

PHASE EQUILIBRIUM MEASUREMENTS AND
MODELING OF SELECTED ASYMMETRIC
TERNARY MIXTURES

By

Khalid Farouk Omar

Bachelor of Science
Texas A&M University
College Station, TX
1989

Master of Chemical Engineering
University of Houston – University Park
Houston, TX
1993

Submitted to the Faculty of the
Graduate College of the
Oklahoma State University
in partial fulfillment of
the requirements for
the Degree of
DOCTOR OF PHILOSOPHY
December, 2002

PHASE EQUILIBRIUM MEASUREMENTS AND
MODELING OF SELECTED ASYMMETRIC
TERNARY MIXTURES

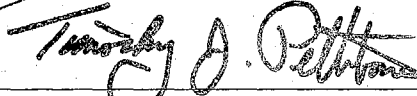
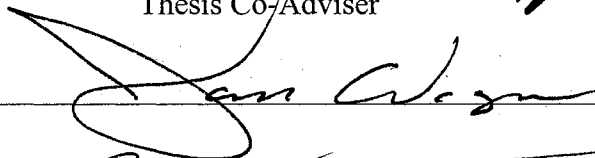
Thesis Approved:



Thesis Co-Adviser



Thesis Co-Adviser



Dean of the Graduate College

PREFACE

The current state of the art indicates that a cubic equation-of-state (CEOS) model capable of precisely representing the vapor-liquid equilibrium (VLE) properties of asymmetric binary mixtures and providing reliable generalized predictions for such mixtures is predicated on: (a) a modified covolume that accounts for molecular size asymmetry, (b) mixing rules reflective of the local-composition mixing, and (c) a determination that the model is able to describe asymmetric multi-component mixtures based on pair-wise interactions.

Accordingly, the specific objectives of the study were to: (a) evaluate the efficacy of the existing one-fluid and excess free energy mixing rules in representing the selected binary and ternary asymmetric mixtures, (b) develop improved excess Gibbs/Helmholtz energy mixing rules, (c) modify the CEOS covolume utilizing the combinatorial contribution to excess free energy formulation, (d) design and construct a mercury-free, high-pressure experimental apparatus to facilitate accurate solubility measurements for systematically selected ternary asymmetric systems, and (e) evaluate the correlative and predictive abilities of the new thermodynamic model developed in this work in comparison with recent literature models advanced by Boukavalas, et al. (1994) and Orbey and Sandler (1997).

A new, constant-volume, synthetic-type, mercury-free, high-pressure experimental apparatus was designed and constructed based on a new experimental

technique. Solubility measurements for asymmetric ternary mixtures of (a) hydrogen and carbon dioxide in eicosane, octacosane, and hexatriacontane were determined at 323.15, 344.26, 373.15 and 473.15 K and pressures to 15.3 MPa; and (b) ethane and carbon dioxide in eicosane, octacosane, and hexatriacontane were determined at 323.15, 344.26, 373.15 and 473.15 K and pressures to 14.17 MPa. Internal and external consistency tests validate the viability of the newly-acquired ternary solubility measurements, which exhibit experimental uncertainties within 0.002 in mole fraction.

The efficacy of the one-fluid mixing theory in handling binary and ternary asymmetric mixture was evaluated. For the ternary asymmetric mixtures ethane/carbon dioxide/n-paraffin, the Peng-Robinson (PR) equation of state (EOS) with one-fluid mixing rules was capable of predicting ternary mixture bubble point pressures with the same accuracy as it represents the constituent binaries when two temperature-independent parameters were used per binary. In comparison, for the hydrogen/carbon dioxide/n-paraffin, the predictive ability of PR EOS with one-fluid mixing rules is as good as its representation of its binaries when one or two temperature-independent parameters were used. Moreover, in the context of one-fluid mixing rules, molecular pair-wise interactions are effective in describing the asymmetric ternary mixtures considered in this study.

The present effort to improve the mixing rules for asymmetric mixtures based on a sound theoretical approach has been effective. A new semi-theoretical mixing rule was developed for the Peng-Robinson EOS covolume, which accounts effectively for molecular size asymmetry in mixture phase behavior. In general, the new excess Helmholtz energy mixing rule yields predictions with average absolute deviation of about

4.7 % for the systems studied. These results are comparable to those of Orbey and Sandler (1997) and better than those of Boukavalas et al. (1994). Moreover, the new mixing rules produce excellent results for the challenging hydrogen/n-paraffin binaries.

Comparable results were obtained for the excess Gibbs/Helmholtz based models using group contribution method in comparison to predictive model based on the one-fluid mixing rules. Further, for the excess Gibbs/Helmholtz free energy models, functional group pair-wise interactions are effective in describing the asymmetric ternary mixtures considered in this study.

I would like to express my grateful appreciation to my adviser Dr. K. A. M. Gasem. His continuous support, constructive guidance, knowledge, and experience have helped greatly in the completion of this study.

I would like to extend any thanks and appreciation to my co-advisor Dr. R. L. Robinson, Jr. for his valuable suggestions and encouragement provided during this study. Also, I extend my thanks to the committee members Dr. J. Wagner and Dr. J. N. Veenstra for their time and efforts in reviewing this work.

I like to express my thanks to my wife, Azza, and our sons and daughter, Amr, Ahmad and Salma, for their patience and understanding throughout this process.

Finally, I dedicate this dissertation to the memory of my father, Dr. Farouk Omar, whose inspiration, encouragement, moral and financial support made my ambitions throughout the years a reality.

Funding provided by the endowed R. N. Maddox Professorship is greatly appreciated.

TABLE OF CONTENTS

Chapter	Page
I. INTRODUCTION.....	1
Objectives.....	5
Organization.....	8
II. BACKGROUND AND LITERATURE REVIEW.....	9
Vapor-Liquid Equilibrium Framework.....	10
Mixing Rules.....	10
The Importance of the Covolume Constant.....	18
The Importance of using Ternary Mixtures in Evaluating EOS Models.....	21
Non-Random Solution Model.....	22
Group Contribution Concept.....	24
Combinatorial and Free Volume Contributions to Excess Free Energy.....	28
III. EXPERIMENTAL METHODS AND APPARATUS.....	36
Review of Experimental Methods.....	37
A New Experimental Technique.....	40
New Experimental Apparatus.....	42
IV. EXPERIMENTAL PROCEDURE.....	50
Pressure Testing	50
Pressure Calibration	51
Temperature Calibration.....	54
Volume Calibration.....	55
Solvent Preparation.....	55
Solute Preparation	60

Chapter	Page
Planning for an Experiment.....	62
Solute and Solvent Injection.....	65
Determination of Thermodynamic Properties.....	72
Apparatus Clean up and Drying	76
 V	
EXPERIMENTAL DATA ANALYSIS.....	82
Error Analysis.....	82
Consistency Testing of Experimental Data	87
Instrumental Consistency Testing.....	88
Internal Consistency Testing	88
External Consistency Testing.....	95
 VI	
EXPERIMENTAL RESULTS AND DISCUSSIONS	104
High-Pressure Solubility of Ethane and Carbon Dioxide in Eicosane, Octacosane, and Hexatricontane.....	109
High-Pressure Solubility of Hydrogen and Carbon Dioxide in Eicosane, Octacosane, and Hexatricontane.....	120
Summary.....	130
 VII.	
NEW MIXING RULES BASED ON EXCESS HELMHOLTZ FREE ENERGY - 1. EVALUATION WITH BINARY MIXTURES.....	131
Model Development.....	131
Evaluation of Excess Free Energy Combinatorial Expressions.....	135
Database Used	142
Model Evaluations and Comparisons	142
Results and Discussions.....	150
Summary... ..	176
 VIII	
NEW MIXING RULE BASED ON EXCESS HELMHOLTZ FREE ENERGY - 2. EVALUATION WITH TERNARY MIXTURES.....	177
Model Development.....	178
Database Used	178
Results and Discussions.....	178
Summary.....	183

Chapter	Page
IX CONCLUSIONS AND RECOMMENDATIONS	185
Conclusions.....	185
Recommendations.....	187
LITERATURE CITED	189
DATABASE LITERATURE CITED.....	201
APPENDIXES.....	207
APPENDIX A - Flow Diagram for Experiment Planning Program.....	207
APPENDIX B - Error Analysis of Solubility Measurements for Binary and Ternary Mixtures	214
APPENDIX C - The PR Representation of Asymmetric Binary Mixtures..	234
APPENDIX D - Experimental and Calculated Activity Coefficients at Infinite-Dilution using Several Models.....	240
APPENDIX E - Mixing Rules and Component Fugacity Coefficients for the Thermodynamic Models used in this Work.....	247
APPENDIX F - Auxiliary VLE Properties Measurements.....	253

LIST OF TABLES

Table	Page
1. Selected Asymmetric Ternary Mixtures and their Compositions and Temperatures.....	6
2. Selected Cubic Equation-of-State Mixing Rules.....	13
3. Selected Combinatorial Expressions.....	32
4. Suppliers and Stated Purities of the Chemicals used in this Work.....	85
5. Pure-Fluid Properties used in this Work.....	86
6. Vapor Pressure of Pure Butane.....	88
7. Solubility of Nitrogen in Hexane.....	91
8. PR Equation-of-State Representations of the Solubility of Nitrogen in Hexane using One Interaction Parameter.....	93
9. PR Equation-of-State Representations of the Solubility of Nitrogen in Hexane using Two Interaction Parameters.....	94
10. Asymmetric Ternary Mixtures in the Literature.....	106
11. Solubility of Carbon Dioxide and Ethane in Eicosane.....	110
12. Solubility of Carbon Dioxide and Ethane in Octacosane.....	111
13. Solubility of Carbon Dioxide and Ethane in Hexatricosane.....	112
14. The Critical Properties and Acentric Factors used in the PR CEOS Evaluations.....	113

Table	Page
15. PR EOS Prediction/Representation of Carbon Dioxide /Ethane /n-Paraffins Systems Based on Binary Interaction Parameters.....	116
16. PR Equation-of-State Prediction/Representation of the Solubilities of Carbon Dioxide and Ethane in Eicosane.....	117
17. PR Equation-of-State Prediction/Representation of the Solubilities of Carbon Dioxide and Ethane in Octacosane.....	118
18. PR Equation-of-State Prediction/Representation of the Solubilities of Carbon Dioxide and Ethane in Hexatricontane.....	119
19. PR EOS Prediction/Representation of Carbon Dioxide /Ethane /n-Paraffin Systems Based on Binary Interaction Parameters.....	121
20. Solubility of Carbon Dioxide and Hydrogen in Eicosane.....	122
21. Solubility of Carbon Dioxide and Hydrogen in Octacosane.....	123
22. Solubility of Carbon Dioxide and Hydrogen in Hexatricontane.....	124
23. PR EOS Prediction/Representation of Carbon Dioxide /Hydrogen /n-Paraffin Systems Based on Binary Interaction Parameters.....	126
24. PR Equation-of-State Prediction/Representation of the Solubilities of Carbon Dioxide and Hydrogen in Eicosane.....	127
25. PR Equation-of-State Prediction/Representation of the Solubilities of Carbon Dioxide and Hydrogen in Octacosane.....	128
26. PR Equation-of-State Prediction/Representation of the Solubilities of Carbon Dioxide and Hydrogen in Hexatricontane.....	129
27. Comparison among Several Combinatorial Expressions using Infinite-Dilution Activity Coefficients of n-Paraffins Binary Mixtures.....	137
28. van der Waals Gas Parameters.....	138

Table	Page
29. Mixing Rules For Models Evaluated in this Work.....	139
30. PR Equation-of-State One-Fluid Mixing Rules Generalized Correlations for Selected Systems.....	140
31. Models Comparison for Several Combinatorial Expressions Using Ethane/n-Paraffin Binary Mixtures.....	141
32. The Database of Binary Systems used in this Study.....	143
33. UNIFAC Interaction Parameters Regressed for Models Evaluated.....	149
34. Models Comparison for Ethane/n-Paraffin Systems.....	151
35. Models Comparison for Carbon Dioxide/n-Paraffin Systems.....	154
36. Models Comparison for Methane/n-Paraffin Systems.....	156
37. Models Comparison for Hydrogen/n-Paraffin Systems.....	157
38. Models Comparison for Carbon Monoxide/ n-Paraffin Systems.....	160
39. Summary of Overall Results for all the Binary Systems Considered.....	161
40. Summary of Results for Asymmetric Binary Mixtures involving C ₂₀ and above.....	161
41. Comparison among the Number of Parameters for the Models Evaluated.....	175
42. The Database of Ternary Systems used in this Study.....	179
43. Summary of Model Evaluation Results for Asymmetric Ternary Systems.....	180
44. Models Comparison for Asymmetric Binary and Ternary Mixtures.....	182

LIST OF FIGURES

Figure	Page
1. Experimental Methods for High Pressure Phase Equilibria.....	38
2. Concept of the New Experimental Technique.....	41
3. Schematic Diagram of the New High-Pressure Experimental Apparatus.....	43
4. Bubble Point Pressures for CO ₂ /Butane Binary System.....	66
5. Bubble Point Pressures for CO ₂ /Decane Binary System.....	67
6. Symbolic Representation of Sequence in Experimental Phase Behavior.....	73
7. Experimental Pressure-Volume Trends of Carbon Dioxide/Butane Binary Mixture.....	74
8. Experimental Pressure-Volume Trends of Carbon Dioxide/Decane Binary Mixture.....	77
9. Bubble Point Pressures of Nitrogen/Hexane System.....	90
10. Comparison of Bubble Point Pressures of Nitrogen/ Hexane System.....	92
11. Comparison of Bubble Point Pressures for the Carbon Dioxide /Butane System at 377.6 K.....	96
12. Comparison of Carbon Dioxide Solubilities in Butane System at 377.6 K....	97
13. Comparison of Bubble Point Pressures for Carbon Dioxide/Decane System.....	99

Figure	Page
14. Comparison of Carbon Dioxide Solubilities in Decane.....	100
15. Comparison of Bubble Point Pressures for Nitrogen/ Decane System at 410.9 K.....	101
16. Comparison of Nitrogen Solubilities in Decane at 410.9 K.....	102
17. The Effect of Combinatorial Expression on CHV Model for Ethane/Hexatricontane Binary Mixture.....	152
18. Model-1 Correlations for Excess Combinatorial Helmholtz Free Energy Parameter.....	158
19. Comparison of the Covolume Deviations for Ethane /n-Paraffin Mixtures.....	163
20. Comparison of the Covolume Deviations for Carbon Dioxide /n-Paraffin Mixtures.....	164
21. Comparison of the Covolume Deviations for Methane /n-Paraffin Mixtures.....	165
22. Comparison of the Covolume Deviations for Hydrogen /n-Paraffin Mixtures.....	166
23. Comparison of the Covolume Deviations for Carbon Monoxide /n-Paraffin Mixtures.....	167
24. Covolume Interaction Parameter Variations for VDW-2 Model – Case 1.....	169
25. Covolume Interaction Parameter Variations for VDW-2 Model – Case 2.....	170
26. Covolume Interaction Parameter Variations for CHV Model.....	171
27. Infinite-Dilution Activity Coefficients of Solutes in n-Paraffins at 373 K.....	173
28. Combinatorial Infinite-Dilution Activity Coefficients of Solutes in n-Paraffins at 373 K.....	173

29. Excess Helmholtz Combinatorial Values of Several Solutes in n-Octacosane at 373.3 K.....	174
---	-----

NOMENCLATURE

a	CEOS molecular interaction parameter
A	Helmholtz free energy
\bar{A}_{ij}	UNIFAC empirical parameter
A_{vdw}	van der Waals surface area
b	CEOS covolume parameter
B	empirical constant
\bar{B}_{ij}	UNIFAC empirical parameter
CEOS	cubic equation-of-state
\bar{C}	UNIFAC empirical parameter
CHV	corrected Huron Vidal model by Orbey and Sandler (1997)
C_{ij}, D_{ij}	CEOS interaction parameters
C_M	MHV model CEOS dependent constant
C_N	new model CEOS dependent constant
C_{os}	CHV model CEOS dependent constant
C_V	HV model CEOS dependent constant
CN	n-paraffin carbon number
e	potential energy
FV	free volume
G	Gibbs free energy
g_{12}	energy of interaction between a 1-2 pair of molecules
k	empirical parameter
m	empirical parameter
MHV	modified Huron Vidal model by Michelsen (1990b)
n	number of moles

N_o	Avogadro's number
p	pressure
q_i	molecular surface area
Q_k	group area parameter
r	number of segments
\bar{r}	distance
R	universal gas constant
RMSE	root mean square error
r_i	molecular volume
R_k	group volume parameter
S	entropy
T	temperature
u	packing factor
U_{mn}	energy of interaction between groups m and n
V_{vdw}	van der Waals group volume
w	volume fraction exponent
V	volume
x	liquid phase composition
X_{21}	local mole fraction of molecule 2 in the neighborhood of molecule 1
z	mole fraction of vapor or liquid phase
Z_c	coordination number

Greek Letters

Γ_k^i	activity coefficient of group k at a group composition corresponding to pure component
Ω	configuration factor
δ	empirical constant
Γ	group activity coefficient
Θ	group area fraction in mixture

Ψ_{nm}	group interaction parameter between groups n and m
ε_{ij}	interaction energy between molecules i and j
σ_{ij}	intermolecular interaction distance between molecules i and j
Ψ_i	modified volume fraction
γ_i	molecular activity coefficient
θ_i	molecular area fraction
ϕ_i	molecular volume fraction
ξ	non-sphericity of molecule
ν_{ki}	number of groups of type k in molecule i
ρ	density
τ	non randomness factor
ω	acentric factor

Subscripts and Superscripts

0	reference
c	critical property
cal	calculated
comb	combinatorial
exe	excess
exp	experimental
FV	free volume
i, j	component or group identifier
res	residual

CHAPTER I

INTRODUCTION

Phase equilibrium thermodynamics is a subject of fundamental importance in the chemical and petroleum process industries. Phase equilibrium properties (in particular, temperature, pressure, and composition) are required for the design of essential separation operations in these industries. The chemical process industry is the fourth largest manufacturing industry in the United States. In the petroleum industry, refining accounts for 10% of total industrial energy usage in the United States. As reported by Humphrey, et al. (1991), 43% of the energy consumed in the chemical and petroleum industries can be attributed to separation processes. Separation processes account for 40-70% of both capital and operating costs in these industries. Beyond separation processes, phase equilibrium properties affect rates of reaction, mass transfer, and selectivity in synthesis processes. Therefore, the proper design, operation, and optimization of many processes depend heavily on knowledge of the phase behavior of the mixtures encountered in these processes.

The understanding of intermolecular forces responsible for thermodynamic properties of pure substance and mixtures is far from complete. Quantitative results have been obtained for only simple and idealized models of real fluids. Frequently, the theory

of intermolecular forces gives us no more than a qualitative, or perhaps semi quantitative, basis for understanding phase behavior (Prausnitz, et al., 1999).

Knowledge of the thermodynamics and phase behavior of asymmetric mixtures (molecules differing greatly in size and shape) is central to the understanding and comprehensive modeling of many important processes including coal liquefaction, enhanced oil recovery, and supercritical fluid extraction.

Indirect coal liquefaction using slurry phase Fisher-Tropsch (F-T) technologies offers several advantages over other methods (e.g., direct coal liquefaction, and gas phase F-T). In the early 1980s, the United States Department of Energy (DOE) began to support a research and development program to advance the slurry phase reactor technology aimed at coal-based applications. Recent publications (e.g., Eisenberg, et al., 1998) indicate that industrial companies also have been active in the area of slurry phase F-T technology development (Shen, et al., 1997). Accurate modeling of F-T reactor performance and subsequent process operations are strongly dependent on the composition of the wax phase (high molecular weight hydrocarbons, mostly n-paraffins (Shah, et al., 1988)), whose composition is constrained (in addition to catalyst properties) by the vapor-liquid equilibrium (VLE) that exists in the reactor (e.g., the F-T reactor temperature controls the wax yield (Kuo, 1985)).

Many factors contribute to the challenge in dealing with asymmetric mixtures due to non-idealities that result from differences in molecular size, shape, and polarity. In coal processing, mixtures of light gases dissolved in high molecular weight solvents, such as CH₄, CO, CO₂, C₂H₆, and H₂ in n-paraffin solvents, are typically encountered. The presence of near-critical and supercritical components with a broad variation of physical

properties (e.g., quantum, quadrupole, and polar fluids) has limited the ability to generalize phase behavior models.

The most convenient form for representing the equilibrium phase behavior in process design and optimization has long been recognized as the analytical equation of state. Among many equations of state proposed for predicting the phase behavior of systems, cubic equations of state (CEOS) have been used because of their simplicity and accuracy.

Use of CEOS to model complex behavior of highly non-ideal mixtures, however, requires mixing rules other than the commonly employed van der Waals (vdW) one-fluid mixing rules (Wong and Sandler, 1992). In addition, the largely empirical nature of the CEOS parameters, as determined from vdW mixing rules, limits the interpretation that can be placed upon these parameters (Gasem, et al., 1993).

Recently developed mixing rules based on excess Gibbs/Helmholtz mixing rules (e.g., Wong and Sandler, 1992; Orbey and Sandler, 1995; Fischer and Gmehling, 1996) have greatly expanded CEOS useful application. This is accomplished by relating the CEOS attraction constant, a , for a mixture to activity coefficient model parameters and the vdW covolume, b (Orbey and Sandler, 1996). Several of these models specifically targeted asymmetric mixtures (Boukvalas, et al., 1994; Zhong and Musuoka, 1996; Orbey and Sandler, 1997). A shortfall of these models is in not taking into consideration the non-ideality due to variation in size when determining the equation of state covolume, b , as it applies to asymmetric mixtures. In addition, these models have not been evaluated with asymmetric ternary or multi-component mixtures.

The non-ideality due to large variation in molecular size ratio is critically important in modeling asymmetric mixtures. The modification of CEOS covolume when dealing with asymmetric mixtures offers a physically meaningful representation (Kwak and Mansoori, 1986) and better results (Gasem and Robinson, 1985; Peters, 1986; Gasem, et al., 1989; Darwish, et al., 1993) of these systems.

Beyond asymmetry in binary systems, thermodynamic model evaluation and development must take into consideration the ability to correctly predict the VLE of a mixture of at least three components (BenMekki and Mansoori, 1988). The description of multi-component phase behavior in terms of pair-wise interactions (molecule interaction only with its nearest neighbor) has been validated for mixtures composed of molecules of similar size and structure; however, additional study is needed to extend such validation to molecules of widely differing type, size and structure (Azevedo and Prausnitz, 1988; Gasem and Robinson, 1995). Due to the lack of experimental data for asymmetric ternary and higher mixtures, thermodynamic models were not evaluated for these mixtures. The overall objective of this research is to develop an accurate predictive thermodynamic model of asymmetric binary and ternary mixtures phase equilibrium properties typically encountered in coal-conversion processes.

Research to validate any theoretical development requires pertinent and accurate experimental data covering an adequate range of experimental conditions. Nevertheless, the quantity of data required can be reduced dramatically if the experiments are carefully designed to serve a specific, critical role in the development and testing of theoretical and empirical models. Such a research program should logically include (a) critical evaluation of existing literature data, (b) identification of viable correlation frameworks

that contain a minimum number of input parameters (and those parameters should be amenable to generalization), and (c) an experimental facility able to provide the data for the correlation and process development efforts (Gasem and Robinson, 1995).

Due to lack of experimental data for asymmetric ternary and multi-component mixtures, solubility measurements were performed for systematically selected asymmetric ternary mixtures, as presented in Table 1, in this work. The composition ranges selected for the ternary mixtures were based on the upper and lower limits of the solute compositions in the corresponding binary mixtures. The temperature ranges of available binary mixture data set the temperatures used. Differences in the lowest temperatures (i.e., 323.1 K for eicosane and 373.1 K for hexatriacontane) at which the systems were studied were often dictated by the melting points of the n-paraffins, which are solids at room temperature. The systems investigated were systematically selected to determine the effect of solute and solvent properties; specifically, ethane is a normal fluid, carbon dioxide represents a quadrupole fluid, and hydrogen is a quantum fluid. The n-paraffin solvents show molecular size effects.

Objectives

The current state of the art indicates that a CEOS model capable of (a) precisely representing the vapor-liquid equilibrium (VLE) properties of binary asymmetric mixtures and (b) providing reliable generalized predictions for such mixtures requires:

1. A modified covolume that accounts for molecular size asymmetry.
2. Mixing rules reflective of the local-composition mixing attributed to aggregation.

Table 1. Selected Asymmetric Ternary Mixtures and their Compositions and Temperatures

	T/ K	Molar Composition, %				
Eicosane	323.15	34	43	49	51	51
+ CO ₂	344.26	3	9	17	27	38
+ C ₂ H ₆	373.15	63	48	34	22	11
	423.15					
Eicosane	323.15	80	75	70	63	56
+ CO ₂	344.26	8	16	24	33	42
+ H ₂	373.15	12	9	6	4	2
	423.15					
Octacosane	348.15	46	49	49	44	36
+ CO ₂	373.15	5	15	27	42	58
+ C ₂ H ₆	423.15	49	36	24	14	6
Octacosane	348.15		70	60	49	38
+ CO ₂	373.15		20	34	47	60
+ H ₂	423.15		10	6	4	2
Hexatriacontane	373.15		52	55	55	51
+ CO ₂	423.15		10	20	31	44
+ C ₂ H ₆	473.15		38	25	14	5
Hexatriacontane	373.15		69	63	56	48
+ CO ₂	423.15		17	27	37	48
+ H ₂	473.15		14	10	7	4

3. A confirmation that the model is able to describe multi-component asymmetric mixtures based on pair-wise interactions.

The goal of this study was to develop a CEOS model that meets the above requirements. Specifically, we implemented the Peng-Robinson (PR) (Peng and Robinson, 1976) equation of state (EOS) using newly developed excess Gibbs/Helmholtz free energy mixing rules. To successfully complete this development effort, an extensive VLE database for asymmetric binary mixtures involving five light gases and n-paraffins extending from C₃ to C₄₄ were assembled, and selected ternary VLE measurements were conducted.

The specific objectives of the study were:

1. Evaluate the efficacy of the existing one-fluid and excess Gibbs/Helmholtz free energy mixing rules in representing the selected asymmetric binary and ternary mixtures.
2. Develop improved excess Helmholtz free energy mixing rules.
3. Modify the CEOS covolume utilizing the UNIFAC (Universal Quasi-chemical Functional-group Activity Coefficients) excess Helmholtz free energy formulation.
4. Design and construct a mercury-free, high-pressure experimental apparatus to permit accurate solubility measurements for the asymmetric ternary systems.
5. Evaluate the correlative and predictive abilities of new model in comparison with recent literature models advanced by Boukvalas, et al. (1994) and Orbey and Sandler (1997).

Organization

This dissertation is organized as follows. Chapter II presents a brief background and a literature review on vapor-liquid equilibrium modeling. Chapter III gives a review of experimental methods, presents the new experimental technique, and provides a description of the new experimental apparatus. Chapter IV details the experimental procedures. Chapter V presents error analysis and consistency tests of the experimental data. Chapter VI includes measurements acquired in this study, as well as the results and discussions for systems investigated. Chapter VII presents the new semi-theoretical mixing rule and gives an evaluation of several mixing rules as they apply to binary mixtures. Chapter VIII presents an evaluation of mixing rules as they apply to ternary mixtures, particularly asymmetric mixtures. Chapter IX outlines the conclusions of this research and suggestions for future work.

CHAPTER II

BACKGROUND AND LITERATURE REVIEW

The purpose of this chapter is to present background information and a literature review of the current state in modeling VLE of non-ideal mixtures using CEOS. The emphasis is on recently developed mixing rules that combine an EOS with an excess free energy model. A summary of the development of CEOS mixing rules is presented. The importance of the CEOS covolume in dealing with asymmetric mixtures is explored. Phase behavior of a ternary mixture is likely to be more indicative of multi-component fluid-phase equilibria than phenomena exhibited by a binary mixture; the importance of model evaluation/development using asymmetric ternary mixtures is considered. Several important issues are also addressed including: (a) the local composition concept and two-fluid theory, which form the basis for many successful liquid solution models (for example, NRTL [non-random, two-liquid], UNIQUAC [Universal Quasi-chemical] and UNIFAC) are presented, (b) the group-contribution methods and the extension of interaction among molecules to functional groups, and (c) combinatorial and free volume expressions and developments in these areas.

Vapor-Liquid Equilibrium Framework

The determination of equilibrium phase behavior of complex mixtures over broad ranges of temperature and pressure is an important problem in chemical process design. The most convenient form for representation of equilibrium phase behavior for process design and optimization calculation has long been recognized as an analytic EOS (Prausnitz, 1977).

Two approaches commonly used in modeling VLE incorporate (a) an EOS with classical one-fluid mixing rules for both liquid and vapor phases or (b) an EOS for the vapor phase and activity coefficient model for the liquid phase. The first approach using one-fluid mixing rules can be applied over a broad range of temperature and pressure, but is limited to simple and normal fluid mixtures. The second approach can be used to model liquids of any complexity. The deficiencies of the second approach are: (1) hypothetical standard states are assumed for supercritical components, (2) a separate method is required for determining volumetric and calorimetric properties, and, (3) there is difficulty in modeling near-critical regions. As such, an EOS applicable to both vapor and liquid phases has a definite advantage over activity coefficient models.

Mixing Rules

Among many equations of state proposed for predicting the phase behavior of non-polar systems, CEOS have been used because of their simplicity and accuracy. Among the CEOS, two equations that have enjoyed widespread acceptance in the refinery and gas-processing industries are the SRK EOS (Soave, 1972) and the PR EOS. For pure

substances, they give acceptable results for practical purposes; for mixtures, the results are strongly dependent on the mixing rules used and the systems evaluated.

The one-fluid theory is the simplest procedure to extend the use of CEOS to mixtures. The fundamental idea of the one-fluid theory is that a mixture can be considered to be a hypothetical fluid whose characteristic properties are the composition-average of the corresponding properties of the mixture components (Prausnitz, et al., 1999). The most commonly used mixing rules are the van der Waals one-fluid mixing rules, where mixing rules are quadratic in mole fraction. For a multi-component mixture,

$$a = \sum_i \sum_j z_i z_j a_{ij} \quad (2-1)$$

$$b = \sum_i \sum_j z_i z_j b_{ij} \quad (2-2)$$

In addition, combining rules are needed for the cross energy and covolume constants. The usual combining rules are:

$$a_{ij} = \sqrt{a_{ii} a_{jj}} (1 - C_{ij}) \quad (2-3)$$

$$b_{ij} = \frac{b_{ii} + b_{jj}}{2} (1 + D_{ij}) \quad (2-4)$$

Where C_{ij} and D_{ij} are empirical “binary interaction parameters” obtained by fitting EOS predictions to experimental data.

To use a CEOS to model complex behavior of highly non-ideal mixtures, however, mixing rules other than the commonly employed van der Waals one-fluid mixing rules are required. Several authors (e.g., Panagiotopoulos and Reid, 1986; Adachi and Sugie, 1986; Sandoval, et al., 1989; Schwartzenruber and Renon, 1989) have proposed modified forms of the van der Waals mixing rules that use composition-

dependent binary interaction parameters. While these largely empirical mixing rules have been successful for some highly non-ideal mixtures, they are not generally applicable; since in the low-density limit they are inconsistent with the statistical mechanical result that the second virial coefficient must be a quadratic function of composition. Further, these rules may fail for simple mixtures (Shibata and Sandler, 1989).

To correct these problems, attempts have been made to develop density-dependent mixing rules (e.g., Luedecke and Prausnitz, 1985; Panagiotopoulos and Reid, 1986b) so that the correct low density is recovered. Such an approach, however, is *ad hoc* and does not preserve the cubic nature of EOS when used for mixtures. Moreover, as pointed out by Michelsen and Kistenmacher (1990), some of the mixing rules that have been proposed lead to inconsistencies when a component is split into two or more identical fractions (i.e., 50% A and 50% B mixture should have the same properties as 50% A, 25% B and 25% B mixture). Ongoing efforts have attempted to correct such deficiencies (Schwartzentruber and Renon, 1991; Mathias, et al., 1991), but with little success (Wong and Sandler, 1992). A review of density- and composition-dependent mixing rules is given elsewhere (Zavala, et al., 1996; Trivedi, 1996). A partial list of mixing rules for the CEOS is shown in Table 2 to demonstrate the highly empirical nature of its parameters.

Because of inadequacies in empirical mixing rules, such as the classical mixing rules, the CEOS approach to VLE long has been limited to systems exhibiting modest and well-behaved deviations from ideal solution behavior in the liquid phase, e.g., systems containing hydrocarbons. However, the developments of a certain class (Huron-Vidal type) of mixing rules for CEOS have greatly expanded their useful application.

Table 2. Selected Cubic Equation-of-State Mixing Rules

Composition-Dependent Binary Interaction Parameters

$a = \sum_i \sum_j x_i x_j \sqrt{a_i a_j} \left(1 - k_{ij} + x_i (k_{ij} - k_{ji}) \right)$	Panagiotopoulos-Reid (1986)
$a = \sum_i \sum_j x_i x_j \sqrt{a_i a_j} \left(1 - x_i k_{ij} - x_j k_{ji} \right)$	Stryjek-Vera (1986b)
$a = \sum_i \sum_j \sqrt{a_i a_j} \left(1 - \frac{k_{ij} k_{ji}}{x_i k_{ij} + x_j k_{ji}} \right)$	Stryjek-Vera (1986b)
$a = \sum_i \sum_j x_i x_j \sqrt{a_i a_j} \left[1 - k_{ij} + m_{ij} (x_i - x_j) \right]$ $k_{ji} = k_{ij}, \quad m_{ji} = -m_{ij}$	Adachi and Sugie (1986)
$a = \sum_i \sum_j x_i x_j a_{ij}$ $a_{ij} = 1 - \bar{k}_{ij} - x_j \Delta k_{ji} - x_i \Delta k_{ij} - l_{ij}$ $\left(x_i - x_i^2 + x_j - x_j^2 \right)$ $\bar{k}_{ij} = \frac{k_{ij} + k_{ji}}{2}, \quad \Delta k_{ij} = k_{ij} - \bar{k}_{ij}, \quad \Delta k_{ji} = k_{ji} - \bar{k}_{ij}$	Sandoval-Wilczek-Vera (1989)
$a = \sum_i \sum_j x_i x_j \sqrt{a_i a_j} \left(1 - k_{ij} - l_{ij} (x_i - x_j) \right)$ $k_{ji} = k_{ij}, \quad l_{ji} = -l_{ij}$	Schwartzentruber and Renon (1989)
$a = \sum_i \sum_j x_i x_j \sqrt{a_i a_j} \left(1 - k_{ij} + \lambda_{ij} x_i \right)$ $k_{ij} = k_{ji}, \quad \lambda_{ji} = -\lambda_{ij}$	Melhem (1990) and Saini (1990)

Table 2. Selected Cubic Equation-of-State Mixing Rules - *continued*

$$a = \sum_i \sum_j x_i x_j \sqrt{a_i a_j} (1 - k_{ij}) + \sum_j x_j \left[\sum_j x_j \left(\frac{a_i a_j}{6} \right)^{\frac{1}{6}} \left(k_{ij} - k_{ji} \right)^{\frac{1}{3}} \right]^3$$

Mathias-Klotz-Prausnitz (1991)

$$a = \sum_i \sum_j x_i x_j \sqrt{a_i a_j} \left(\left[1 - \frac{k_{ij}}{T} \right] + \left[\frac{H_{ij} G_{ij} x_j^2}{x_i + G_{ij} x_j} \right] \right)$$

$$H_{ij} = \frac{[k_{ji} - k_{ij}]}{T} \quad G_{ij} = \exp \left[-\beta_{ij} H_{ij} \right]$$

Twu, et al. (1991)

Density-Dependent Binary Interaction Parameters

$$a = \sum_i \sum_j x_i x_j \sqrt{a_i a_j} (1 - k_{ij}) + \left(\frac{\rho}{RT} \right) \sum_{i \neq j} \sum_{i \neq j} x_i x_j (x_i c_{i(j)} + x_j c_{j(i)})$$

Luedecke and Prausnitz (1985)

$$a = \sum_i \sum_j x_i x_j \sqrt{a_i a_j} (1 - k_{ij}) + \frac{\rho b}{RT} \sum_i \sum_j x_i x_j (x_i \lambda_{ij} + x_j \lambda_{ji})$$

$$k_{ij} = k_{ji}, \quad \lambda_{ij} = -\lambda_{ji}$$

Panagiotopoulos and Reid (1986b)

Following is a brief literature review of the developments pertaining to this type of mixing rule.

The use of CEOS for the systems containing non-ideal asymmetric components requires a proper definition of the mixing rules for CEOS attraction and covolume constants.

Huron and Vidal (1979) pioneered linking the EOS attraction constant to the excess free energy at infinite pressure. The use of this mixing rule was limited due to the pressure dependency of excess Gibbs free energy, and the lack of experimental excess Gibbs free energy data at high pressures. Huron-Vidal mixing rules are defined as follows:

$$G_{p=\infty}^{\text{exc}} = -\left(\frac{a}{b} - \sum_i^n \frac{a_{ii}}{b_{ii}} x_i\right) \ln 2 \quad (2-5)$$

$$b = \sum_{i=1}^n b_{ii} x_i \quad (2-6)$$

Gupta, et al. (1986) used the same method, but at the temperature and pressure of the system. Simplifying assumptions led to mathematical inconsistency. Gani, et al. (1989) corrected the mathematical inconsistency by considering the volume dependency of the “a” constant in deriving the component fugacity coefficient. The new model relates the pressure and volume through a differential equation rather than through an algebraic equation. Analytical treatment of the equation is difficult, and the fugacity coefficients are cumbersome to evaluate.

Several models developed by Mollerup (1986), Heidemann and Kokal (1990), Michelsen (1990a, 1990b), Dahl and Michelsen (1990) and Dahl, et al. (1991) are all

based on a zero-pressure standard state for excess Gibbs free energy. The model requires the determination of liquid volumes at zero pressure, which were determined from an EOS where a root, or roots, may exist. The modified Huron-Vidal mixing rule (MHV1) developed by Michelsen (1990b) is as follows:

$$\alpha_{\text{mix}} = \left(\frac{a}{bRT} \right)_{\text{mix}} = \sum_{i=1}^n z_i \alpha_{ii} + \frac{1}{C_M} \left[\frac{G^{\text{exe}}}{RT} + \sum_{i=1}^n z_i \ln \left(\frac{b}{b_{ii}} \right) \right] \quad (2-7)$$

To overcome the problem of finding a liquid volume in some cases at this hypothetical zero pressure, a constant packing factor (u) assumption was made for pure fluids and mixtures. The constant packing assumption sets the value of the mixing rule constant as follows:

$$C_M = \left[-1 - \ln(u-1) - \alpha_{\text{mix}} \ln \left(\frac{u+1}{u} \right) \right]_{p=\text{zero}} \quad (2-8)$$

Studies have shown (e.g., Fischer and Gmehling, 1996) that the mixing rule accuracy is sensitive to the value of u . In all of these models, one can use a liquid-activity coefficient model directly, since the connection with the EOS is made in the limit of zero pressure.

All publications from the University of Delaware (Wong and Sandler, 1992; Wong, et al., 1992; Orbey, et al., 1993; Orbey and Sandler, 1995a, 1995b, 1997) used infinite-pressure excess Helmholtz energy as their reference state. Two advantages are gained by this approach. First, the excess Helmholtz energy is nearly pressure independent, so the already available excess Gibbs free energy data at low pressure can be

used. Second, at infinite pressure, the assumption of close packing ($V/b = 1$) is valid based on the lattice model, where all sites are occupied.

Three of these models specifically targeted mixtures that contain components with large differences in size (Orbey and Sandler, 1997; Boukouvalas, et al., 1994; Zhong and Musuoka, 1996). These three models used linear mixing rules (typically used for spherical molecules of equal size) for the EOS covolume constant and were not tested with asymmetric ternary or higher mixtures.

Orbey and Sandler (1997) compared several models (Holderbaum and Gmehling, 1991; Michelsen, 1990b; Orbey and Sandler, 1995a; Dahl and Michelsen, 1990; Boukouvalas, et al., 1994) in representing asymmetric binary mixtures. As the asymmetry of the mixture is decreased, the performance of all models becomes similar and, in general, is better. Both models by Boukouvalas, et al. (1994) and Orbey and Sandler (1997) perform better than the other models for mixtures of molecules with large difference in sizes. The Orbey and Sandler (1997) model (CHV) is given as follows:

$$\alpha = \frac{a}{bRT} = \frac{A^{exe}}{C_{os}RT} + \frac{(1-\delta_1)}{C_{os}} \sum_i z_i \ln\left(\frac{b}{b_i}\right) + \sum_i z_i \frac{a_i}{b_i RT} \quad (2-9)$$

$$b = \sum_i b_i z_i \quad (2-10)$$

Although the empirical LCVM model (Boukouvalas, et al., 1994) provides reasonable results for highly asymmetric binary mixtures, the LCVM model has no explicit reference pressure and lacks a theoretical justification. The model developed by Orbey and Sandler (1997) received limited testing for asymmetric mixtures, where the ethane /eicosane binary mixture represents the highest asymmetry used.

Zhong and Musuoka (1996, 1997) used the MHV1 mixing rule developed by Michelsen (1990b). A correction factor was used to compensate for excess Gibbs free energy parameter error as determined from the original UNIFAC. For each solute/n-paraffin series, a correlation was introduced to relate the excess Gibbs free energy correction factor to the n-paraffin member carbon number.

An alternative approach has been suggested by Gasem (1989) to address some of the limitations of the VLE framework (Trivedi, 1996). The basic premise of this new method is to use a fugacity deviation function to augment the fugacity generated from an EOS. This concept was demonstrated through the work of Trivedi (1996). The correlative abilities of this approach are compared with the modified Wong-Sandler (MWS) (Orbey and Sandler, 1995a) mixing rule. The Redlich-Kister model (Walas, 1985) was used for the fugacity deviation function. The new approach shows accuracy comparable to the MWS mixing rule for correlating highly asymmetric binary systems. In addition, either approach extends the applicability of EOS to highly non-ideal systems.

The Importance of the Covolume Constant

Leland and co-workers (Leland, et al., 1968a, 1968b, 1969) were able to re-derive the van der Waals mixing rules with the use of statistical-mechanics theory of radial distribution functions (Kwak and Mansoori 1986). According to these investigators, for a fluid mixture with a pair intermolecular potential energy function between molecules of the mixture in the form

$$e_{ij}(r) = \epsilon_{ij} f\left(\frac{\bar{r}}{\sigma_{ij}}\right) \quad (2-11)$$

the following mixing rules were derived:

$$\sigma^3 = \sum_i^n \sum_j^n X_i X_j \sigma_{ij}^3 \quad (2-12)$$

$$\varepsilon \sigma^3 = \sum_i^n \sum_j^n X_i X_j \varepsilon_{ij} \sigma_{ij}^3 \quad (2-13)$$

In these equations, ε_{ij} is the interaction energy parameter between molecules i and j and σ_{ij} is the intermolecular interaction distance between the two molecules.

For PR EOS, the vdW constant b_{ii} for pure component is defined as follows:

$$b_{ii} = 0.07796 R \frac{T_{ci}}{P_{ci}} \propto N_0 V_{ci} \propto N_0 \sigma_{ii}^3 \quad (2-14)$$

From Equations (2-12) and (2-14), the correct mixing rule for the covolume that satisfies statistical mechanics theory is defined as follows:

$$b = \sum_i^n \sum_j^n X_i X_j b_{ij} \quad (2-15)$$

Knowing that σ_{ij} for ($i \neq j$), the unlike interaction diameter, for spherical molecules, is equal to:

$$\sigma_{ij} = \frac{(\sigma_{ii} + \sigma_{jj})}{2} \quad (2-16)$$

This gives the following expression for b_{ij} of spherical molecules:

$$b_{ij} = \left[\frac{b_{ii}^{1/3} + b_{jj}^{1/3}}{2} \right]^3 \quad (2-17)$$

Then for non-spherical molecules, the expression for b_{ij} as defined by Kwak and Mansoori (1986) is:

$$b_{ij} = (1 - D_{ij}) \left[\frac{b_{ii}^{1/3} + b_{jj}^{1/3}}{2} \right]^3 \quad (2-18)$$

This rule represents a physically meaningful concept that should be applicable to a mixture of molecules that vary largely in size and shape regardless of EOS used.

Gasem (1986) concluded that the SRK with one-fluid mixing rules with a single interaction parameter, C_{ij} , proved inadequate in dealing with CO_2 /n-paraffin asymmetric mixtures. Thus, two parameters, C_{ij} and D_{ij} , have been used to successfully fit the available data. Peters (1986) concluded that in binary mixtures of a volatile and a non-volatile n-alkane, the binary parameter D_{ij} is more important than C_{ij} to describe VLE of ethane/eicosane binary mixture using a simple CEOS. The success of EOS representation for the asymmetric mixtures is attributed to proper accounting for both temperature and molecular size effects (Gasem, 1986; Peters, 1986; Gasem, et al., 1989; Darwish, et al., 1993).

Solubilities of five aromatic compounds in supercritical carbon dioxide were evaluated by Sheng, et al. (1992). The attraction constant of the CEOS is evaluated by equating the excess free energy calculated by the CEOS to that from a UNIFAC group contribution liquid model. A new mixing rule for the excluded volume parameter of the EOS is proposed. The new mixing rule is defined as follows:

$$b_{\text{mixture}} = \sum_i x_i b_i + b^{\text{exe}} \quad (2-19)$$

The composition dependence of the excess term is expressed as follows:

$$b^{\text{exe}} = x_1 x_2 (K_1 + K_2 x_2) \quad (2-20)$$

where K_1 and K_2 are two constants, which are to be fitted as function of the characteristic properties of pure solute. With the new mixing rules, solubilities of aromatic solids in supercritical carbon dioxide were calculated satisfactorily.

In summary, the modification of the CEOS covolume when dealing with asymmetric mixtures offered a physically meaningful (Kwak and Mansoori, 1986) and better representation (Gasem and Robinson, 1985; Peters, 1986; Gasem, et al., 1989; Darwish, et al., 1993) of asymmetric mixtures. Therefore, a modification to the CEOS covolume is required to account for the size and shape of chain-like molecules. Accordingly, a new semi-theoretical equation for the covolume was derived and evaluated in Chapter VII.

The Importance of using Ternary Mixtures in Evaluating EOS Models

Mixing rules that produce good VLE predictions of binary systems may produce unacceptable results for multi-component mixtures (Zavala, et al., 1996). The description of multi-component phase behavior in terms of pair-wise interactions (molecule interaction only with its nearest neighbor) has been validated for mixtures composed of molecules of similar size and structure; however, additional study is needed to extend such validation to molecules of widely differing type, size and structure (Azevedo and Prausnitz, 1988; Gasem and Robinson, 1995). Several evaluations demonstrated that equations of state, which are built on pure component and binary data, are sometimes incapable of accurately predicting ternary and multi-component properties due to unlike-three-body interactions. Therefore, mixing rule evaluation/development must take into consideration the ability to correctly predict the VLE of a mixture of at least three

components (BenMekki and Mansoori, 1988). As stated by Soave (1984), vdW classical mixing rules have been shown to apply well to binary mixtures of polar compounds. Unfortunately, as shown by several authors (e.g., Leland, 1980; Gupta, et al., 1980), such rules although theoretically well supported and completely adequate for binary systems, fail when applied to some multi-component mixtures. Due to the lack of experimental data for multi-component asymmetric mixtures, mixing rule evaluations were not performed for these mixtures.

Non-Random Solution Model

One-fluid theory based on random mixing of molecules is effective when the constituent molecules are similar in size and chemical nature. When molecules differ greatly in size, shape, or intermolecular interactions, the molecular environment of one type of molecule is different from that of the other type leading to the non-random solution model. The non-randomness concept has been introduced for the non-ideality of asymmetric liquid mixtures. Examples are the liquid-state activity coefficient models such as that of Wilson (1964), NRTL (Renon and Prausnitz, 1968), and UNIQUAC (Abrams and Prausnitz, 1975).

Wilson conceived that interaction between molecules depends primarily on “local concentrations”. To take into account non-randomness in liquid mixtures, Wilson suggested a relation between local mole fraction x_{11} of molecules 1 and local mole fraction x_{21} of molecules 2 which are in the immediate neighborhood of molecule 1:

$$\frac{x_{21}}{x_{11}} = \frac{x_2}{x_1} \frac{\exp(-g_{21}/RT)}{\exp(-g_{11}/RT)} \quad (2-21)$$

We expect, therefore, that as the temperature rises, the orientations of molecules become more random.

The NRTL model took into consideration non-randomness by an expression similar to that used by Wilson, except that an additional constant was added to account for the degree of non-randomness of the mixture. In this case, the local composition is defined as follows:

$$\frac{x_{21}}{x_{11}} = \frac{x_2}{x_1} \frac{\exp(-\tau_{12}g_{21}/RT)}{\exp(-\tau_{12}g_{11}/RT)} \quad (2-22)$$

The assumption used in the NRTL model is similar to that of the quasi-chemical theory of Guggenheim; however, it is different from Guggenheim's assumption, where the lattice model is not used, and τ_{12} is considered as an empirical constant, independent of temperature and not always related to the lattice coordination number.

To obtain a semi-theoretical equation for the excess Gibbs energy of a liquid mixture, Guggenheim's quasi-chemical analysis is generalized through the introduction of the local area fraction as the primary concentration variable. The effects of molecular size and shape are introduced through a structural parameter obtained from pure-component data and through use of Staverman-Guggenheim (SG) combinatorial entropy as a boundary condition for athermal mixture equation (Abrams and Prausnitz, 1975). The local composition concept introduced by Wilson was utilized in the resulting universal quasi-chemical (UNIQUAC) model.

The UNIQUAC equation is derived by phenomenological arguments based on two-fluid theory. The two-fluid theory is based on the fundamental idea that a mixture can be considered to be two hypothetical fluids. The two-fluid theory assumes that an

extensive configurational property (i.e., a property dependent on intermolecular forces) is the average of the properties (usually mole-fraction) of two hypothetical pure fluids (Hicks, 1976). The essential step in the derivation is the adoption of Wilson's assumption that local composition can be related to overall composition through Boltzmann factors. The use of an additional universal parameter similar to NRTL model leads to only marginal improvement (Maurer and Prausnitz, 1978).

Computer simulation has made it possible to model local composition and thereby to examine the validity of models. Local composition of binary Lennard-Jones fluid mixtures with either the same (Nakanishi and Toukubo, 1979; Nakanishi and Tanaka, 1983) or different (Gierycz and Nakanishi, 1984; Hoheisel and Kohler, 1984) sizes of molecules has been examined using Monte Carlo (MC) simulation at liquid-like densities (Lee and Chao, 1986). In addition, local composition of square-well molecules of diverse sizes was evaluated (Lee and Chao, 1987; Lee and Sandler, 1989) using MC simulation. Lee and Chao (1987) evaluated the effect of interaction energy, density, and size ratio (size ratio ≤ 2). The study revealed that the larger the size ratio, the greater the departure of local composition from the bulk composition.

Group Contribution Concept

Extension of the group-contribution idea to mixtures is extremely attractive because while the number of pure fluids in chemical technology is already very large, the number of different mixtures is still larger by many orders of magnitude. Numerous multi-component liquid mixtures of interest in the chemical industry can be constituted

from perhaps twenty, fifty, or at most one hundred functional groups (Fredenslund and Prausnitz, 1975).

The concept of treating a mixture in terms of the interacting structural groups received some attention by Derr and co-workers (Redlich, et al., 1959; Derr and Papadopoulos, 1959) in correlating heats of mixing, followed by Wilson and Deal (1962), who developed the solution-of-group method for activity coefficients (Fredenslund and Prausnitz, 1975).

The analytical solution of groups (ASOG) method developed by Derr and Deal (1969) proved to be effective in correlating activity coefficients through structural-group parameters. The method is based on the assumption that (a) molecular-molecular interactions are given by the properly weighted sums of group-group interactions, and (b) the contribution made by one group is assumed to be independent of that made by another group. The chemical potential or simply the logarithm of the activity coefficient of a component in a solution is treated as a sum of two terms: The first term provides contribution due to size effect, and the second is due to molecular interaction. The “interaction” term is treated as the difference between group contributions, which arise in the solution and in the molecular standard states. Those contributions are summed over all “interaction” groups comprising the solute molecule of interest. Thus,

$$\ln \gamma_i^{\text{res}} = \sum_k \nu_{ki} (\ln \Gamma_k - \ln \Gamma_k^i) \quad (2-23)$$

The UNIFAC model is based on combining solution-of-group concept with the UNIQUAC equation. In UNIFAC, the combinatorial part of the UNIQUAC activity

coefficient is used directly. Parameters r_i and q_i are calculated as the sum of the group volume and area parameters, R_k and Q_k .

Group parameters R_k and Q_k are obtained from the van der Waals group volume and surface area, V_{vdw} and A_{vdw} , given by Bondi (1968) relative to those of standard segment coefficients (Fredenslund and Prausnitz, 1975).

The choice of a standard segment is somewhat arbitrary. Abrams and Prausnitz (1975) defined it as a sphere such that, for a linear polymethylene molecule of infinite length, the identity

$$(Z_c/2)(r - q) = r - 1 \quad (2-24)$$

is satisfied. The result is a standard segment volume of $15.17 \text{ cm}^3/\text{mole}$ and a standard segment area of $2.5 \times 10^9 \text{ cm}^2/\text{mole}$.

The group activity coefficient Γ_k is found from an expression similar to one used in UNIQUAC to define the component activity coefficient:

$$\ln \Gamma_k = Q_k \left[1 - \ln \left(\sum_m \Theta_m \Psi_{mk} \right) - \sum_m \left(\frac{\Theta_m \Psi_{km}}{\sum_n \Theta_n \Psi_{nm}} \right) \right] \quad (2-25)$$

where

$$\Psi_{ij} = \exp \left[-\frac{U_{ij} - U_{jj}}{RT} \right] = \exp \left(-\frac{\bar{A}_{ij}}{T} \right) \quad (2-26)$$

The group interaction parameters \bar{A}_{ij} (two parameters per binary mixture of groups) are regressed from experimental data.

The modified UNIFAC (Larsen, et al., 1987) offers two modifications over the original model. First, the combinatorial term responsible for non-idealities due to size

effect was slightly modified. Second, the group-interaction parameters have been made temperature dependent using three parameters, where

$$\psi_{ji} = \exp \left[\bar{A}_{ji} + \bar{B}_{ji}(T - T_0) + \bar{C}_{ji} \left(T \ln \frac{T_0}{T} + T - T_0 \right) \right] \quad (2-27)$$

Similarly, Holderbaum and Gmehling (1991) used three interaction parameters. In comparison, two interaction parameters for the pairs gas/CH₂ and CH₂/gas were used in the LCVm model, where a linear temperature dependency was chosen for the UNIFAC interaction parameters due to the relatively narrow temperature range of the data used (typically 273-423 K) (Boukvalas, et al., 1994).

The ASOG and UNIFAC methods are classical examples of applying group contribution concept to phase equilibrium computations for liquid and gas mixtures. Until the late 1980s, the application of the group contribution concepts to high-pressure phase equilibrium computation was limited to the parameters from the group-contribution equation (PFGC) introduced by Cunningham and Wilson (1974) and the group-contribution equation of state (GC-EOS) developed by Skjold-Jorgensen (1984, 1988).

The PFGC is based on modified Flory-Huggins and Wilson equations. The cubic equation of state was derived from Helmholtz free energy by differentiation with respect to volume at constant temperature and composition. The PFGC equation was further advanced and evaluated by Moshfeghian, et al. (1980) and Majeed and Wagner (1986) to broad range of systems, particularly of interest in natural gas processing. The PFGC equation of state has five adjustable parameters. In addition, there is one binary interaction coefficient for each pair of groups (Majeed and Wagner, 1986).

The GC-EOS is based on the generalized van der Waals partition function and uses local-composition mixing rules similar to NRTL model (Renon and Prausnitz, 1968) for excess Helmholtz function. All thermodynamic properties of interest in phase-equilibrium calculations can be derived from the configurational Helmholtz function by differentiation with respect to composition or density (Skjold-Jorgensen, 1984). The contribution to configurational Helmholtz function from external rotation and vibration degrees of freedom is neglected. The resulting equation of state is thereby applicable only to molecules of limited size (Skjold-Jorgensen, 1984). Six adjustable parameters are required for the GC-EOS equation of state.

A review of group-contribution methods is given by Gmehling (1998).

Combinatorial and Free Volume Contributions to Excess Free Energy

Combinatorial Contribution

The accuracy of the combinatorial contribution to excess free energy, which arises from differences in the size and shape of the molecules, plays an important role in modeling asymmetric mixtures using UNIFAC or UNIQUAC. Mixtures containing exclusively normal, branched and cyclic alkanes, as well as saturated hydrocarbon polymers are known to exhibit almost athermal behavior, i.e., the enthalpy of mixing is approximately zero. These types of mixtures are usually used to evaluate/modify different combinatorial expressions.

The well-known Flory-Huggins expression for athermal polymer systems (Flory, 1941; Flory, 1942; Huggins, 1941; Huggins, 1942) was the basis for the development of many combinatorial activity coefficient models (Voutsas et al., 1995). Staverman (1950)

and Guggenheim (1952) performed further theoretical developments to improve the combinatorial effect.

All these models are based on the lattice model, which assumes the existence of a regular lattice having Z_c nearest neighbor sites surrounding each lattice site, where Z_c is the coordination number of the lattice. Each molecule of species (i) in the mixture is assumed to be formed by r_i equal size segments, each occupying one lattice site. Finally, a parameter q_i is defined such that $Z_c q_i$ is the number of nearest-neighbor sites to molecule i. The relation between $Z_c q_i$ and r_i is given in general by:

$$Z_c q_i = (Z_c - 2) r_i + 2(1 - L_i) \quad (2-28)$$

The term “ $2L_i$ ” takes into account the bulkiness of the molecule; it represents the difference between the number of external contact points of an actual (bulky) molecule i and an open-chain molecule having the same r_i . For open chain, branched or unbranched molecules ($L_i = 0$).

The excess molar combinatorial entropy, S^{exe} , is related by statistical thermodynamics to the number of possible configurations Ω (microstates) of the system having the same energy:

$$\frac{S^{exe}}{R} = \frac{1}{n N_0} \left[\frac{\Omega(N_1, N_2, \dots, N_c)}{\sum_i^c \Omega(N_i, 0, \dots, 0)} \right] + \sum_i x_i \ln x_i \quad (2-29)$$

The difference between the models lies in the way the number of possible configurations is determined. The Flory-Huggins equation takes the form for r-mer/monomer multi-component mixture:

$$\left(-\frac{S^{\text{exc}}}{R}\right) = \sum_i x_i \ln\left(\frac{\phi_i}{x_i}\right) \quad (2-30)$$

where the volume fraction, ϕ_i , is defined as

$$\phi_i = \frac{x_i r_i}{\sum_i x_i r_i} \quad (2-31)$$

In addition, the Staverman-Guggenheim (SG) equation is defined as:

$$\left(-\frac{S^{\text{exc}}}{R}\right) = \sum_i x_i \ln\left(\frac{\phi_i}{x_i}\right) + \frac{1}{2} \sum_i x_i (Z_c q_i) \ln\left(\frac{\theta_i}{\phi_i}\right) \quad (2-32)$$

The second term of the right-hand side of Equation (2-32) represents non-ideality due to the variation in shape, where θ_i is the surface area fraction of compound i:

$$\theta_i = \frac{x_i q_i}{\sum_i x_i q_i} \quad (2-33)$$

It has been demonstrated (Donohue and Prausnitz, 1975; Kikic, et al. 1980) that the SG combinatorial contribution to excess Gibbs energy models exhibits too large a deviation from ideality for alkane mixtures by predicting activity coefficients that are too low.

Therefore, many investigators (Kikic, et al., 1980; Weidlich and Gmehling, 1987; Larsen, et al., 1987; Sheng and Chen, 1989; Voutsas, et al., 1995; Ye and Zhong, 2000) have made slight modifications in the Flory-Huggins part of the SG expression. The main variation among these models is in the exponent, w , of the Flory-Huggins volume fraction.

$$\Psi_i = \frac{x_i r_i^w}{\sum_j x_j r_j^w} \quad (2-34)$$

Sheng and Chen (1989) correlate the exponent, w , to non-sphericity of each component. Voutsas et al. (1995) and Ye and Zhong (2000) relate the volume-fraction exponent to the molecular size ratio. Table 3 presents a list of selected combinatorial expressions.

Free Volume Contribution

Free volume contribution is due to the free-volume difference between polymer and solvent molecules; such difference is usually insignificant for liquid mixtures of small molecules (Prausnitz, et al., 1999). Oishi and Prausnitz (1978) proposed a model similar to UNIFAC, but with an additional term to account for free-volume effect. The activity coefficient of the solvent is the product of three contributions:

$$\gamma_i = \gamma_i^{\text{comb}} \gamma_i^{\text{res}} \gamma_i^{\text{FV}} \quad (2-35)$$

A combined combinatorial-free volume activity coefficient models have been proposed (e.g., Elbro, et al., 1990; Kontogeorgis, et al., 1994). The combined combinatorial-free volume activity coefficient for the Elbro-FV model (Elbro, et al., 1990) is defined as:

$$\ln \gamma_i^{\text{Comb-FV}} = \ln \frac{\phi_i^{\text{FV}}}{x_i} + 1 - \frac{\phi_i^{\text{FV}}}{x_i} \quad (2-36)$$

Equation (2-36) is similar to the Flory-Huggins Equation (2-30), but the free-volume fraction is now used instead of volume or segment fraction:

$$\phi_i^{\text{FV}} = \frac{x_i V_{fi}}{\sum_j x_j V_{fj}} \quad (2-37)$$

where V_{fi} is the free-volume of component i , and is defined by equation

Table 3. Selected Combinatorial Expressions

$$\frac{G_{\text{comb}}^{\text{exe}}}{RT} = \sum_i x_i \ln \frac{\phi_i}{x_i} - \frac{Z_c}{2} \sum_i q_i x_i \ln \frac{\phi_i}{\theta_i}$$

$$\theta_i = \frac{q_i x_i}{\sum_j q_j x_j} \quad \phi_i = \frac{r_i x_i}{\sum_j r_j x_j}$$

Fredenslund et al., 1975

$$\frac{G_{\text{comb}}^{\text{exe}}}{RT} = \sum_i x_i \ln \frac{\phi_i}{x_i} \quad \Psi_i = \frac{x_i r_i^{w_i}}{\sum_j r_j x_j^{w_j}}$$

$$w_i = f\left(r, \frac{q}{r}\right)$$

Donohue and Prausnitz, 1975

$$\frac{G_{\text{comb}}^{\text{exe}}}{RT} = \sum_i x_i \ln \frac{\Psi_i}{x_i} - \frac{Z_c}{2} \sum_i q_i x_i \ln \frac{\phi_i}{\theta_i}$$

$$\theta_i = \frac{q_i x_i}{\sum_j q_j x_j} \quad \Psi_i = \frac{x_i r_i^{2/3}}{\sum_j x_j r_j^{2/3}}$$

Kikic, et al., 1980

$$\phi_i = \frac{x_i r_i}{\sum_j x_j r_j}$$

$$\frac{G_{\text{comb}}^{\text{exe}}}{RT} = \sum_i x_i \ln \frac{\Psi_i}{x_i}$$

$$\Psi_i = \frac{x_i r_i^{2/3}}{\sum_j x_j r_j^{2/3}}$$

Larsen, et al., 1987

Table 3. Selected Combinatorial Expressions-*continued*

$$\frac{G_{\text{comb}}^{\text{exe}}}{RT} = \sum_i x_i \ln \frac{\Psi_i}{x_i} - \frac{Z_c}{2} \sum_i q_i x_i \ln \frac{\phi_i}{\theta_i}$$

$$\theta_i = \frac{q_i x_i}{\sum_j q_j x_j} \quad \Psi_i = \frac{x_i r_i^{w_i}}{\sum_j x_j r_j^{w_i}}$$

Sheng, et al., 1989

$$w_i = 1 - \frac{1}{[0.8(\xi_i - 1)^{1.5} + 1]} \quad \xi_i = r_i^{1/3} \left(\frac{q_i}{r_i} \right)$$

$$\frac{G_{\text{comb}}^{\text{exe}}}{RT} = \sum_i x_i \ln \frac{\Psi_i}{x_i} - \frac{Z_c}{2} \sum_i q_i x_i \ln \frac{\phi_i}{\theta_i}$$

$$\theta_i = \frac{q_i x_i}{\sum_j q_j x_j} \quad \Psi_i = \frac{x_i r_i^R}{\sum_j x_j r_j^R}$$

Voutsas, et al., 1995

$$\phi_i = \frac{x_i r_i}{\sum_j x_j r_j} \quad R = 0.9 \left(1 - \frac{r_{\text{small}}}{r_{\text{large}}} \right)$$

$$\frac{G_{\text{comb}}^{\text{exe}}}{RT} = \sum_i x_i \ln \frac{\Psi_i}{x_i} - \frac{Z_c}{2} \sum_i q_i x_i \ln \frac{\phi_i}{\theta_i}$$

$$\theta_i = \frac{q_i x_i}{\sum_j q_j x_j} \quad \Psi_i = \frac{x_i r_i}{\sum_j x_j r_j}$$

Ye and Zhong, 2000

$$\phi_i = \frac{x_i r_i}{\sum_j x_j r_j} \quad n = \frac{r_{\text{large}}}{r_{\text{small}}}$$

$$r_i' = \left(0.6583 + \frac{0.3417}{n} \right) r_i \quad \text{For Large Molecules}$$

$$r_i' = r_i \quad \text{For Small Molecules}$$

$$V_f = V - V_{vdw} \quad (2-38)$$

where V is the actual volume, and V_{vdw} is the van der Waals volume.

Several activity coefficient models containing both combinatorial and free-volume contributions were tested and compared to the classical model (Kontogeorgis, et al., 1994). Based on this evaluation, the modified UNIFAC (Larsen, et al., 1987) was the best model in representing infinite-dilution activity coefficients of short-chain alkane solutes in various long-chain solvents, but it cannot be extended to mixtures containing polymers (Kontogeorgis, et al., 1994).

An extensive comparison of combinatorial expressions (i.e., developed by Kontogeorgis, et al., 1994; Elbro, et al., 1991; Larsen, et al., 1987) containing both combinatorial and free-volume contributions was conducted by Voutsas, et al. (1995). The model by Voutsas, et al. (1995) performs satisfactorily in all cases examined, with the added advantage that it avoids the use of pure-component liquid molar volumes. This represents a significant advantage when experimental data are not available, especially for systems containing supercritical compounds (Voutsas, et al., 1995).

A liquid-volume-free model (UNIFAC-r) developed by Ye and Zhong (2000) was compared to combinatorial expression (UNIFAC-R) developed by Voutsas, et al. (1995). Both models were tested against systems that included polymer/solvent, small/large molecules, as well as normal/normal fluid systems. For systems containing small and large molecules, the UNIFAC-r model shows comparable accuracy to the UNIFAC-R model, and both models do not need liquid molar volumes.

In addition to previous studies (e.g., Voutsas, et al., 1995), a recently published article by Abildskov, et al. (2001) stressed the importance of combinatorial terms for

some mixtures and how they can be essential to the success of correlations based on UNIFAC or UNIQUAC. Therefore, several expressions based on the quasi-crystalline lattice model (Kikic, et al., 1980; Larsen, et al., 1987; Sheng and Chen, 1989; Voutsas, et al., 1995; Ye and Zhong, 2000) were evaluated in this work against infinite-dilution activity coefficient and VLE data of short-chain alkane solutes in various long-chain solvents. The objective was to extend the evaluation to ethane/n-paraffin VLE data, which cover a broad range of size ratios in comparison to previous studies.

CHAPTER III

EXPERIMENTAL METHODS AND APPARATUS

The purpose of this chapter is to describe (a) experimental methods typically used for high-pressure vapor liquid equilibria, (b) a new experimental technique and (c) the apparatus designed and used in this work.

Numerous chemical processes operate at high pressure and, primarily for economic reasons, many separation operations (distillation, absorption) are conducted at high pressure. The design of processes (e.g., enhanced oil recovery, coal liquefaction, supercritical extraction) typically operated at high pressure requires quantitative information about the thermodynamic properties of fluids and their mixtures. Predicting the properties of mixtures in many industrial chemical processes using a theoretically based or semi-empirical EOS, especially without an adjustable binary interaction parameter, is not reliable when the system exhibits large non-idealities. Non-idealities can result from differences in molecular size, shape, and polarity. In coal processing, mixtures of light gases dissolved in high molecular weight solvents are typically encountered (e.g., CO, CO₂, C₂H₆, and H₂ in n-paraffin, naphthene and aromatic solvents). The presence of a large database of phase equilibria experimental data for binary asymmetric mixtures has led to successful modeling efforts involving binary asymmetric mixtures. In comparison, experimental data for asymmetric ternary and higher mixtures are rare; consequently, modeling efforts dealing with such systems are

limited. To fulfill our needs of ternary mixtures experimental data, a new high-pressure experimental apparatus was designed and constructed in this work.

Review of Experimental Methods

The experimental techniques used to investigate multi-phase equilibria can be classified by the method employed to determine the composition: analytical or synthetic. Methods are further subdivided by the technique used to achieve equilibrium conditions: static, continuous flow and recirculation method (e.g., Deiters and Schneider, 1986; Fornari, et al., 1990; Dohrn and Brunner, 1995). Figure 1 gives the classification of experimental methods in high-pressure fluid phase equilibria.

The analytical method involves the determination of the composition of the coexisting phases. To minimize the effect of pressure changes on phase compositions, small samples (taken in a micro cell) are usually taken from the recirculating gas and/or liquid stream using a fast-acting sample valve. The samples are analyzed externally at normal pressure. In addition, physicochemical methods (e.g., spectroscopic method) of analysis have been used to determine equilibrium compositions at system operating temperature and pressure.

In the analytical approach, several methods are used to attain equilibrium. The static method uses either a mechanical stirrer (e.g., Laursen, et al., 2002) or the equilibrium cell is rocked. In the recirculation method (e.g., Hsu, et al., 1985; Gamse, et al., 2001; Cebola, et al., 2000), one or more phases are recirculated to ensure complete mixing and allow the sample volume to be filled isobarically. In the recirculation

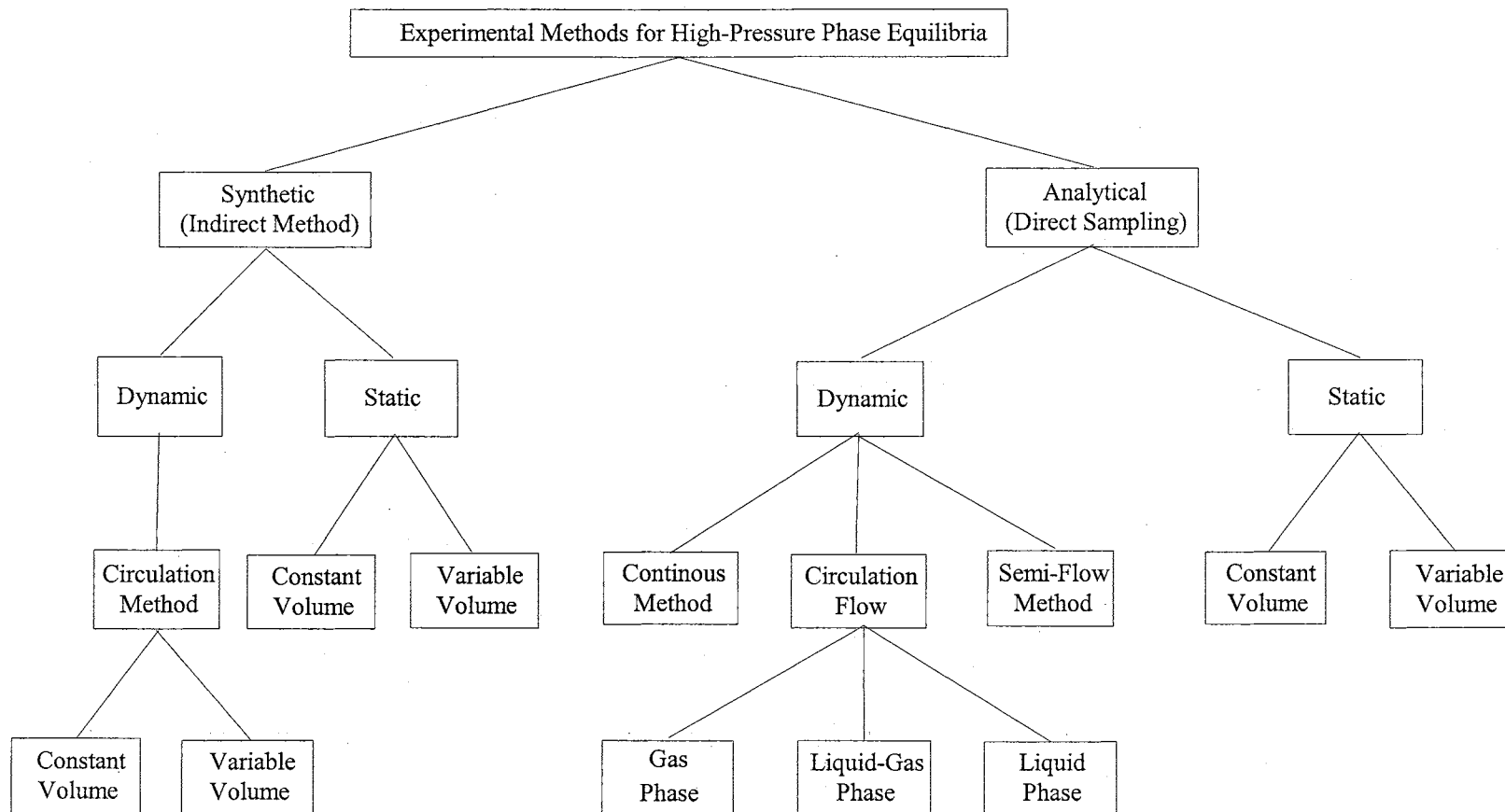


Figure 1. Experimental Methods for High Pressure Phase Equilibria.

method, thorough mixing in a short period is required to ensure a rapid approach to equilibrium. The continuous flow method is usually used with temperature sensitive substances and with systems that do not require a long residence time to reach equilibrium. Lee and Chao (1988) used a semi-flow method to determine the solubility of supercritical gases in high molecular weight hydrocarbons. A major uncertainty is the possible lack of attainment of equilibrium using the semi-flow method (Dohn and Brunner, 1995).

In the synthetic method, a mixture of known composition is placed inside the equilibrium cell. This method has the benefits of reducing costly equipment required for sample analysis and any possible system disturbance during sampling. The main limitation of this method occurs when phase compositions are required for multi-phase, multi-component mixtures.

The transition or appearance of a new phase is usually detected by (a) a visual cell, (b) microwave techniques (e.g., Fogh, et al., 1991), where the new phase creates a characteristic change in the dielectric properties of the sample, (c) abrupt change in slope on the pressure-volume plots and, (d) a vibrating tube densimeter (e.g., Makamura, et al., 1997), where a phase change is indicated by the change in vibrating period of a one-dimensional resonator.

Several of these methods have been used in the thermodynamics research laboratories at Oklahoma State University to generate highly reliable experimental data at high pressures. The type of apparatus used has depended mainly on the experimental objective and the systems to be examined. Mundis, et al. (1977) used an analytical, variable-volume experimental apparatus for determining multi-phase equilibrium

compositions at high pressures. Hsu, et al. (1985) established an analytical-gas phase recirculation apparatus for measurements of equilibrium phase compositions, densities, and interfacial tensions of mixtures. An analytical-continuous flow apparatus was developed by Chen and Wagner (1994) to determine the mutual solubility of water and hydrocarbons. Most of the publications on the solubility of supercritical fluids in high molecular weight hydrocarbon were determined using a static-type variable-volume apparatus designed and developed by Gasem (1986). Traditionally, in this static, variable-volume approach, mercury is used as an incompressible, nonvolatile fluid piston. One of the experimental objectives of this work is to design and construct a high-pressure apparatus of comparable reliability to the static-type apparatus of Gasem (1986), but without the potential health hazards involved with the use of mercury.

A New Experimental Technique

A new experimental technique was proposed by Gasem (1986). The concept for this new approach is shown in Figure 2. The bubble point pressure (for the mixture of known composition) is identified graphically from the discontinuity in a pressure vs. total-volume (or composition)-of-solvent-injected plot as the mixture passes from the more compressible two-phase state to the less compressible single-liquid-phase state. The technique is based on the observation that (barring retrograde behavior) a temperature reduction from the saturated or slightly compressed liquid region results in a reduction in the liquid molar volume and, consequently, two-phase formation in a constant volume equilibrium cell. This allows the determination of another bubble point at a lower temperature by the introduction of additional solvent. The dew point can be

determined in a similar way to the bubble point; i.e., where a change in the slope of the pressure-volume plot (or pressure-composition plot) is observed. Given the equilibrium cell volume and the amount of substances injected, the volumetric properties at these two points can be determined. The experimental technique as demonstrated in Figure 2 shows two-phase equilibrium envelopes at two temperatures, T_1 and T_2 . Figure 2 shows

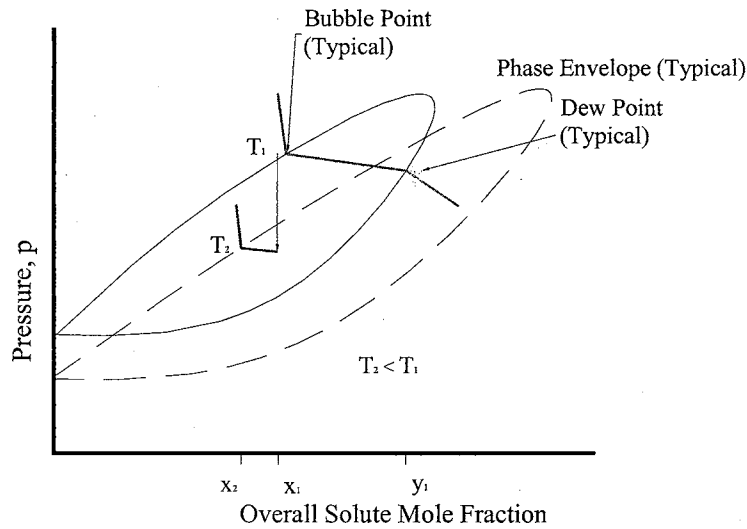


Figure 2. Concept of the New Experimental Technique.

conceptually the dew point and the bubble point pressures determined at high temperature, T_1 , and compositions y_1 and x_1 , respectively. A reduction in temperature to T_2 at constant volume produces a system in the two-phase region with an overall composition equals to x_1 . Upon injection of additional solvent, a new bubble point is reached with a composition of x_2 at temperature T_2 . This technique is repeated to the lowest desired experimental temperature.

New Experimental Apparatus

The new apparatus has enhanced features designed to accommodate a wide range of operating conditions. Schematic representation of the apparatus is shown in Figure 3.

Its features include the following:

- A mercury-free environment (no compressing media required).
- The ability to handle multi-component mixtures.
- The ability to handle solvents that are solid at room temperature.
- The capability to determine phase equilibrium and volumetric properties such as the bubble point (Bp), the dew point (Dp), and the molar volume of liquid and gas phase at Bp and Dp, respectively.
- A wide operating range with a pressure up to 35 MPa at 600 K.
- A blind equilibrium cell that is interchangeable with a visual cell, allowing the observation of multi-phase formation.
- A data acquisition system to record automatically temperatures and pressures.

These features facilitate an efficient and accurate way for experimentation with multi-component mixtures.

Figure 3 is a schematic representation of the new apparatus. The new apparatus employs two temperature-controlled ovens. The first oven (Oven-1) includes a blind equilibrium cell and a rocking mechanism for the equilibrium cell. The second oven (Oven-2) includes a solvent storage vessel and three high precision injection pumps. The two air-bath ovens and the interface connection between them are maintained at

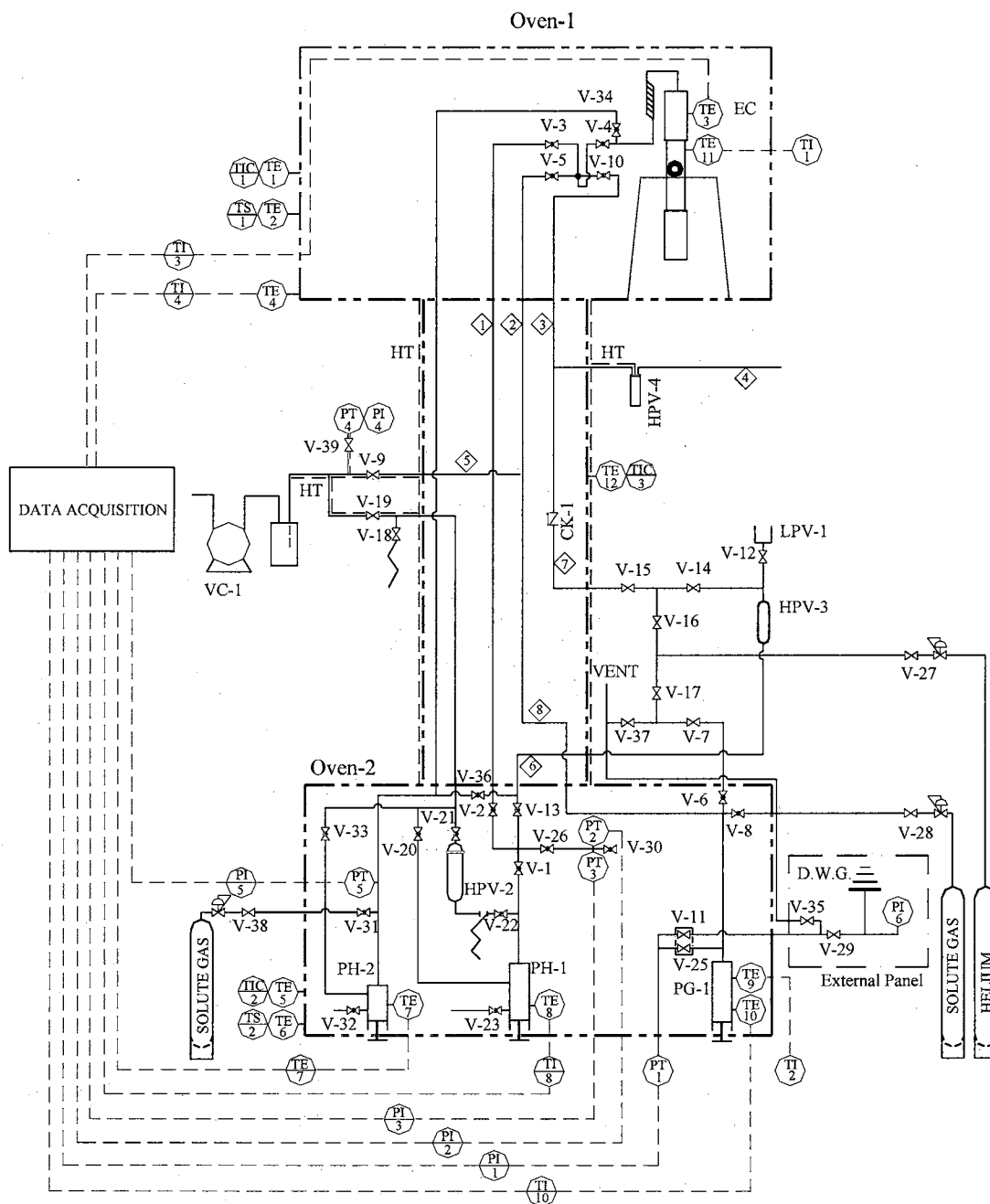


Figure 3. Schematic Diagram of the New High-Pressure Experimental Apparatus: Solvent Injection Pumps (PH-1 & 2), Solute Injection Pump (PG-1), Vacuum Pump (VC-1), Equilibrium Cell (EC), Solvent Storage Vessel (HPV-2), Cleaning Solution Vessel (HPV-3), Waste Vessel (HPV-4), Temperature Element (TE), Temperature Controller (TIC), Temperature Switch (TS), Pressure Transducer (PT), Pressure Indicator (PI), Heat Trace (HT).

controlled temperatures (± 0.05 K) using three Proportional-Integral-Derivative (PID) controllers.

Injection Pumps

The three positive displacement injection pumps manufactured by Tempco, Inc. were used in this experiment. All three pumps are housed in Oven-2. Two pumps [PH-2 (Model 10-1-12-H), PG-1 (Model 25-1-10-hat)] each with a total displacement of 10 and 25 cm³, respectively, are used for solute injections, and a 25 cm³ [PH-1 (Model HP-25-10)] pump is used for solvent injection. All wetted parts of the pumps are 316 stainless steel and are rated for 10,000 psia maximum operating pressure. The pumps provide a scale and dial for readings within 0.01 cm³. Each pump has its own pressure transducer and temperature sensing elements.

Equilibrium Cell

A static-type, constant-volume, blind-equilibrium cell was used in this apparatus. The cell is constructed from 316 stainless steel with a maximum allowable operating pressure of 15,000 psia. Operations at temperatures up to 800 °F are made possible by the metal-to-metal seal construction. The cell (supplied by High Pressure Equipment, Inc., Model MS-16) is 9/16 inch inside diameter (ID), 6 inches overall length, and has a total capacity of 24 cm³.

Efficient vapor-liquid mixing is required in the equilibrium cell in order to reduce the time required for the mixture to reach equilibrium. To accomplish this, the cell is mounted on a rotating central shaft that controls the speed and the angle of the rotation of

the equilibrium cell. This rocking action is controlled by a microprocessor board (Minarik Corp., RG101UC) that controls the action of a 1/8 Hp, 90 VDC (direct current volt), adjustable speed motor. The motor is connected to the shaft indirectly through a gearbox. Two stainless steel balls, 3/8 inch in diameter, are placed inside the cell to enhance the gas/liquid mixing action as it rotates 180 degrees from top to bottom. Two temperature-sensing elements are used to sense equilibrium cell metal temperature. The equilibrium cell has two connections: one is plugged, and the other allows the injection of substances and the discharge of waste. To allow the equilibrium cell rocking action, a coil of 12 inch long (1/16" inch diameter) tubing is used to connect the EC with the metering valves (V-34, V-4).

Ovens and Interface Connections

1. Equilibrium Cell Oven

The equilibrium cell oven (Oven-1) is manufactured by Gallenkamp, Inc. (model 300 plus series). A microprocessor-based mechanism for equilibrium cell rocking is part of Oven-1. The oven is temperature controlled up to 600 °F within ± 0.1 °F. High temperature limit switches are used to disconnect heating elements if the temperature exceeds the preset limit.

2. Pump Oven

In the second oven (Oven-2), control and valve panels are constructed from 14-gauge carbon steel then sandblasted and painted with protective coating. The oven dimensions are 48 inches width, 36 inches length, and 13 inches height. It is insulated with 1-inch thick fiberglass on five sides. In addition to the three pumps, a high air-

circulation blower, a solvent storage vessel, and a heating element are located inside the oven. To allow visual observation of the oven contents, including pumps scale and dial, a clear ½ inch thick cover made from polycarbonate is used. The heating element is located in front of the forced-air draft of the blower, and for safety reasons, is interlocked with the blower operation. The oven is temperature controlled up to 220 °F within ± 0.1 °F. A high temperature safety switch is used to disconnect heating elements if the temperature exceeds the specified limit. The oven is temperature controlled for two reasons: (a) first, the oven temperature needs to be above the melting point temperature of the solvent to be injected, (b) second, the volume of solute and solvent injected needs to be determined at constant temperature and pressure. The upper limit for the oven temperature is set by the operating temperature limitations of polycarbonate cover material and pressure transducers (which is 250 °F for each of them).

3. Interface Connection between Ovens

All connections between the two ovens are passed through a heat-traced, temperature-controlled ½ inch pipe. In addition, all tubes emerging from this interface to the vacuum pump are heat traced as indicated in Figure 3. These measures were taken to be able to transfer solvents that are solid at room temperature between the two ovens and to prevent any possible tube plugging while venting or evacuating the solvent or equilibrium cell sections.

Cleaning System

The cleaning solution in the storage vessel (HPV-3, 250 cm³ capacity) is displaced into the solvent injection pump, equilibrium cell and associated piping using pressurized

helium gas. A drain port machined in the bottom of the horizontally positioned solvent pump (PH-1) ensures complete drainage of the pump contents. After the solvent is drained, the solvent injection pump and associated components are pressurized several times with the cleaning solution and then flushed. The liquid or melted solid waste is disposed in the discharge waste vessel (HPV-4).

Vacuum System

Vacuum is achieved by a rotary vane oil-sealed, two-stage, high-vacuum pump (Sargent-Welch, model 1400). The pump has a free air displacement of 0.90 cubic feet per minute. The vacuum level achieved is indicated by the vacuum meter (PI-4) (GCA/Precision Scientific, Model, 10477), which receives its input signal from the vacuum gauge tube (PT-4) (Sargent-Welch, Model S-39705-58) installed in the vacuum line. Vacuum levels down to 150 millitorr were achieved using this system.

Fitting, Tubing, and Valves

1. Valves

The majority of valves (total of 22) are 316 stainless steel rated for a maximum allowable pressure of 30,000 psia (Autoclave Engineering Inc., 30VM-4071). The remaining valves (total of 9) are supplied by Whitey Inc. and are rated for 5000 psia maximum allowable pressure.

2. Tubing and Fitting

A 316 stainless steel, seamless tubing with 1/8 inch OD and 0.06 inches ID is used in most of the connections. In addition, tubing with 1/16 inch OD and 0.03 inch ID

is used in other lines. All tubing is rated for 15,000 psia working pressure. The 316 stainless steel fittings were supplied by Autoclave Engineering, Inc. and Crawford fitting Co. (Swaglock®).

Pressure Measurements

Several pressure transducers are used to sense the pressures in the pumps. Each of the two solute pumps (PG-1, PH-2) has its independent transducer with a range from 0-2000 psia (Sensotec Inc, Model STJE/1890). The solvent pump has two transducers: the first covers the pressure range from 0-2000 psia and the second, a maximum pressure of 3000 psia. The equilibrium cell pressure is determined indirectly through the capillary tube connecting the equilibrium cell to the solvent injection components. A correction for liquid head is used to determine the true equilibrium pressure in the cell. The output electrical signals from the pressure transducers are directed to four pressure indicators (Sensotec Inc., Model 450 D).

Data Acquisition

The main components of data acquisition system consist of an analog-to-digital conversion electronic board (Omega Inc, Daqboard-100), resistance temperature detectors (RTD), signal conditioner board (Omega Inc., OMB-DBK9), and interface software (Labtech Control). This configuration can handle a total of 16 single-ended or 8 differential inputs directly in addition to 8 RTD temperature signals.

A total of four 0-5 VDC output signals from the pressure indicators and five RTD temperature signals are directed to the data acquisition system for continuous pressure and temperature monitoring and recording.

Temperature Measurements

A total of seven of RTD temperature elements were used in the apparatus, of which five are directly forwarded to data acquisition system, and two are directed to digital temperature indicators (Fluke, Model 2180A). Two RTD elements (TE-3, TE-11) are allocated to the equilibrium cell and another two elements (TE-9, TE-10) are assigned to the solute injection pump (PG-1). The RTD elements TE-8 and TE-7 are directly connected to each pump PH-1 and PH-2, respectively. The last element, TE-4, is used to monitor Oven-2 temperature. All temperature elements are placed and secured firmly in ½ inch deep temperature wells associated with each of the pumps and equilibrium cell. Other RTD temperature elements are used to control the operation of the two ovens. Three temperature controllers are used, one for each oven and the third for the interface connection between them. The temperature controller, (TIC-1) is manufactured by LFE Instrument Division (Model PuP 2004), and the other two controllers, TIC-2 and TIC-3, are supplied by Omega Inc. (model CN9000A).

CHAPTER IV

EXPERIMENTAL PROCEDURE

This chapter includes a description of the experimental procedure used in determining VLE equilibrium properties (bubble point pressures, dew point pressures, and molar volumes). Starting with a clean and dry apparatus, the following sequences were followed in performing the experiment: (a) Pressure testing, (b) Pressure and temperature calibration, (c) Solvent and solute preparation, (d) Planning for the experiment, (e) Solute and solvent injection, (f) Determination of thermodynamic properties, and (g) Apparatus clean up and drying. The careful execution of each step in this procedure is critical to the accuracy and the precision of experimental data obtained. The objective of this chapter is to describe in detail the purpose and actions taken in the execution of each stage in this experiment.

Pressure Testing

The solubility (or bubble point) apparatus must be leak-free to generate accurate measurements. Another issue that needs to be considered is the internal valve leak problem, which arises due to deterioration of valve packing caused by frequent use, particularly for the metering valve (V-4) to the EC. Pressure testing is initially performed at room temperature, where the system is pressurized with helium gas in 500 psi pressure increments up to 3000 psia. Verifying that the pressure is not declining is necessary

before stepping to higher pressure; otherwise, all connections, fittings, valves and pumps seals need to be leak tested using a highly-sensitive helium leak detector (Gow Mac Instrument Co., Model 21-150). The system can be partitioned to several sections (solvent, solute, and EC sections) to speed up the process of locating the leaks. Next, pressure testing is conducted at the system operating temperature and pressure in the range between 2000-3000 psia, depending upon the system to be examined. For the apparatus to pass the pressure-testing stage, the pressure must be constant, with a maximum tolerance of 0.5 psia, for 24 hours. The inlet valve (V-4) to equilibrium cell must be capable of holding a high differential pressure. To verify that, the EC is evacuated and isolated, then the opposite direction of V-4 toward the pump side is pressurized to 2000 psia. The pump side is always maintained at a higher pressure than at the EC; therefore, the direction toward EC is the direction of interest for internal valve leak testing. The EC needs to hold vacuum for at least four hours to verify the viability of the valve. To verify absence of any leaks and the dryness of the system, the system needs to hold 200-millitorr vacuum (with a tolerance of 100 millitorr) for eight hours under the highest operating temperature for the mixtures to be examined.

Pressure Calibration

Calibrating the pressure transducers is done on a regular basis, typically before and after experimentation with any system (i.e., one mixture at several compositions and isotherms). All four transducers are calibrated simultaneously against a dead-weight gauge (DWG) (Ruska Instrument Co., Model 2470-701-00). The factory calibration was made by comparing the above DWG with Ruska Instrument Corporation laboratory gauge

piston No. C-1C. The piston is referenced to the National Bureau of Standards (currently, the National Institute of Science and Technology) Test Number TN215451. Due to the high melting point (above room temperature) of the solvents used in the experiment, three of the transducers are located in Oven-2. The pressure calibration is performed at the operating temperature of Oven-2, typically 15 °F above the melting point of the solvent. As a starting point, all valves are closed except the following valves: V-1, V-2, V-3, V-4, V-5, V-6, V-17, V-25, V-26, V-27, V-34, and V-38. For each step, through out this Chapter, the objective is stated first then the procedure is explained. The steps of the pressure calibration procedure are as follows:

1. Make the interface connection between the external panel (i.e., dead-weight gauge and associated valves) and the apparatus. Connect the vent line to V-35 and V-29 to V-11.
2. Record ambient pressure, temperature, and DWG piston temperature. Prepare a cross-reference between DWG weights and expected pressures in 100 psi increments up to 2200 psia (highest possible pressure for DWG available).
3. Calibrate the data acquisition system simultaneously with digital pressure instruments. Set the pressure indicator range (for first time use or when needed) by adjusting the pressure indicator zero and span (i.e., the output signal needs to be 5 VDC at the highest required pressure for that particular indicator and 0 VDC at full vacuum). The output signal from the pressure indicators (0-5 VDC) monitored at the computer screen is recorded against dead-weight gauge loading.

4. Fill the system with helium to 150 psia. Adjust the pressure regulator of the helium cylinder to the lowest setting, then open V-7 gradually and adjust the pressure regulator to reach 150 psia. This corresponds to the lowest possible calibration pressure using the dead-weight gauge. Verify that valve arrangements are correct (i.e., all four pressure indicators should indicate the pressure rise).
5. Open the system to the dead-weight pressure tester. With the dead-weight tester loaded with a weight equivalent to 150 psia, open V-11 and wait until the temperature stabilizes in Oven-2 as represented by the temperature elements, TE-7, TE-8, TE-9, and TE-10. Open V-29 and note the pressure in the pressure indicator (PI-6).
6. Balance the pressure against the dead-weight gauge reference point. Close V-29, and adjust either the helium cylinder pressure regulator to increase the pressure, or close V-7 and gradually open V-35 to reduce the pressure. The final adjustment is made with a manually operated pump (PG-1) with both V-7 and V-35 closed. The system pressure is balanced when the index line of the sleeve weight is within 1 mm of the line on the index post. (Refer to dead-weight gauge operating manual for detailed instructions.) Record the pressure indicator readings and data acquisition input signals when the system pressure is balanced.
7. Calibrate pressure transducers at higher pressures. With V-29 closed, add the next sleeve weight in position on the piston. Raise the pressure gradually (360 psi per minute maximum) to the next required pressure using the helium

cylinder pressure regulator and then open V-7. Follow the same procedure given in Step 6 to balance the pressure against the dead-weight gauge.

8. Repeat Step 7 until system pressure reaches the highest targeted pressure.
9. At the end of calibration, record the ambient temperature, pressure, and piston temperature. Disconnect the external panel shown in Figure 3, and plug the interface connections with the external panel in the apparatus side (two terminal points). Close V-11, V-7, and V-17.

Accurate pressure indicator readings are determined by applying two corrections. First, the pressure readings are correlated against the dead-weight pressure (true pressure). Second, a liquid head due to the elevation difference between the equilibrium cell and the pressure transducers (PT-2 and PT-3) is accounted for. The pressure measurement using the dead-weight gauge “air-piston gauge” has an accuracy range of 0.015 percent. The random error in the pressure measurement is considered in the error analysis section.

Temperature Calibration

Calibrations for temperature elements (RTD) are done on a regular basis, typically, before the start of system run. All seven-temperature elements are calibrated simultaneously against a standard platinum resistance thermometer (Minco Inc., Model XS7929). The standard thermometer resistance was factory measured at fixed temperature points by comparison with a calibrated platinum resistance thermometer traceable to the National Institute of Standards and Technology. Calibration Table, RT07-C, by Minco Inc., listed the resistances for temperatures from -189 to 500 °C in 0.1 °C increments for the model above.

The temperature calibration is typically performed in Oven-1. All seven RTDs and the standard platinum resistance thermometer are placed in the central core of an aluminum metal block. After temperature stabilizes for all the RTDs, the standard platinum thermometer resistance and the readings of all temperature elements are recorded. The above procedure was applied to other fixed temperature points that cover the full operating temperature range for the planned experiment.

Volume Calibration

The volume of solute or solvent injected using either of three positive displacement pumps (PH-1, PH-2, and PG-1) is determined based on the dimension of the piston and the scale associated with piston displacement. For 10 cm³ capacity pump (PH-2), the piston is 0.4407 inch in diameter and 4.0 inches in length (pump scale is 4.0 inches). For 25 cm³ capacity pumps (PH-1 and PG-2), the piston is 0.6233 inch in diameter and 5.0 inches in length (pump scale is 5.0 inches). The thermal expansion of 316 stainless steel piston material from the standard dimensions reported at 25 °C was considered in determining the true volume injected. The main contribution is due to the expansion of the piston diameter. For 25 cm³ volume displaced using PH-1 pump, the variation due to thermal expansion is about 0.19% in volume for 56 °C temperature rise.

Solvent Preparation

The presence of any non-condensable (e.g., air), either in the system or in a dissolved form in the solvent, can have a negative effect on the accuracy of experimental data. The objective in this section is to present the procedure used in degassing the

solvent, either in a liquid or solid form, and the way it is supplied to the solvent pump (PH-1).

Degassing of Liquid Solvent

Degassing of the solvent and the subsequent filling of the solvent pump is done externally. A total of 50 cm³ of liquid solvent is placed in a flask with a side connection to a vacuum hose and a stopper. With the solvent under constant stirring (using magnetic stirring plate), the contents of the flask are placed under continuous vacuum. This process is continued until no bubbling is observed in the liquid phase, then the stirring is stopped, the vacuum hose is disconnected, and the stopper is removed. At this stage, the content of the flask is ready for the immediate filling of the solvent pump, with the exception of the upper solvent layer exposed to atmosphere.

The differential pressure between atmospheric pressure and the vacuum condition in the pump provides the driving force for filling the solvent pump. The vapor pressure of the solvent reduces the differential pressure by an amount equivalent to its vapor pressure. To minimize solvent vapor pressure, this procedure is performed at ambient temperature.

The following steps are performed to prepare the system, degas the solvent and fill the solvent pump.

1. Release any pressure in the system through the vent line. Open V-7 and V-37.

At this stage, all pressure indicators should read atmospheric pressure. Note, only these valves are initially open: V-1, V-2, V-3, V-4, V-5, V-6, V-25, V-26 and V-34.

2. Evacuate the system. Close V-37 and open V-9, V-19, V-21 and V-22 (interface tubing between HPV-2 and V-22 is connected). Then turn on the vacuum pump until system vacuum reaches 150 millitorr, close V-9 and V-19.
3. Flush the system with solute gas. Open V-28 and adjust pressure regulator to 500 psi. Open V-8 gradually until the pressure reaches 500 psia. Stop solute supply by closing V-8.
4. Flush the system several times with the solute gas. Repeat Steps 1 to 3 five times, then proceed to Step 5.
5. Release any pressure in the system through the vent line. Open V-37; at this stage, all pressure indicators should read atmospheric pressure.
6. Evacuate the system. Close both V-37 and open V-9 and V-19, and then turn vacuum pump on. Once the system reaches 150 millitorr, close V-9 and V-19.
7. Verify the system is tight and leak free. If the system holds vacuum for four hours, then go to Step 8; otherwise, first check that the valves are tightly closed before proceeding to pressure testing. (Note: never tighten valves more than “finger tight” to avoid damage to the valves.)
8. Set valves to admit solvent. Close V-2, V-3, V-4, V-5, and V-34. Turn vacuum pump on, and then place the end of 1/8 inch plastic tubing connected to V-18 in the bottom of the solvent flask. Open V-19, then gradually open V-18 to allow the vacuum pump to withdraw the air in the plastic tubing, then close V-18.
9. Admit solvent to the pump. Close V-19 after system vacuum reaches 200 millitorr, then close vacuum pump. Turn manual pump handle all the way

counter-clockwise to allow the fill of the pump to its full capacity of 25 cm³. By opening V-18, the solvent is admitted to the solvent pump through the HPV-2 vessel. Close V-18 either when the pump is filled or before the liquid height in the flask gets below ½ inch.

10. Admit additional solvent if required (the solvent is degassed and the air trapped in plastic tubing is removed in the same way as mentioned above and then admitted to solvent pump).
11. Remove non-condensable gases directly from the pump (this is an extra measure). The pump horizontal cylinder has an upper vent connection connected to the vacuum pump. To avoid withdrawing liquid from the pump, allow free space above the liquid level in the pump. Turn pump handle counter-clockwise all the way, then turn the vacuum pump on. Open V-19 and V-20 for a few minutes and then close. Turn off the vacuum pump.

Degassing of Solid Solvent (Solid at Room Temperature)

Degassing of solid solvent is performed externally similar to liquid solvent degassing, with the exception that the solid solvent is melted before degassing. The subsequent solvent pump filling is done internally. An equivalent to 50 cm³ of solid solvent is placed in a flask. The flask is connected to an operating vacuum pump, and the flask is placed in a heated water bath oven until the solvent is melted and heated to a high temperature. The use of heated water bath to melt the solid was limited to the first few experiments. In most of the cases, the flask is placed in a high temperature oven until the solid solvent is melted and heated to a suitable temperature. The solvent is then degassed

in similar fashion to liquid-solvent degassing. During the process, both ovens are temperature controlled at the planned experimental operating temperature. The following steps are performed to prepare the system, degas the solvent and fill the solvent pump:

1. Follow Steps 1 through 7 as for a liquid solvent, with the exception that in Step 2, V-21 and V-22 are always closed (interface between HPV-2 and V-22 disconnected).
2. Set valves to admit solvent. Close V-2, V-3, V-4, V-5 and V-34, and then turn vacuum pump on. Open V-20 and V-19. Place the end of the 1/8 inch stainless steel tubing connected to V-22 in the bottom of the melted and degassed solvent flask. Gradually, open V-22 to allow the vacuum pump to withdraw the air in 1/8 inch stainless steel tubing, and then close V-22.
3. Admit the solvent to the pump. Allow the system vacuum to reach 150 millitorr. Close V-19, V-20 and then turn off the vacuum pump. Turn manual pump handle all the way counter-clockwise to allow the fill of the pump to its full capacity of 25 cm³. Open V-22 to admit solvent to the solvent pump. Close V-22 either when the pump is filled or before the liquid height in the flask gets below ½ inch.
4. Admit additional solvent if required. The solvent is melted and degassed in the same way as mentioned above and then admitted to the solvent pump. Typically, the 1/8 inch tubing from V-22 is filled with solvent. This can be verified by compressing the remaining liquid in the pump, and then slightly opening V-22 to bleed some of the solvent out of the 1/8 inch tubing submerged in the flask.

5. Remove non-condensable gases directly from the pump (an extra measure).

The pump horizontal cylinder has an upper vent connection connected to the vacuum pump. To avoid withdrawing liquid from the pump, allow free space above the liquid level in the pump by allowing full pump capacity to withhold the partially filled pump. Turn pump's handle counter-clockwise all the way, and then turn the vacuum pump on. Open V-19 and V-20 for a few minutes and then close off vacuum pump, V-19, and V-20. Turn off the vacuum pump.

Solute Preparation

Two pumps, PG-1 and PH-2, were used for solute injections. The capacities of the pumps are 25 cm³ and 10 cm³, respectively. The objective in this section is to purge gas, flush, and fill solute pumps with solute gases.

Solute Pump (PG-1)

Based on experimental solute injections planned, a high-volume solute injection is allocated to this relatively high capacity pump. As a starting point, the following valves need to be closed: V-3, V-4, V-7, V-8, V-9, V-10, V-11, V-34, V-37 and the following valves need to be open: V-5, V-6, V-25. The following sequence was used in filling the pump with solute gas.

1. Vent any pressure in the targeted solute section. Open V-7 and V-37, until solute pressure reading reaches atmospheric pressure.

2. Evacuate the targeted solute section. Turn on vacuum pump, and then open V-9. Once system reaches 150 millitorr, close V-9 and then turn off vacuum pump.
3. Flush solute section with solute gas. Set solute cylinder pressure regulator at 500 psia and then open V-28 and V-8. Close V-8 when pressure reaches 500 psia.
4. Flush of section several times with solute gas by repeating Steps 1 to 3 five times, then go to Step 5.
5. Fill pump with solute gas. The pressure and the volume of gas are set to optimum values as determined by (a) error analysis and (b) equilibrium cell pressure as solute is injected (i.e., higher injection pressure than equilibrium cell pressure required). Set solute cylinder pressure regulator and pump accessible volume to predetermined values. Open V-8 to admit solute to the pump. The pressure is fine tuned by allowing excess pressure to be vented by opening V-7 and V-37 until pressure drops to required value or by increasing pressure regulator setting to increase the pressure. The final adjustment is made with a manually operated pump (PG-1) with V-6 closed.

Solute Pump (PH-2)

This low capacity pump (10 cm³) can be used either for solvent or solute injection due to the availability of a drain port. As a starting point, the following valves need to be closed: V-31, V-32, V-33, V-34, and V-36. The following steps are performed in filling the pump with solute gas.

1. Vent any pressure in the targeted solute section. With vacuum pump connection disconnected from the apparatus, Open V-33 and V-19 until solute pressure readings reaches atmospheric pressure.
2. Evacuate the targeted solute section. Connect and then turn on the vacuum pump. Once the system reaches 150 millitorr, close V-33 and V-19, turn off vacuum pump.
3. Flush solute section with solute gas. With solute cylinder pressure regulator set at 500 psia, open V-38 and V-31. Close V-31 when pressure reaches 500 psia.
4. Flush of solute section several times with solute gas by repeating Steps 1 to 3 five times, then go to Step 5.
5. Fill pump with solute gas. The pressure and amount of gas are set to optimum values as determined by error analysis and equilibrium cell content pressure as solute is injected. Set solute cylinder pressure regulator and pump accessible volume to predetermined values from experimental planning and error analysis methods. Open V-31 to admit solute to the pump. The pressure is fine tuned by allowing excess pressure to be vented by opening V-33 and V-19 (vacuum pump disconnected) until pressure drops to required value or by increasing pressure regulator setting to increase the pressure.

Planning for an Experiment

Careful planning of an experiment before its execution has many benefits. Planning the amount of solvent and solute to be injected and a rough estimate of bubble

point pressures narrows the bubble point search region, which is the main interest in this study. Several factors contribute to reducing the uncertainty in the bubble point pressure measurement, including the injection pressure and initial and final volumes of solute and solvent in the pumps, etc. (Refer to error analysis section.) These variables can be controlled to reduce the uncertainties in experimental data. The sequence of solute gas injections and the injection pressures to be used needs to be planned. The injection pressure always needs to be higher than the equilibrium cell pressure. For the solvent, the injection pressure needs to be higher than the anticipated bubble point pressure at the corresponding temperature. For the solute, the injection pressure needs to be higher than the equilibrium pressure of the equilibrium cell contents at the highest operating temperature, taking into consideration the pressure rise upon admitting additional solute.

In performing the experiment, if the injection goes beyond the bubble point pressure (or dew point pressure) state without getting an adequate number of data points, there is no way to go back and recover the run. Thus, careful planning the experiment is critical.

The bubble point pressure is determined in a constant-volume equilibrium cell. Knowing the molar volume of the mixture and the volume of the equilibrium cell, the number of moles is determined. Accordingly, the volume of each component of the mixture can be determined. After the bubble point pressure is determined in the initial isotherm, the equilibrium cell temperature is reduced to a lower temperature. A reduction in temperature is associated with it a reduction in mixture molar volume, and since a constant volume method is used, two phases form in the equilibrium cell. The amount of

solvent required to reach the mixture bubble point at this lower temperature, and at a subsequent reduction in temperature, needs to be determined.

The method used in planning the experiment is accurate and representative of the experiment in the single- and two-phase regions as long as the binary interaction parameter for the CEOS is regressed from the initial experiment data points. The method calls for determining the following variables in sequence: (a) determine the molar volume and bubble point pressure at the specified temperature and composition (bubble point measurements); (b) determine the amount of solute and solvent required based on a constant-volume equilibrium cell and knowledge of pure components densities; (c) determine the two-phase equilibrium pressure and liquid/vapor ratio. A flash calculation is performed at constant temperature and overall solute composition subject to constant volume constraint as small increments of solvent are admitted to the equilibrium cell; (d) determine the pressure in the liquid-phase region. As the mixture composition reaches beyond the bubble point composition, the pressure is determined in this liquid region from EOS based on knowledge of molar volume, temperature and composition; (e) determine the molar volume, the bubble point pressure and the amount of solvent required to reach the bubble point pressure at a lower temperature. After a temperature reduction, the pressure and the molar volume at the bubble point are determined by iteration subject to variable liquid-phase solute mole fraction until the constant equilibrium cell volume constraint and the bubble point equilibrium condition are satisfied; (f) determine the two-phase equilibrium pressure and liquid/vapor ratio. A flash calculation is performed at constant temperature and overall solute composition subject to

constant volume constraint as small increments of solvent are admitted to the equilibrium cell.

The same procedure continues as the equilibrium cell temperature is reduced further. A flow diagram for the experiment planning program developed by Gasem (1989-1999) is presented in Appendix A. Figures 4 and 5 show comparison between experimental data and simulation results at different isotherms in the single and two-phase regions for CO₂/butane and CO₂/decane binaries. A single temperature-independent binary interaction parameter was used in the simulation of each system.

Solute and Solvent Injection

Accurate determination of mixture composition in the equilibrium cell relies on precise volumetric injection of mixture components at constant pressure and temperature. In this section, a description of the procedure is presented.

Before making any injection, the pressure and temperature of solute and solvent need to be stable for at least 4 hours. Due to the low compressibility of liquids, a large fluctuation in pressure (in the range of 10 psi) is observed for temperature changes in the order of ± 0.1 °F.

Solute (1) and Solute (2) Injections

As a starting point, the equilibrium cell is put under vacuum and isolated from solute (1) by V-4 and from solute (2) by V-34. The following steps are used in injecting both solutes to the equilibrium cell:

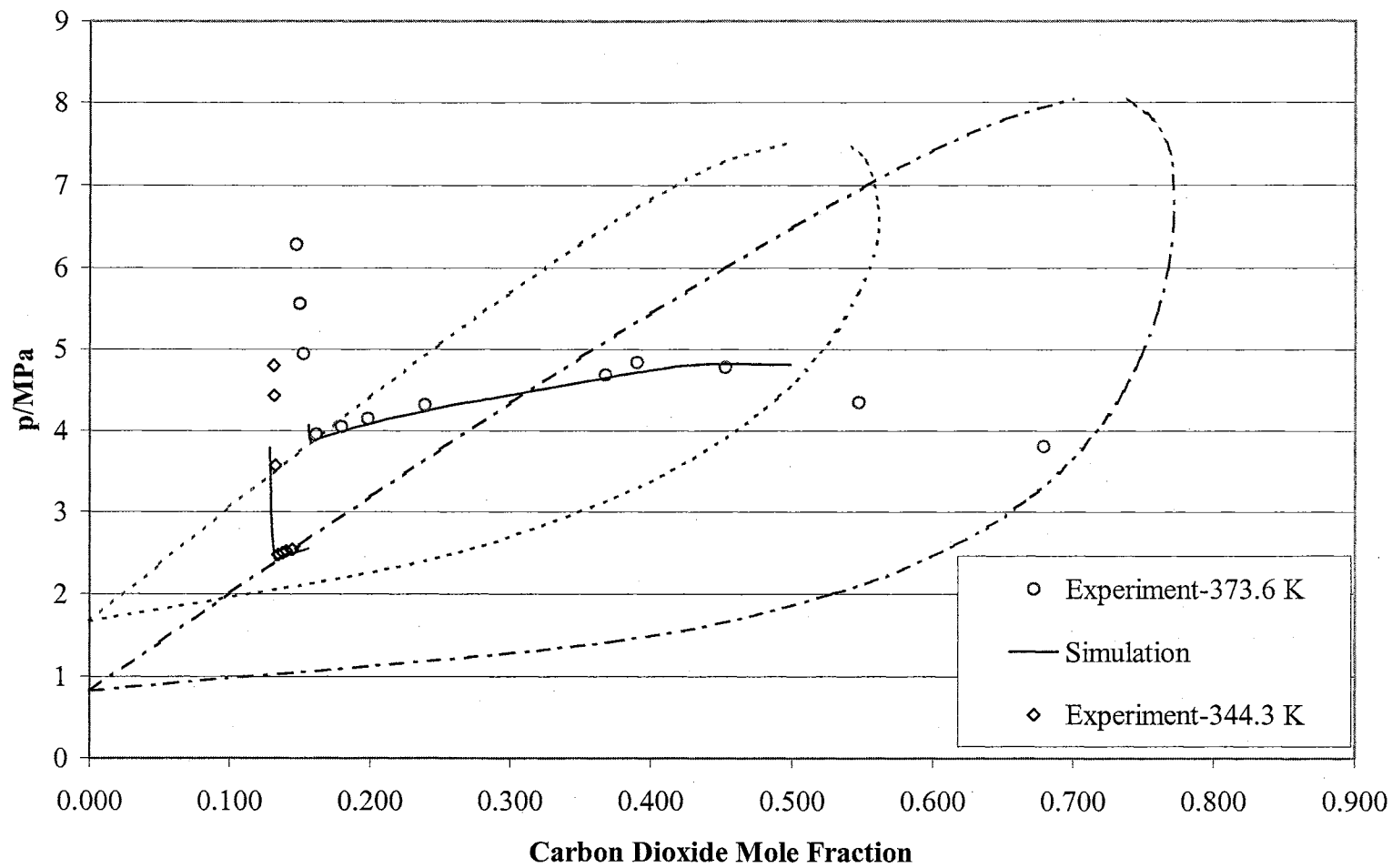


Figure 4. Bubble Point Pressures for CO₂/Butane Binary System.

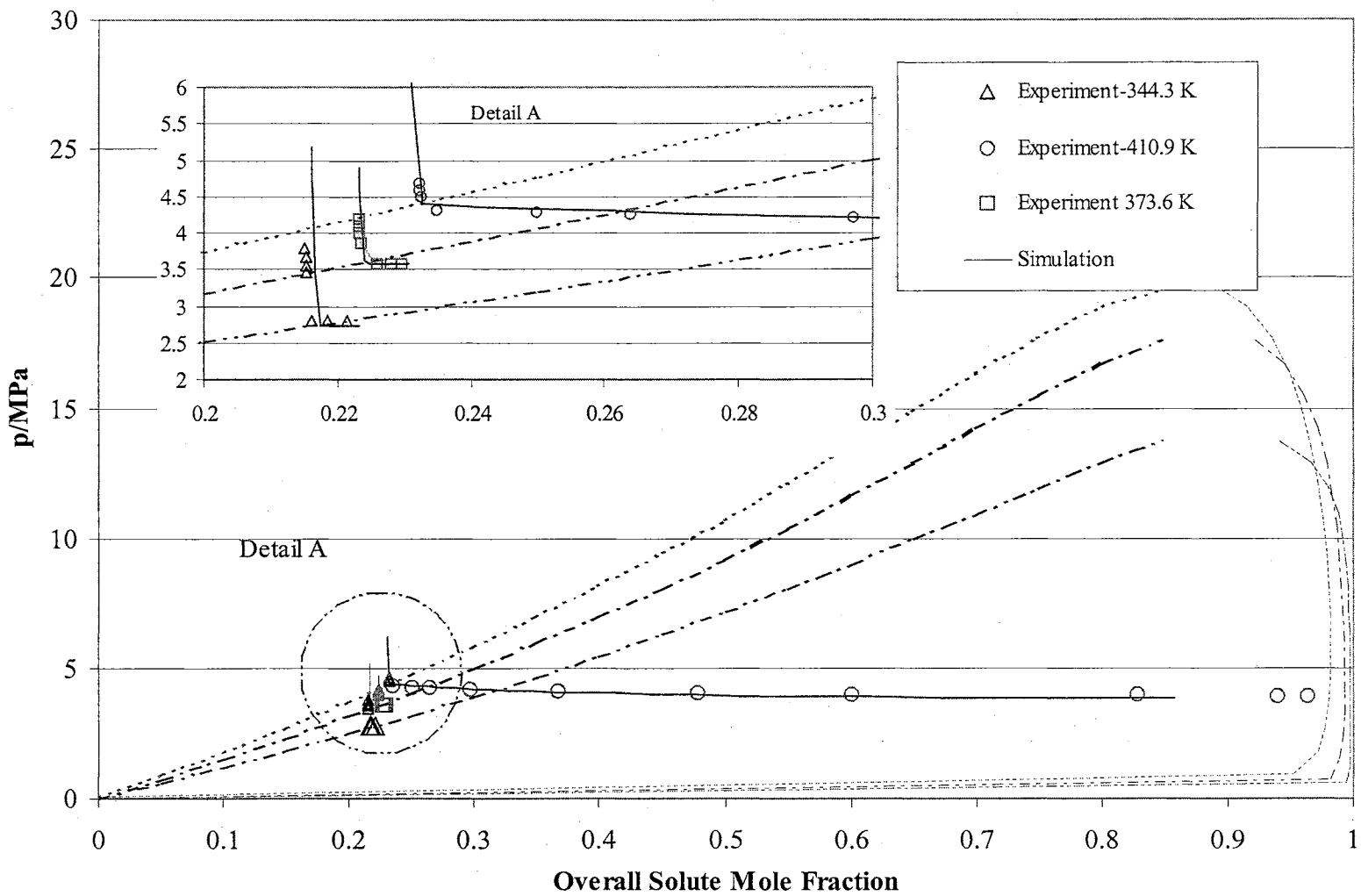


Figure 5. Bubble Point Pressures for CO₂/Decane Binary System.

1. Record injection pump temperature from the two temperature elements TE-9 and TE-10. Record solute gas pressure from pressure indicator PI-1.
2. Confirm the volume of solute to be injected based on solute density. Record temperature and pressure. Record the initial volume from the pump (PG-1) scale and dial to a tolerance within 0.005 cc.
3. Forward pump (PG-1) piston to final volume (i.e., sum of initial volume + volume to be injected); note the increase in solute pressure (PI-1) as solute gas is compressed.
4. Open V-4 slightly until the solute pressure (PI-1) reaches the initial value, and then close V-4.
5. Fine-tune the final pressure against the initial value by adjusting the pump piston to slightly compress or expand gas. Record the final temperature, pressure, and volume after the temperature and pressure stabilize.
6. For ternary mixture measurements, inject solute (2) in a similar way to solute (1). After recording the initial temperature (TE-7) and the initial pressure (PI-5), confirm the amount of volume required for the injection. Record the initial pump volume.
7. Forward pump (PH-2) piston to the final volume (sum of initial volume + volume to be injected); note the increase in the solute pressure (PI-5) as the solute gas is compressed.
8. Slightly open V-34 until the PI-5 reaches the initial value, and then close V-34.

9. To fine-tune the final pressure against the initial value, adjust the pump piston to slightly compress or expand gas. Record the final temperature, pressure, and volume.

Solvent Injection

10. The solute gas needs to be removed from the section bordered by V-2, V-4, V-6, V-10, and V-34. Close V-6 and open V-3, and then vent the solute gas through line 5 by disconnecting the vacuum pump connection with the apparatus, then open V-9. Once the pressure reaches ambient condition, connect and turn on the vacuum pump. After the vacuum reaches 200 millitor as indicated by PI-4, close V-9 and V-5, then turn off the vacuum pump.
11. Admit the solvent up to V-4. Open V-2 and forward the pump piston (PH-1) to maintain positive pressure.
12. Allow the solvent section temperature to stabilize. The expansion and contraction of fluids usually leads to thermal instability; allow enough time for the solvent temperature to stabilize.
13. Record initial conditions. Forward the piston pump (PH-1) to predetermined pressure, typically 100 psia above the estimated mixture bubble point. Record the solvent pump initial volume, pressure (PI-2 or PI-3), and temperature (TE-8).
14. Prepare the solvent for injection. Forward the pump piston (PH-1) to the final volume required, based on the amount to be injected. Inject the solvent in suitable increments to support the experimental objective. Three regions are

of particular interest: the capillary tube effect region, the dew point region, and the bubble point region. These will be discussed in the next section.

15. Admit the solvent to the equilibrium cell. Open V-4 and allow equilibrium cell pressure to reach equilibrium. The time for the contents of the equilibrium cell to reach equilibrium depends upon the system: for the solubility of carbon dioxide and ethane in n-paraffins, it was approximately 15-20 minutes; for hydrogen in the same solvent, it was about 30 minutes. After the EC contents reach the equilibrium, record the equilibrium cell pressure from the solvent pump pressure indicators (PI-2 and PI-3) and the equilibrium cell temperature (TI-1 and TI-3).
16. Determine the amount of solvent injected. Close V-4, and move the solvent pump piston until the initial solvent pressure is reached. Record the final volume, temperature, and pressure.
17. Admit more solvent. Steps 14, 15 and 16 continue until the bubble point is determined as shown graphically in the next section.
18. Plot the pressure-volume data after each equilibrium point is determined.
19. Determine the net volume of the solvent injected. Upon the determination of the bubble point, the total volume of solvent injected exceeds the amount to reach bubble point. Close V-4, and move the solvent pump piston until the initial solvent pressure is reached. Record the final volume, temperature, and pressure.
20. Determine the bubble point at a lower temperature. Reduce the equilibrium cell temperature to the next selected experimental temperature, and determine

the initial volume, temperature, and pressure of the solvent pump after the system stabilizes. Note that the initial pump pressure needs to be higher than the estimated bubble point of solvent at the new temperature.

21. Prepare solvent for injection. Forward the pump piston (PH-1) to the final volume required. The injection increment is based on the total amount of solvent to be injected. Be sure to collect at least three data points before and three after bubble point.
22. Admit the solvent to the equilibrium cell. Open V-4 and allow the equilibrium cell pressure to reach equilibrium.
23. Determine the amount of solvent injected. Close V-4, and move the solvent pump piston until the initial solvent pressure is reached. Record the final volume, temperature, and pressure.
24. Plot pressure-volume (p-V) trend after each equilibrium point is determined.
25. Admit more solvent. Steps 14, 15, and 16 continue until the bubble point is determined as shown graphically in the next section.
26. Repeat Steps 20 through 25 as the temperature is reduced further to determine the bubble point pressure at a lower temperature.
27. Upon completion of one initial solute composition at several temperatures, the apparatus must be cleaned and prepared for the next run.
28. The procedure is repeated several times, starting each run with a different composition to cover the desired composition range.

Determination of Thermodynamic Properties

In the synthetic type experimental method used in this work, the phase change is determined by the abrupt change in the slope of the pressure-volume plot. The purpose of this section is to show the way the thermodynamic properties (bubble point pressure, composition, and molar volume; dew point pressure, composition and molar volume) were determined. Experimental data for the butane/carbon dioxide mixture is used to demonstrate this method. Figure 6 shows symbolic representation of the sequence of phase transitions in the experimental procedure.

In generating a pressure-volume plot, four p-V trends were observed with volatile solvents. This leads to three discontinuities in the plot as shown in Figure 7. Following is an explanation for these discontinuities in the p-V trends.

The equilibrium cell is connected to V-4 with 1/6 inch tubing. To determine the size of this tubing, small increments of solvent were injected. A linear p-V relation was observed as the solvent forwarded in the capillary tube (prior to reaching the cell). The pressure increases due to compression of the solute(s) in the equilibrium cell. The assumption made is that no solute mixing with or diffusion into the solvent occurs in the equilibrium cell and within the capillary tube.

A different pressure-volume pattern is observed when the solvent passes beyond the capillary tube and into the cell. This p-v trend supports the assumption that mixing takes place only when the solvent reaches the cell. The capillary tube volume corresponds to the volume of solvent injected up to the discontinuity point in the pressure-volume relation. The volume of the solvent present in the capillary tube is

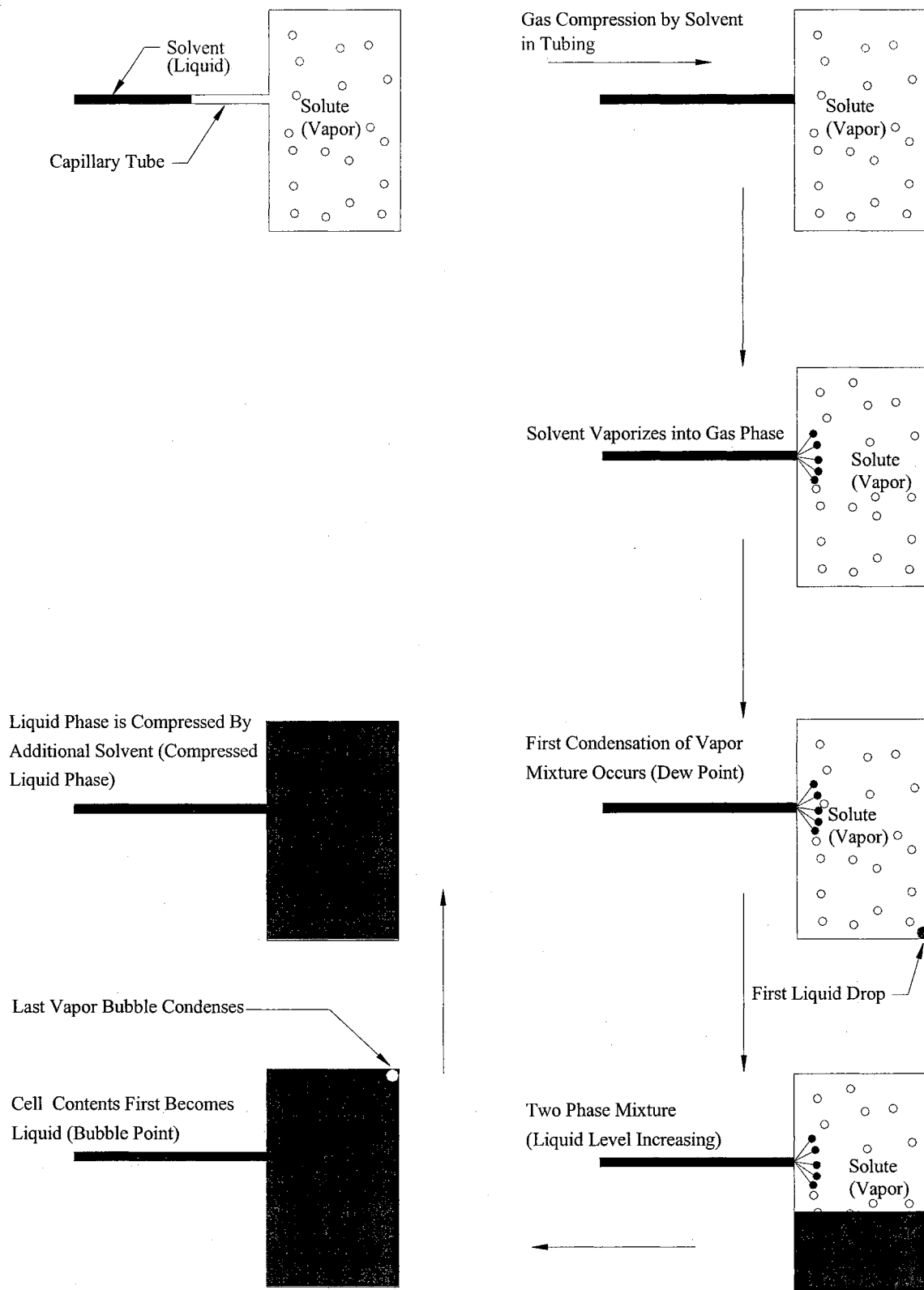


Figure 6. Symbolic Representation of Sequence in Experimental Phase Behavior.

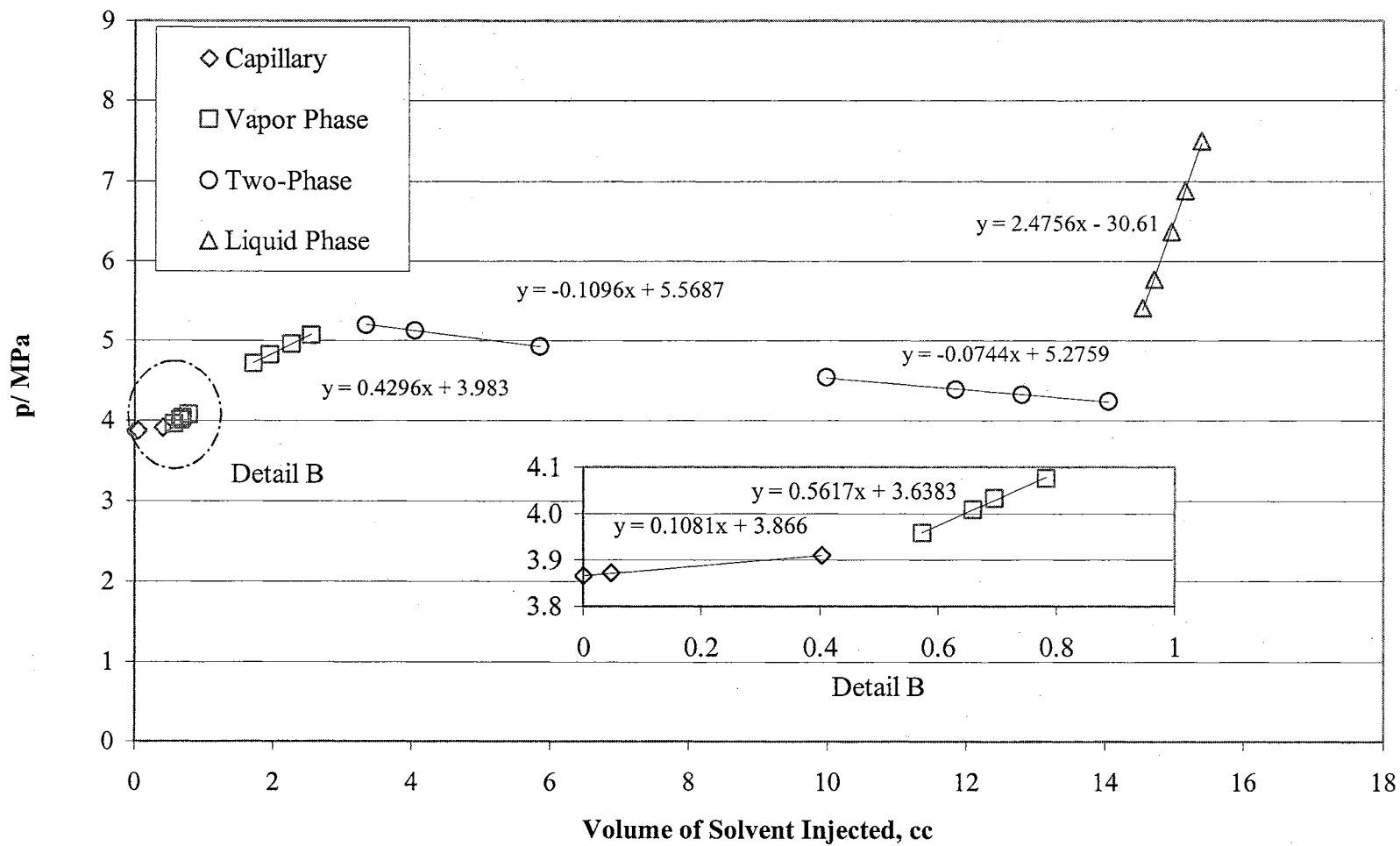


Figure 7. Experimental Pressure-Volume Trends of Carbon Dioxide/Butane Binary Mixture.

considered dead volume that needs to be subtracted from the total volume of solvent injected.

For the butane/carbon dioxide binary mixture, the change in the p-v trend as the solvent is injected beyond the capillary tube volume is due to the vaporization of butane into the carbon dioxide when it reaches the equilibrium cell. Consequently, the molar volume of the gas mixture present in the equilibrium cell is reduced. As more solvent is added, the molar volume decreases and the pressure increases. The pressure continues to increase until the mixture reaches its dew point, then a different p-v trend is observed due to two-phase formation. The intersection point between the two p-v trends represents the dew point pressure of the mixture injected. At this intersection, the molar volume can also be determined. This second discontinuity in the p-v relation was not observed with non-volatile solvents, since they condensed almost immediately upon entering the cell.

The p-v trend in the two-phase region is dependent on the mixture used. A nearly linear trend was observed with ethane/carbon dioxide/n-paraffin in comparison with hydrogen/carbon dioxide/n-paraffin mixture. This variation is due to the different degrees of solubility of the solutes in the n-paraffin. The two-phase region continues until an abrupt change in the p-v relation is observed, which signifies a transition to a nearly incompressible liquid-phase region. This point of intersection is defined as the bubble point pressure. The point of intersection is determined by solving simultaneously the two (linear) equations representing the p-v trends. At any point in the p-v plot, the overall molar volume of equilibrium cell content can be determined, since the moles of each component are known, and the volume of the cell can be determined as described in Appendix F.

Contributing to the efficiency of this new technique is that additional bubble point pressures can be determined at lower temperatures during a single experimental run. The experimental results for the carbon dioxide/decane mixture, as presented in Figure 8, demonstrate this approach. Due to the low volatility of decane, no discontinuity in the p-v trend is shown for the dew point pressure at 410 K. Four bubble point pressures are shown at four different temperatures. Upon determining the bubble point at the highest temperature, the contents of the equilibrium cell are cooled to the next lower experimental temperature. Then, additional solvent is added to generate enough data points in the two-phase and single-phase regions for the bubble point pressure to be determined accurately. The bubble point pressures and molar volumes are determined at lower temperatures in the same manner as mentioned above. This procedure is repeated to the lowest experimental temperature.

Apparatus Clean Up and Drying

After performing the experiment at the lowest temperature, the contents of the apparatus were discharged, and the apparatus was cleaned and dried. The following steps are used in accomplishing this objective:

1. Discharge the contents of the equilibrium cell. Close V-3, and then open V-10 to allow the equilibrium cell contents to be discharged to the HPV-4 vessel. Allow the equilibrium cell pressure to decrease to ambient pressure, and then close V-10.

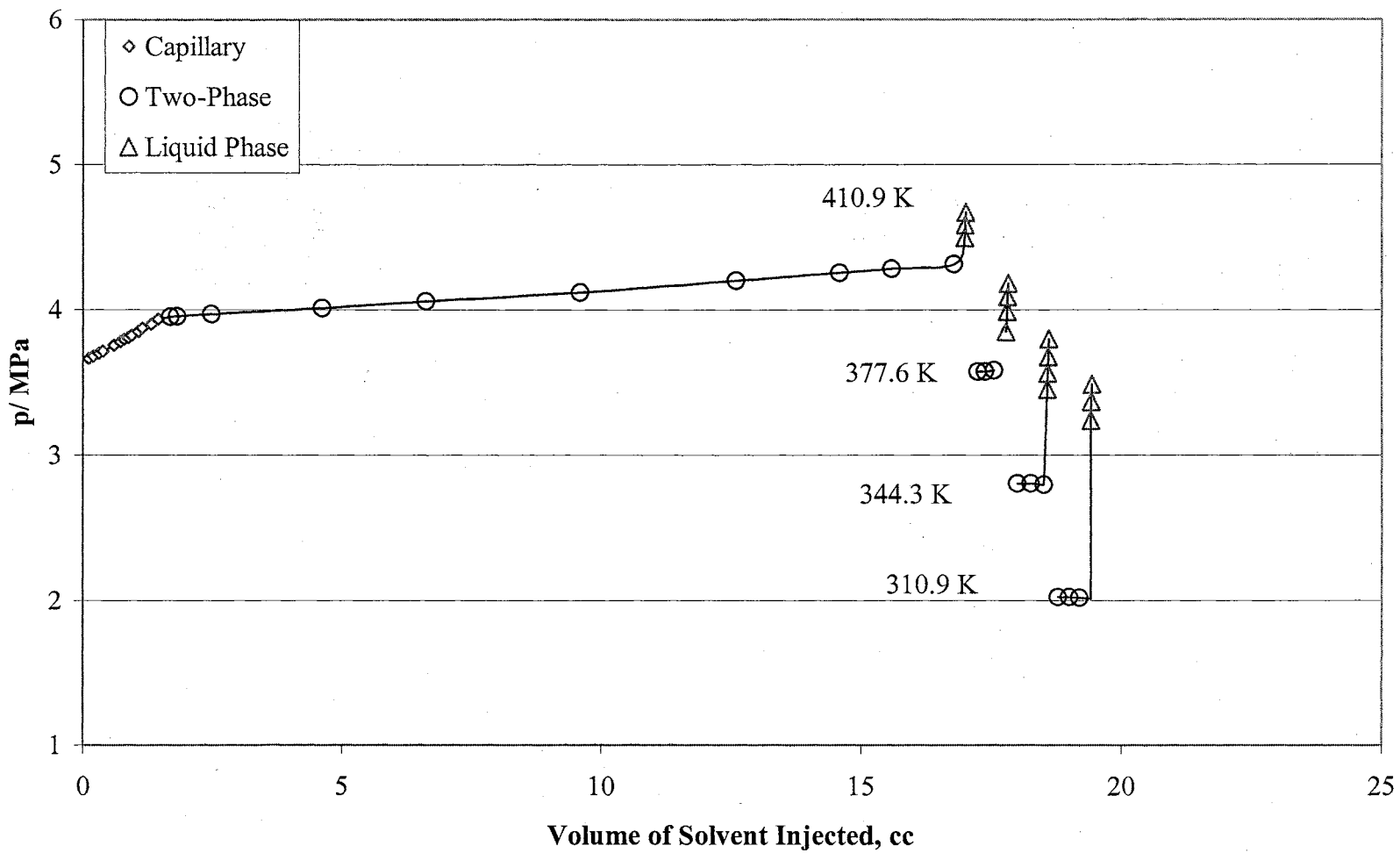


Figure 8. Experimental Pressure-Volume Trends of Carbon Dioxide/Decane Binary Mixture.

2. Inject a high-pressure gas into the equilibrium cell. Admit high-pressure carbon dioxide (cleaning agent) to the equilibrium cell. The valve opened depends on which pump contains carbon dioxide. Use V-34 for the PH-2 pump and V-5 for the PG-1 pump. Open V-28 and V-8 to maintain constant supply of carbon dioxide to the pump. Assuming carbon dioxide is placed in the PG-1 pump, open V-5 until pressure reaches 800 psi, and then close V-5.
3. Mix the equilibrium cell contents with carbon dioxide then discharge. Allow contents of the cell to mix by turning the rocking mechanism on, then discharge to the HPV-4 vessel by opening V-10.
4. Repeat this process of filling and mixing with carbon dioxide, and then discharging. Repeat Steps 2 and 3 fifteen times. The emptiness of the cell can be observed by the sound of internal steel balls as they move inside the cell. In addition, to ensure that the content of the equilibrium cell is discharged, and the cell is clean, the equilibrium cell is opened and examined occasionally.
5. End the cleaning process if the same solvent (e.g., n-paraffin) will be used in the following experiment; otherwise, the solvent pump and associated tubing need to be drained and cleaned with the cleaning solution (e.g., pentane for n-paraffin).
6. Determine the temperature required to drain the solvent pump. Depending on the solvent present (either liquid or solid at room temperature), the Oven-2 temperature is set. Use ambient temperature for a liquid solvent and 15 °F above the melting point for solid solvents. The potential hazard for using a

high temperature for the liquid solvent is in the formation of a vapor/air mixture within the lower/upper explosion limits that can be ignited by the high temperature heating element present in the oven. Two possible ways to overcome this problem either to (a) inert Oven-2 enclosure with an inert gas (e.g., nitrogen or helium), or (b) extend the drain tubing from Oven-2 through the ½ inch heat-traced pipe and into HPV-4 vessel.

7. Drain the solvent pump. Three valves are used to drain the PH-1 pump and the pressure transducers (PT-2, PT-3). The three valves, V-30, V-22, and V-23 are connected to 1/8 inch tubing, with the other tubing end placed in the flasks. Use the three valves to drain the content of the solvent pump.
8. Use helium gas to pressurize the solvent, and then drain. Close V-30, V-22, and V-23. Admit helium to HPV-3 vessel, by opening V-27, V-16, V-14 and regulate helium pressure at 800 psia. Open V-13, then open V-30, and allow all the solvent to drain. Close V-30 after all the solvent is drained, and only helium gas is released. Repeat the same with V-22 and V-23, then close V-22, V-23. Close V-14 and release helium pressure by opening V-23 until it reaches ambient pressure, and then close V-23.
9. Select a suitable cleaning solution, depending upon the solvent present. For n-paraffins, pentane is typically used. Carbon dioxide gas was used only for cleaning the EC between runs as long as the same solvent was used. Carbon dioxide was used mainly because it can be easily handled in comparison to pentane, but with the disadvantage that the process of filling and discharging

the EC with carbon dioxide has to be repeated many times to reach the same level of cleanness.

10. Evacuate the solvent pump. Turn the vacuum pump on, open V-20 and V-19. Allow the system to reach the lowest possible pressure, and then close V-19.
11. Admit the cleaning solution to HPV-3. Fill the LPV-1 vessel with cleaning solution, and then open V-12. The vacuum condition in HPV-3 and the liquid head facilitate the filling of HPV-3 (250 cc capacity) with the cleaning solution. Close V-12 after HPV-3 is filled.
12. Forward cleaning solution to pumps. Helium is used to forward and compress the cleaning solution to the solvent pump and the equilibrium cell. With helium pressure regulated at 800 psi, open V-14 then turn PH-1 pump counter-clockwise to fill total pump capacity with the cleaning solution. Open V-23, V-30, and V-22 sequentially to allow cleaning solution to drain until only helium is released. Stop helium flow, by closing V-14 and let the pump pressure reach ambient pressure, then close V-23, V-30, and V-22. Note the drained cleaning solution needs to be removed quickly from the oven when operating at high temperature.
13. Repeat the cleaning process several times. Repeats Steps from 10 to 12 four times or until there is no sign of contaminant present in the drained cleaning solution.
14. Clean the equilibrium cell with the cleaning solution. Repeat Steps 10 to 12 four times, but in this case, open V-2 to allow the cleaning solution to reach the equilibrium cell. Allow the equilibrium cell contents to mix while it is

pressurized with the cleaning solution, and then discharge the contents by opening V-10. Verify, by opening and inspecting, that the internal volume of the equilibrium cell is clean.

15. Dry the wetted portion of the apparatus (the solvent pump and equilibrium cell and associated tubing) under moderate temperature (i.e., 122 °F) and vacuum.

CHAPTER V

EXPERIMENTAL DATA ANALYSIS

The main objective in the experimental work was to acquire accurate and precise measurements to support the effort in developing reliable phase behavior models for the targeted systems. An error analysis of the uncertainties associated with measured and calculated variables due to random error is presented. Consistency testing of experimental data is used to ensure that the experimental procedures employed are free of systematic errors and to show the degree of data scatter associated with random errors.

Error Analysis

The objectives of error analysis are to determine the precision of the data and to identify the means to increase this precision. Errors can be classified as random and systematic. Random errors or random variations are generally inherent in all measurements, whereas systematic errors can be assigned to identifiable causes. To prevent bias in experimental results, the experiment needs to be free of any systematic error.

The specific objectives of performing error analysis in this study are to: (a) determine the uncertainties in the measured solute mole fractions and bubble point pressures of binary and ternary mixtures, (b) identify the contributing factors to these

uncertainties, and then (c) find ways to reduce these uncertainties. In this work, statistical methods were used to analyze and improve the precision of our experimental data.

The error analysis used in this work is based on the theory of multivariate error propagation. The experiment model is expressed as a function y of several independent variables x_1, x_2, \dots, x_n , or $y = f(x)$. The usual procedure is to linearize $f(x)$ by a Taylor series and thereafter compute the variance by

$$\sigma_y^2 \cong \sum_i^n \left[\frac{\partial f(x)}{\partial x_i} \right]^2 \sigma_{x_i}^2 \quad (5-1)$$

The first-order Taylor series expansion is not a valid approximation if (a) the standard deviation in the input variable is large, (b) the second- and higher-order derivatives with respect to x are significant (Asbjornsen, 1975), and (c) the errors in the independent variables are correlated.

Using error propagation techniques, as shown in Appendix B, the uncertainty in bubble point pressure (σ_{Bp}) estimated for binary mixtures is as follows:

$$\sigma_{Bp}^2 = \varepsilon_{Bp}^2 + \left(\frac{\partial P}{\partial x_1} \right)_T^2 \sigma_{x_1}^2 + \left(\frac{\partial P}{\partial T} \right)_{x_1}^2 \sigma_T^2 \quad (5-2)$$

Similarly, the uncertainty in mole fraction (σ_{x_1}) is expressed as:

$$\frac{\sigma_{x_1}}{(x_1(1-x_1))} = \left(\frac{\sigma_{V_1}^2}{(V_{1f} - V_{1i})^2} + \frac{(V_{1f}^2 + V_{1i}^2)\sigma_{\rho_1}^2}{(V_{1f} - V_{1i})^2 \rho_1^2} + \frac{\sigma_{V_{2T}}^2}{(V_{2f} - V_{2i})^2} + \frac{(V_{2f}^2 + V_{2i}^2)\sigma_{\rho_2}^2}{(V_{2f} - V_{2i})^2 \rho_2^2} \right)^{1/2} \quad (5-3)$$

As can be deduced from Equations (5-2) and (5-3), three types of errors contribute to the uncertainty in the bubble point pressure.

1. Errors due to the intrinsic variability of the measuring devices like pressure and temperature instruments. The imprecision of the instruments was determined from calibration trends over short intervals of time.
2. Errors due to propagated error in calculated variables. The precision in the calculated mole fraction is a function of the several independent variables (ρ_1 , ρ_2 , V_{1i} , V_{1f} , V_{2i} , V_{2f}) and the uncertainties in their measured or calculated values.

As shown in Table 4, high purity chemicals were used in this study. No further purification of the chemicals was attempted. The densities of pure gases were calculated from accurate literature correlations. The pure solvent densities were correlated from tabulated results. Table 5 gives the sources used in determining pure-fluid densities. The uncertainties in measured volumes were determined using error propagation techniques as shown in Appendix B.

3. Errors associated with a particular experimental technique. To quantify this error in a simple way, variations were performed involving the slopes of the two lines that intersect at the bubble point pressure, subject to experimental data constraints (i.e., different combinations of experimental data points were used to form lines). The standard deviation, ϵ_{pp} , in the bubble point pressure due to the variation of the line slopes in the pressure-volume plots was determined for each bubble point pressure measured. ϵ_{bp} is due to the uncertainty in pressure reading and ϵ_{pp} .

Table 4. Suppliers and Stated Purities of the Chemicals used in this Work

Chemical Names	Supplier	Purity (mol %)
Butane	Phillips 66	99.98
Hexane	Aldrich Chemical Company	99+
Decane	Aldrich Chemical Company	99+
Eicosane	Aldrich Chemical Company	99
Octacosane	Aldrich Chemical Company	99
Hexatricontane	Aldrich Chemical Company	98
Carbon Dioxide	Aeriform	99.99
Ethane	Airgas	99.99
Hydrogen	Union Carbide Corporation	99.995
Nitrogen	Airgas	99.995

Table 5. Pure-Fluid Properties used in this Work

Chemical Names	Reference (Affiliation)
Butane	Haynes and Goodwin, 1982 (NBS)
Hexane	API Research Project 44 (TRC)
Decane	Gehrig and Lentz, 1983 API Research Project 44 (TRC) Vargaftik, 1975
Eicosane	Doolittle, 1964
Octacosane	Flory, et al., 1964
Hexatricosane	Flory, et al., 1964
Carbon Dioxide	Span and Wagner, 1996 Vukalovich and Altunin, 1968
Ethane	Younglove and Ely, 1987 (NBS) Friend, et al., 1991 (NIST)
Hydrogen	McCarty, et al., 1981 (NBS)
Nitrogen	IUPAC, 1977

IUPAC: International Union of Pure and Applied Chemistry

NIST: National Institute of Science and Technology

TRC: Thermodynamic Research Center - Texas A&M University

To verify error analysis results, solubility measurements were performed twice for two systems (nitrogen/hexane, nitrogen/decane) at fixed composition and temperature. In the two cases, the uncertainties in both the bubble point pressure and in the composition fall within the expected uncertainties as determined by the error analysis. As shown in Equation (5-3), the initial and final volumes of both the solute and the solvent do have an effect on the uncertainty in mole fraction and consequently on the bubble point pressure. To minimize this error, the volume factor, $\left[\frac{V_i^2 + V_f^2}{(V_i - V_f)^2} \right]$, needs to be minimized to near unity. This was accomplished by retaining in the pumps only the amounts required for injection at the lowest possible pressures, thus minimizing the numerator in the above expression.

A detailed derivation, a case study, and tabulated results are given in Appendix B.

Consistency Testing of Experimental Data

Consistency testing of experimental data may be divided into four categories: (a) instrumental consistency test to verify the accuracy of the temperature and pressure measurements and establish their precisions, (b) internal consistency tests which determine the imprecision of a single set of measurements performed on the same apparatus, (c) external consistency tests which seek to compare data from different sources, and (d) thermodynamic consistency tests, which verify the internal thermodynamic consistency of the experimental data.

Thermodynamic consistency tests are based on the Gibbs-Duhem equation. For supercritical components at high pressure, the direct application of the Gibbs-Duhem equation is not convenient due to non-ideality of the vapor phase, where an empirical

constant needs to be introduced, and a hypothetical standard state may be required for supercritical fluid. Therefore, instrumental, internal, and external consistency tests were used to assess the quality of the experimental data.

Instrumental Consistency Test

Instrumental consistency for the temperature and pressure devices was ascertained by frequent calibration against standard devices traceable to the National Institute of Science and Technology (NIST). Seven RTD temperature elements were calibrated against a standard platinum resistance thermometer before each system measurement. Similarly for pressure transducers, all four transducers were calibrated against a dead-weight gauge before and after each system run. The accuracy of the temperature and pressure measurements was verified by measuring the vapor pressure of pure butane at several temperatures, as exemplified by Table 6 shown below.

Table 6. Vapor Pressure of Pure Butane

T (K)	Vapor Pressure (MPa)		
	This Work	Literature	Reference
409.5	2.931	2.929	National Bureau of Standard (NBS) Monograph 169
409.7	2.948	2.940	

Internal Consistency Test

Assessment of scatter among data points can be performed graphically and analytically. Graphical evaluation of the data, such as a plot of $(p - p_i^s)/x_i$ versus x_i , provides a measure of the scatter of a single set of measurements, where the deviations in

pressure can be magnified by the reciprocal of mole fraction. The amount of scatter in $(p-p_i^s)/x_i$ versus x_i plot indicates the precision of experimental data, and the quality of variation of $(p-p_i^s)/x_i$ versus x_i among the different isotherms reflects the consistency of these data. Two sets of data were used to demonstrate the implementation of internal consistency test to the experimental measurements. Figure 9 and Table 7 represent the experimental results performed in this work for the solubility measurement of nitrogen in hexane and the experimental data by Poston and McKetta (1966). In Figure 10 the p/x_1 versus x_1 plot shows the trends of both sets of data (solute in supercritical region; vapor pressure ignored). Our experimental results show near-linear trends for the different isotherms and no crossovers in comparison to Poston and McKetta's (1966) data. This suggests that our data have a better internal consistency than Poston and McKetta's (1966) data.

The analytical approach relies on checking the ability of an EOS to represent the experimental results. The excellent EOS fit of the data on an isotherm-by-isotherm basis illustrates both the ability of the EOS and the precision of the data. As shown in Table 8, our data can be described with root-mean-square deviation (RMS) in solute composition of about 0.003 by the PR EOS using one temperature-independent interaction parameter. This deviation reduces to 0.001 maximum, as shown in Table 9, when two interaction parameters per isotherm were used. This falls within the expected uncertainty of our experimental data, and accordingly, indicates the precision of our experimental data. From Poston and McKetta's (1966) data, a RMS deviation of 0.011 was obtained for the 310.9 K isotherm. This can be observed from Figures 9 and 10, where the 310.9 K

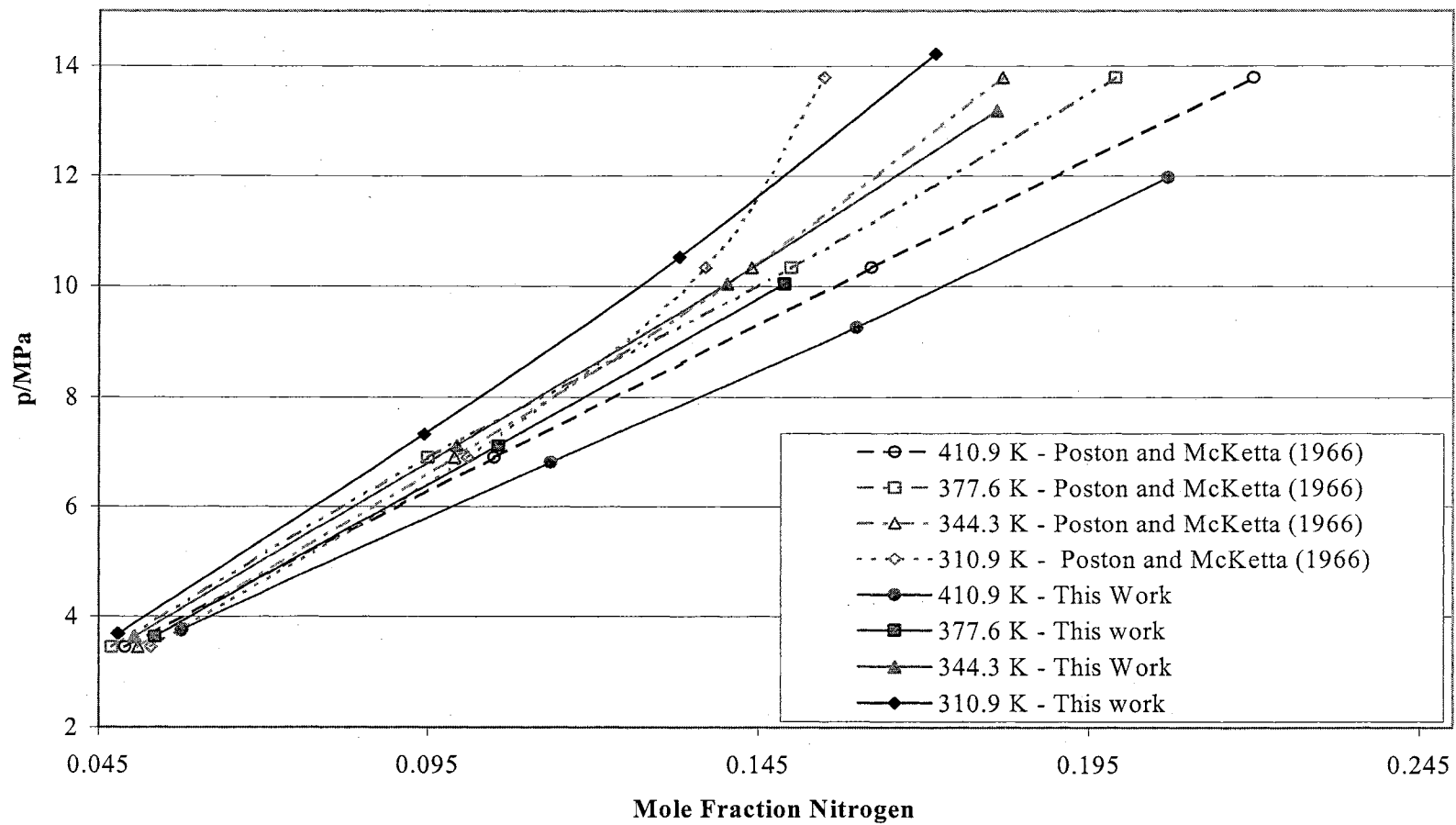


Figure 9. Bubble Point Pressures of Nitrogen/Hexane System.

Table 7. Solubility of Nitrogen (1) in Hexane (2)

x_1	p/MPa		x_1	p/MPa
		310.9 K		
0.0479	3.679		0.1331	10.532
0.0480	3.686		0.1718	14.219
0.0944	7.322			
		344.3 K		
0.0504	3.636		0.1403	10.049
0.0505	3.636		0.1811	13.185
0.0994	7.115			
		377.6 K		
0.0536	3.635		0.1056	6.884
0.0536	3.633		0.1490	9.637
		410.9 K		
0.0576	3.740		0.1598	9.263
0.0577	3.757		0.2070	11.974
0.1136	6.807			

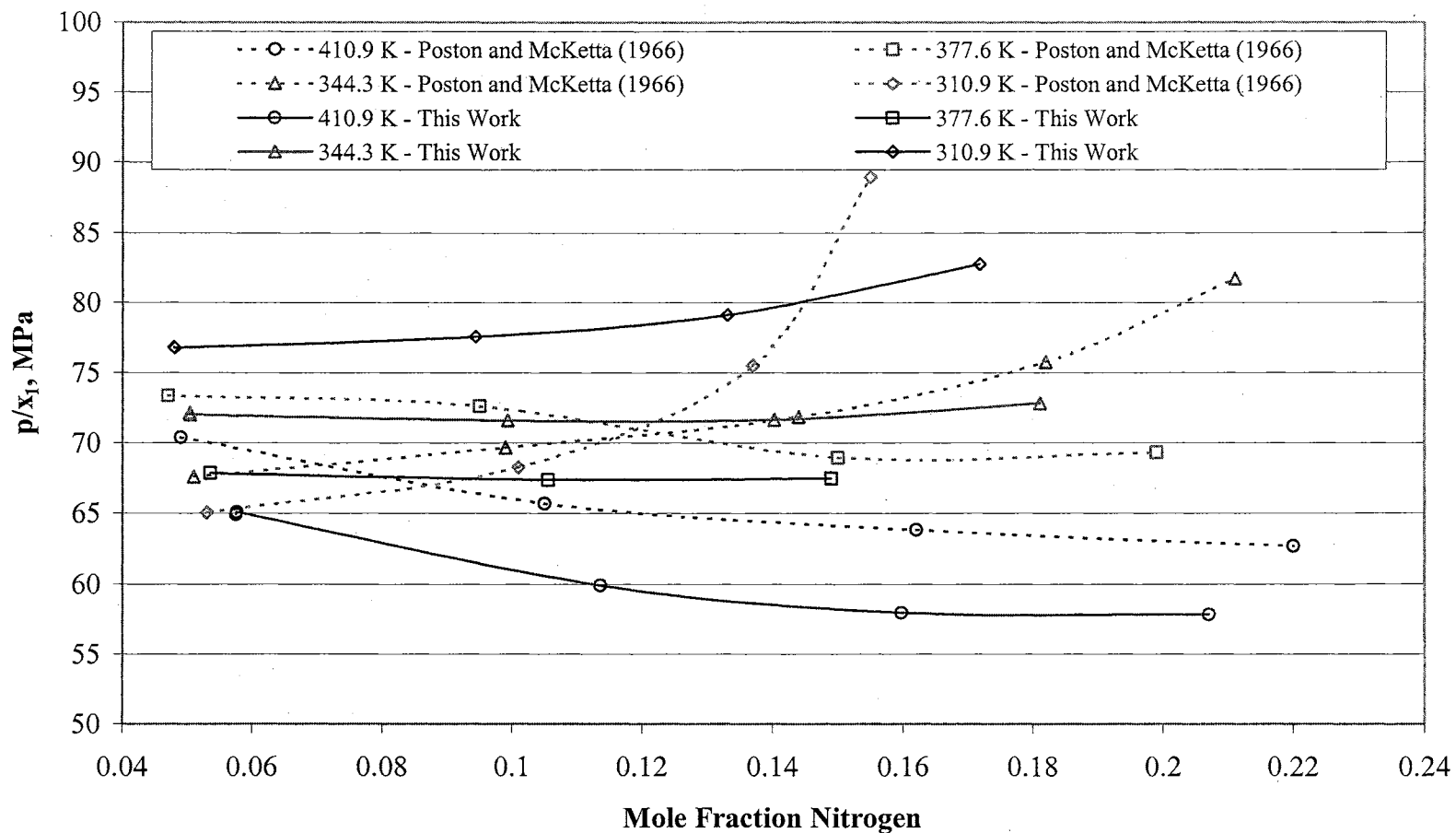


Figure 10. Comparison of Bubble Point Pressures of Nitrogen (1)/ Hexane (2) System.

Table 8. PR Equation-of-State Representations of the Solubility of Nitrogen (1) in Hexane (2) using One Interaction Parameter

T/K	This Work			Poston and McKetta (1966)		
	PR Parameters C_{12}	Deviation in Solute Mole Fraction, x_1		PR Parameters C_{12}	Deviation in Solute Mole Fraction, x_1	
		RMS*	MAX		RMS	MAX
310.9	0.1530	0.0020	0.0030	0.1175	0.0106	0.0228
344.3	0.1446	0.0032	0.0060	0.1347	0.0016	0.0034
377.6	0.1642	0.0010	0.0019	0.1982	0.0035	0.0059
410.9	0.1472	0.0037	0.0066	0.2130	0.0041	0.0085
(310.9 - 410.9)	0.1513	0.0032	0.0080	0.1394	0.0075	0.0138

$$\text{Dev} = (x_{\text{cal}} - x_{\text{exp}})$$

n = Number of data points

$$*\text{RMS} = \sum \sqrt{\left(\frac{\text{Dev}^2}{n}\right)}$$

Table 9. PR Equation-of-State Representations of the Solubility of Nitrogen (1) in Hexane (2) using Two Interaction Parameters

T/K	This Work				Poston and McKetta (1966)			
	PR Parameters		Deviation in Solute Mole Fraction, x_1		PR Parameters		Deviation in Solute Mole Fraction, x_1	
	C_{12}	D_{12}	RMS	MAX	C_{12}	D_{12}	RMS	MAX
310.9	0.0506	0.0347	0.0010	0.0016	0.1136	0.0012	0.0107	0.0323
344.3	0.0186	0.0565	0.0005	0.0008	0.1323	0.0008	0.0016	0.0350
377.6	0.0928	-0.0242	0.0004	0.0007	0.0594	0.0464	0.0024	0.0034
410.9	-0.0635	0.0789	0.0008	0.0013	0.0624	0.0570	0.0015	0.0024
(310.9 - 410.9)	0.1513	0.000	0.0032	0.0080	0.2828	-0.0485	0.0060	0.0112

isotherm does not follow the nearly linear trend as other isotherms, and the same conclusion can be deduced from the results presented in Tables 8 and 9. The results in Tables 8 and 9 revealed that our data are more precise than Poston and McKetta's (1966) data for the same pressure range.

External Consistency Test

To validate the experimental procedures used, our experimental measurements were compared against experimental data from reliable published sources. The comparisons are shown in terms of deviations of the experimental solubilities and bubble point pressures from values correlated by the PR EOS, using temperature-dependent interaction parameter (C_{ij}) values determined from the combined data sets. Interaction parameter values were optimized to minimize the RMS deviations in the calculated bubble point pressures at fixed temperature and liquid mole fraction. Three systems were examined, and the evaluation for each system is presented below.

The carbon dioxide/butane binary was the first system examined. Figures 11 and 12 show that our results are in excellent agreement with Olds, et al. (1949) data, where the maximum deviations in mole fraction and pressure are approximately 0.0015 and 0.02 MPa, respectively. The experimental uncertainties of our data are 0.002 in mole fraction and 0.031 MPa in pressure. The uncertainties in mole fractions reported by Hsu et al. (1985) and Fernandez et al. (1989) are 0.002 and 0.005, respectively. Differences in liquid phase mole fractions between the data set from the present work and that of Hsu, et al. (1985) are typically 0.004–0.006. A maximum deviation of 0.0075 in mole fraction is observed between our data and that of Fernandez, et al. (1989). The observed differences

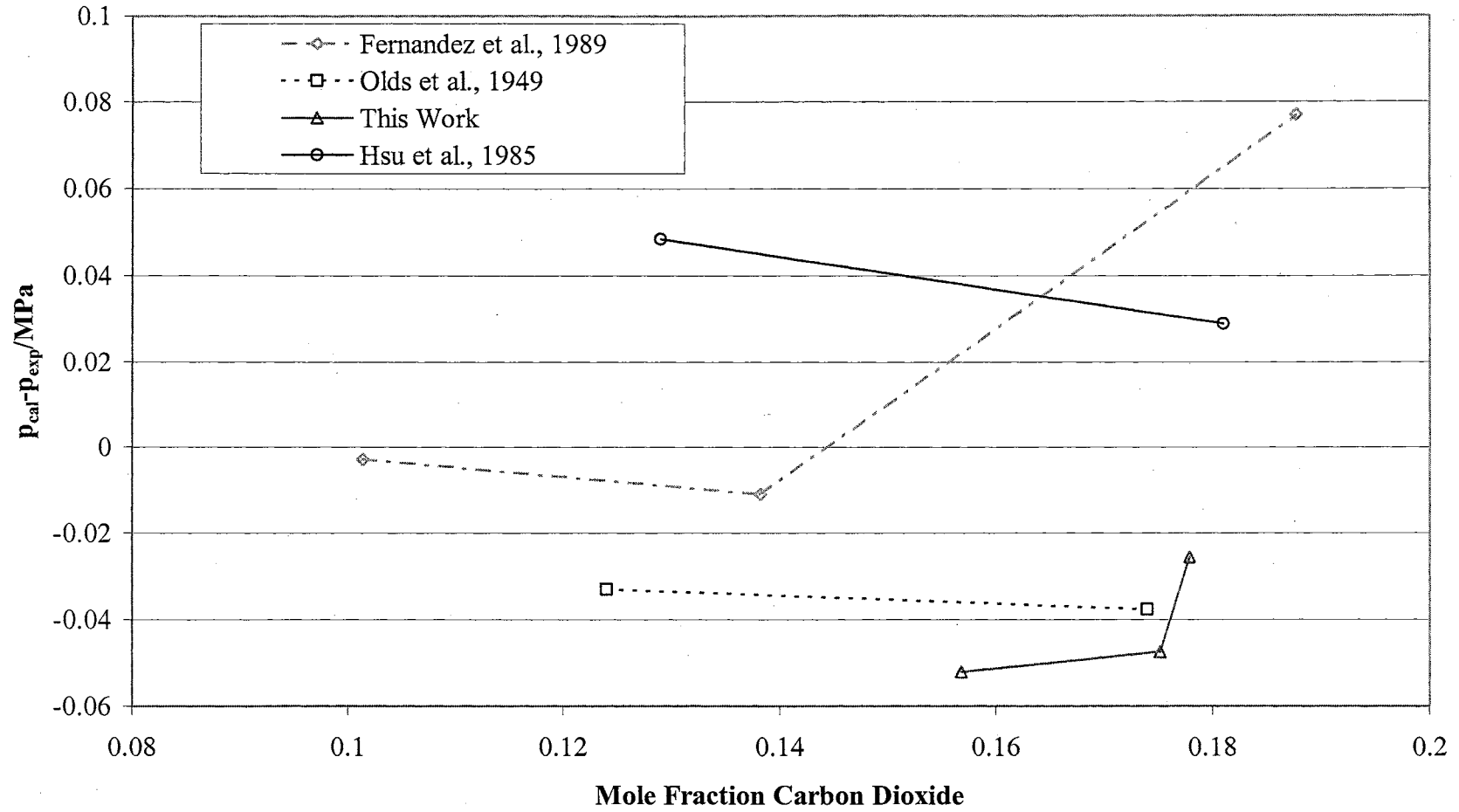


Figure 11. Comparison of Bubble Point Pressures for the Carbon Dioxide/Butane System at 377.6 K.

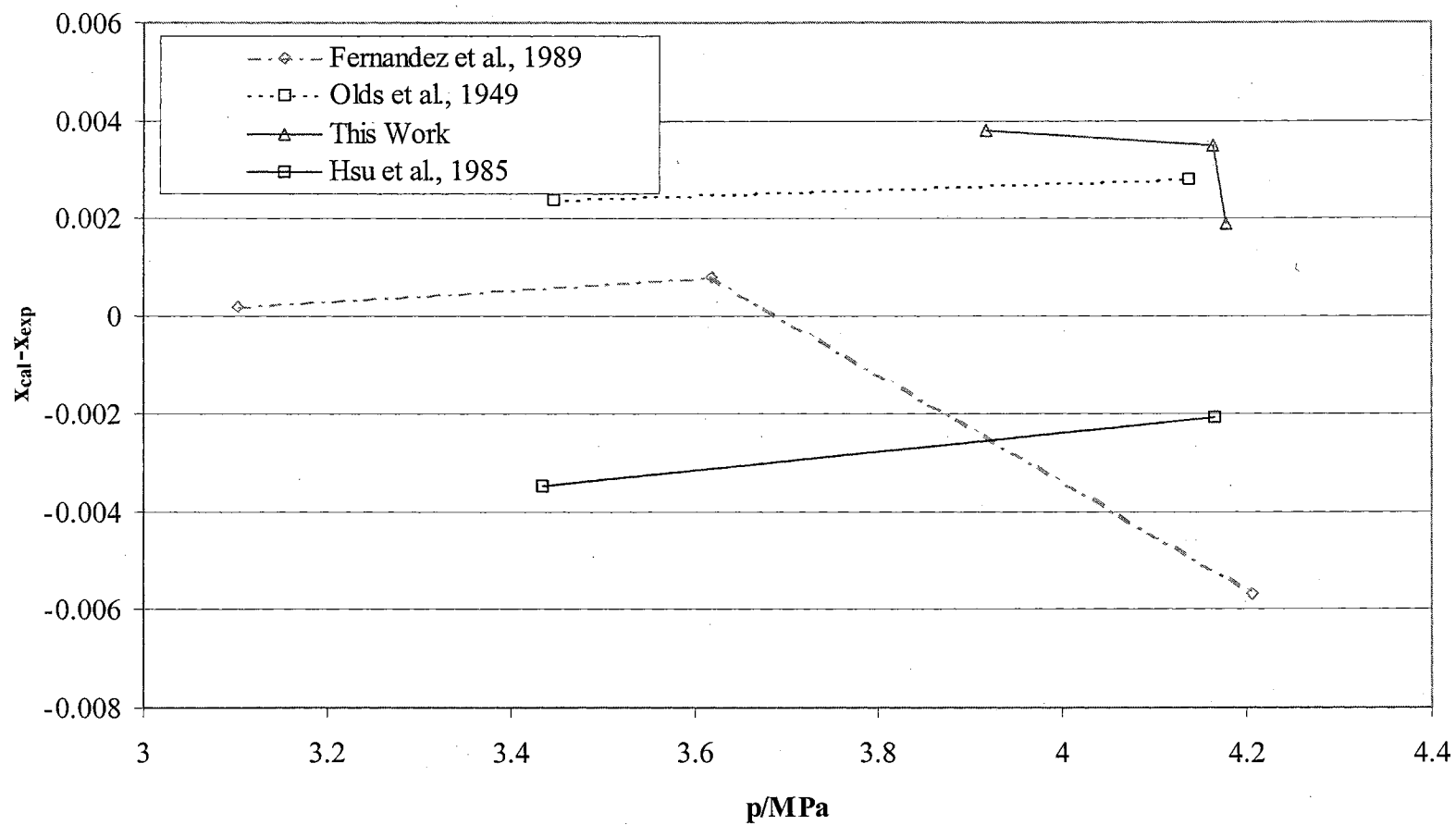


Figure 12. Comparison of Carbon Dioxide Solubilities in Butane System at 377.6 K.

between this work data set and the data sets of Hsu et al. (1985) and Fernandez et al. (1989) are slightly greater than the combined estimated uncertainties in the experimental results of each data set reported.

For the carbon dioxide/decane system, as shown in Figures 13 and 14, a comparison was made for three isotherms. For the three isotherms at 410.9 K, 377.6 K and 344.3 K, excellent agreement is seen between our data and Reamer and Sage's (1963) data, where the maximum deviation in solute mole fractions and pressures between the two sets of data are 0.0017 and 0.034 MPa, respectively. These deviations are within the experimental uncertainties of our data ($\sigma_{Bp} = 0.041$ MPa, $\sigma_{x_1} = 0.002$). Similarly, Shaver, et al. (2001) data measured at 344.3 K are in excellent agreement with our data. Reasonable agreement is observed with Bufkin's (1986) data.

Figures 15 and 16 show our experimental results for the nitrogen/decane system in comparison to experimental data reported by others (Gao, 1999; Azornoosh and McKetta, 1963; Tong, et al., 1994). In comparison to experimental data measured by Gao (1999) and Azonoosh and McKetta (1963), a good agreement in results is indicated where maximum deviations of 0.001 in nitrogen mole fraction and 0.079 MPa in bubble point pressure are observed between our data and others. These deviations are slightly over the experimental uncertainties of our data ($\sigma_{Bp} = 0.065$ MPa, $\sigma_{x_1} = 0.0007$), but within the experimental uncertainty in mole fractions of 0.001 reported by Gao (1999) in his experimental data. Therefore, our data set are within the combined uncertainties in both data sets. In comparison with Tong, et al. (1999) data, a fair agreement between both sets

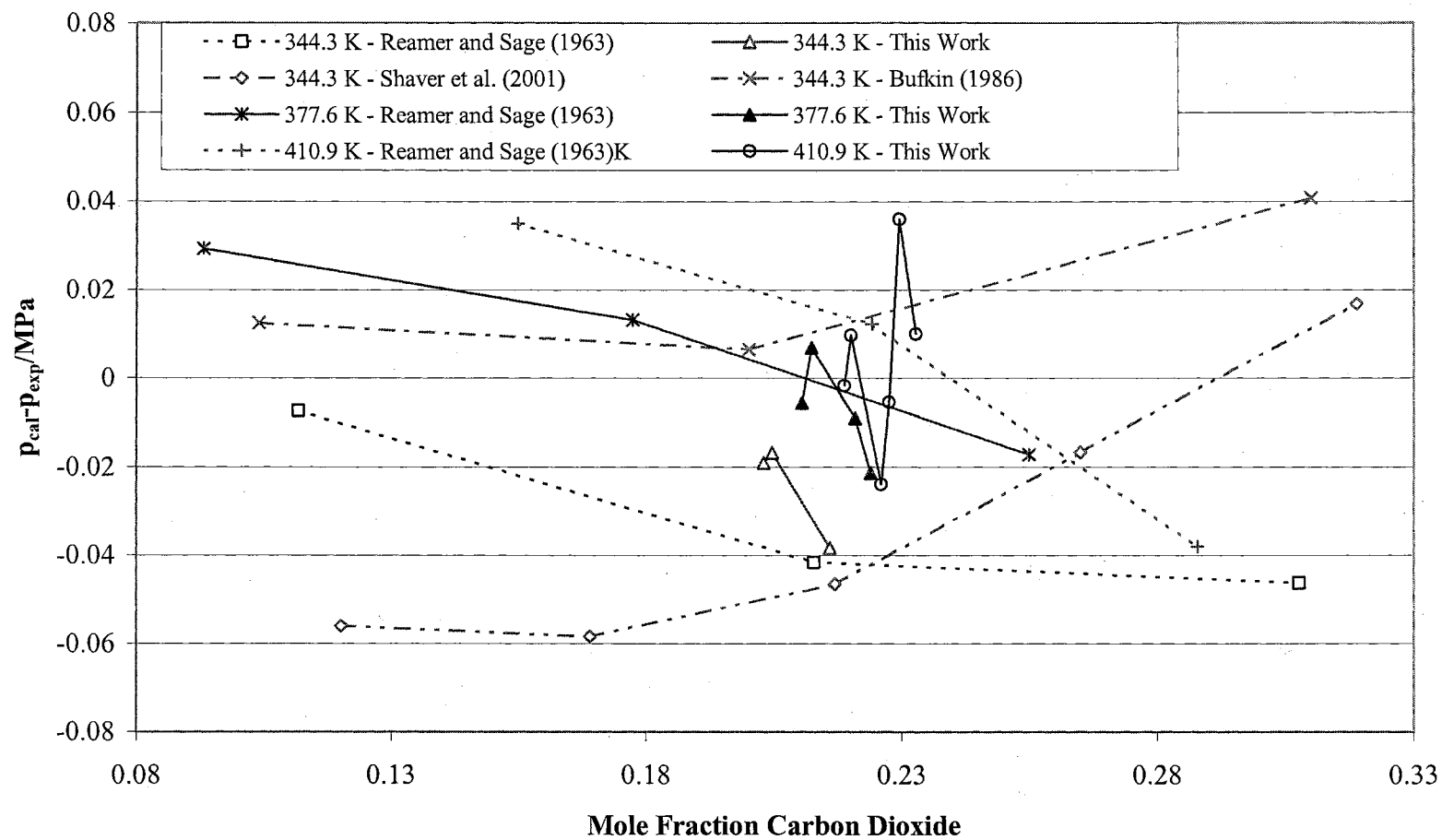


Figure 13. Comparison of Bubble Point Pressures for Carbon Dioxide/Decane System.

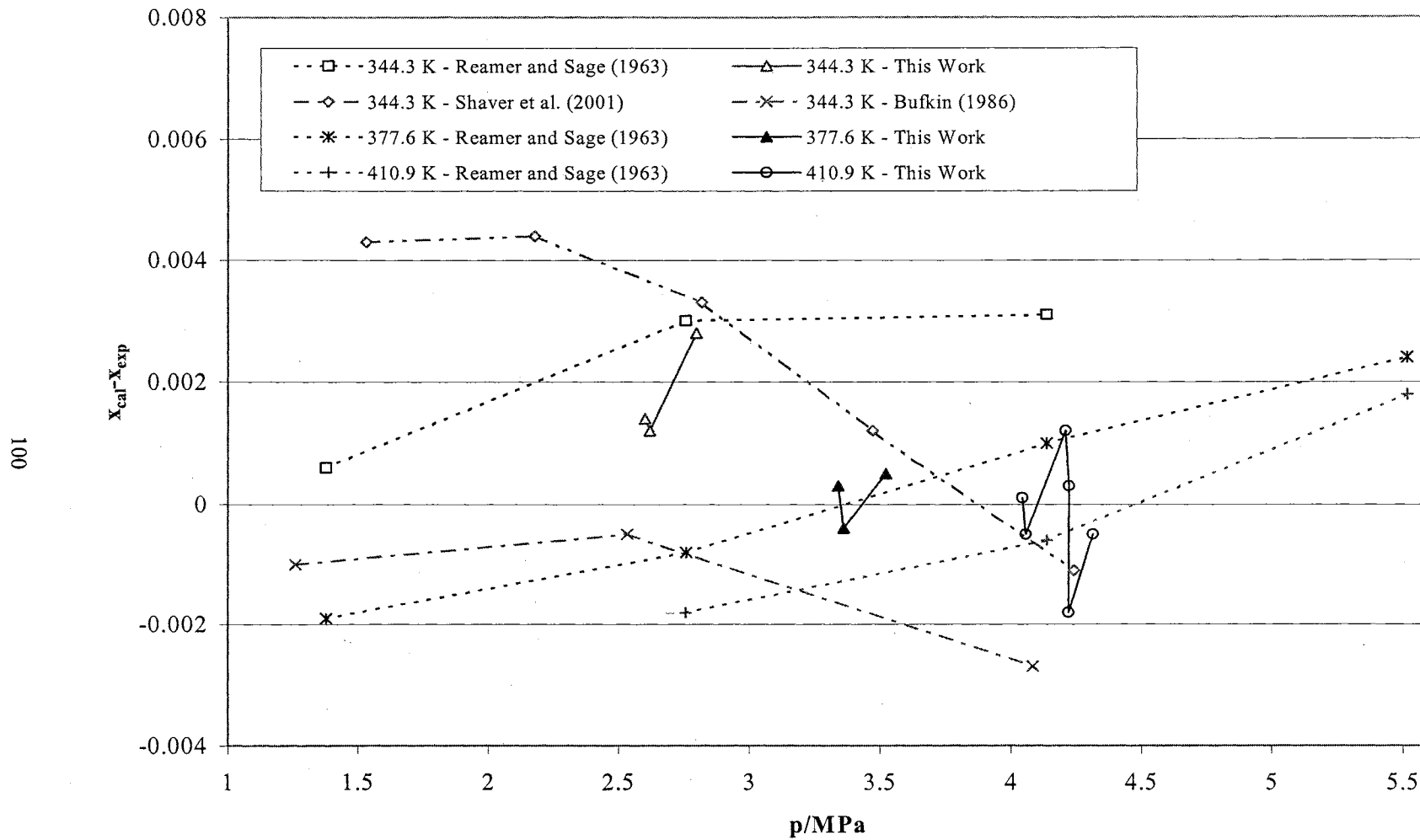


Figure 14. Comparison of Carbon Dioxide Solubilities in Decane.

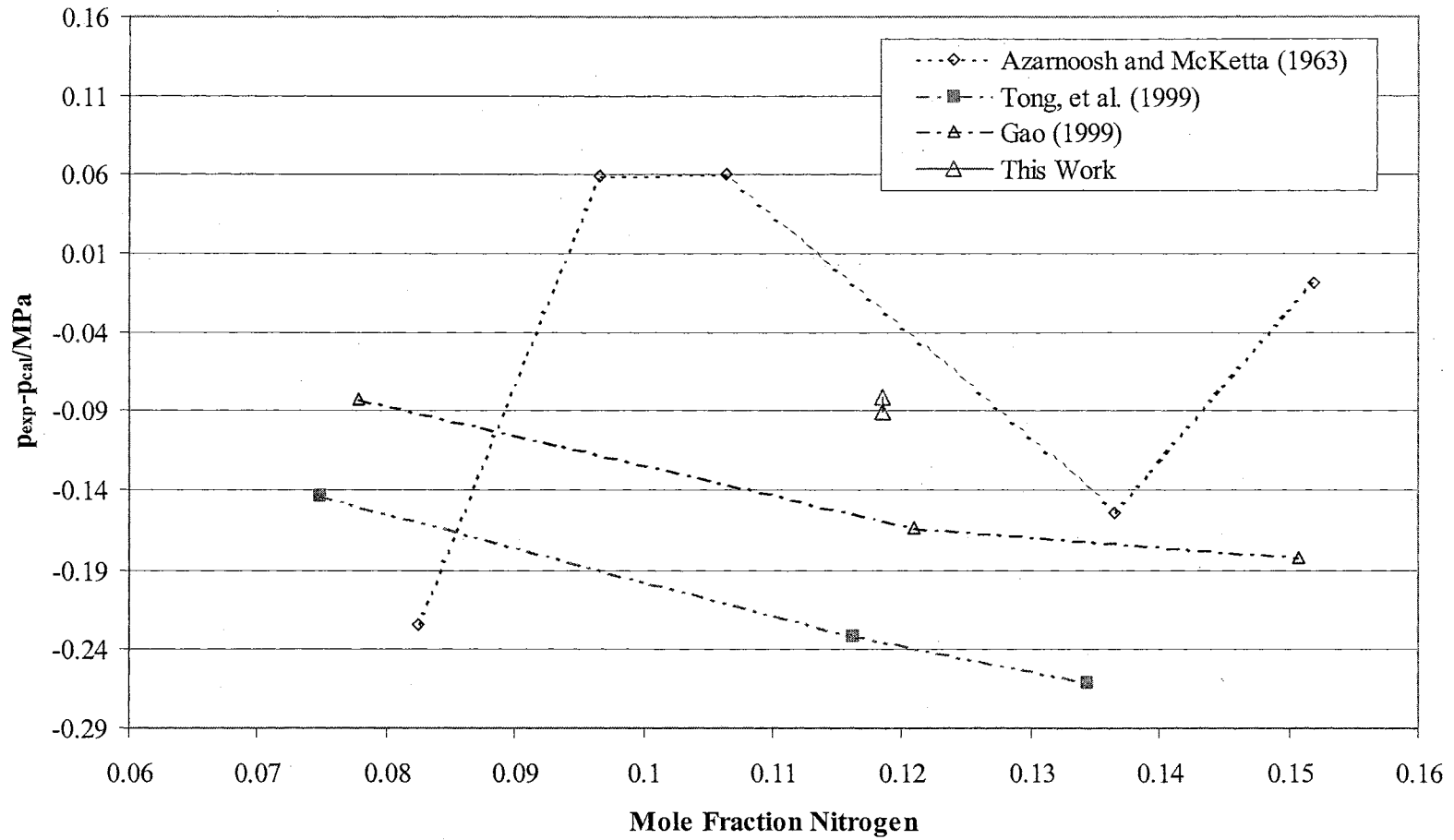


Figure 15. Comparison of Bubble Point Pressures for Nitrogen/Decane System at 410.9 K.

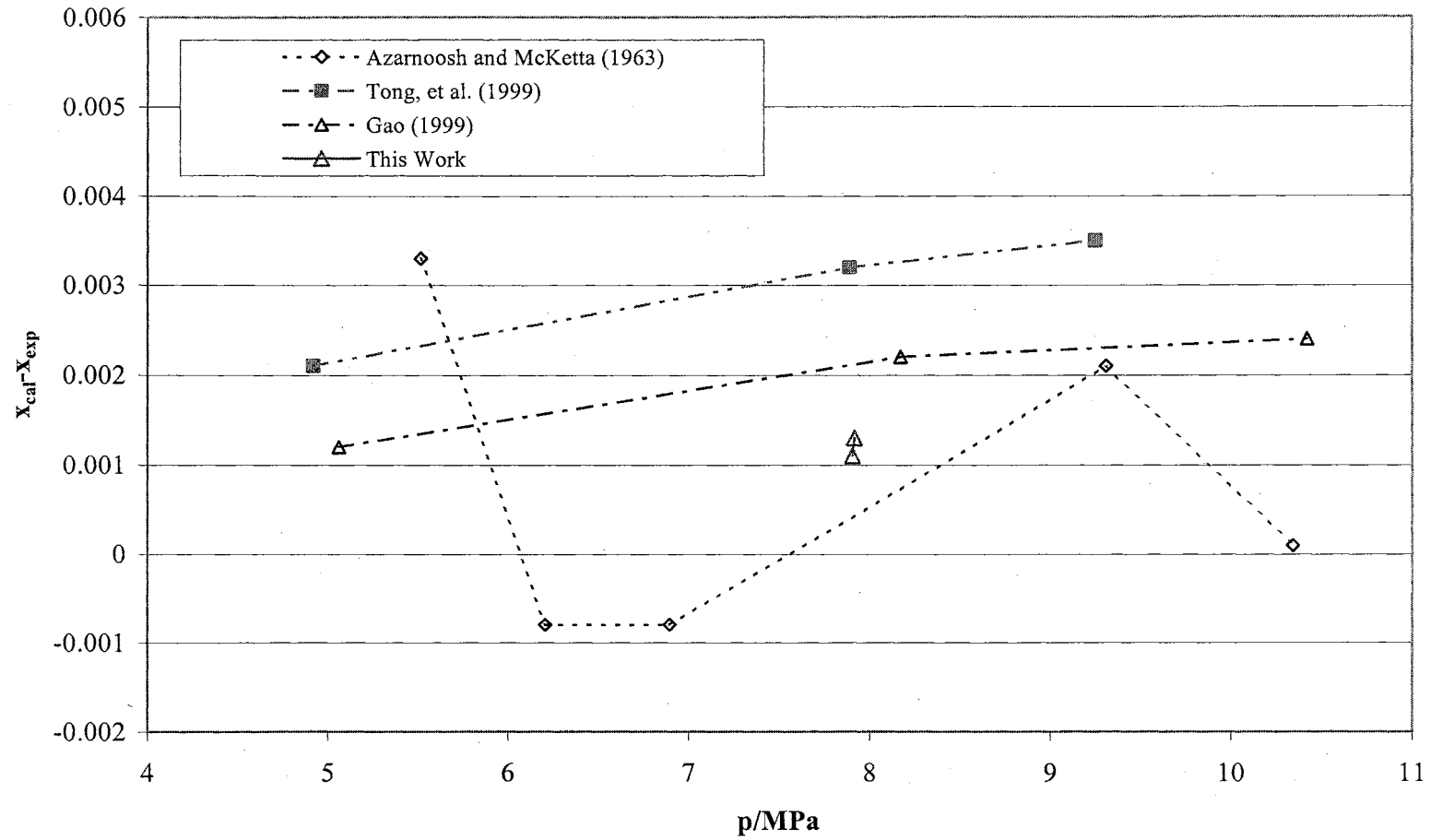


Figure 16. Comparison of Nitrogen Solubilities in Decane at 410.9 K.

of data is observed, where the differences in mole fractions are slightly over the combined estimated uncertainties in the two works.

In this Chapter, consistency tests were mainly focused on bubble point pressure measurements. Appendix F presents external consistency tests of liquid densities and a few dew point pressures measured in this work.

The consistency tests performed confirm the viability of the new experimental apparatus and procedure.

CHAPTER VI

EXPERIMENTAL RESULTS AND DISCUSSIONS

Multi-component asymmetric mixtures are typically encountered in many important processes. In indirect coal liquefaction, mixtures of light gases dissolved in high molecular weight solvents, such as carbon monoxide, hydrogen, ethane, and carbon dioxide in high molecular weight n-paraffin solvents, are typically encountered (Kuo, 1985; Shah, et al., 1988). In addition, multi-component asymmetric mixtures of gases, such as methane, ethane and propane dissolved in n-paraffins (e.g., eicosane, docosane), were used to model gas condensates encountered in enhanced oil recovery (Gregorowicz, et al., 1993).

The behavior of these mixtures is affected by the interactions of unlike molecules, particularly if some are polar. Interaction between triplets and higher combinations usually are less important than those between pairs of components (Walas, 1985); However, interaction between triplet combinations becomes significant at high reduced-pressures (Lee, et al., 1978). Higher-order interactions often are small, and thus hidden by imperfection in an EOS; therefore, ternary mixture may provide a better description of multi-component equilibrium in general (Sadus, 1999). Mixing rules that can represent accurately VLE phase behavior of binary mixtures may give unacceptable prediction results for multi-component mixtures (Zavala, 1996). As stated by Soave (1984), vdW

classical mixing rules have been shown to apply well to binary mixture of polar compounds. Unfortunately, as shown by several authors (e.g., Leland, 1980; Gupta, et al., 1980), such rules, although completely adequate for binary systems, fail when applied to some multi-component mixtures. Non-ideality due to size variation represents an additional measure that was considered in modeling multi-component asymmetric mixtures. Therefore, mixing rules evaluation/development must take into consideration the ability to predict correctly the VLE of a mixture of at least three components (BenMekki and Mansoori, 1988).

An extensive literature review of VLE data for ternary and higher asymmetric mixture was conducted. The targeted systems were asymmetric mixtures involving light gases (methane, carbon dioxide, carbon monoxide, nitrogen, hydrogen, and ethane) and n-paraffins extending from eicosane to the highest n-paraffin available. A comprehensive list was compiled from several databases. DECHEMA chemistry data series (Knapp, et al., 1989) provides references to ternary VLE data from 1900 to 1987. Fornari (1990) listed ternary systems investigated between 1978 and 1987. Similarly, Dohn and Brunner (1995) covered the period from 1988 to 1993. In addition, SciFinder Scholar search engine, which covers about 1750 journals, including those that publish VLE data, was used. A complete list of the systems found is presented in Table 10.

Gregorowics, et al. (1992, 1993a, 1993b), Floter, et al. (1998) and Jangkamolkulchai and Lukes (1989) examined the multi-phase behavior, especially liquid-liquid-vapor (LLV) immiscibility phenomena in prototype rich gases dissolved in n-paraffin mixtures. Table 10 shows the temperature and composition ranges for experiments performed.

Table 10. Asymmetric Ternary Mixtures in the Literature

Ternary Mixture Components order: (1)/(2)/(3)	Composition Range	Temperature, K	Reference
Ethane/Propane/Eicosane	x_1 : 0.958 x_3 : 0.0268	310.4 Maximum	Gregorowicz, J.; de Loos, T.; de Swaan A. (1992)
Methane/Ethane/Eicosane	x_1 : 0.0314 - 0.1516 x_3 : 0.0148	290.0 - 307.0	Gregorowicz, J.; Smits, P.; de Loos, T.; de Swaan A. (1993)
Propane/Ethylene/Eicosane	x_1 : 0.0566 - 0.1982 x_3 : 0.0072 - 0.0049	290.5 - 308.0	Gregorowicz, J.; de Loos, T.; de Swaan Arons (1993)
Carbon dioxide/Decane/Eicosane	L-L-V Region	302.2 - 306.2	Huie, N.; Luks, K.; Kohn, J. (1973)
Ethane/Nonadecane/Eicosane	x_1 : 0.2718 - 0.7481	308.3 - 310.4	Kim, Y.; Carfagno, J.; McCaffrey, D.; Kohn, J. (1967)
Methane/Propane/Tetracosane	x_2 : 0.0859 - 0.1501 x_3 : 0.0952 - 0.0852	322.6 - 448.2	Floter, E.; Hollanders, B.; de Loss, T.; de Swaan, A. (1998)
Methane/Docosane/Tetracosane	x_2 : 0.0000 - 0.1026 x_3 : 0.0952 - 0.0000	315.0 - 362.0	Floter, E.; Hollanders, B.; de Loss, T.; de Swaan, A. (1998)
Methane/Decane/Docosane	x_1 : 0.47, 0.45, 0.40 x_3 : 0.05, 0.1, 0.20	293.0 - 423.0	Daridon, J.; Bessieres, D.; Xans, P.; Faissat, B. (1997)
Methane/Ethane/Docosane	x_2 : 0.8477 - 0.9915	298.2 - 303.2	Jangkamolkulchai, A.; Luks, K. (1989)
Methane/Hexane/Hexatricontane	x_3 : 0.5304 - 0.4929 x_1 : 0.0544 - 0.3263	343.2 - 347.2	Hong, S.-P.; Green, K.; Luks, K. (1993)
Carbon dioxide/Hexane/Hexatricontane	x_1 : 0.3329 - 0.5831 x_3 : 0.2640 - 0.0220	337.0 - 323.5	Hong, S.-P.; Luks, K. (1991)
Hydrogen/Carbon Dioxide/Octacosane	x_1 : 0.0164 - 0.088 x_2 : 0.0181 - 0.0964	473.2 - 573.2	Huang, et al. (1988)

Two systems were examined by Hong, et al. (1991) and Hong and Luks (1992) to determine the binary interaction parameters below the melting point for n-paraffins from ternary data. In the two systems listed in Table 10, hexane was used to depress the melting point of hexatriacontane (i.e., which is 348 K).

Molecules that belong to a homologous series and differ only in size (such as, decane/eicosane, nonadecane/eicosane, hexane/hexatriacontane, and docosane/tetracosane) are usually treated with negligible binary interaction parameters. The thermodynamic equilibrium properties of a mixture of chain molecules depend on the chain length (Hijmans, 1961). Thus, an equimolar mixture of C₈ and C₁₆ will have the same molar volume as pure C₁₂ (Marano and Holder, 1997). Ternary mixtures that contain these binary molecules are referred to as quasi-binary systems. Several of the systems listed in Table 10 belong to this category.

Accordingly, the literature data are scarce for asymmetric ternary mixtures involving high molecular weight n-paraffins, limited to low temperatures, and do not cover broad composition ranges for n-paraffins. As observed, most investigators targeted a narrow pressure-temperature window in the phase envelope specific to the system under investigation.

The objective of this work is to investigate the effect of temperature, pressure, solute, and solvent properties in the behavior of asymmetric ternary mixtures. The systems investigated, as presented in Table 1, were systematically selected to determine the effect of these variables; specifically, Ethane is a normal fluid, carbon dioxide represents a quadrupole fluid, and hydrogen is a quantum fluid. The n-paraffin solvent varies to show size effect. The temperature and composition ranges were set by the

available experimental data for binary components that constitute the ternary mixture, where most of the experimental data of binary systems were performed at the Thermodynamic Research Laboratories at Oklahoma State University. Specifically, the composition ranges selected for the ternary mixtures were based on the upper and lower limits of the solute compositions in the corresponding binary mixtures; this is due to the composition dependence of CEOS binary interaction parameters. High composition ranges up to 0.60 mole fractions were used for carbon dioxide and ethane. Hydrogen concentration was limited to a mole fraction of 0.14 due to the high bubble point pressures experienced at higher concentrations. Differences in the lowest temperatures at which the systems were studied were often dictated by the melting points on n-paraffins, which are solids at room temperature.

Following are the experimental results for a total of six asymmetric ternary systems investigated in this study. A schematic diagram of the experimental apparatus was presented in Figure 3. A complete description of the experimental apparatus was given in Chapter III and detailed description of experimental procedures was given in Chapter IV. The uncertainties in measured bubble point pressures (σ_{Bp}), calculated liquid phase compositions (σ_{x_i}) and molar volumes (σ_{Bp}) were determined using error propagation methods detailed in Chapter V, Appendix B and Appendix F. The uncertainties in the reported values are presented with the experimental results. The purities and suppliers of the materials used in this study are listed in Table 4. No further purification of these chemicals was attempted.

High-Pressure Solubility of Ethane and Carbon Dioxide in Eicosane, Octacosane, and Hexatricontane

The solubility and molar volume measurements and the estimated uncertainties of the bubble point pressures, compositions, and molar volumes of mixtures of carbon dioxide and ethane in eicosane, octacosane and hexatricontane are shown in Tables 11-13. As observed with binary mixtures of carbon dioxide (Gasem and Robinson, 1985) and ethane (Gasem, et al., 1989) with n-paraffins, the gas solubility decreases with the rise in temperature.

The PR EOS was used to correlate the experimental data. The PR EOS is:

$$p = \frac{RT}{V - b} - \frac{a}{V(V + b) + b(V - b)} \quad (6-1)$$

where

$$a = a_c \alpha(T) \quad (6-2)$$

$$b = 0.0778 \frac{RT_c}{P_c} \quad (6-3)$$

and

$$a_c = 0.45724 \frac{R^2 T_c^2}{P_c} \quad (6-4)$$

The α function by Gasem, et al. (2001) was used, where

$$\ln(\alpha(T, \omega)) = (2.000 + 0.836T_r)(1 - T_r^{(0.134 + 0.508\omega - 0.0467\omega^2)}) \quad (6-5)$$

Equations (2-1) to (2-4) are the one-fluid mixing rules used in the experimental data evaluation. The parameters for pure components (critical constant, T_c , critical pressure, P_c and the acentric factor, ω) are given in Table 14.

Table 11. Solubility of Carbon Dioxide (1) and Ethane (2) in Eicosane (3)

x_1	x_2	p MPa	V_{Bp} $cm^3/gmol$	T/K	σ_{x_1}	σ_{x_2}	σ_{Bp} MPa	$\sigma_{V_{Bp}}$ $cm^3/gmol$
323.15								
0.0285	0.547	3.21	191		0.0005	0.0015	0.03	1.1
0.0841	0.457	3.37	222		0.0007	0.0017	0.03	1.2
0.1748	0.303	3.63	220		0.0011	0.0019	0.03	1.1
0.2439	0.197	3.71	228		0.0012	0.0012	0.02	1.1
0.3551	0.099	4.48	224		0.0015	0.0010	0.02	1.1
344.26								
0.0289	0.554	4.22	193		0.0005	0.0015	0.03	1.1
0.0852	0.464	4.35	226		0.0007	0.0017	0.03	1.2
0.1771	0.307	4.56	223		0.0011	0.0019	0.04	1.1
0.2478	0.199	4.59	232		0.0012	0.0012	0.03	1.1
0.3594	0.101	5.53	227		0.0015	0.0010	0.02	1.1
373.15								
0.0293	0.563	5.75	197		0.0005	0.0015	0.04	1.1
0.0869	0.473	5.81	230		0.0007	0.0018	0.04	1.2
0.1604	0.323	5.47	229		0.0011	0.0022	0.05	1.1
0.1802	0.312	5.89	227		0.0012	0.0019	0.04	1.1
0.2521	0.203	5.86	236		0.0012	0.0012	0.03	1.1
0.3659	0.102	6.99	231		0.0015	0.0010	0.03	1.1
410.93								
0.1646	0.3310	7.12	235		0.0011	0.0022	0.06	1.2
423.15								
0.0302	0.580	8.50	203		0.0005	0.0015	0.05	1.1
0.0899	0.489	8.40	239		0.0008	0.0018	0.05	1.2
0.1862	0.323	8.14	235		0.0012	0.0020	0.06	1.1
0.2606	0.210	7.92	244		0.0012	0.0012	0.04	1.1
0.3779	0.106	9.28	239		0.0016	0.0011	0.04	1.1

Table 12. Solubility of Carbon Dioxide (1) and Ethane (2) in Octacosane (3)

x_1	x_2	p MPa	V_{Bp} cm^3/gmol	T/K	σ_{x_1}	σ_{x_2}	σ_{Bp} MPa	$\sigma_{V_{Bp}}$ cm^3/gmol
348.15								
0.0455	0.4618	3.33	290		0.0003	0.0008	0.01	0.8
0.1393	0.3374	3.81	300		0.0005	0.0008	0.01	0.9
0.2618	0.2284	4.80	293		0.0007	0.0004	0.02	1.1
0.4165	0.1084	6.27	275		0.0008	0.0003	0.02	1.4
0.5485	0.0588	8.80	237		0.0008	0.0002	0.03	1.4
0.5493	0.0581	8.78	235		0.0009	0.0002	0.03	1.1
373.15								
0.0461	0.4674	4.27	294		0.0003	0.0008	0.01	0.8
0.1411	0.3417	4.74	304		0.0005	0.0008	0.02	0.9
0.2651	0.2312	5.89	297		0.0007	0.0005	0.02	1.1
0.4221	0.1099	7.62	279		0.0008	0.0003	0.02	1.4
0.5541	0.0594	10.73	240		0.0008	0.0002	0.03	1.4
0.5551	0.0587	10.73	238		0.0009	0.0002	0.03	1.1
423.15								
0.0473	0.4799	6.24	303		0.0003	0.0009	0.02	0.8
0.1450	0.3513	6.62	313		0.0005	0.0008	0.02	0.9
0.2723	0.2375	7.97	306		0.0008	0.0007	0.02	1.1
0.4322	0.1125	10.14	287		0.0008	0.0003	0.03	1.4
0.5663	0.0607	14.17	246		0.0009	0.0002	0.04	1.4
0.5672	0.0599	14.16	243		0.0009	0.0002	0.04	1.1

Table 13. Solubility of Carbon Dioxide (1) and Ethane (2) in Hexatricontane (3)

x_1	x_2	p MPa	V_{Bp} cm ³ /gmol	T/K	σ_{x_1}	σ_{x_2}	σ_{Bp} MPa	$\sigma_{V_{Bp}}$ cm ³ /gmol
373.15								
0.0945	0.3576	3.43	396		0.0008	0.0011	0.02	2.1
0.1872	0.2348	3.74	413		0.0009	0.0010	0.02	1.7
0.3304	0.1250	5.09	391		0.0009	0.0006	0.02	1.9
0.4171	0.0479	5.59	386		0.0018	0.0007	0.03	2.1
423.15								
0.0971	0.3675	4.80	408		0.0008	0.0011	0.02	2.1
0.1923	0.2412	5.06	425		0.0009	0.0010	0.02	1.7
0.3394	0.1284	6.62	403		0.0009	0.0007	0.02	1.9
0.4277	0.0491	7.30	396		0.0018	0.0007	0.04	2.1
473.15								
0.0997	0.3774	6.09	420		0.0008	0.0012	0.03	2.1
0.1977	0.2480	6.25	438		0.0010	0.0010	0.03	1.7
0.3482	0.1317	7.92	414		0.0009	0.0007	0.03	1.9
0.4383	0.0504	8.76	407		0.0018	0.0008	0.05	2.1

Table 14. The Critical Properties and Acentric Factors used in the PR CEOS Evaluations

Component	p_c / MPa	T_c / K	ω	Reference
Nitrogen	3.39	126.2	0.039	Reid, et al. (1987)
Hydrogen	1.30	33.2	-0.218	Reid, et al. (1987)
Carbon Monoxide	3.50	132.9	0.066	Reid, et al. (1987)
Carbon Dioxide	7.38	304.2	0.225	Reid, et al. (1987)
Methane	4.60	190.6	0.011	Reid, et al. (1987)
Ethane	3.87	305.3	0.100	Reid, et al. (1987)
C ₃	4.25	369.8	0.153	Reid, et al. (1987)
C ₄	3.80	425.2	0.199	Reid, et al. (1987)
C ₅	3.37	469.7	0.251	Reid, et al. (1987)
C ₆	3.01	507.5	0.299	Reid, et al. (1987)
C ₇	2.74	540.3	0.349	Reid, et al. (1987)
C ₈	2.49	568.8	0.398	Reid, et al. (1987)
C ₉	2.29	594.6	0.445	Reid, et al. (1987)
C ₁₀	2.13	618.8	0.489	Gao, et al. (2001)
C ₁₂	1.83	658.9	0.575	Gao, et al. (2001)
C ₁₆	1.39	720.9	0.737	Gao, et al. (2001)
C ₁₈	1.23	745.5	0.814	Gao, et al. (2001)
C ₁₉	1.16	756.6	0.851	Gao, et al. (2001)
C ₂₀	1.09	766.9	0.888	Gao, et al. (2001)
C ₂₁	1.03	776.6	0.925	Gao, et al. (2001)
C ₂₂	0.97	785.7	0.961	Gao, et al. (2001)
C ₂₄	0.87	802.3	1.031	Gao, et al. (2001)
C ₂₈	0.71	830.3	1.167	Gao, et al. (2001)
C ₃₆	0.48	871.5	1.421	Gao, et al. (2001)
C ₄₄	0.34	899.8	1.656	Gao, et al. (2001)

The PR EOS predictive ability of ternary mixtures bubble point pressures based on binary interaction parameters (BIP) (C_{ij} , D_{ij}) is presented. BIPs were determined by fitting the experimental data to minimize the objective function, SS, which represents the sum of squared-relative deviations in bubble point pressure, i.e.:

$$SS = \sum_i^n \left(\frac{P_{cal} - P_{exp}}{P_{exp}} \right)_i^2 \quad (6-6)$$

The BIPs for the carbon dioxide/ethane and carbon dioxide/hydrogen (for carbon dioxide/hydrogen/n-paraffins referred to later) systems were regressed from VLE data in the subcritical region and were linearly extrapolated to the operating temperature range used in this work. Another analysis was made by regressing the BIPs from ternary data, where the other two binary temperature-dependent interaction parameters are given (i.e., carbon dioxide/n-paraffin; ethane/n-paraffin for carbon dioxide/ethane/n-paraffin). An upper and lower bounds were placed on the regressed BIPs to avoid unrealistic values (for ethane/carbon dioxide: -0.02 min and 0.5 max; for hydrogen/carbon dioxide: -0.53 min and 0.3 max).

For some systems, more than one data source was available, and where binary interaction parameters vary, the evaluation of BIPs from different sources was considered in some cases.

The experimental data were limited to bubble point pressures and the corresponding liquid densities. The dew point pressures and corresponding densities are presented for selected systems in Appendix F. Bubble point pressure can be determined accurately; therefore, its been used to validate one-fluid mixing rules extensions to ternary mixtures. Most equations of state show moderate success in calculation of liquid

densities without additional tuning. A brief review of several techniques used to improve CEOS determined liquid densities is given by Shaver (1993).

The ability of the PR EOS to predict/represent the experimental data is shown in Table 15. As indicated in Table 15, the prediction results improved significantly, when two temperature-*independent* interaction parameters per binary system were used. This is in agreement with an earlier observation of many investigators (Gasem and Robinson, 1985; Gasem, et al., 1989; Peters, 1986) who modeled asymmetric binary mixtures, particularly, ethane/n-paraffin and carbon dioxide/n-paraffin binaries. As presented in Tables 16, 17 and 18, the predictive ability of PR EOS to ternary mixtures bubble point pressure is as good as its representation of its binaries when two temperature-*independent* interaction parameters per binary were used. The prediction results did not improve when two temperature-*dependent* interaction parameters per binary system were used as is typically experienced with binary mixtures.

To evaluate the predictive ability of EOS, two issues were examined: first, the precision of the experimental data, and second, the accuracy of the linearly-extrapolated interaction parameters for the carbon dioxide/ethane binary, determined in the subcritical region (show a linear trend in subcritical region), in predicting the ternary mixture bubble point pressure. Experimental data were regressed using two temperature-*dependent* interaction parameters per system (i.e., total of six for ternary mixture). The PR EOS was capable of representing the bubble point pressures within the experimental uncertainties, which indicates the precision of the experimental data. The temperature-*dependent* interaction parameters for carbon dioxide/ethane were regressed from ternary data within upper and lower constraints; the results for this case are presented in Table 19. Only one

Table 15. PR EOS Prediction/Representation of Carbon Dioxide /Ethane/n-Paraffin Systems Based on Binary Interaction Parameters*(Extrapolated)

CN	T, K	C_{ij}	$C_{ij}(T)$	C_{ij}, D_{ij}	$C_{ij}(T), D_{ij}(T)$	$C_{ij}(T), D_{ij}(T)$	NPTS
		%AAD in Bubble Point Pressure					
					Prediction	Regression**	
20	323.15	7.8	5.2	2.5	3.2	0.8	5
	344.26		5.1		***	0.8	5
	373.15		5.4		3.1	0.7	5
	423.15		6.0		***	1.2	5
28	348.15	13.9	11.4	3.9	4.1	0.4	6
	373.15		13.4		4.5	0.6	6
	423.15		18.8		6.8	0.4	6
36	373.15	10.2	11.8	2.6	3.2	1.0	4
	423.15		10.8		2.5	0.1	4
	473.15		13.0		5.2	0.0	4
%AAD		10.6	10.1	3.0	4.1	0.6	50

* Extrapolated carbon dioxide/ethane interaction parameter.

** Two binary interaction parameters per binary system (total of six for ternary mixture).

*** Binary data were not available at this isotherm.

Table 16. PR Equation-of-State Prediction/Representation of the Solubilities of Carbon Dioxide (1) and Ethane (2) in Eicosane (3)

T/ K	Binary Interaction Parameters		% AAD in Bubble Point Pressure			Ref.
			Binary	Ternary		
				Prediction	Regression**	
323.15	C ₁₂	0.1979 {0.5}				62*
	C ₁₃ , D ₁₃	0.1074, -0.0034	0.5	3.2	0.8	18
	C ₂₃ , D ₂₃	0.0177, -0.0206	0.7	{1.6}		64
373.15	C ₁₂	0.2779 {0.5}				62*
	C ₁₃ , D ₁₃	0.0981, -0.0080	0.3	3.1	0.7	18
	C ₂₃ , D ₂₃	0.0150, -0.0213	0.7	{2.9}		64
323.15- 423.15	C ₁₂	0.278 {0.5}				62*
	C ₁₃ , D ₁₃	0.1007, -0.0035	3.9	2.5		18
	C ₂₃ , D ₂₃	0.0165, -0.0227	2.8	{2.0}		64
323.15	C ₁₂	0.1979 {0.5}				62*
	C ₁₃	0.097	1.1	5.2		18
	C ₂₃	-0.0061 (-0.025)	(7.3)	{3.6} (9.4)		20*, 64
344.26	C ₁₂	0.2317 {0.5}				62*
	C ₁₃	0.0900		5.1		18*
	C ₂₃	-0.0110		{4.3}		20*
373.15	C ₁₂	0.2779 {0.5}				62*
	C ₁₃	0.0780	1.4	5.3		20
	C ₂₃	-0.0132 (-0.023)	(8.3)	(7.3) {5.1}		20*, 64
423.15	C ₁₂	0.3579 {0.5}				62*
	C ₁₃	0.0575		6.0		18*
	C ₂₃	-0.015 (-0.049)	(4.7)	(11.2) {6.1}		20*, 64
323.15- 423.15	C ₁₂	0.278 {0.5}				62*
	C ₁₃	0.090	3.8	7.8		18
	C ₂₃	-0.03	7.2	{9.0}		64

* Indicates extrapolation or interpolation of binary interaction parameters values.

** Two binary interaction parameters per binary system (total of six for ternary mixture).

{ } Indicated regressed carbon dioxide/ethane binary interaction parameter from ternary data.

() Alternative interaction parameter.

Table 17. PR Equation-of-State Prediction/Representation of the Solubilities of Carbon Dioxide (1) and Ethane (2) in Octacosane (3)

T/ K	Binary Interaction Parameters	% AAD in Bubble Point Pressure			Ref.
		Binary	Ternary		
			Prediction	Regression**	
348.15	C ₁₂	0.2379 {-0.02}			62*
	C ₁₃ , D ₁₃	0.1125, -0.0110	0.3	4.1	18
	C ₂₃ , D ₂₃	-0.0022, -0.0166	1.1	{3.5}	64
373.15	C ₁₂	0.2779 {-0.02}			62*
	C ₁₃ , D ₁₃	0.1112, -0.0129	0.4	4.5	18
	C ₂₃ , D ₂₃	-0.0062, -0.0159	1.1	{3.5}	64
423.15	C ₁₂	0.3579 {-0.02}			62*
	C ₁₃ , D ₁₃	0.1086, -0.0178	1.9	6.8	18
	C ₂₃ , D ₂₃	-0.0113, -0.0213	0.6	{5.4}	64
348.15- 423.15	C ₁₂	0.298 {-0.02}			62*
	C ₁₃ , D ₁₃	0.1163, -0.0145	3.0	3.9	18
	C ₂₃ , D ₂₃	-0.0007, -0.0187	2.9	{2.9}	64
348.15	C ₁₂	0.2379 {-0.02}			62*
	C ₁₃	0.0760	6.4	11.4	18
	C ₂₃	-0.052	6.1	{11.2}	64
373.15	C ₁₂	0.2779 {-0.02}			62*
	C ₁₃	0.058	3.7	13.4	18
	C ₂₃	-0.058	6.8	{12.8}	64
423.15	C ₁₂	0.3579 {-0.02}			62*
	C ₁₃	0.0270	6.2	18.8	18
	C ₂₃	-0.054 (-0.085)	(4.8)	{11.8}	21*, 64
348.15- 423.15	C ₁₂	0.298 {-0.02}			62*
	C ₁₃	0.06	7.2	13.9	18
	C ₂₃	-0.06	7.1	{13.3}	64

* Indicates extrapolation or interpolation of binary interaction parameters values.

** Two binary interaction parameters per binary system (total of six for ternary mixture).

{ } Indicated regressed carbon dioxide/ethane binary interaction parameter from ternary data.

() Alternative interaction parameter.

Table 18. PR Equation-of-State Prediction/Representation of the Solubilities of Carbon Dioxide (1) and Ethane (2) in Hexatricontane (3)

T/ K	Binary Interaction Parameters	% AAD in Bubble Point Pressure			Ref.
		Binary	Ternary		
			Prediction	Regression**	
373.15	C ₁₂	0.2779 {-0.02}			62*
	C ₁₃ , D ₁₃	0.1014, -0.0113	0.7	3.2	18
	C ₂₃ , D ₂₃	-0.0062, -0.0168	0.7	{2.5}	64
423.15	C ₁₂	0.3579 {-0.02}			62*
	C ₁₃ , D ₁₃	0.1240, -0.0186	0.7	2.5	18
	C ₂₃ , D ₂₃	-0.0010, -0.0215	1.3	{1.5}	64
473.15	C ₁₂	0.4379 {-0.02}			62*
	C ₁₃ , D ₁₃	0.0693, -0.0096	1.1	5.2	14
	C ₂₃ , D ₂₃	-0.0194, -0.0180	1.2	{3.6}	14
373.15- 473.15	C ₁₂	0.358 {-0.02}			62*
	C ₁₃ , D ₁₃	0.1065, -0.0133	2.4	2.6	18
	C ₂₃ , D ₂₃	-0.0056, -0.0180	2.1	{1.7}	64
373.15	C ₁₂	0.2779 {-0.02}			62*
	C ₁₃	0.0316	5.0	11.8	18
	C ₂₃	-0.083	7.6	{11.2}	64
423.15	C ₁₂	0.3579 {-0.02}			62*
	C ₁₃	0.019	6.2	10.8	18
	C ₂₃	-0.087	7.9	{9.7}	64
473.15	C ₁₂	0.4379 {-0.02}			62*
	C ₁₃	-0.007	2.4	13.0	14
	C ₂₃	-0.103	3.9	{11.8}	64
373.15- 473.15	C ₁₂	0.358 {-0.02}			62*
	C ₁₃	0.027	5.7	10.2	18
	C ₂₃	-0.085	7.8	{9.1}	64

* Indicates extrapolation or interpolation of binary interaction parameters values.

** Two binary interaction parameters per binary system (total of six for ternary mixture).

{ } Indicated regressed carbon dioxide/ethane binary interaction parameter from ternary data.

() Alternative interaction parameter.

temperature-*dependent* interaction parameter (C_{ij}) for the carbon dioxide/ethane binary was regressed per isotherm (D_{12} insignificant for nearly equal molecular sizes), using two temperature-*dependent* interaction parameters for the other two binaries (carbon dioxide/n-paraffin and ethane/n-paraffin). Despite the difference between the extrapolated and correlated binary interaction parameter (C_{12}) values used in predicting ternary mixture bubble point pressures, both %AAD in asymmetric ternary mixture bubble point pressure predictions are comparable as shown in Tables 15 and 19. Accordingly, the difference between the prediction and representation results of ternary mixture bubble point pressures when using two temperature-*dependent* interaction parameters per binary system may be the degree of precision of binary and ternary bubble point pressure measurements, and consequently, the uncertainties in BIPs applied

High-Pressure Solubility of Hydrogen and Carbon Dioxide in Eicosane, Octacosane, and Hexatricosane

Tables 20 through 22 present solubility and molar volume measurements and the expected uncertainties in the reported experimental data for the ternary mixtures of carbon dioxide and hydrogen in eicosane, octacosane, and hexatricosane. The solubility behavior of the mixtures depends on the composition of the gas mixture. The carbon dioxide dominated mixture shows a decrease in solubility with rise in temperature, this is in contrary to hydrogen-dominated mixtures.

Table 19. PR EOS Prediction/Representation of Carbon Dioxide /Ethane/n-Paraffin Systems Based on Binary Interaction Parameters* (Regressed)

CN	T, K	C_{ij}	$C_{ij}(T)$	C_{ij}, D_{ij}	$C_{ij}(T), D_{ij}(T)$	$C_{ij}(T), D_{ij}(T)$	NPTS
		%AAD in Bubble Point Pressure				Prediction	
20	323.15	9.0	3.6	2.0	1.6	0.8	5
	344.26		4.3		***	0.8	5
	373.15		5.1		2.9	0.7	5
	423.15		6.1		***	1.2	5
28	348.15	13.3	11.2	2.9	3.5	0.4	6
	373.15		13.4		3.5	0.6	6
	423.15		11.8		5.4	0.4	6
36	373.15	9.1	11.2	1.7	2.5	1.0	4
	423.15		9.7		1.5	0.1	4
	473.15		11.8		3.6	0.0	4
%AAD		10.5	8.82	2.2	3.1	0.6	50

* Regressed carbon dioxide/ethane interaction parameter from ternary Data.

** Two binary interaction parameters per binary system (total of six for ternary mixture).

*** Binary data were not available at this isotherm.

Table 20. Solubility of Carbon Dioxide (1) and Hydrogen (2) in Eicosane (3)

x_1	x_2	p MPa	V_{Bp} $cm^3/gmol$	T/K	σ_{x_1}	σ_{x_2}	σ_{Bp} MPa	$\sigma_{V_{Bp}}$ $cm^3/gmol$
323.15								
0.0800	0.1108	13.94	299		0.0008	0.0006	0.08	0.8
0.1640	0.0688	9.79	288		0.0013	0.0004	0.05	0.9
0.2451	0.0568	8.95	264		0.0014	0.0005	0.07	0.9
0.3271	0.0322	7.78	250		0.0016	0.0005	0.06	1.0
0.4124	0.0143	6.44	230		0.0013	0.0003	0.04	1.1
344.26								
0.0812	0.1126	13.17	304		0.0008	0.0006	0.08	0.8
0.1665	0.0698	9.46	293		0.0013	0.0004	0.05	0.9
0.2484	0.0575	8.70	268		0.0014	0.0005	0.07	0.9
0.3316	0.0327	7.97	254		0.0016	0.0005	0.06	1.0
0.4184	0.0145	7.25	233		0.0013	0.0003	0.05	1.1
373.15								
0.0830	0.1151	12.03	311		0.0008	0.0006	0.07	0.8
0.1702	0.0714	8.51	300		0.0014	0.0004	0.05	0.9
0.2534	0.0587	8.52	274		0.0014	0.0006	0.07	0.9
0.3380	0.0333	8.55	259		0.0017	0.0005	0.07	1.0
0.4252	0.0147	8.51	237		0.0013	0.0003	0.05	1.1
423.15								
0.0863	0.1197	10.77	324		0.0008	0.0007	0.07	0.8
0.1767	0.0741	8.80	312		0.0014	0.0004	0.05	0.9
0.2623	0.0608	8.44	284		0.0015	0.0006	0.06	0.9
0.3496	0.0344	9.69	268		0.0017	0.0005	0.06	1.0
0.4393	0.0152	10.43	246		0.0014	0.0003	0.04	1.1

Table 21. Solubility of Carbon Dioxide (1) and Hydrogen (2) in Octacosane (3)

x_1	x_2	p MPa	V_{Bp} $cm^3/gmol$	T/K	σ_{x_1}	σ_{x_2}	σ_{Bp} MPa	$\sigma_{V_{Bp}}$ $cm^3/gmol$
348.15								
0.1994	0.0945	10.719	380		0.0006	0.0004	0.04	1.6
0.3260	0.0620	9.890	337		0.0007	0.0003	0.04	2.1
0.4536	0.0361	9.928	290		0.0008	0.0002	0.03	1.4
0.5697	0.0195	10.625	243		0.0009	0.0002	0.04	1.2
373.15								
0.2025	0.0959	10.452	387		0.0006	0.0004	0.04	1.6
0.3306	0.0628	10.064	342		0.0007	0.0003	0.03	2.1
0.4594	0.0366	10.769	294		0.0008	0.0002	0.03	1.4
0.5757	0.0198	12.269	246		0.0009	0.0002	0.04	1.2
423.15								
0.2090	0.0991	10.048	400		0.0006	0.0004	0.04	1.6
0.3401	0.0646	10.717	353		0.0008	0.0003	0.03	2.1
0.4710	0.0375	12.477	302		0.0009	0.0002	0.03	1.4
0.5881	0.0202	15.296	252		0.0010	0.0002	0.04	1.2

Table 22. Solubility of Carbon Dioxide (1) and Hydrogen (2) in Hexatricontane (3)

x_1	x_2	p MPa	V_{Bp} cm^3/gmol	T/K	σ_{x_1}	σ_{x_2}	σ_{Bp} MPa	$\sigma_{V_{Bp}}$ cm^3/gmol
373.15								
0.1640	0.1396	12.02	477		0.0006	0.0007	0.06	2.1
0.2576	0.0990	10.35	446		0.0012	0.0003	0.04	2.4
0.2734	0.0515	6.59	469		0.0010	0.0002	0.03	1.8
0.4700	0.0356	9.49	358		0.0009	0.0003	0.04	2.1
423.15								
0.1692	0.1440	10.82	493		0.0006	0.0007	0.06	2.1
0.2651	0.1018	10.05	460		0.0012	0.0003	0.04	2.4
0.2820	0.0531	6.89	484		0.0013	0.0002	0.03	1.8
0.4810	0.0364	10.92	367		0.0009	0.0003	0.04	2.1
473.15								
0.1742	0.1482	10.39	508		0.0006	0.0007	0.06	2.1
0.2726	0.1047	10.13	474		0.0012	0.0004	0.05	2.4
0.2886	0.0543	7.45	497		0.0013	0.0003	0.04	1.8
0.4911	0.0372	12.21	375		0.0009	0.0003	0.05	2.1

The predictive ability of the PR EOS using one-fluid mixing rules and employing binary interaction parameters is presented in Table 23. The accuracy of the prediction for the ternary experimental data depends on the fit of the binary systems, which form the boundaries of the ternary system (Shibata and Sandler, 1989). As shown in Tables 24, 25, and 26, the predictive ability is as good as the representation of the binaries when one or two temperature-*independent* interaction parameters were used. The prediction results did not improve when one or two temperature-*dependent* interaction parameters per binary system were used as is typically experienced with some binary mixtures. As presented in Tables C1-C3, PR EOS representation of hydrogen/n-paraffin asymmetric binary mixtures is better using one temperature-*dependent* interaction parameter in comparison to two temperature-*independent* interaction parameters, which is in contrary to ethane/n-paraffin mixtures. Carbon dioxide/n-paraffins show almost no difference in this comparison. Using one temperature-*dependent* interaction parameter did not show any noticeable improvement, this is similar to CO₂/C₂₈ and CO₂/C₃₆ results shown in Table C1. Accordingly, the high concentrations of carbon dioxide have dominated influence over that of hydrogen.

The PR EOS was able to represent ternary mixture data within the experimental uncertainties of our experimental data, in most cases, when two temperature-*dependent* interaction parameters were used per binary; this indicates the precision of the experimental data. The use of regressed BIPs from high temperature ternary data show moderate improvement in the bubble point pressure predictions over BIPs determined from the extrapolated temperature-*dependent* interaction parameter from hydrogen/carbon

Table 23. PR EOS Prediction/Representation of Carbon Dioxide /Hydrogen /n-Paraffin Systems Based on Binary Interaction Parameters* (Extrapolated)

CN	T, K	C _{ij}	C _{ij} (T)	C _{ij} , D _{ij}	C _{ij} (T), D _{ij} (T)	C _{ij} (T), D _{ij} (T)		NPTS
						%AAD in Bubble Point Pressure		
						Prediction	Regression**	
20	323.15	5.0	6.7	4.5	7.1	0.8		4
	344.26		5.3		***	0.3		4
	373.15		5.2		3.8	2.2		4
	423.15		4.3		***	0.4		4
28	348.15	9.1	7.1	3.0	4.3	1.3		4
	373.15		8.8		2.9	0.6		4
	423.15		11.9		2.8	0.1		4
36	373.15	5.2	7.2	2.5	1.6	0.1		4
	423.15		5.1		0.9	0.2		4
	473.15		8.4		2.5	0.0		4
%AAD		6.4	5.18.0	3.3	3.2	0.08		40

* Extrapolated carbon dioxide/hydrogen binary interaction parameter.

** Two binary interaction parameters per binary system (total of six for ternary mixture).

*** Binary data were not available at this isotherm.

Table 24. PR Equation-of-State Prediction/Representation of the Solubilities of Carbon Dioxide (1) and Hydrogen (2) in Eicosane (3)

T/ K	Binary Interaction Parameters		% AAD in Bubble Point Pressure			Ref.
			Binary	Ternary		
				Prediction	Regression**	
323.15	C ₁₂	-0.053 {-0.5}				63*
	C ₁₃ , D ₁₃	0.1074, -0.0034	0.5	7.1	0.8	18
	C ₂₃ , D ₂₃	0.1255, 0.0055	0.3	{3.4}		50
373.15	C ₁₂	-0.098 {0.3}				63*
	C ₁₃ , D ₁₃	0.0981, -0.0080	0.3	3.8	2.2	18
	C ₂₃ , D ₂₃	0.1036, 0.0043	0.6	{2.1}		50
323.15- 423.15	C ₁₂	-0.098				63*
	C ₁₃ , D ₁₃	0.1007, -0.0035	3.9	4.5		18
	C ₂₃ , D ₂₃	0.2294, 0.0000	5.1			47
323.15	C ₁₂	-0.0533 {-0.5}				63*
	C ₁₃	0.097	1.1	6.7		18
	C ₂₃	0.254	0.5	{5.9}		50
344.26	C ₁₂	-0.0723				63*
	C ₁₃	0.0900		5.3		18*
	C ₂₃	0.2266				50*
373.15	C ₁₂	-0.098 {0.3}				63*
	C ₁₃	0.078	1.4	5.2		20
	C ₂₃	0.199	0.6	{4.5}		50
423.15	C ₁₂	-0.143				63*
	C ₁₃	0.0575		4.3		18*
	C ₂₃	0.1447	0.3			50
323.15- 423.15	C ₁₂	-0.098				63*
	C ₁₃	0.090	3.8	5.0		18
	C ₂₃	0.2294	5.1			47

* Indicates extrapolation or interpolation of binary interaction parameters values.

** Two binary interaction parameters per binary system (total of six for ternary mixture).

{ } Indicated regressed carbon dioxide/hydrogen binary interaction parameter from ternary data.

() Alternative interaction parameter.

Table 25. PR Equation-of-State Prediction/Representation of the Solubilities of Carbon Dioxide (1) and Hydrogen (2) in Octacosane (3)

T/ K	Binary Interaction Parameters	% AAD in Bubble Point Pressure			Ref.
		Binary	Ternary		
			Prediction	Regression**	
348.15	C ₁₂	-0.076 {-0.5}			63*
	C ₁₃ , D ₁₃	0.1125, -0.0110	0.3	4.3	1
	C ₂₃ , D ₂₃	0.142, 0.0066	0.2	{2.2}	50
373.15	C ₁₂	-0.098 {-0.5}			63*
	C ₁₃ , D ₁₃	0.1112, -0.0129	0.3	2.9	18
	C ₂₃ , D ₂₃	0.1661, 0.0044	0.1	{1.2}	50
423.15	C ₁₂	-0.143 {0.114}			63*
	C ₁₃ , D ₁₃	0.1086, -0.0178	1.9	2.8	18
	C ₂₃ , D ₂₃	0.1104, 0.0057	0.4	{1.0}	50
348.15- 423.15	C ₁₂	-0.109			63*
	C ₁₃ , D ₁₃	0.1163, -0.0145	2.9	3.0	18
	C ₂₃ , D ₂₃	0.1127, 0.0059	3.5		3
348.15	C ₁₂	-0.0758			63*
	C ₁₃	0.0760	6.4	7.1	18
	C ₂₃	0.3550	0.5		50
373.15	C ₁₂	-0.0980			63*
	C ₁₃	0.058	(5.6)	8.8	18
	C ₂₃	0.3070	0.4		50
423.15	C ₁₂	-0.1433			63*
	C ₁₃	0.027	6.2	11.9	18
	C ₂₃	0.1928	0.4		50
348.15- 423.15	C ₁₂	-0.109			63*
	C ₁₃	0.06	7.2	9.1	18
	C ₂₃	0.2775	2.2		47

* Indicates extrapolation or interpolation of binary interaction parameters values.

** Two binary interaction parameters per binary system (total of six for ternary mixture).

{ } Indicated regressed carbon dioxide/hydrogen binary interaction parameter from ternary data.

() Alternative interaction parameter.

Table 26. PR Equation-of-State Prediction/Representation of the Solubilities of Carbon Dioxide (1) and Hydrogen (2) in Hexatricontane (3)

T/ K	Binary Interaction Parameters	% AAD in Bubble Point Pressure			Ref.
		Binary	Ternary		
			Prediction	Regression**	
373.15	C ₁₂	-0.098 {-0.047}			63*
	C ₁₃ , D ₁₃	0.1014, -0.0113	0.7	1.6	18
	C ₂₃ , D ₂₃	0.47, 0.00	0.8	{0.6}	50
423.15	C ₁₂	-0.1427 {-0.004}			63*
	C ₁₃ , D ₁₃	0.1240, -0.0186	0.7	0.9	18
	C ₂₃ , D ₂₃	0.2346, 0.0034	0.3	{0.8}	50
473.15	C ₁₂	-0.188 {0.30}			63*
	C ₁₃ , D ₁₃	0.0693, -0.0096	1.1	2.5	14
	C ₂₃ , D ₂₃	0.3503, -0.0002	3.7	{0.9}	47
373.15- 473.15	C ₁₂	- 0.143			63*
	C ₁₃ , D ₁₃	0.1065, -0.0133	2.4	2.5	18
	C ₂₃ , D ₂₃	0.178, 0.006	2.5		50
373.15	C ₁₂	- 0.098 {-0.6514}			63*
	C ₁₃	0.0316	5.0	7.2	18
	C ₂₃	0.4730	0.8	{5.6}	50
423.15	C ₁₂	- 0.1427{-0.0046}			63*
	C ₁₃	0.0190	6.2	5.1	18
	C ₂₃	0.3720	0.5	{5.3}	50
473.15	C ₁₂	- 0.1880 {-1.463}		8.4	63*
	C ₁₃	- 0.0070	2.4	(7.1)	14
	C ₂₃	0.2710 (.35)	(3.61)	{6.7}	50*, 47
373.15- 473.15	C ₁₂	- 0.1430			63*
	C ₁₃	0.0270	5.7	5.2	18
	C ₂₃	0.4330	2.7		50

* Indicates extrapolation or interpolation of binary interaction parameters values.

** Two binary interaction parameters per binary system (total of six for ternary mixture).

{ } Indicated regressed carbon dioxide/hydrogen binary interaction parameter from ternary data.

() Alternative interaction parameter.

dioxide subcritical region. Accordingly, the difference between the prediction and representation results of ternary mixture bubble point pressures when using two temperature-*dependent* interaction parameters per binary system may be due to the degree of uncertainties of binary and ternary bubble point pressure measurements, and consequently, the uncertainties in BIPs applied.

Summary

Solubility measurements of ternary mixtures of hydrogen and carbon dioxide in eicosane, octacosane, and hexatricosane were determined at 323.15, 344.26, 373.15 and 423.15 K and pressures to 15.3 MPa. Similarly, solubility measurements of ethane and carbon dioxide in eicosane, octacosane, and hexatricosane were determined at 323.15, 344.26, 373.15 and 423.15 K and pressures to 14.17 MPa.

For the carbon dioxide/hydrogen/n-paraffin systems investigated, the predictive ability of the PR EOS with one-fluid mixing rules is as good as its representation of its binaries when one or two temperature-independent parameters are used. For the carbon dioxide/ethane/n-paraffin systems examined, the PR EOS with one-fluid mixing rules is capable of predicting ternary mixture bubble point pressures with the same accuracy as it represents its binaries when two temperature-independent parameters are used per binary mixture. In conclusion, the concept of pair-wise interactions is justified for one-fluid mixing rules when size effect is taken into consideration, particularly with mixtures involving ethane.

CHAPTER VII

NEW MIXING RULES BASED ON EXCESS HELMHOLTZ FREE ENERGY

1. EVALUATION WITH BINARY MIXTURES

The objectives in this chapter are to: (a) develop a new semi-theoretical mixing rule for the covolume to account for the non-ideality of asymmetric mixtures, (b) evaluate several combinatorial expressions using infinite-dilution activity coefficient and VLE data of ethane/n-paraffins, and (c) evaluate the applicability of new and recently developed thermodynamic models (PR EOS + mixing rules + UNIFAC) based on excess free energy mixing rules (CHV and LCVM) and the commonly used one-fluid mixing rules as they apply to binary mixtures. Evaluation with ternary mixtures is examined in Chapter VIII.

Model Development

In this study, a new semi-theoretical expression for the CEOS covolume was developed. The new expression is based on equating combinatorial contribution to excess Helmholtz free energy determined from the CEOS with a corresponding one determined from the lattice model at infinite pressure, thus making use of the nearly pressure-independent Helmholtz free energy. Following is the model derivation.

For the PR EOS, the fugacity coefficient of a component in a mixture is expressed

as:

$$\ln \hat{\phi}_i = -\ln(Z-B) + \frac{\bar{b}_i}{b} (Z-1) - \frac{a}{2\sqrt{2} bRT} \left[\frac{\bar{a}_i}{na} - \frac{\bar{b}_i}{b} \right] \ln \left[\frac{Z+2.414B}{Z-0.414B} \right] \quad (7-1)$$

where $B = \frac{bp}{RT}$ and $Z = \frac{pV}{RT}$

and

$$\bar{a}_i = \frac{\partial n^2 a}{\partial n_i} \quad (7-2)$$

and

$$\bar{b}_i = \frac{\partial nb}{\partial n_i} \quad (7-3)$$

The excess Gibbs and Helmholtz energies can be determined from the EOS fugacity coefficients, where

$$\frac{G^{exe}}{RT} = \ln \phi - \sum z_i \ln \phi_i \quad (7-4)$$

and

$$\frac{A^{exe}}{RT} = \frac{G^{exe}}{RT} - \frac{PV^{exe}}{RT} \quad (7-5)$$

From the above, the excess Helmholtz energy is derived as:

$$\begin{aligned} \frac{A^{exe}}{RT} = & \sum z_i \ln \left(\frac{Z_i - B_i}{Z - B} \right) + \frac{\tilde{A}}{2\sqrt{2}B} \ln \left(\frac{Z - 0.414B}{Z + 2.414B} \right) - \\ & \sum z_i \frac{\tilde{A}_i}{2\sqrt{2}B_i} \ln \left(\frac{Z_i - 0.414B_i}{Z_i + 2.414B_i} \right) \end{aligned} \quad (7-6)$$

where $\tilde{A} = \frac{ap}{R^2T^2}$

The CEOS constant “a” was related to excess Helmholtz free energy by several authors (Wong and Sandler, 1992; Orbey and Sandler, 1995a,b; Orbey and Sandler, 1997). A similar expression as used by Orbey and Sandler (1997) in the CHV model is used in this work. The expression is given as:

$$\alpha = \frac{a}{bRT} = \frac{1}{C_N} \left[\frac{A^{exe}}{RT} + (1 - \delta_1) \sum_1^{NC} z_i \ln \frac{b}{b_i} \right] + \sum_1^{NC} z_i \frac{a_i}{b_i RT} \quad (7-7)$$

From Equation (7-6), the excess Helmholtz combinatorial expression is

$$\frac{A_{comb}^{exe}}{RT} = \sum z_i \ln \left(\frac{Z_i - B_i}{Z - B} \right) = \sum z_i \ln \left(\frac{V_i - b_i}{V - b} \right) \quad (7-8)$$

Where the combinatorial contribution does not contain the attraction constant that accounts for molecular attractions.

$$\frac{A_{comb}^{exe}}{RT} = \sum z_i \ln \left(\frac{\frac{V_i - b_i}{b_i}}{\frac{V - b}{b}} \right) + \sum z_i \ln \left(\frac{b_i}{b} \right) \quad (7-9)$$

The excess Helmholtz combinatorial expression was determined from the lattice model, where no free sites exist. Thus at infinite pressure, the molecules are so closely packed that there is no free volume (Wong and Sandler, 1992), i.e.,

$$\lim_{p \rightarrow \infty} V = b \quad (7-10)$$

$$\lim_{p \rightarrow \infty} V_i = b_i \quad (7-11)$$

Assuming a constant packing factor (V/b) larger than unity for pure substances and their mixtures at any temperature (Orbey and Sandler, 1995b), this leads to:

$$\left(\frac{A_{\text{comb}}^{\text{exe}}}{RT}\right)_{p \rightarrow \infty} = \left[\sum z_i \ln\left(\frac{b_i}{b}\right)\right]_{p \rightarrow \infty} = \sum z_i \ln\left(\frac{b_i}{b}\right) \quad (7-12)$$

In addition, excess Helmholtz energy is nearly pressure independent, then

$$b = \exp\left(\sum_i z_i \ln b_i - \frac{A_{\text{comb}}^{\text{exe}}}{RT}\right) \quad (7-13)$$

As defined in Equation (7-13), the covolume “b” is dependent on CEOS pure-component covolume “b_i” and the excess Helmholtz combinatorial expression.

The pure-component covolume for the PR EOS is defined as:

$$b_i = 0.0778 R \frac{T_c}{P_c} \quad (7-14)$$

The pure-component covolume depends on the accuracy of the pure component critical constants. Therefore, the Asymptotic Behavior Correlations (ABC) for n-paraffin critical constants recently developed by Gao, et al. (2001) were used in this work. The ABC correlations can represent the available experimental data for critical temperature and pressure with accuracy of 0.2% and 0.8%, respectively. The critical constants are listed in Table 14.

A second model was developed in this work based on equating the residual contribution from the EOS to a corresponding one derived from the local composition model. The residual contribution from the PR EOS was extracted from Equation (7-7) by retaining only the contributions due to molecular attractions. The equation is

$$\alpha = \frac{1}{C_N} \left(\frac{A_{\text{residual}}^{\text{exe}}}{RT}\right) + \sum_1^{\text{NC}} z_i \frac{a_i}{b_i RT} \quad (7-15)$$

In evaluating Equation (7-15), both Equation (7-13) and a linear mixing rule for the covolume were used.

Evaluation of Excess Free Energy Combinatorial Expressions

A recent article by Abildskov (2001) expressed the importance of combinatorial terms for some mixtures, and how they can be essential to the success of models based on UNIFAC or UNIQUAC. Three recently developed models (Orbey and Sandler, 1997; Boukouvalas, 1994; Zhong and Musuoka, 1996) specifically targeted mixtures that contain components with large differences in size. All these models used an excess Gibbs or Helmholtz free energy expressions based on the original UNIFAC combinatorial expression that is known for its inaccuracy, with the exception of Zhong and Musuoka (1996), where a correction factor to excess Gibbs free energy was used. Equations (7-7) and (7-13) reveal that the accuracy of the combinatorial contribution to excess Helmholtz free energy has a direct impact on EOS energy and covolume constants.

For athermal mixtures (i.e., those that mix without any energetic effects) of molecules of arbitrary size and shape (Guggenheim, 1952),

$$\left(\frac{A^{\text{exe}}}{RT}\right)_{\text{athermal}} = -\left(\frac{S^{\text{exe}}}{R}\right)_{\text{comb}} \quad (7-16)$$

Where an expression for excess entropy can be determined from statistical mechanics as shown in Equation (2-29) and partially listed in final form in Table 3.

At low to moderate pressures (Hildebrand and Scott (1964)),

$$\left(A^{\text{exe}}\right)_{T,V} \approx \left(G^{\text{exe}}\right)_{T,P} \quad (7-17)$$

The approximation in Equation (7-17) was used only in calculating infinite-dilution activity coefficients. The advantage of using the excess Helmholtz free energy over the excess Gibbs free energy is that it is nearly pressure independent, since

$$\left(A^{exc}\right)_{T,V,p\rightarrow\infty} \approx \left(A^{exc}\right)_{T,V,Low\ p} \quad (7-18)$$

In modifying the combinatorial term, it is assumed that for mixtures containing alkanes only, the residual excess Gibbs or Helmholtz free energy is zero. Several publications (Abrams and Prausnitz, 1975; Kikic et al, 1980; Larsen, et al., 1987; Sheng et al, 1989; Voutsas et al, 1995; Ye and Zhong, 2000) proposed certain modifications to the excess combinatorial expressions. In all cases, infinite-dilution activity coefficients of n-alkane mixtures and/or VLE data were used to validate the model handling of asymmetric mixtures. The databases used in all publications were limited to small size ratios, where the size ratio is defined as the vdW volume of the large molecule over the vdW volume of the small molecule. In this study, infinite-dilution activity coefficient experimental data of n-paraffin binary mixtures and VLE data of mixtures of ethane/n-paraffins up to C₄₄ (with the largest vdW size ratio of 20) were used to evaluate excess combinatorial expressions.

Evaluation of Combinatorial Expressions using Infinite-dilution Activity Coefficients

Data

All six models listed in Table 3 were evaluated using 263 data points published in DECHEMA Chemistry data series (Tiegs, et al. 1986). All data points were for n-paraffin binary mixtures with the largest size ratio of 5.6. The results presented in Table 27 show that original UNIFAC combinatorial expression has the highest percentage-average-absolute deviation (%AAD) in the infinite-dilution activity coefficient in comparison to the modified UNIFAC combinatorial expression. This is in excellent agreement with the published results by Tiegs, et al. (1986). Detailed results are shown

Table 27. Comparison among Several Combinatorial Expressions using Infinite-Dilution Activity Coefficients of n-Paraffins Binary Mixtures

	Original UNIFAC 1975	Kikic, et al. 1980	Modified UNIFAC 1987	Sheng 1989	Voutsas 1995	Zhong 2000
AAD	0.17	0.03	0.04	0.15	0.04	0.06
%AAD	20.78	4.75	5.61	20.17	5.28	8.72
BIAS	-0.16	-0.01	-0.03	0.15	0.01	-0.06

in Appendix D. This evaluation serves as an initial screening of different combinatorial expressions that appear in the literature.

Evaluation of Combinatorial Expressions for the New Model (Model-1) using Ethane/n-Paraffin Data

The new model was evaluated with the six combinatorial expressions listed in Table 27. In this case, the comparison is not limited to evaluating the combinatorial expressions, but also to the new model performance as it applies to VLE data of n-paraffin asymmetric binary mixtures.

For the UNIFAC model used in this work, the volume and area group parameters R and Q used in model evaluations are the ones suggested by Holderbaum and Gmehling (1991) and are presented in Table 28.

Table 28. Van der Waals Gas Parameters

Gas	R	Q
Ethane	1.80	1.696
Carbon Dioxide	1.30	0.982
Methane	1.129	1.124
Carbon Monoxide	0.711	0.828
Hydrogen	0.416	0.571

A list of the excess Gibbs/Helmholtz based mixing rules evaluated throughout this work is presented in Table 29.

In addition to the mixing rules listed in Table 29, the commonly used one-fluid theory mixing rules were used as a reference to the potential capability of the excess free energy based mixing rules. The one (VDW-1 model) and two (VDW-2 model) temperature-independent binary interaction parameters were regressed per binary mixture. The PR EOS [Equation (6-1)] and one-fluid mixing rules [Equations (2-1) to (2-4)] were used for VDW-2 model. For VDW-1 model, the same equations were used except D_{12} were set equal to zero. The predictive ability of the generalized form of CEOS parameter C_{ij} (VDW-G model) developed by Gao (1999) was assessed, where CEOS parameter C_{ij} is correlated linearly to n-paraffin acentric factor for each solute/n-paraffin systems. The PR EOS generalized prediction correlations are presented in Table 30.

The number of parameters for excess free energy models includes four group contribution parameters plus one universal parameter, δ_1 , for LCVM and CHV models. For Model-1, an additional universal parameter, δ_2 , was used for covolume mixing rule, which is directly related to δ_1 . Both parameters tend to balance the effect of combinatorial contribution from excess free energy determined from EOS to the corresponding value determined from UNIFAC.

Table 29. Mixing Rules for Models Evaluated in this Work

Model-1 (This Work)

$$\alpha^* = \frac{1}{C_N} \left[\frac{A^{\text{exe}}}{RT} + (1 - \delta_1) \sum_1^{\text{NC}} z_i \ln \frac{b}{b_i} \right] + \sum_1^{\text{NC}} z_i \frac{a_i}{b_i RT} \quad (7-19)$$

$$b = \exp \left(\sum_1^{\text{NC}} z_i \ln b_i - (1 - \delta_2) \frac{A^{\text{exe comb}}}{RT} \right) \quad (7-20)$$

Model-2 (This Work)

$$\alpha = \frac{1}{C_N} \left(\frac{A^{\text{exe residual}}}{RT} \right) + \sum_1^{\text{NC}} z_i \frac{a_i}{b_i RT} \quad (7-21)$$

$$b = \exp \left(\sum_1^{\text{NC}} z_i \ln b_i - (1 - \delta_2) \frac{A^{\text{exe comb}}}{RT} \right) \quad (7-22)$$

Model-3 (This Work)

$$\alpha = \frac{1}{C_N} \left(\frac{A^{\text{exe residual}}}{RT} \right) + \sum_1^{\text{NC}} z_i \frac{a_i}{b_i RT} \quad (7-23)$$

$$b = \sum_1^{\text{NC}} z_i b_i \quad (7-24)$$

LCVM Model (Boukvalas, et al., 1994)

$$\alpha = \left(\frac{\delta_1}{C_V} + \frac{1 - \delta_1}{C_M} \right) \frac{G^{\text{exe}}}{RT} + \frac{1 - \delta_1}{C_M} \sum_1^{\text{NC}} z_i \ln \frac{b}{b_i} + \sum_1^{\text{NC}} z_i \frac{a_i}{b_i RT} \quad (7-25)$$

$$b = \sum_1^{\text{NC}} z_i b_i \quad (7-26)$$

CHV Model (Orbey and Sandler, 1997)

$$\alpha = \frac{1}{C_{\text{os}}} \left(\frac{A^{\text{exe}}}{RT} \right) + \frac{1 - \delta_1}{C_{\text{os}}} \sum_1^{\text{NC}} z_i \ln \frac{b}{b_i} + \sum_1^{\text{NC}} z_i \frac{a_i}{b_i RT} \quad (7-27)$$

$$b = \sum_1^{\text{NC}} z_i b_i \quad (7-28)$$

* $\alpha = \frac{a}{bRT}$

Table 30. PR Equation-of-State One-fluid Mixing Rules Generalized Correlations for Selected Systems (Gao, 1999)

Systems	C_{ij}	D_{ij}
H ₂ /n-paraffin	0.211 + 0.060 ω	0
CO/n-paraffin	0.001 + 0.107 ω	0
CO ₂ /n-paraffin	0.139 - 0.062 ω	0
CH ₄ /n-paraffin	0.053 - 0.063 ω	0
C ₂ H ₆ /n-paraffin	0.035 - 0.072 ω	0

The universal parameters (δ_1 and/or δ_2 depending on the model used) were determined by fitting the experimental data of ethane/n-paraffin mixtures to minimize the objective function:

$$SS = \sum_i^n \left[\frac{p_{cal} - p_{exp}}{p_{exp}} \right]_i^2 \quad (7-29)$$

Where n is the number of data points, p_{cal} is the calculated pressure, and p_{exp} is the experimental pressure. Further details of the data reduction technique are given by Gasem (1986).

Based on a commonly used assumption, no group interaction parameters were regressed for n-paraffin mixtures. The results of applying several combinatorial expressions to the new model are presented in Table 31, where the original UNIFAC, the modified UNIFAC, and the model developed by Ye and Zhong (2000) performed better than the other models (%AAD in bubble point pressure are 3.9, 4.6, and 4.9, respectively).

Even though the original UNIFAC had the best results due to the introduction of an empirical constant, the original UNIFAC predictions had the highest deviation when evaluated using infinite-dilution activity coefficient data. The modified UNIFAC

Table 31. Models Comparison for Several Combinatorial Expressions using Ethane/n-Paraffin Binary Mixtures

	Model-1				NPTS	Ref.	
	Original UNIFAC	Modified UNIFAC	Kikic	Voutsas			Zhong
δ_1	0.36	0.68	0.68	0.43	0.407		
δ_2	0.20	-1.34	-1.95	-1.50	-1.07		
%AAD in Bubble Point Pressure							
C ₃	0.77	0.76	0.81	1.65	0.92	37	7
C ₄	2.01	2.55	1.78	3.73	1.46	35	6
C ₅	1.03	2.05	1.13	6.94	1.71	25	11
C ₆	1.25	1.50	2.10	15.27	4.93	48	12
C ₇	4.04	3.62	5.02	12.08	4.67	8	8
C ₈	4.59	6.93	4.49	10.27	2.80	31	13
C ₁₀	3.21	3.62	5.52	18.15	7.45	28	1
C ₁₁	3.03	4.14	8.52	12.12	6.45	19	3
C ₁₂	3.15	5.64	6.74	10.55	4.33	58	5
C ₁₆	3.24	6.40	11.05	7.46	4.50	30	2
C ₂₀	7.61	4.59	9.00	10.67	10.89	15	12
C ₂₂	3.31	5.65	12.77	2.13	3.17	35	9
C ₂₄	6.51	9.64	17.93	4.75	5.82	20	10
C ₂₈	5.98	2.28	3.13	4.07	7.36	36	12, 4
C ₃₆	5.32	5.85	6.30	7.47	5.76	25	12, 14
C ₄₄	7.89	8.59	10.61	8.27	6.81	16	12
Total	3.93	4.61	6.68	8.47	4.94	466	

combinatorial expression had more consistent and better results in the overall comparison; therefore, it was used in new model evaluations involving the other solutes/n-paraffin systems. Use of the Zhong and Voutsas combinatorial expressions with the new mixing rule should be feasible with polymer solutions since both combinatorial expressions represent polymer solutions accurately (Ye and Zhong, 2000).

Database Used

The VLE test systems employed involved five solutes (ethane, carbon dioxide, methane, hydrogen, and carbon monoxide) dissolved in n-paraffins. This corresponds to a total of sixty binary systems encompassing 1466 data points. Table 32 documents the database used in the model evaluations.

Model Evaluations and Comparisons

In this study, the predictive capabilities of several thermodynamic models based on PR EOS and the mixing rules listed in Table 29 were evaluated. The mixing rule parameter is highly correlated (non linear) with n-paraffin carbon number in the model developed by Zhong and Musuoka (1997); therefore, their model was not considered in this work. Derivations for the fugacity coefficient of a component in a mixture for all the models evaluated in this study are listed in Appendix E.

The CHV and LCVM models were evaluated using original UNIFAC/UNIQAUC combinatorial expression by their respective authors. In comparison to LCVM model, the CHV is theoretically justified, so it was also evaluated with the modified UNIFAC. The PR EOS, the new alpha function (Gasem, et al., 2001) and n-paraffin critical constants

Table 32. The Database of Binary Systems used in this Study

Solvent	Ethane				
	Temperature Range, K	Pressure Range, MPa	Solute Mole Fraction Range	NPTS	Reference
C ₃	283.10 - 355.40	0.689 - 4.137	0.0253 - 0.7810	37	Matschke and Thodos, 1965
C ₄	303.15 - 363.40	0.441 - 4.877	0.0440 - 0.8370	35	Lhotak and Wichterle, 1981
C ₅	310.93 - 444.26	0.345 - 4.137	0.0048 - 0.8503	25	Reamer, et al., 1960
C ₆	310.93 - 394.26	0.393 - 5.399	0.0720 - 0.6519	48	Robinson and Gasem, 1987
C ₇	338.71 - 449.82	3.923 - 7.598	0.2960 - 0.8480	8	Mehra and Thodos, 1965
C ₈	323.15 - 373.15	0.405 - 5.269	0.0470 - 0.8630	31	Rodrigues, et al., 1968
C ₁₀	311.11 - 411.11	0.423 - 8.236	0.1050 - 0.6380	28	Bufkin, 1986
C ₁₁	298.15 - 318.15	1.286 - 5.427	0.278 - 0.969	19	Estrera, et al., 1987
C ₁₂	273.15 - 373.15	0.405 - 6.282	0.1010 - 0.9350	58	Lee and Kohn, 1969
C ₁₆	285.00 - 345.00	0.575 - 6.633	0.1990 - 0.8750	30	De Goede, et al., 1989
C ₂₀	323.15 - 423.15	0.504 - 6.645	0.1180 - 0.6530	15	Robinson and Gasem, 1987
C ₂₂	310.00 - 360.00	0.205 - 7.143	0.0541 - 0.8529	35	Peters, et al., 1988
C ₂₄	310.00 - 360.00	0.460 - 7.820	0.1197 - 0.7833	20	Peters, et al., 1987
C ₂₈	348.15 - 573.15	0.563 - 5.182	0.1020 - 0.5200	36	Robinson and Gasem, 1987; Huang, et al., 1988
C ₃₆	373.15 - 573.05	0.368 - 4.760	0.0870 - 0.5320	25	Robinson and Gasem, 1987; Tsai, et al., 1987
C ₄₄	373.15 - 423.15	0.387 - 3.170	0.0986 - 0.5161	16	Robinson and Gasem, 1987

Table 32. The Database of Binary Systems used in this Study – *continued*

Solvent	Carbon Dioxide				Reference
	Temperature Range, K	Pressure Range, MPa	Solute Mole Fraction Range	NPTS	
C ₄	319.26 - 377.59	2.180 - 6.965	0.088 - 0.778	19	Hsu, et al., 1985
C ₅	273.41	0.269 - 3.247	0.0451 - 0.9274	11	Cheng, et al., 1989
C ₆	298.15 - 393.15	0.444 - 7.620	0.0495 - 0.8856	40	Ohgaki and Katayama, 1976; Wagner and Wichterle, 1987; Li, et al., 1981
C ₇	310.65 - 477.21	0.186 - 8.694	0.0220 - 0.9290	44	Kalra, et al., 1978
C ₁₀	310.93 - 410.93	0.689 - 8.618	0.0730 - 0.6000	24	Reamer and Sage, 1963
C ₁₆	463.05 - 663.75	2.006 - 5.087	0.0897 - 0.2575	14	Sebastian, et al., 1980
C ₁₈	396.60 - 673.20	1.016 - 6.190	0.0519 - 0.3890	25	Kim, et al., 1985
C ₁₉	313.15 - 333.15	0.936 - 7.958	0.0899 - 0.6342	34	Fall, et al., 1985
C ₂₀	323.15 - 373.15	0.620 - 6.757	0.0730 - 0.5010	33	Gasem, 1986; Huang, et al., 1988
C ₂₁	318.15 - 338.15	0.931 - 7.820	0.0999 - 0.6496	26	Fall, et al., 1985
C ₂₂	323.15 - 373.15	0.962 - 7.178	0.0833 - 0.5925	44	Fall, et al., 1985
C ₂₄	373.15	1.013 - 5.066	0.0819 - 0.3531	5	Tsai and Yau, 1990
C ₂₈	348.15 - 573.40	0.807 - 9.604	0.0700 - 0.6170	39	Gasem, 1986; Huang, et al., 1988
C ₃₆	373.15 - 423.15	0.524 - 8.653	0.0620 - 0.5020	18	Gasem, 1986
C ₄₄	373.15 - 423.15	0.579 - 7.081	0.0800 - 0.5020	14	Gasem, 1986

Table 32. The Database of Binary Systems used in this Study – *continued*

Methane					
Solvent	Temperature Range, K	Pressure Range, MPa	Solute Mole Fraction Range	NPTS	Reference
C ₄	277.59 - 377.59	1.379 - 10.342	0.0256 - 0.4513	11	Wiese et al, 1970; Roberts et al, 1962
C ₆	298.33 - 410.95	1.014 - 17.237	0.0300 - 0.6380	53	Shim and Kohn, 1962
C ₇	311.11 - 411.11	2.193 - 10.466	0.1000 - 0.4000	12	Reamer, et al., 1956
C ₈	298.33 - 423.33	1.013 - 7.093	0.0380 - 0.2870	27	Kohn and Bradish, 1964
C ₉	323.15 - 423.15	1.014 - 10.135	0.0329 - 0.3471	39	Shipman and Kohn, 1966
C ₁₀	310.93 - 477.59	0.138 - 10.342	0.0141 - 0.3639	68	Reamer, et al., 1942
C ₁₂	323.15 - 373.15	1.330 - 10.380	0.0615 - 0.3566	12	Srivatsan, 1991
C ₁₆	462.45 - 703.55	2.029 - 15.189	0.0801 - 0.5958	19	Lin , et al., 1980
C ₂₀	373.35 - 423.15	1.008 - 5.052	0.0427 - 0.2030	15	Huang, et al., 1988
C ₂₈	348.15 - 573.15	0.926 - 7.740	0.0566 - 0.3250	34	Darwish, et al., 1993; Huang, et al., 1988
C ₃₆	373.15 - 573.15	0.838 - 7.928	0.0567 - 0.3506	29	Darwish, et al., 1993; Tsai, et al., 1987

Table 32. The Database of Binary Systems used in this Study – *continued*

Solvent	Hydrogen			NPTS	Reference
	Temperature Range, K	Pressure Range, MPa	Solute Mole Fraction Range		
C ₄	327.65 – 394.25	2.778 - 16.847	0.0190 - 0.2660	49	Klink et al, 1975
C ₅	273.15-373.15	0.693 - 20.680	0.0044 - 0.2590	29	Freitag and Robinson, 1986
C ₆	344.26 – 410.93	1.287 - 15.11	0.0107 - 0.1430	29	Gao, 1999
C ₇	424.15 - 498.85	2.4203 - 29.035	0.0230 - 0.2950	13	Peter and Reinhartz, 1960
C ₈	463.15 - 513.15	1.379 - 10.342	0.0127 - 0.2010	36	Connolly, 1965
C ₁₀	344.26 - 423.15	3.710 - 15.040	0.0367 - 0.1286	15	Park, et al., 1995
C ₁₂	344.26 - 410.93	1.422 - 13.235	0.0144 - 0.1204	23	Gao, et al., 1999
C ₁₆	461.65 – 664.05	2.032 - 25.220	0.0311 - 0.3597	23	Lin , et al., 1980
C ₂₀	323.15 - 423.15	2.230 - 10.400	0.0273 - 0.1246	18	Park, et al., 1995
C ₂₈	348.15 - 423.15	2.860 - 13.100	0.0452 - 0.1487	16	Park, et al., 1995
C ₃₆	373.15 - 423.15	3.560 - 16.750	0.0677 - 0.2271	12	Park, et al., 1995
C ₂₀	373.35 – 573.25	1.009 - 5.035	0.0113 - 0.0866	13	Huang, et al., 1988
C ₂₈	373.25 – 573.15	0.986 - 5.070	0.0149 - 0.1360	15	Huang, et al., 1988
C ₃₆	373.15 – 573.15	1.022 - 5.066	0.0154 - 0.150	15	Huang, et al., 1988

Table 32. The Database of Binary Systems used in this Study – *continued*

Solvent	Carbon Monoxide			NPTS	Reference
	Temperature Range, K	Pressure Range, MPa	Solute Mole Fraction Range		
C ₆	323.15 - 423.15	1.179 - 8.687	0.0099 - 0.1466	18	Yi, 1992
C ₈	463.15 - 533.15	0.669 - 6.569	0.0027 - 0.1570	42	Connolly and Kandalic, 1984
C ₁₀	310.93 - 377.59	2.227 - 10.004	0.0385 - 0.1400	17	Yi, 1992
C ₁₂	344.26 - 410.93	0.690 - 8.751	0.0113 - 0.1493	27	Gao, 1999
C ₂₀	323.15 - 423.15	1.991 - 8.384	0.0403 - 0.1614	20	Srivatsan, 1991
C ₂₈	373.15 - 423.15	1.903 - 8.412	0.0463 - 0.1853	10	Yi, 1992
C ₃₆	373.15 - 423.15	1.800 - 8.956	0.0494 - 0.2099	12	Yi, 1992
C ₂₈	348.15 - 423.15	2.080 - 6.630	0.0519 - 0.1502	17	Srivatsan, 1991
C ₂₈	373.45 - 573.45	1.008 - 5.069	0.0227 - 0.1310	13	Huang, et al., 1988
C ₃₆	373.15 - 572.95	1.015 - 5.080	0.0257 - 0.1730	15	Huang, et al., 1988

(Gao, et al., 2001) were used in all our model evaluations, with the exception of LCVMM model, where the alpha function for nonpolar compounds (Boukovalas, et al., 1994) was used. Improved predictions were obtained when n-paraffin critical constants (Gao, et al., 2001) were used instead of the values used by Boukovalas, et al. (1994). Although the CHV model was developed for asymmetric mixtures, in the original work it was evaluated with five binary mixtures, where the ethane/eicosane binary mixture has the largest asymmetry.

The group-interaction parameters were determined by fitting the experimental data to minimize the objective function, SS, in Equation (7-29). In determining the group-interaction parameters, the gas solute is considered to be a separate group. The group-interaction parameters were determined by regression, where:

$$\psi_{ij} = \exp \left[- \frac{\bar{A}_{ij} + \bar{B}_{ij} (T - 298.15)}{T} \right] \quad (7-30)$$

Group-interaction parameters were regressed for Model-1, Model-2, Model-3, and the CHV model, since Orbey and Sandler (1997) model evaluations were based on the UNIQUAC (i.e., molecular interactions). The LCVMM model reported only group-interaction parameters for ethane, carbon dioxide and methane; therefore, the interaction parameters for other solutes were regressed.

The UNIFAC group-interaction parameters for all models used in this work are listed in Table 33.

Table 33. UNIFAC Interaction Parameters Regressed for Models Evaluated

Modified UNIFAC Interaction Parameters for Model-1

i	j	\bar{A}_{ij}	\bar{A}_{ji}	\bar{B}_{ij}	\bar{B}_{ji}
CO ₂	CH ₂ *	-52.77	383.76	-0.538	-0.007
CH ₄	CH ₂	-0.346	68.63	0.170	0.001
H ₂	CH ₂	182.83	483.30	0.038	0.046
CO	CH ₂	147.29	160.39	-0.314	0.214
CO ₂	H ₂	400.42	8606.90	4.411	60.625

*In all cases CH₂ and CH₃ are considered as one group

Modified UNIFAC Interaction Parameters for CHV Model

i	j	\bar{A}_{ij}	\bar{A}_{ji}	\bar{B}_{ij}	\bar{B}_{ji}
CO ₂	CH ₂	4.156	311.48	-0.253	-0.867
CH ₄	CH ₂	25.185	9.46	0.336	-0.620
H ₂	CH ₂	91.099	406.81	-0.101	-0.028
CO	CH ₂	5.147	218.68	-0.489	-0.050
CO ₂	H ₂	400.420	8606.90	4.411	60.615

Original UNIFAC Interaction Parameters for LCVM Model

i	j	\bar{A}_{ij}	\bar{A}_{ji}	\bar{B}_{ij}	\bar{B}_{ji}
CO ₂ *	CH ₂	110.6	116.7	0.5003	-0.9106
CH ₄ *	CH ₂	-25.0	88.0	-0.3000	0.3000
H ₂	CH ₂	179.0	460.9	0.5106	0.0442
CO	CH ₂	27.0	219.8	-0.0477	0.1728
CO ₂	H ₂	223.9	1958.7	1.6054	-0.4735

Supplied by Bokouvalas, et al (1994)

Modified UNIFAC Interaction Parameters for Model-2

i	j	\bar{A}_{ij}	\bar{A}_{ji}	\bar{B}_{ij}	\bar{B}_{ji}
CO ₂	CH ₂	-0.0045	326.1	-1.4900	0.9425
CH ₄	CH ₂	45.10	26.42	0.3501	-0.4911

Modified UNIFAC Interaction Parameters for Model-3

i	j	\bar{A}_{ij}	\bar{A}_{ji}	\bar{B}_{ij}	\bar{B}_{ji}
CO ₂	CH ₂	98.84	232.5	0.4445	-1.396
CH ₄	CH ₂	28.91	-14.76	0.1005	-0.1642
H ₂	CH ₂	18.71	284	-0.5423	-0.1828
CO	CH ₂	1.272	301.01	-0.2554	-0.0864

Results and Discussions

Ethane/n-Paraffin Systems

Several models were compared as presented in Table 34. The optimum parameter “ δ_1 ” for the CHV model suggested by Orbey and Sandler (1997) is 0.36 for UNIQUAC. This is similar to the value used in the LCVM model. In the CHV model, the value tends to decrease as the asymmetry is increased. For the ethane/n-paraffin mixtures, the optimum values found for δ_1 (CHV model) in this work were 0.275 for the original UNIFAC and 0.573 for the modified UNIFAC. Also, better results are shown for the CHV model with the modified UNIFAC, rather than the original UNIFAC. The CHV, Model-1, and Model-2 models gave comparable results (4.0, 4.6, and 4.0 %AAD, respectively). The VDW-G result (5.88 %AAD) is higher than other predictive models evaluated. This is due to the higher dependency of ethane/n-paraffin mixtures in D_{12} than C_{12} (Peters, et al., 1987), as indicated by the increase in %AAD as the solvent molecular size increases. For vdW mixing rules the use of two interaction parameters per binary significantly improved the results (2.0 %AAD) over the use of one interaction parameter (4.2 %AAD). Model-2 gave exceptionally better results than Model-3, specifically above C_{11} . In both cases, the importance of correcting the CEOS covolume “b” is indicated. The CHV and LCVM models are slightly dependent on the combinatorial expression used. The inaccuracy of the combinatorial expression is compensated for by the universal parameter “ δ_1 ” correction to F-H-like term as represented by F-H-C in Figure 17. Where,

$$F - H - C = (1 - \delta_1) \sum_1^{NC} z_i \ln \frac{b}{b_i} \quad (7-31)$$

Table 34. Models Comparison for Ethane/n-Paraffin Systems

	Model-1		Model-2	Model-3	LCVM	CHV		VDW-1	VDW-2	VDW-G	NPTS	Ref
	Original UNIFAC	Modified UNIFAC	Modified UNIFAC	NA	Original UNIFAC	Modified UNIFAC	Original UNIFAC	$C_{12}/$ Binary	C_{12}/D_{12} Binary	$C_{12} = f(\omega)$		
δ_1	0.36	0.68		NA	0.36	0.573	0.275					
δ_2	0.20	-1.34	-1.60									
%AAD in Bubble Point Pressure												
C ₃	0.77	0.76	0.76	0.77	0.70	0.77	0.77	0.77	0.69	3.45	37	7
C ₄	2.01	2.55	2.67	2.35	2.88	2.31	2.55	1.51	1.50	2.53	35	6
C ₅	1.03	2.05	2.26	1.87	2.58	1.66	2.16	0.73	0.72	2.26	25	11
C ₆	1.25	1.50	1.90	1.67	2.56	1.02	2.04	0.72	0.68	3.54	48	12
C ₇	4.04	3.62	2.59	1.73	1.49	1.81	1.54	3.38	3.38	2.40	8	8
C ₈	4.59	6.93	7.48	8.71	9.62	7.15	8.90	1.87	1.89	4.80	31	13
C ₁₀	3.21	3.62	3.45	3.81	5.55	2.04	4.00	1.99	1.80	1.98	28	1
C ₁₁	3.03	4.14	3.55	3.81	3.73	1.46	3.06	1.24	0.96	2.18	19	3
C ₁₂	3.15	5.64	5.73	9.36	10.82	5.52	8.83	1.91	1.63	6.32	58	5
C ₁₆	3.24	6.40	5.66	13.42	12.67	6.62	10.08	4.22	2.53	10.38	30	2
C ₂₀	7.61	4.59	4.67	7.85	6.05	5.90	4.86	7.16	2.79	7.26	15	12
C ₂₂	3.31	5.65	4.32	17.11	13.75	7.18	10.17	10.43	2.31	12.25	35	9
C ₂₄	6.51	9.64	6.47	18.11	14.28	6.80	9.57	10.12	5.22	10.63	20	10
C ₂₈	5.98	2.28	2.70	10.87	6.36	4.77	4.55	6.29	2.65	6.49	36	12, 4
C ₃₆	5.32	5.85	3.50	18.37	7.08	4.38	5.24	6.86	1.85	6.98	25	12, 14
C ₄₄	7.89	8.59	6.16	24.91	6.84	5.14	6.28	8.59	1.55	10.65	16	12
Total	3.93	4.61	3.99	9.05	6.68	4.03	5.29	4.24	2.01	5.88	466	

NA: Not applicable

Refer to Table-41 for detail listing of the number of parameters used

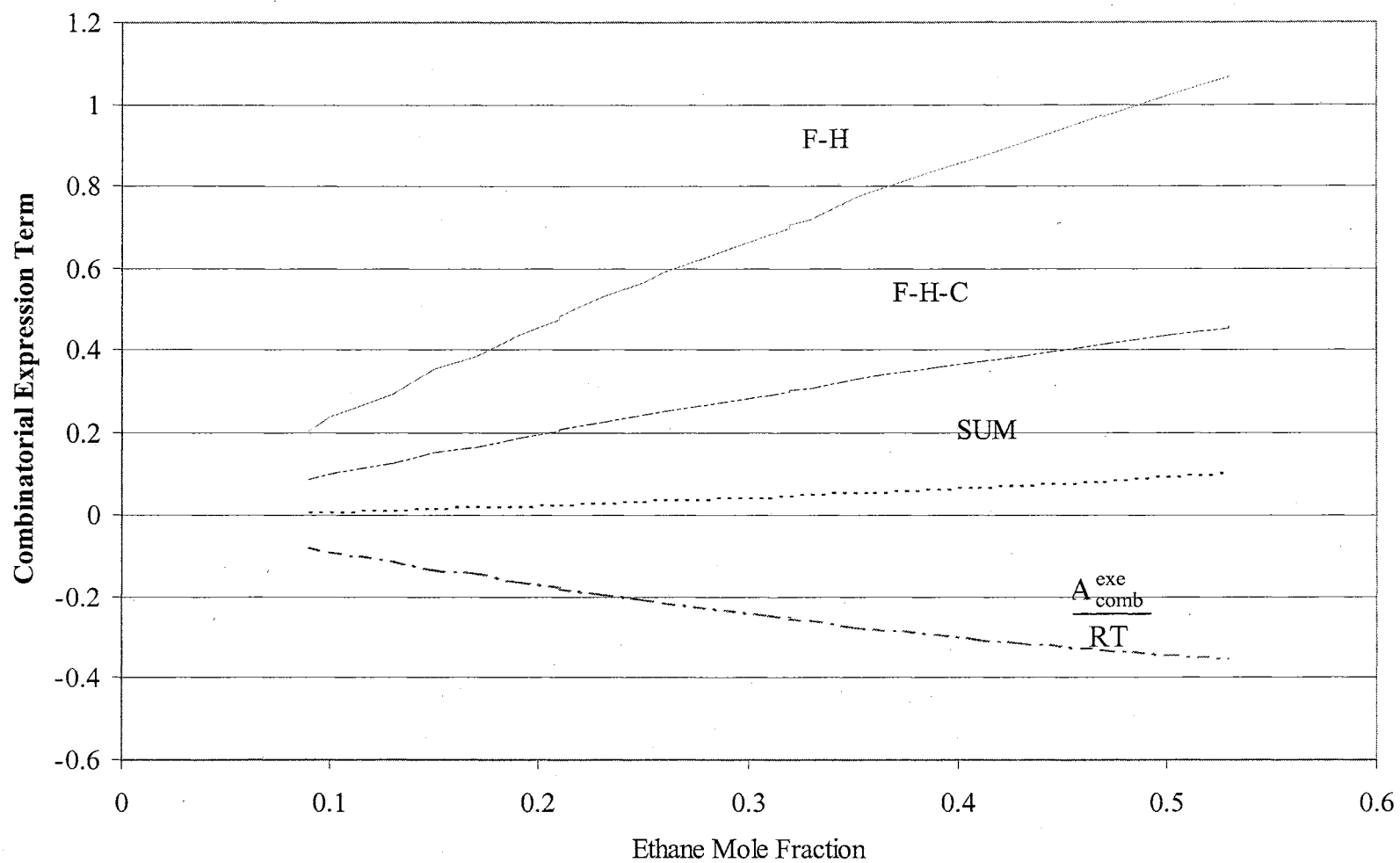


Figure 17. The Effect of Combinatorial Expression on CHV Model for Ethane/Hexatricontane Binary Mixture.

and

$$\text{SUM} = \left(\frac{A_{\text{comb}}^{\text{exc}}}{RT} \right) + (1 - \delta_1) \sum_1^{\text{NC}} z_i \ln \frac{b}{b_i} \quad (7-32)$$

Also, as shown in Figure 17, for the ethane/hexatricontane system, the sum of the two effects (SUM), as represented in Equation (7-32), is gradually increased as the asymmetry becomes larger. This small deviation from equality had an effect on α or a/b ratio, as indicated in Equation (7-27), to compensate for the inaccuracy in the covolume.

Carbon dioxide/n-Paraffin Systems

Table 35 presents a comparison among several models for representing the bubble point pressures of carbon dioxide/n-paraffin systems. Comparable results are obtained for Model-1, CHV, LCVM, and VDW-G models, which are 5.4, 4.6, 4.5, and 5.4 %AAD, respectively. Better results obtained for VDW-1 (4.1 %AAD) and VDW-2 (3.0 %AAD) models. Comparing the results of Model-2 and Model-3 and VDW-2 and VDW-1, particularly for C_{20} and above, indicates a smaller dependency on the covolume parameters than for ethane/n-paraffin systems. As observed, LCVM and CHV models gave very close results although the two models are based on different combinatorial expressions.

A comparison between Model-1 and CHV model indicates that Model-1 performed better in most cases with the exception of C_{36} and C_{44} . The correction to covolume in Model-1 takes systematic deviation according to athermal or combinatorial Helmholtz variation, which also showed higher deviations for ethane/ C_{36} and ethane/ C_{44}

Table 35. Models Comparison for Carbon Dioxide/n-Paraffin Systems

	Model-1		Model-2	Model-3	CHV	LCVM	VDW-1	VDW-2	VDW-G	NPTS	Ref.
	Modified UNIFAC	Original UNIFAC	Modified UNIFAC	NA	Modified UNIFAC	Original UNIFAC	C ₁₂ / Binary	C ₁₂ /D ₁₂ Binary	C ₁₂ = f (ω)		
δ ₁	0.68	0.36		NA	0.57	0.36					
δ ₂	-1.34	0.20	-1.60								
%AAD in Bubble Point Pressure											
C ₄	2.39	4.18	1.85	1.97	1.70	1.12	0.60	0.67	0.85	19	19
C ₅	4.39	5.50	2.20	3.46	4.48	1.56	2.52	0.49	2.89	11	15
C ₆	2.67	5.37	4.08	4.65	3.86	3.85	5.01	3.35	4.99	40	25, 30, 24
C ₇	7.29	8.92	5.93	6.50	5.65	4.81	2.47	2.40	4.95	44	22
C ₁₀	4.08	1.52	1.88	1.21	0.96	3.18	2.89	2.60	3.22	24	26
C ₁₆	7.00	8.68	12.50	7.52	8.01	5.96	7.16	7.16	7.16	14	27
C ₁₈	8.06	7.62	12.34	8.85	9.20	6.49	3.92	3.84	8.46	25	23
C ₁₉	4.04	4.21	6.03	5.61	4.86	7.54	2.97	2.98	4.97	34	16
C ₂₀	3.27	5.67	3.14	3.54	4.20	6.01	3.91	3.88	4.57	33	18, 20
C ₂₁	3.11	4.23	6.09	7.12	5.64	6.27	2.80	2.82	4.39	26	16
C ₂₂	3.67	5.78	5.46	5.87	6.78	4.38	4.79	3.12	4.80	44	16
C ₂₄	3.71	10.65	4.21	6.23	4.03	5.54	3.42	3.41	3.49	5	29
C ₂₈	4.06	11.98	6.79	9.77	5.06	4.04	6.44	3.18	7.0	39	18, 21
C ₃₆	8.39	17.31	6.50	14.08	2.42	2.73	5.68	2.27	9.93	18	18
C ₄₄	14.64	22.38	11.70	21.07	2.86	4.23	7.16	2.44	9.27	14	18
Total	5.38	8.27	6.05	7.16	4.64	4.51	4.12	2.97	5.40	276	

Refer to Table-41 for detail listing of the number of parameters used

binary mixtures. The results of the CHV model show a different pattern in comparison to VDW-1 and VDW-2 models. The deviations are higher in the middle range (C_{16} to C_{24}), then they decrease to show comparable results to VDW-2 model at C_{36} and C_{44} . This is an indication of the random nature of the CHV model in correcting for the CEOS covolume.

Methane/n-Paraffins Systems

In Table 36, comparable results are obtained for Model-1, Model-3, and LCVM model which are 3.9, 4.4, and 4.4 %AAD in bubble point pressure, respectively. The difference in results between VDW-1 and VDW-2 suggest that modifying the covolume produces no significant improvement. This is also supported by the good results of Model-3 (4.4 %AAD). This is due, in partial, to the positive contribution of the increase in excess Helmholtz combinatorial contribution term, as indicated by Equation (7-20), to covolume as the asymmetry increased.

Hydrogen/n-Paraffin Systems

As shown in Table 37, models based on excess Gibbs /Helmholtz free energy show a high deviation in the bubble point pressure predictions. Hydrogen/n-paraffin systems are considered a challenge, due to the asymmetric nature of the mixture involved and the quantum behavior of Hydrogen (Huang, et al., 1994). For Model-1, correlating the parameter " δ_2 " against n-paraffin carbon number produced a straight-line correlation, as shown in Figure 18. In addition to the improved results, the linear trend allows us to extrapolate to systems where no experimental data exist. Model-1 results are significantly better than the LCVM and CHV models, which are 5.4,

Table 36. Models Comparison for Methane/n-Paraffin Systems

	Model-1		Model-2	Model-3	CHV	LCVM	VDW-1	VDW-2	VDW-G	NPTS	Ref.
	Modified UNIFAC	Original UNIFAC	Modified UNIFAC	Modified UNIFAC	Modified UNIFAC	Original UNIFAC	C ₁₂ /Binary	C ₁₂ /D ₁₂ Binary	C ₁₂ = f(ω)		
δ_1	0.68	0.36		0.57	0.57	0.36					
δ_2	-1.34	0.20	-1.60								
	%AAD in Bubble Point Pressure										
C ₄	1.41	2.42	2.14	3.46	4.02	2.98	6.37	6.37	6.36	11	39, 44
C ₆	2.64	2.19	4.88	3.71	5.00	2.54	1.03	1.03	1.19	53	40
C ₇	2.59	2.66	4.55	2.28	3.42	1.55	0.69	0.65	2.19	12	38
C ₈	5.62	3.30	9.71	6.60	8.83	7.26	1.68	1.32	4.05	27	34
C ₉	2.74	3.25	5.94	4.35	6.02	5.07	2.00	2.01	2.73	39	41
C ₁₀	2.85	4.92	6.97	3.93	3.75	3.42	2.52	1.64	3.60	68	37
C ₁₂	3.07	3.73	3.37	2.72	0.33	1.90	2.66	2.58	2.84	12	42
C ₁₆	6.49	6.65	8.41	6.67	10.09	6.21	6.47	6.47	9.04	19	35
C ₂₀	4.05	5.23	7.93	4.36	3.81	2.77	3.43	3.49	5.67	15	32
C ₂₈	4.13	10.69	7.61	4.06	5.96	6.30	4.57	4.57	6.32	34	31, 33
C ₃₆	6.87	18.74	5.60	6.06	4.12	8.88	4.24	3.14	4.29	29	31, 43
Total	3.86	5.80	6.10	4.38	5.03	4.44	3.24	3.02	4.39	319	

Refer to Table-41 for detail listing of the number of parameters used

Table 37. Model Comparison for Hydrogen/n-Paraffin Systems

	Model-1		Model-1	Model-3	CHV	LCVM	VDW-1	VDW-2	VDW-G	NPTS	Ref.
	Modified UNIFAC	Modified UNIFAC	Original UNIFAC	Modified UNIFAC	Modified UNIFAC	Original UNIFAC	C ₁₂ / Binary	C ₁₂ /D ₁₂ Binary	C ₁₂ = f(ω)		
δ ₁	0.68	0.68	0.36		0.5734	0.36					
δ ₂	f(CN)	-0.5732	0.20								
	%AAD in Bubble Point Pressure										
C ₄	5.35	9.40	5.06	10.05	8.21	5.06	5.26	5.27	5.26	49	48
C ₅	7.97	12.44	7.25	11.42	10.11	7.71	8.14	8.25	7.97	29	46
C ₆	2.52	12.67	2.47	12.62	11.78	7.30	2.55	2.36	4.79	29	52
C ₇	3.27	8.12	3.32	8.36	7.22	5.84	3.30	3.09	3.31	13	51
C ₈	7.85	14.79	4.89	11.75	12.15	10.83	5.44	4.21	8.42	36	45
C ₁₀	1.37	4.36	2.58	4.45	6.90	5.14	0.70	0.67	0.67	15	50
C ₁₂	4.71	3.74	4.83	2.55	2.46	1.99	1.33	1.27	3.67	23	52
C ₁₆	8.21	10.05	9.75	6.82	7.14	6.88	4.93	4.84	7.11	23	49
C ₂₀	3.10	3.27	9.77	6.00	3.90	3.71	5.14	2.69	4.97	13	47
C ₂₈	5.22	4.07	11.07	7.59	4.91	5.90	2.22	1.33	2.22	15	47
C ₃₆	9.92	33.59	44.39	10.99	12.30	18.10	2.81	2.81	5.41	12	50
Total	5.40	10.59	9.58	8.42	7.91	7.13	3.80	3.34	4.89	257	
C ₂₀	3.18	3.05	9.83	13.00	6.87	6.58	2.29	1.59	4.36	18	50
C ₂₈	5.78	13.54	25.85	14.04	10.73	12.40	3.57	3.53	4.01	16	50
C ₃₆	13.11	14.33	20.01	5.58	5.36	7.74	4.78	3.81	8.81	15	47
Total	5.81	10.53	11.51	8.95	7.85	7.51	3.74	3.26	5.07	306	

Refer to Table-41 for detail listing of the number of parameters used

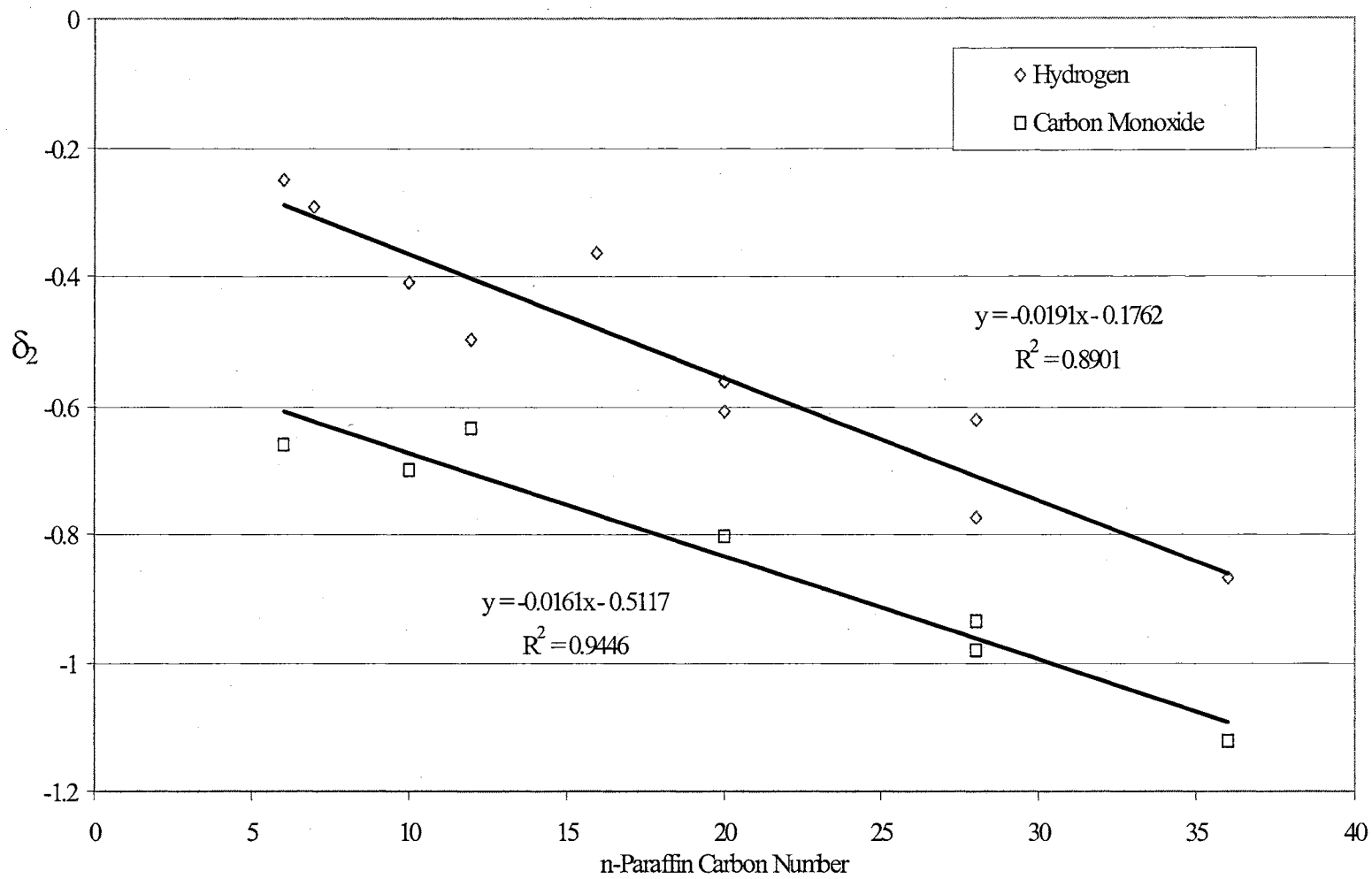


Figure 18. Model-1 Correlations for Excess Combinatorial Helmholtz Free Energy Parameter.

7.1, and 7.9 %AAD, respectively. The VDW-1 and VDW-2 models gave better results than the predictive models evaluated. For the H₂/hexatricontane system, the experimental data reported by Park (1994) has better internal consistency (better representation with PR EOS with one or two temperature-dependent BIP(s)) than reported by Huang, et al. (1988); therefore, Park's (1994) data were considered in evaluating these systems. This consistency is assessed based on how well each set of data points were represented by VDW-1 and VDW-2. Model-2 group interaction parameters were not regressed for these systems since initial evaluation reveals that it works well only with systems where covolume modification is required.

Carbon Monoxide/n-Paraffin Systems

Table 38 shows comparable results for Model-3 and CHV model, which are 3.8 and 3.6 %AAD, respectively. As in the case of hydrogen/n-paraffin, the parameter " δ_2 " was correlated with the n-paraffin carbon number. The results obtained (3.8 %AAD) from this correlation are comparable to the Model-3 and CHV model results. Comparison of VDW-1 and VDW-2 shows no improvement with the use of a second interaction parameter (D_{12}). In addition, the results for Model-3 are comparable to the best result generated by CHV model.

Tables 39 and 40 summarize the overall results for all binary systems examined. Overall comparisons presented in Table 39, reveal the Model-1 developed in this work gave slightly better results among excess free energy-based models for a total of 1469 data points evaluated. As shown in Table 40, for asymmetric mixtures, the CHV model

Table 38. Model Comparison for Carbon Monoxide/n-Paraffin Systems

	Model-1		Model-1	Model-3	CHV	LCVM	VDW-1	VDW-2	VDW-G	NPTS	Ref.
	Modified UNIFAC	Modified UNIFAC	Original UNIFAC	NA	Modified UNIFAC	Original UNIFAC	C ₁₂ /Binary	C ₁₂ /D ₁₂ Binary	C ₁₂ = f(ω)		
δ ₁	0.68	0.68	0.36	NA	0.5734	0.36					
δ ₂	f(CN)	-0.74	0.20								
%AAD in Bubble Point Pressure											
C ₆	4.97	4.21	6.03	4.60	4.31	2.41	1.12	1.12	1.54	18	57
C ₈	5.06	7.92	4.65	8.29	7.87	5.70	1.56	1.56	2.36	42	53
C ₁₀	3.59	2.43	2.40	2.82	2.42	4.84	3.22	3.19	4.52	17	57
C ₁₂	3.61	4.46	2.13	5.63	5.28	5.30	3.57	3.56	3.55	27	56
C ₂₀	3.08	3.36	10.78	0.85	0.68	3.23	6.40	4.94	6.72	20	55
C ₂₈	1.83	5.72	18.66	3.08	3.26	4.17	2.37	2.38	5.08	10	57
C ₃₆	4.21	17.73	31.17	1.22	1.31	5.49	4.18	4.10	4.29	12	57
Total	3.76	6.55	10.83	3.78	3.59	4.45	3.2	2.98	4.01	146	
C ₂₈	3.38	7.15	20.41	2.24	2.31	1.79	2.53	2.52	2.44	17	55
C ₂₈	7.61	3.40	10.77	6.14	6.04	3.62	5.23	4.09	5.41	13	54
C ₃₆	14.55	13.25	23.63	10.40	10.25	3.33	3.33	3.35	4.31	15	54
Total	5.19	6.96	13.06	4.52	4.37	3.99	3.35	3.08	4.02	191	

Refer to Table-41 for detail listing of the number of parameters used

Table 39. Summary of Overall Results for all the Binary Systems Considered

	Model-1 Modified UNIFAC	Model-1 Original UNIFAC	Model-2 Modified UNIFAC	Model-3 Modified UNIFAC	CHV Modified UNIFAC	LCVM Original UNIFAC	VDW-1 (C ₁₂)	VDW-2 (C ₁₂ , D ₁₂)	VDW-G	NPTS
%AAD in Bubble Point Pressure										
Ethane/n-Paraffin	4.61	3.93	3.99	9.05	4.03	6.68	4.24	2.01	5.88	469
CO ₂ /n-Paraffins	5.38	8.27	6.05	7.16	4.64	4.51	4.12	2.97	5.40	276
CH ₄ /n-Paraffins	3.86	5.80	6.10	4.38	5.03	4.44	3.24	3.02	4.39	319
H ₂ /n-Paraffins	5.40	9.58	---	8.42	7.91	7.13	3.80	3.34	4.89	259
CO/n-Paraffins	3.76	10.83	---	3.78	3.59	4.45	3.35	3.08	4.02	146
Total	4.60	7.68	---	6.56	5.04	5.44	3.88	3.17	4.92	1469

Refer to Table 41 for the number of parameters used

Table 40. Summary of Results for Asymmetric Binary Mixtures involving C₂₀ and above

	Model-1 Modified UNIFAC	Model-1 Original UNIFAC	Model-2 Modified UNIFAC	Model-3 Modified UNIFAC	CHV Modified UNIFAC	LCVM Original UNIFAC	VDW-1 (C ₁₂)	VDW-2 (C ₁₂ , D ₁₂)	VDW-G	NPTS
%AAD in Bubble Point Pressure										
Ethane/n-Paraffin	6.10	6.10	4.64	16.20	5.70	9.06	8.24	2.73	9.04	150
CO ₂ /n-Paraffins	5.84	11.14	6.27	9.67	4.43	4.74	4.89	3.02	6.21	179
CH ₄ /n-Paraffins	5.02	11.55	7.05	4.83	4.63	5.98	4.08	3.73	5.43	78
H ₂ /n-Paraffins	6.08	13.64	---	8.19	7.04	9.24	3.39	2.28	4.20	40
CO/n-Paraffins	3.04	20.20	---	1.72	1.75	4.30	4.32	3.81	5.36	42
Total	5.22	12.53	---	6.27	4.71	6.66	4.98	3.11	6.05	489

gave slightly better results than Model-1 and the LCVM model. The use of VDW-2 over VDW-1 led to 52%, 28%, 7%, 12%, and 8% reduction in the average absolute deviation of bubble point pressures for C₂H₆, CO₂, CH₄, H₂, and CO, respectively. This indicates the high influence the modified CEOS covolume has on C₂H₆ and CO₂ binaries. For CH₄, H₂, and CO, the availability of limited asymmetric binary data and broad solute composition range, particularly in the middle range (typically highest non-ideality), limited the interpretation that can be placed upon the importance of the covolume for these systems. The model developed in this work, where several semi-theoretical expressions were used, offers some explanation for the behavior of asymmetric mixtures. These include two-fluid theory, group contribution concept, lattice models, and local composition model. As demonstrated in this work, the CEOS covolume is directly related to the athermal Helmholtz Free energy derived from the lattice model.

The percentage deviations of the covolume based on Equation (7-20) from the values calculated using linear mixing rule are illustrated for the five solutes considered in Figures 19 to 23. The modified UNIFAC was used in determining athermal Helmholtz free energy. For ethane, carbon dioxide, and methane with n-paraffins mixtures, a systematic increase in covolume deviations is noticed as the molecular weight of hydrocarbon increases. For ethane and carbon dioxide mixtures, the deviation reaches around -26% at about 0.5 solute mole fraction. For methane, lower deviations were observed. As mentioned before, linear correlations were used to correct the combinatorial expression of Equation (7-20) for both hydrogen and carbon monoxide mixtures. As shown in Figure 22 for hydrogen/n-paraffins, the deviations of the

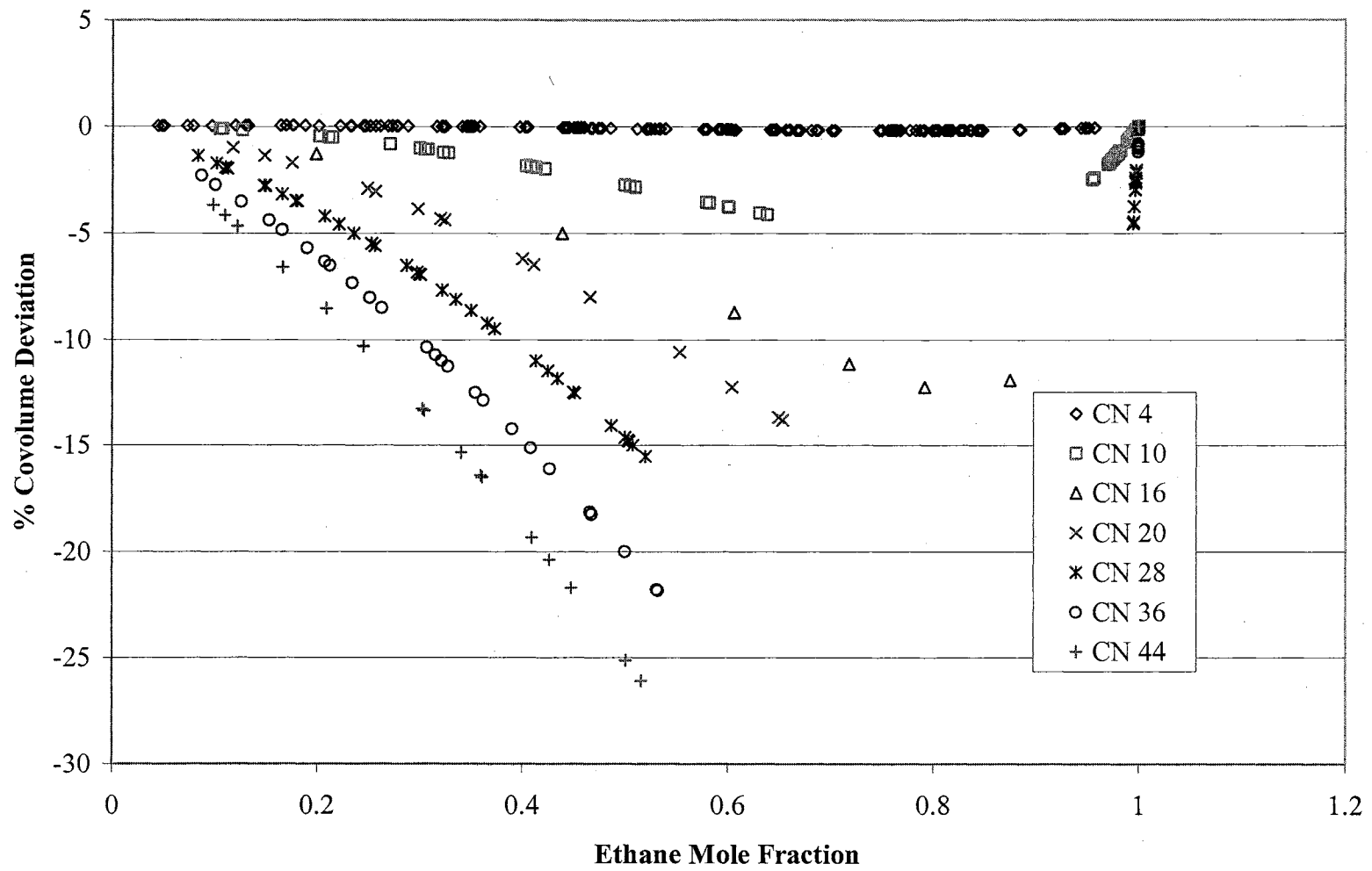


Figure 19. Comparison of the Covolume Deviations for Ethane/n-Paraffin Mixtures.

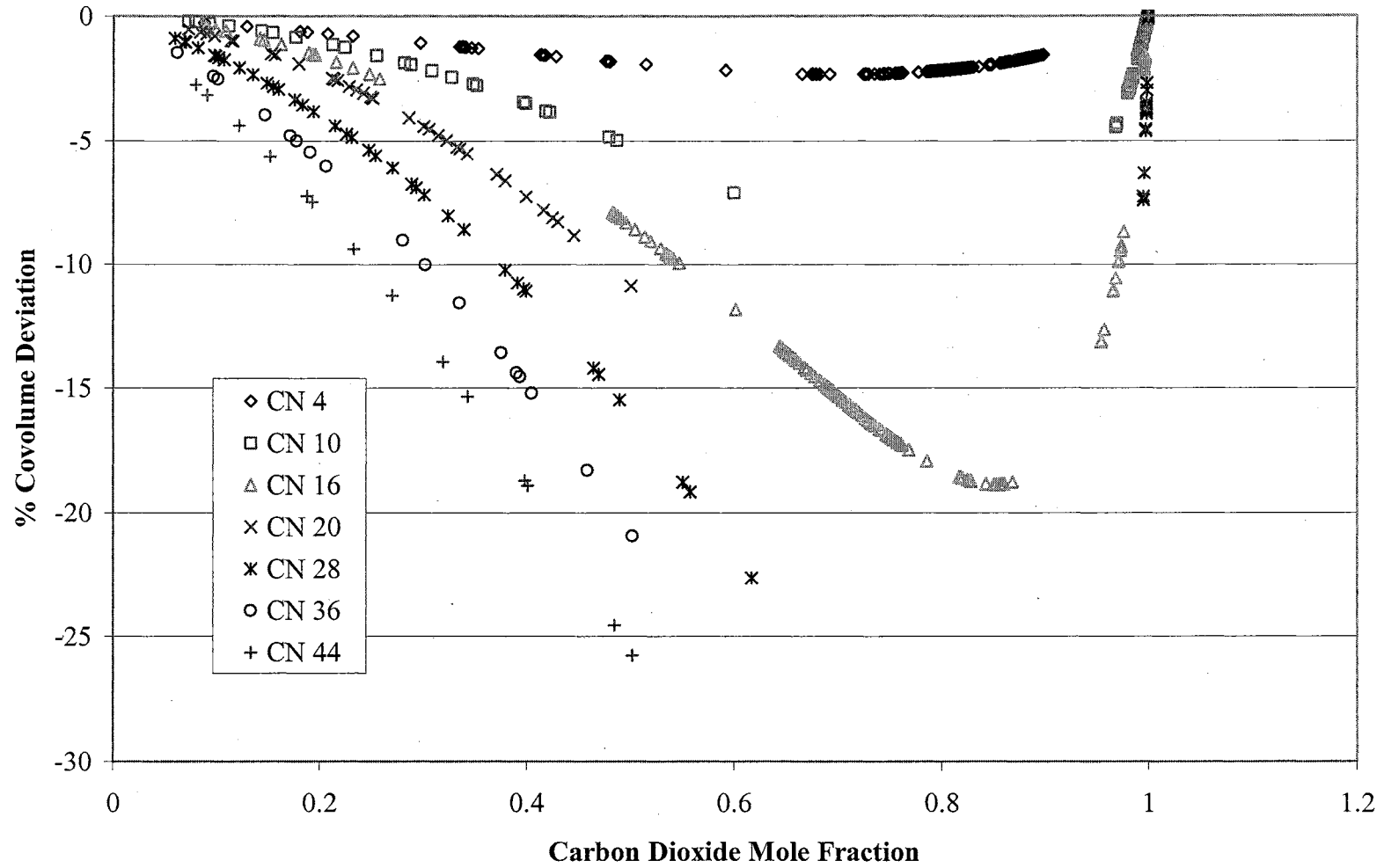


Figure 20. Comparison of the Covolume Deviations for Carbon Dioxide/n-Paraffin Mixtures.

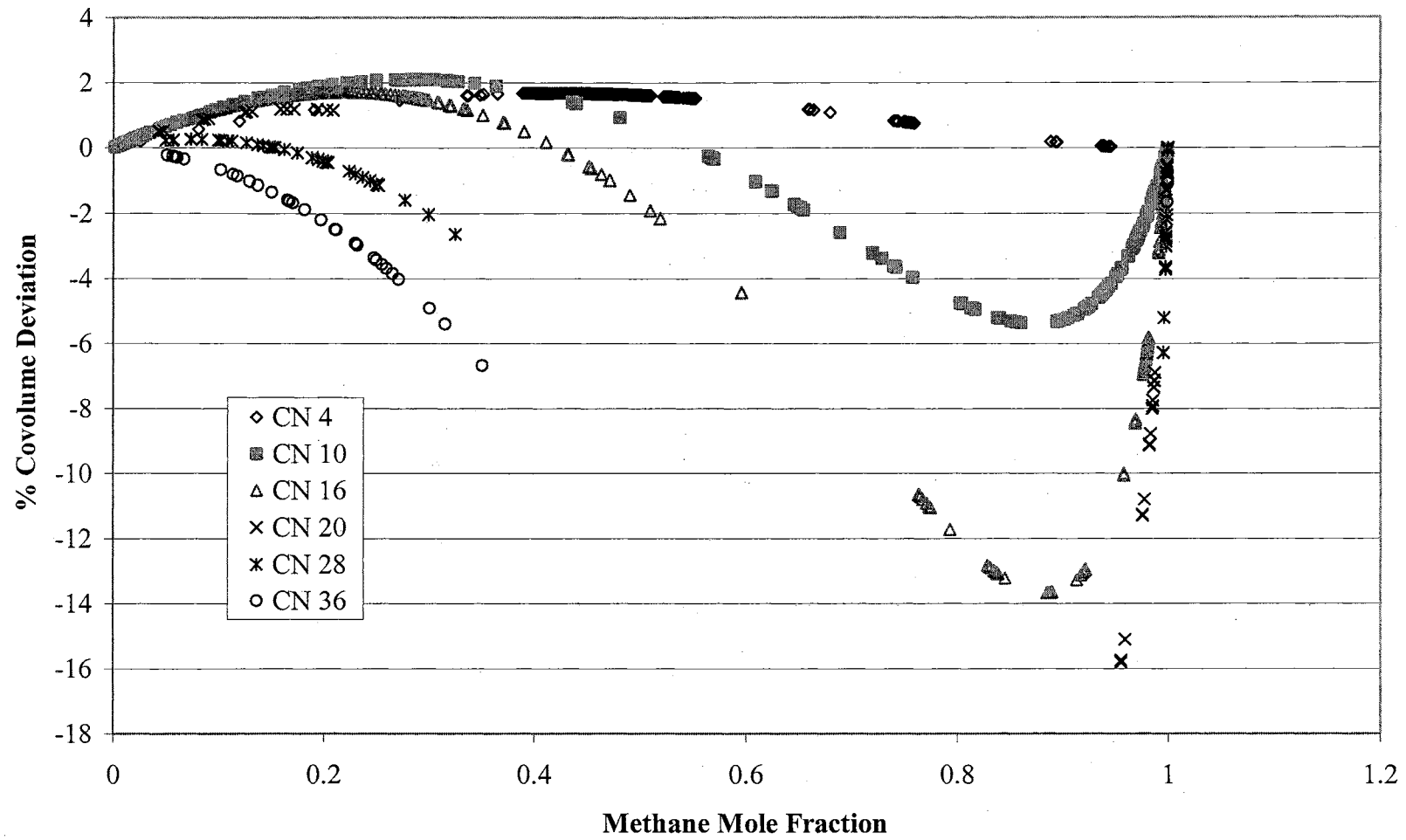


Figure 21. Comparison of the Covolume Deviations for Methane/n-Paraffin Mixtures.

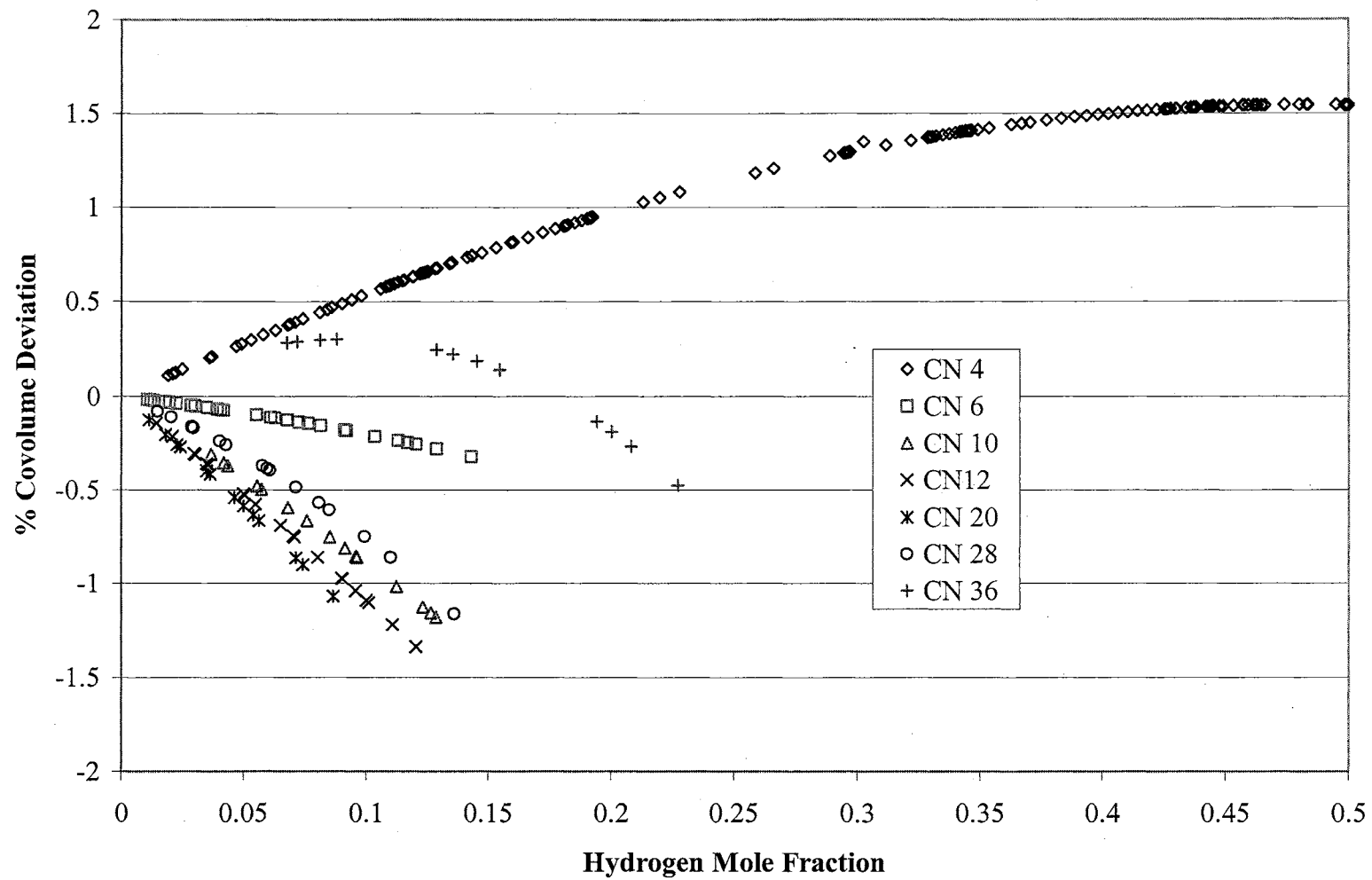


Figure 22. Comparison of the Covolume Deviations for Hydrogen/n-Paraffin Mixtures.

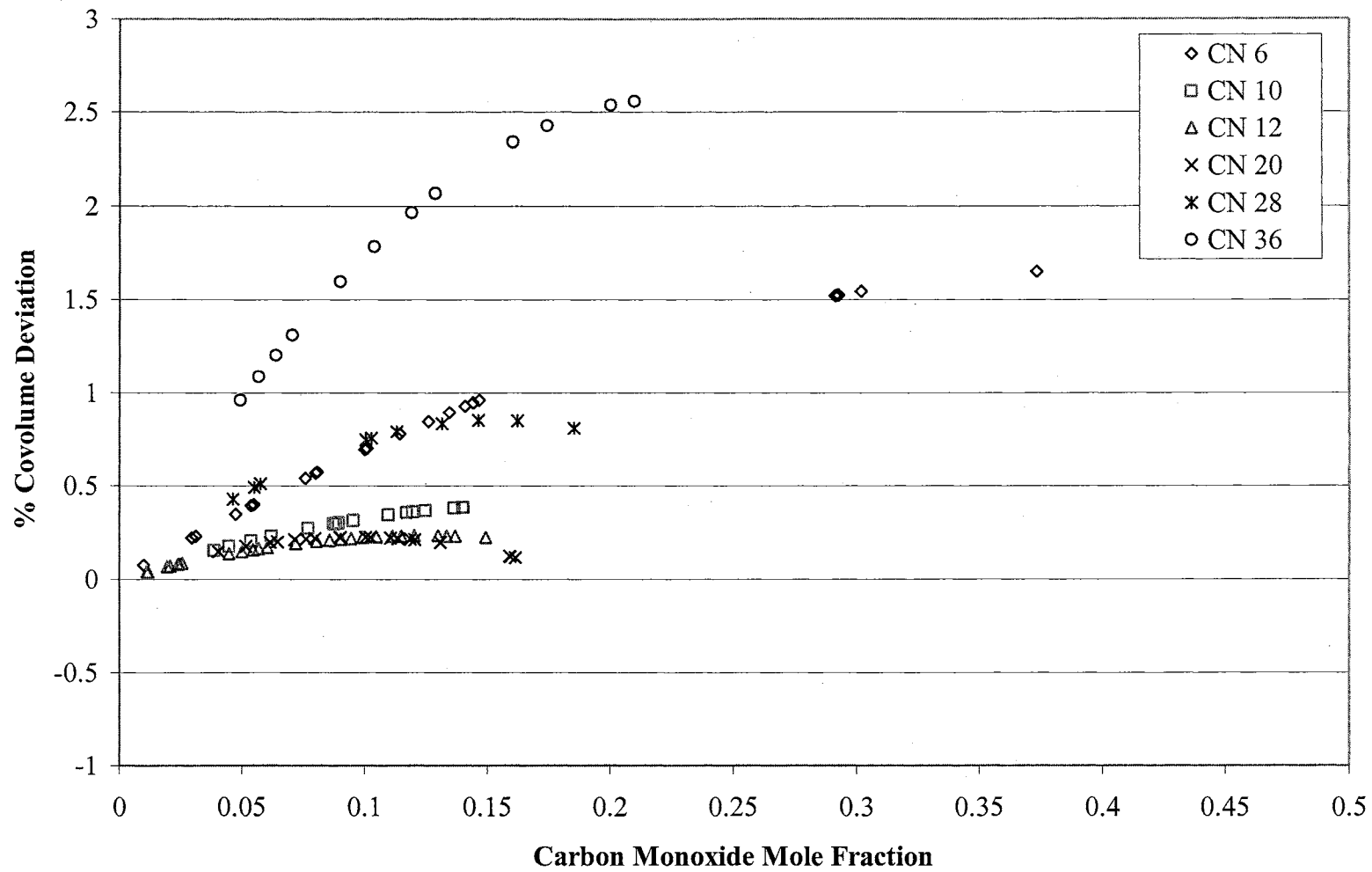


Figure 23. Comparison of the Covolume Deviations for Carbon Monoxide/n-Paraffin Mixtures.

covolume from the value determined using linear mixing rule are very small in comparison to the relative size ratio of hydrogen to n-paraffins (hydrogen is the smallest molecule among the five solutes). This is partially attributed to the narrow hydrogen liquid composition range (0 - 0.15). Another observation is that no systematic deviation was observed as the asymmetry increased. C₂₈ and C₃₆ mixtures have lower deviations than lower molecular weight hydrocarbons. For C₃₆, the result is not representative of H₂/C₃₆ mixture (%AAD is 9.9 for Model-1). For C₂₈, C₂₀, C₁₂, and C₁₀ deviations in covolume are small and close to each other. Carbon monoxide/n-paraffins is another case that is similar to the hydrogen/n-paraffin systems.

In comparison to the new model, as illustrated in Figures 24 and 25, the VDW-2 model covolume parameter D₁₂ shows a nearly systematic deviation, with the exception of few points, for ethane and carbon dioxide with n-paraffin carbon number. For methane, hydrogen, and carbon monoxide, the deviations of the covolume parameter are random and small. To evaluate CHV model covolume trends, the linear mixing rule for covolume was replaced by a quadratic mixing rule (Equations 2-2 and 2-4) similar to VDW-2 model. As shown in Figure 26, random variations in D₁₂ parameter with n-paraffin molecular weights are observed. The CHV model does not reflect the expected systematic deviation in covolume parameter observed with ethane and carbon dioxide with n-paraffin systems as the asymmetry increases.

From the results and figures presented, no correction to the covolume is required for binaries of methane, hydrogen, and carbon monoxide involving n-paraffin in spite of the large size ratios. To investigate these observations, the infinite dilution activity coefficients were determined for several solutes in n-paraffin form modified UNIFAC

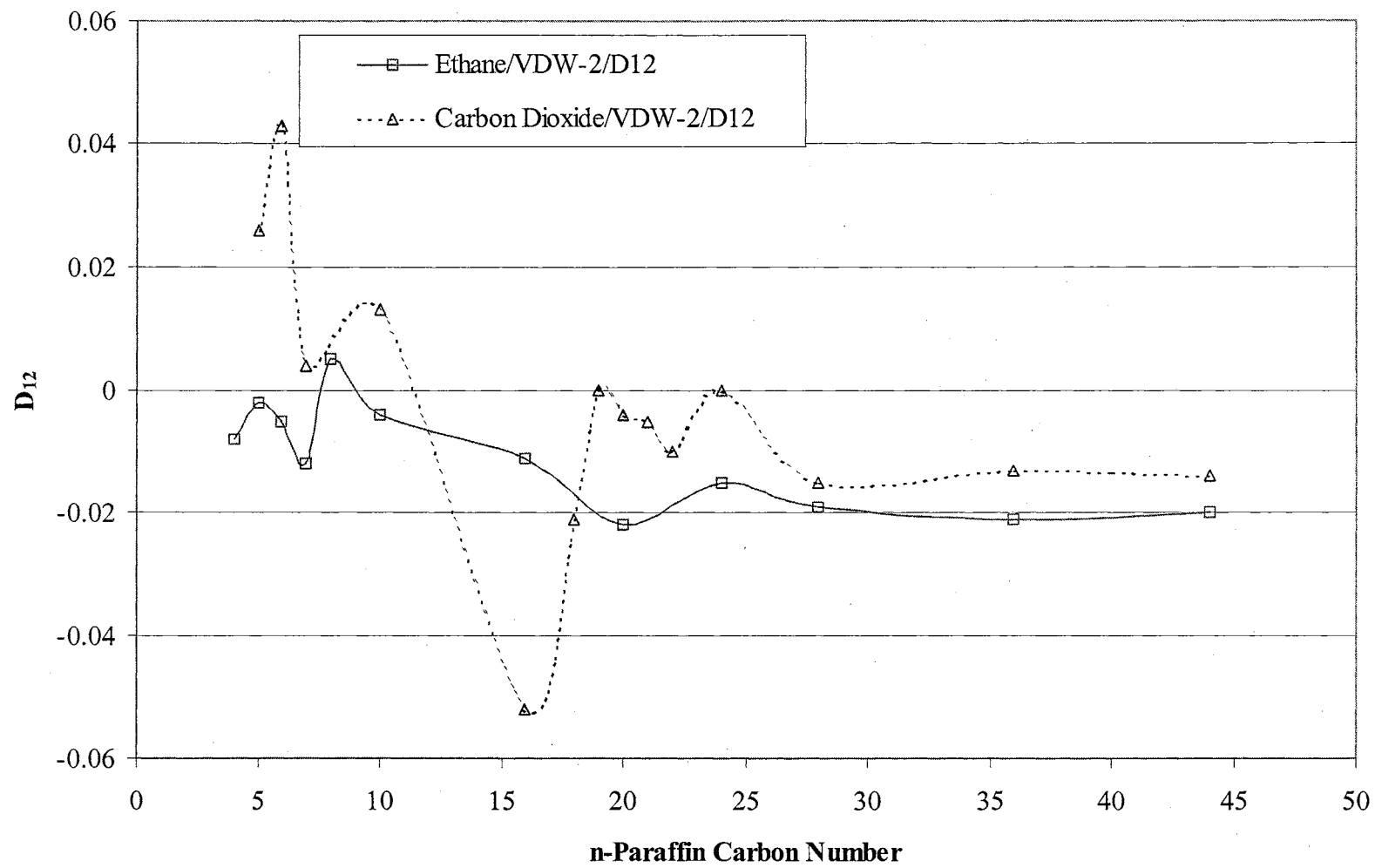


Figure 24. Covolume Interaction Parameter Variations for VDW-2 Model- Case 1.

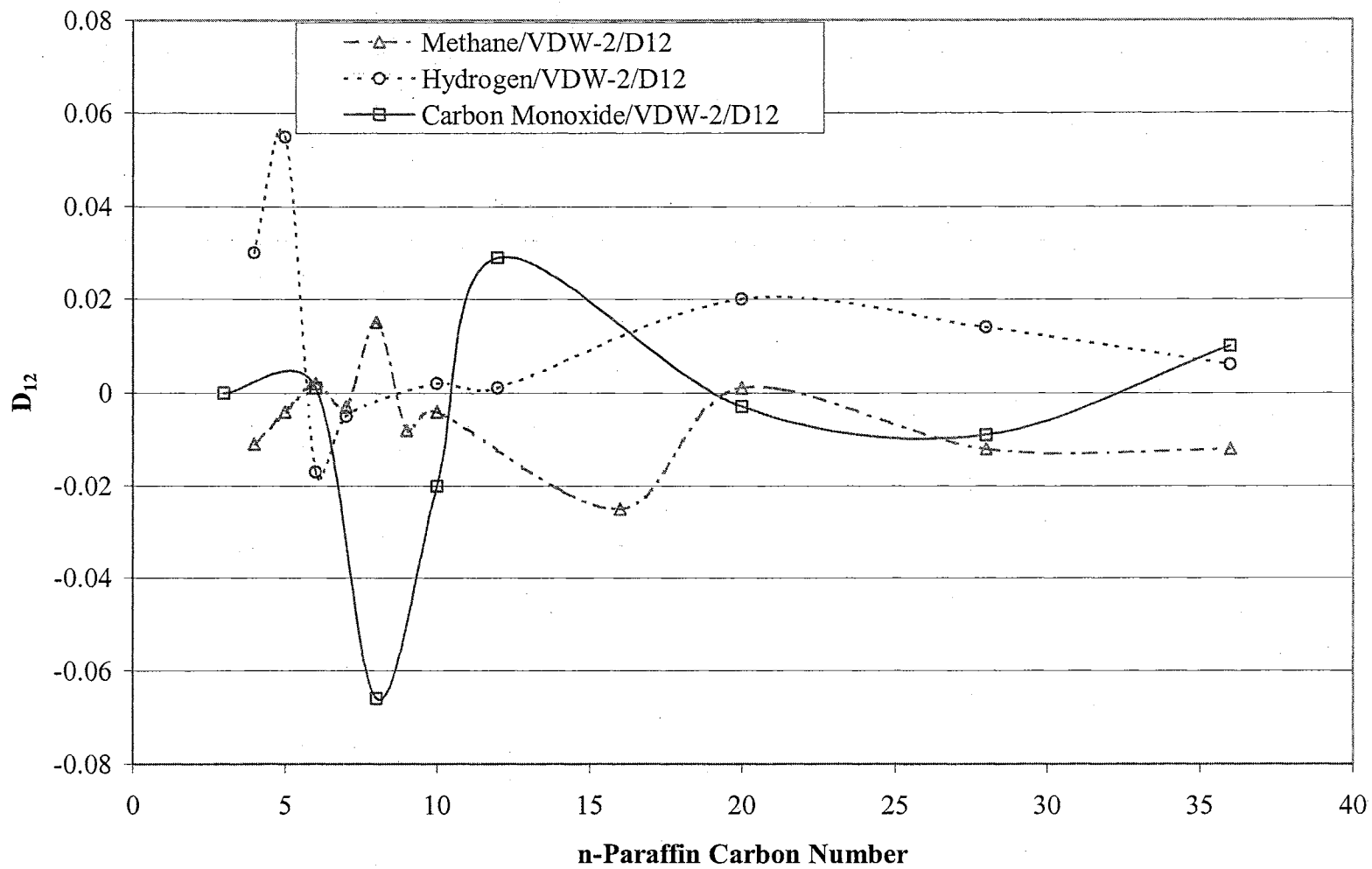


Figure 25. Covolume Interaction Parameter Variations for VDW-2 Model - Case 2.

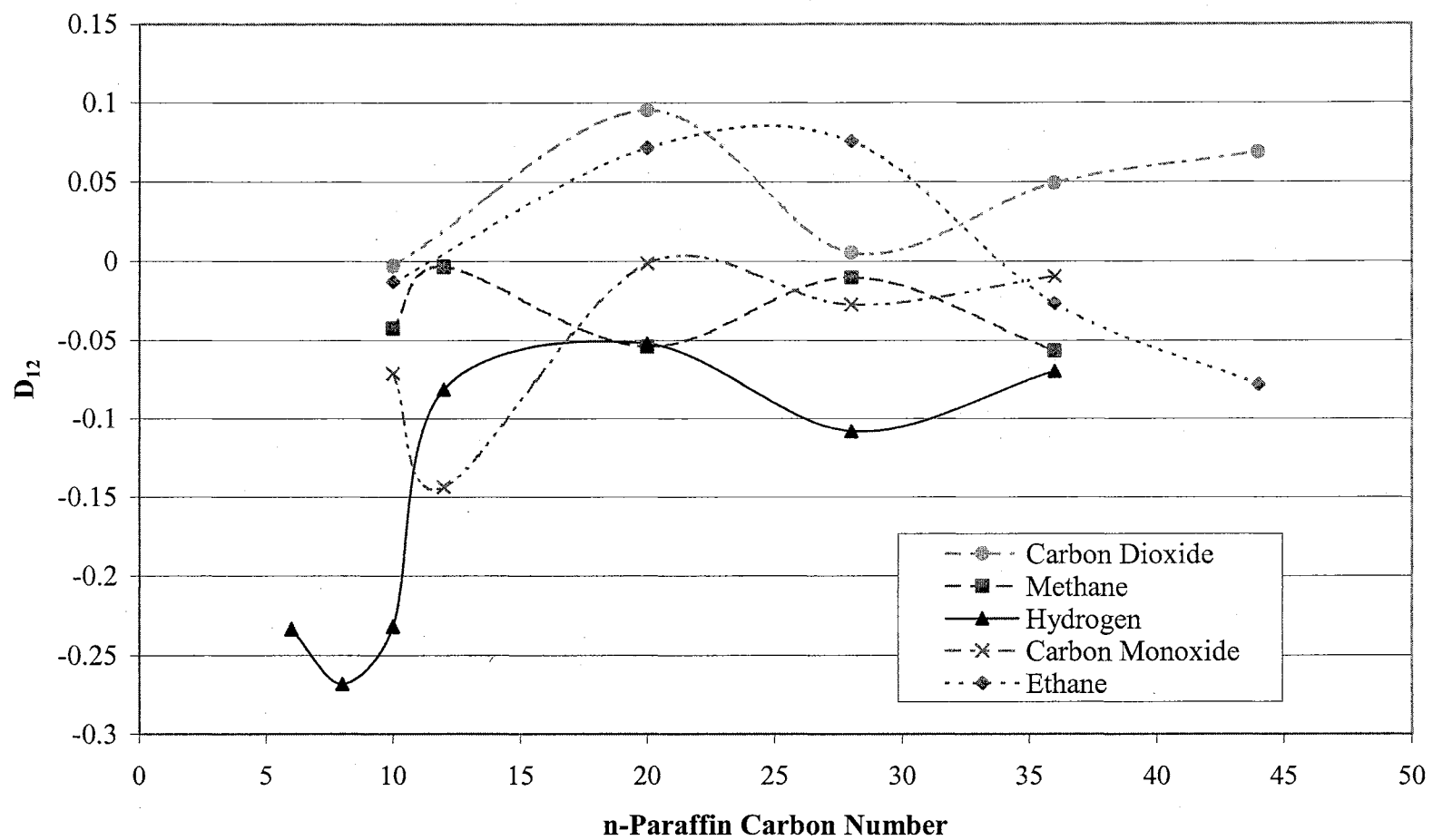


Figure 26. Covolume Interaction Parameter Variations for CHV Model.

model using group interaction parameters regressed for Model-1. The values determined for infinite dilution activity coefficients were based on the approximation that excess Helmholtz free energy are nearly equal to excess Gibbs free energy. As indicated in Figures 27 and 28, the infinite dilution activity coefficient and its combinatorial term decrease as the asymmetry increase. An important aspect of the new mixing rule for the covolume is the interpretation of its parameters and how they affect asymmetric mixtures behavior. As indicated in Equation (7-20), the covolume is dependent on the athermal excess Helmholtz, pure components volumes “ b_i ” and compositions. As shown in Figure 29, as the molecular size ratio increases, the athermal excess Helmholtz absolute value increases and consequently, the covolume increases to reach a value (as shown for methane, hydrogen and carbon monoxide with n-paraffin systems) equal to covolume determined from linear mixing rule. Excellent example in how the new mixing rule reflects the nonideality due to the size effect is methane/n-paraffin and carbon dioxide/n-paraffin binary mixtures. In both cases using two universal constants, the mixing rule for covolume was able to represent both systems reasonably well.

For hydrogen/ and carbon monoxide/n-paraffin mixtures, Model-1 parameter, δ_2 , is correlated to n-paraffin carbon number. The increase in size ratio in comparison to the first three solutes (ethane, carbon dioxide, and methane) dictates the use of non-universal empirical corrections to excess Helmholtz combinatorial expression determined from modified UNIFAC model. The use of excess Helmholtz combinatorial expression by Ye and Zhong (2000) may eliminate the use of these correlations. This is due to the ability of Ye and Zhong (2000) model to represent systems with high asymmetry in comparison to

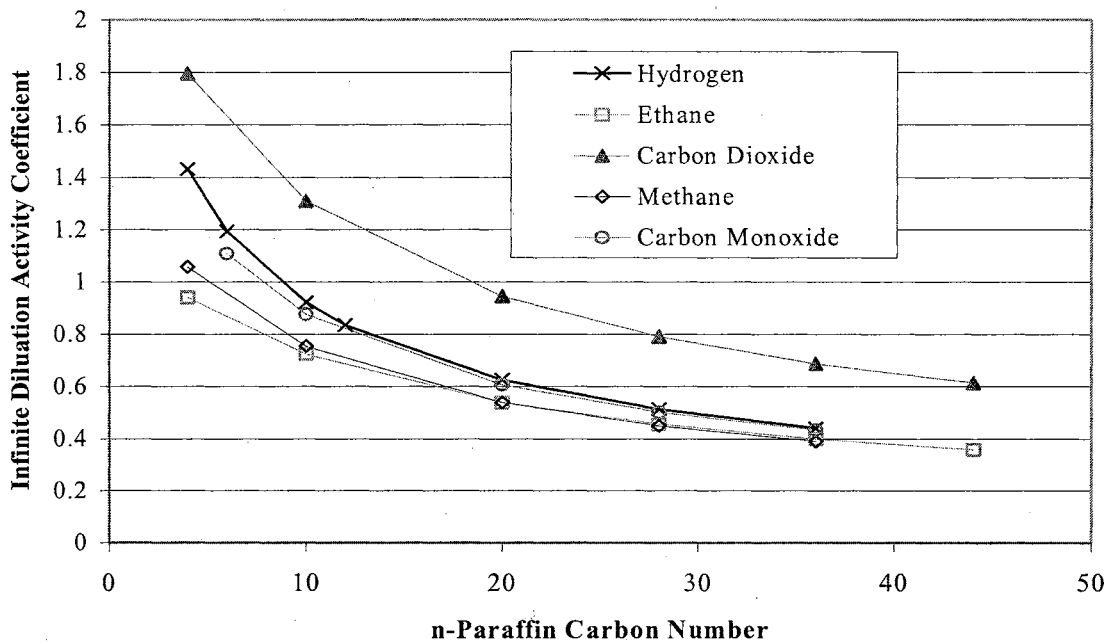


Figure 27. Infinite-Dilution Activity Coefficients of Solutes in n-Paraffins at 373 K.

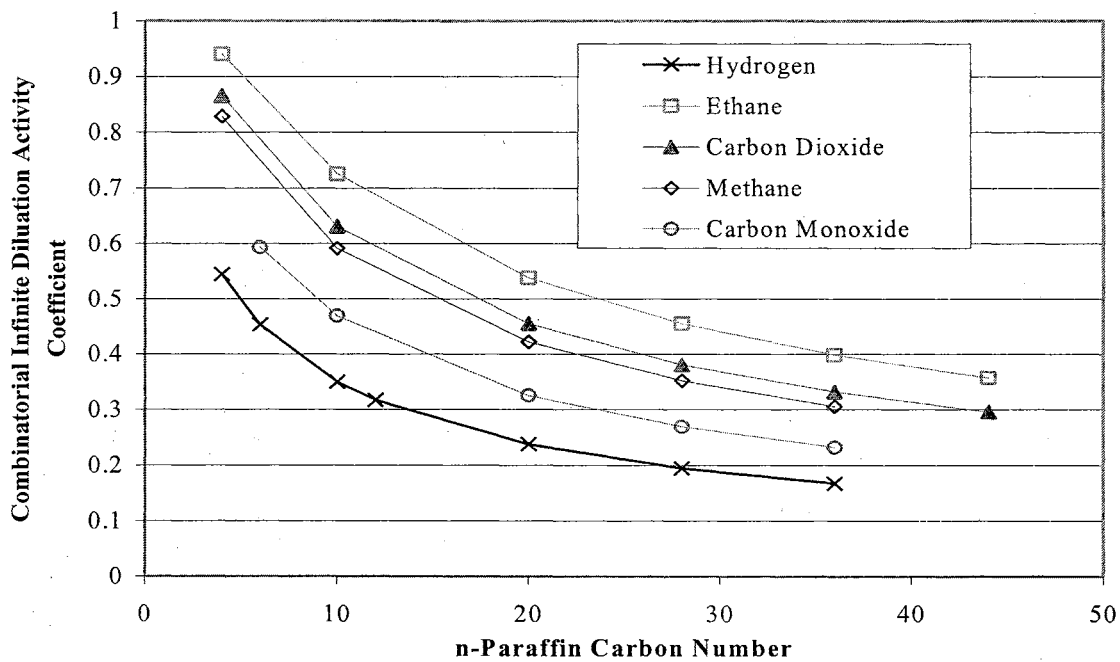


Figure 28. Combinatorial Infinite-Dilution Activity Coefficients of Solutes in n-Paraffins at 373 K.

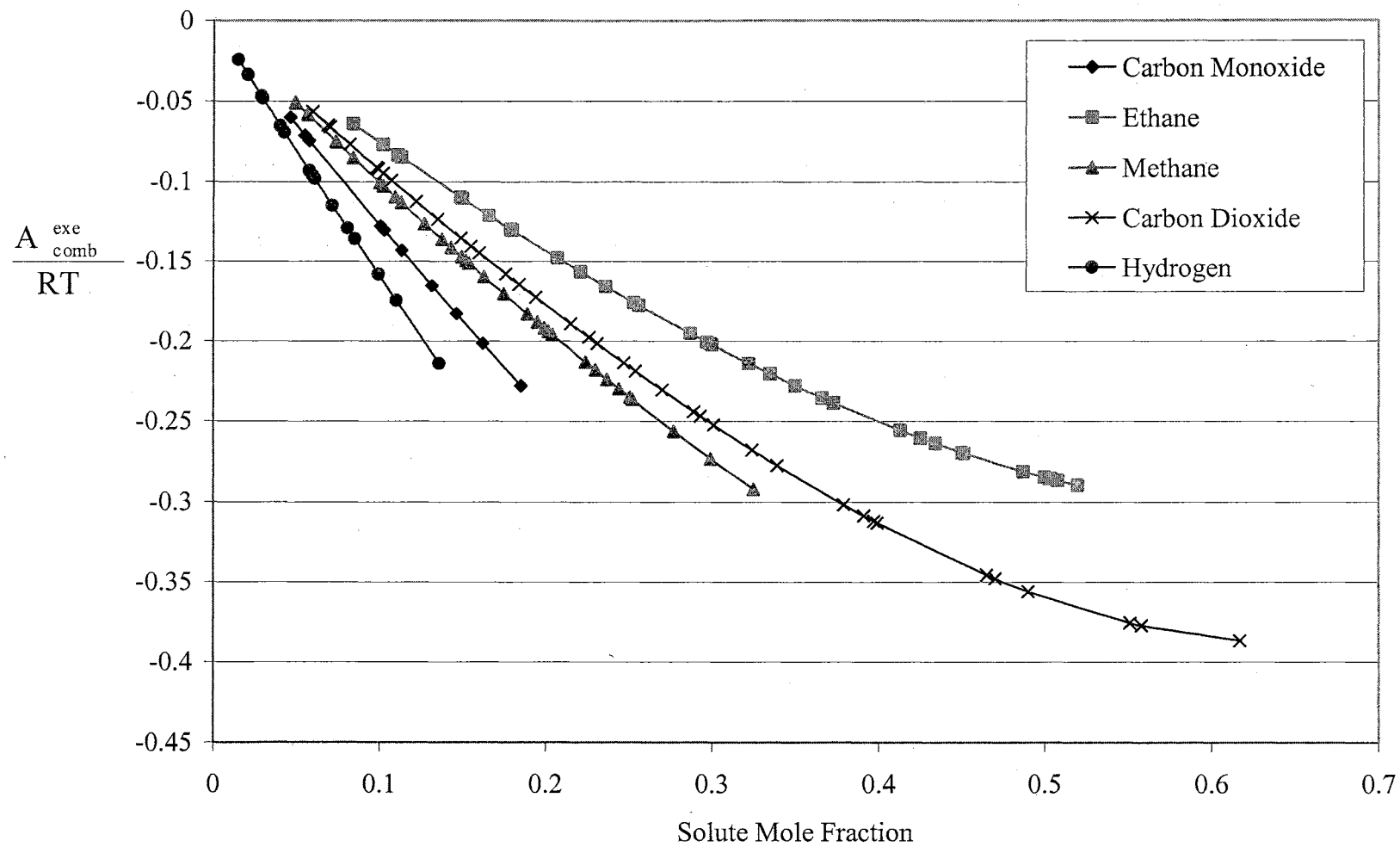


Figure 29. Excess Helmholtz Combinatorial Values for Several Solutes in n-Octacosane at 373.3 K.

modified UNIFAC model (Konlogeorgis, et al., 1994). In addition, as indicated with hydrogen/n-paraffin and carbon monoxide/n-paraffin systems, the deviations in covolume take a positive trend as the asymmetry increased. This is due to the effect of Equation (7-20) parameters, where the increase in both pure n-paraffin covolume and the excess Helmholtz combinatorial contribution tend to shift the deviation to a positive direction.

Number of Parameters Used

The number of parameters used for each model is listed in Table 41. These parameters applied to binary and ternary mixtures tested in the Chapter VIII. The high quality of experimental data fit by the VDW-2 model is at the expense of the high number of parameters required. The VDW-G model gave comparable overall results to Model-1 and CHV model with the least number of parameters for the systems; however, the advantage of group contribution models over models based on molecular interactions is that it can be extended to broad range of systems. In addition, for asymmetric ethane/n-paraffin mixtures, VDW-1 and VDW-G gave the worst results.

Table 41. Comparison among the Number of Parameters for the Models Evaluated

	Model-1	CHV	LCVM	VDW-1	VDW-2	VDW-G
Universal Parameters	2	1	1	0	0	0
	Group Contribution Parameters			Molecular Interaction Parameters		
Ethane	0	0	0	16	32	2*
Carbon Dioxide	4	4	4	15	30	2*
Methane	4	4	4	11	22	2*
Hydrogen	4+ 2*	4	4	11	22	2*
Carbon Monoxide	4+ 2*	4	4	7	14	2*
Total	22	17	17	60	120	10

*Correlations parameters

Summary

A new semi-theoretical equation for the CEOS covolume was developed and evaluated. The new equation related the CEOS covolume to excess Helmholtz combinatorial contribution. Comparison of several combinatorial expressions using infinite-dilution activity coefficients and VLE data of ethane/n-paraffin systems indicate that the modified UNIFAC is the best expression for use in the new model. Among the five solute/n-paraffin systems examined, ethane/n-paraffin and carbon dioxide/n-paraffin systems had the highest dependence on the covolume as indicated by comparing VDW-1 and VDW-2 results. The new model was compared to CHV, LCVM, and VDW-G. Overall models comparison reveals that Model-1 is better than the LCVM and VDW-G models, particularly for asymmetric mixtures and comparable to the CHV model, with the exception of hydrogen/n-paraffin systems, where a significant improvement in representing bubble point pressures is achieved using the new model. The new semi-theoretical mixing rule for the covolume allows interpretation of the fluid behavior due to variation in molecular size ratios. As expected, the van der Waals one-fluid mixing rules with two temperature-independent parameters gave the best results since a significant number of molecular interaction parameters are used.

CHAPTER VIII

NEW MIXING RULES BASED ON EXCESS HELMHOLTZ FREE ENERGY

2. EVALUATION WITH TERNARY MIXTURES

The behavior of mixtures is significantly impacted by the interactions of unlike molecules. Interactions among triplets and higher combinations usually are less important than those between pairs of components (Walas, 1985); however, interactions among triplet combinations become significant at high reduced-pressures (Lee, et al., 1978). Higher-order interactions often are small, and thus they are hidden by imperfection in the EOS used. As such, ternary mixtures may provide a better description of multi-component equilibrium in general (Sadus, 1999).

Mixing rules that can represent accurately the VLE phase behavior of binary mixtures may give unacceptable prediction results for some of the multi-component mixtures (Zavala, 1996). As stated by Soave (1984), vdW classical mixing rules have been shown to apply well to binary mixtures of polar compounds. Unfortunately, although such rules are completely adequate for binary systems, they fail when applied to some multi-component mixtures (see, e.g., Leland, 1980; Gupta, et al., 1980). This situation is further complicated by the non-ideality of size variations in asymmetric multi-component mixtures. Therefore, evaluation and development of mixing rules must take into consideration the ability to predict correctly at least the VLE behavior of ternary mixtures (BenMekki and Mansoori, 1988).

Model Development

In this chapter, Model-1, the CHV, the LCVM, and the VDW-G models were evaluated and compared. A complete evaluation of the predictive ability of VDW-1 and VDW-2 models for asymmetric ternary mixtures was given in Chapter VI. A list of mixing rules for the first three models is given in Table 29.

For Model-1, linear correlations for δ_2 in terms of n-paraffin carbon number were used for the hydrogen/n-paraffin and the carbon monoxide/n-paraffin systems. The mixing rule for the parameter “ δ_2 ” is based on the work of Zhong and Musoka (1996):

$$\delta = \sum_i \sum_j \left(\frac{z_i + z_j}{2} \right) \delta_{ij} \quad (8-1)$$

This mixing rule works well for binary mixtures but not for ternaries. Accordingly, the following modification was implemented in this work:

$$\delta = \frac{1}{(NC-1)} \sum_i \sum_j \left(\frac{z_i + z_j}{2} \right) \delta_{ij} \quad (8-2)$$

where, $\delta_{ii} = 0$

Database Used

Table 42 presents the ternary database used in the model evaluation. The critical constants and the acentric factors listed in Table 14 were used.

Results and Discussions

Table 43 presents the model evaluation results for the bubble point pressure of ternary mixtures. The results for VDW-1 and VDW-2 are presented only for comparison.

Table 42. The Database of Ternary Systems Used in this Study

Ternary Mixture (1)/(2)/(3)	Temperature Range, K	Pressure Range, MPa	Mole Fraction Range Components (1) and (2)	NPTS	Reference
Methane/Propane/Decane	410.93	2.758 – 27.579	0.0632 – 0.7116 0.1874 – 0.0577	13	Wiese et al., 1970
CO ₂ /Butane/Decane	344.30	9.030 – 10.350	0.6370 – 0.7320 0.1570 – 0.1160	5	Nagarajan et al., 1990
Ethane/Butane/Heptane	338.71	3.523 – 6.191	0.5460 – 0.7520 0.0553 – 0.1622	14	Mehra and Thodos, 1966
CO ₂ /Pentadecane/Hexadecane	313.15	1.714 – 6.405	0.1840 – 0.5820 0.4080 – 0.2090	8	Tanaka et al., 1993
CO ₂ /Ethane/Eicosane	323.15 – 423.15	3.210 – 9.278	0.0285 – 0.3779 0.5804 – 0.0993	22	This Work
CO ₂ /Ethane/Octacosane	348.15 – 423.15	3.333 – 14.165	0.0455 – 0.5672 0.4799 – 0.0581	18	This Work
CO ₂ /Ethane/Hexatricontane	373.15 – 473.15	3.430 – 8.760	0.0945 – 0.4277 0.3774 – 0.0479	12	This Work
CO ₂ /Hydrogen/Eicosane	323.15 – 423.15	6.443 – 13.940	0.0800 – 0.4393 0.0143 – 0.1197	16	This Work
CO ₂ /Hydrogen/Octacosane	348.15 – 423.15	9.890 – 15.296	0.1994 – 0.5757 0.0991 – 0.0198	12	This Work
CO ₂ /Hydrogen/Hexatricontane	373.15 – 473.15	6.590 – 12.210	0.1640 – 0.4911 0.1482 – 0.0356	12	This Work

Table 43. Summary of Model Evaluation Results for the Asymmetric Ternary Systems

	Model-1	CHV	LCVM	VDW-1 C ₁₂ / Binary	VDW-2 C ₁₂ /D ₁₂ Binary	VDW-G C ₁₂ Generalized	NPTS
	%AAD in Bubble Point Pressure						
Methane/Propane/Decane	9.12	3.77	3.56	3.07	3.07	1.59	13
CO ₂ /Butane/Decane	4.30	3.30	1.54	4.36	4.36	2.59	10
Ethane/Butane/Heptane	1.53	2.70	3.11	2.15	2.15	1.16	14
CO ₂ /Pentadecane/Hexadecane	1.10	2.68	8.59	1.81	1.81	9.08	8
CO ₂ /Ethane/Eicosane	4.66	2.00	8.33 NC (6)*	7.79	2.48	8.48	22
CO ₂ /Ethane/Octacosane	4.18	2.44	9.63 NC (7)	13.87	3.88	18.34	18
CO ₂ /Ethane/Hexatricosane	10.84	1.97	4.78 NC (1)	10.16	2.59	13.84	12
CO ₂ /Hydrogen/Eicosane	9.61	6.07	4.28	4.92	4.86	4.95	16
CO ₂ /Hydrogen/Octacosane	4.34	7.26	4.75 NC (3)	9.10	3.05	8.01	12
CO ₂ /Hydrogen/Hexatricosane	7.12	12.78	11.21	5.25	2.55	5.11	12
Total	5.68	4.50	5.98	6.25	3.08	7.32	137

NC (6): No conversion in 6 data points

The quality of the bubble point predictions obtained for Model-1, CHV, LCVM, and VDW-G, as signified by the AAD, are 5.7, 4.5, 6.0, and 7.3 %, respectively. As indicated, the VDW-2 gave the best results among the models considered. Further, with few exceptions, all the models performed well with ternary mixtures involving molecules smaller than C₁₆.

The main issue under consideration here is the predictive ability of these models with regard to the bubble point pressures of asymmetric ternary mixtures. Normally, the accuracy of the prediction for the ternary experimental data depends on the fit of the binary systems, which form the boundaries of the ternary system (Shibata and Sandler, 1989), and the precision of the experimental data. The precision of the experimental data acquired in this study was analyzed and established in Chapter VI.

Table 44 presents a comparison among the predictive models as they address the asymmetric binary and ternary mixtures considered in this study. %AAD of 6.8, 5.4, 7.2, and 9.8 are observed for Model-1, CHV, LCVM, and VDW-G, respectively. For Model-1, one out of six systems (CO₂+ H₂ +C₂₀) considered shows considerably larger deviations than those observed for the binary systems, and another system (CO₂ + C₂H₆ + C₃₆) produces by 28% larger deviations than the binary systems maximum deviations. For the CHV model, (CO₂+H₂+C₂₀) and (CO₂+H₂+C₂₈) deviate respectively by 45% and 43% AAD in bubble point pressure beyond the maximum deviations from the binary data. The LCVM model did not converge for several asymmetric mixtures data points; therefore, these data were not included in LCVM model evaluation. The deviations for (CO₂+C₂H₆+C₂₀) and (CO₂+C₂H₆+C₂₈) exceeded the maximum deviations from the binary data. The VDW-G and VDW-1 models prediction of bubble point pressures of

Table 44. Models Comparison for Asymmetric Binary and Ternary Mixtures

	Model-1	CHV	LCVM	VDW-G	NPTS
	% AAD in Bubble Point Pressure				
CO ₂ + Ethane + Eicosane	4.7	2.0	8.3 NC (6)	8.5	22
CO ₂ + Ethane/CO ₂ + Eicosane/Ethane + Eicosane	2.2/3.3/4.6	1.2/4.2/5.9	0.7/6.0/6.0	1.2/4.6/7.4	
CO ₂ + Ethane + Octacosane	4.2	2.4	9.6 NC (7)	18.3	18
CO ₂ + Ethane/CO ₂ + Octacosane/Ethane + Octacosane	2.2/4.1/2.3	1.2/5.1/4.8	0.7/4.0/6.4	1.15/7.0/7.1	
CO ₂ + Ethane + Hexatricontane	10.8	2.0	4.8 NC (1)	13.8	12
CO ₂ + Ethane/CO ₂ + Hexatricontane/Ethane + Hexatricontane	2.2/8.4/5.8	1.2/2.4/4.4	0.7/2.7/7.1	1.1/9.9/8.2	
CO ₂ + Hydrogen + Eicosane	9.6	6.1	4.28	4.9	16
CO ₂ + Hydrogen/CO ₂ + Eicosane/Hydrogen + Eicosane	1.8/3.3/3.1	1.8/4.2/3.9	3.9/6.0/3.7	1.2/4.6/5.0	
CO ₂ + Hydrogen + Octacosane	4.3	7.3	4.75 NC (3)	8.0	12
CO ₂ + Hydrogen/CO ₂ + Octacosane/Hydrogen + Octacosane	1.8/4.1/5.2	1.8/5.1/4.9	3.9/4.0/5.9	1.17/7.0/3.2	
CO ₂ + Hydrogen + Hexatricontane	7.1	12.8	11.2	5.1	12
CO ₂ + Hydrogen /CO ₂ + Hexatricontane/Hydrogen + Hexatricontane	1.8/8.4/9.9	1.8/2.4/12.3	3.9/2.7/18.1	1.17/9.9/5.4	
Total	6.8	5.4	7.2	9.8	137

asymmetric ternary mixtures involving ethane are not accurate. This is due to the inability of the PR EOS using one-fluid mixing rule with single interaction parameter (C_{ij}) to represent accurately these mixtures. As stated by Peters (1986), for binary mixtures of a volatile and non-volatile n-alkanes, the binary parameter D_{ij} is more important than C_{ij} to describe VLE of ethane/eicosane binary mixture using a simple CEOS.

On comparison of all the excess Gibbs/Helmholtz free energy models, no systematic deviations were observed in their predictive ability of asymmetric ternary mixtures, and in most cases, they were able to predict ternary data within the boundaries of binary data. The imprecision of the experimental data for the asymmetric ternary mixture ($\text{CO}_2 + \text{H}_2 + \text{C}_{20}$) may be the cause of the few cases where deviations exceed those of the binary data.

Summary

The present results indicated that the VDW-2 model, where two temperature-independent binary interaction parameters were used, produces the best results among the models considered. This accordingly justifies the use of the one-fluid theory mixing rules when two temperature-independent parameters are employed. VDW-1 and VDW-G models gave the worst results for $\text{C}_2\text{H}_6/\text{CO}_2/\text{n-paraffin}$ mixtures, and the CHV model performed worst for the $\text{H}_2/\text{CO}_2/\text{n-paraffin}$ mixtures. In most cases, Model-1, the CHV and the LCVM models were able to predict the ternary mixture bubble point pressures based solely on pair-wise interactions between functional groups. High deviations in

predicting the bubble point pressures, for most of the ternary mixtures evaluated, were attributed to poor representation of the corresponding binaries.

CHAPTER IX

CONCLUSIONS AND RECOMMENDATIONS

Conclusions

A new, constant-volume, synthetic-type, mercury-free, high-pressure experimental apparatus was designed and operated based on a new experimental technique. Internal and external consistency tests indicate a good level of precision and accuracy for the experimental data acquired. Solubility measurements for asymmetric ternary mixtures of (a) hydrogen and carbon dioxide in eicosane, octacosane, and hexatricosane were determined over the temperature range 323.15 to 473.15 K and pressures to 15.3 MPa; and (b) ethane and carbon dioxide in eicosane, octacosane, and hexatricosane were determined at 323.15, 344.26, 373.15 and 423.15 K and pressures to 14.17 MPa. Internal and external consistency tests validate the viability of the newly-acquired ternary solubility measurements, which exhibit experimental uncertainties within 0.002 in mole fraction.

Evaluation of the one-fluid mixing rules as they apply to asymmetric ternary mixtures was conducted. For the ethane/carbon dioxide/n-paraffin asymmetric ternary mixtures, the PR EOS with one-fluid mixing rules was capable of predicting ternary mixture bubble point pressures with the same accuracy as it represents their constituent binaries when two temperature-*independent* parameters were used per binary. In comparison, for the hydrogen/CO₂/n-paraffin, the predictive ability of the PR EOS with

one-fluid mixing rule was as good as its representation of its binaries when one or two temperature-*independent* parameters were used.

The present effort to improve the CEOS mixing rules for asymmetric mixtures based on a sound theoretical approach has been effective. A new semi-theoretical mixing rule was developed for the Peng-Robinson EOS covolume, which accounts effectively for molecular size asymmetry in mixture phase behavior. In general, the new excess Helmholtz energy mixing rule yields predictions with average absolute deviation of about 4.7% for the systems studied. These results are comparable to those of Orbey and Sandler (1997) and better than those of Boukovalas et al. (1994). Further, the new mixing rules produce excellent results for the challenging hydrogen/n-paraffin binaries.

A comparison of all the models considered in this study revealed that the one-fluid mixing rules, where two *temperature-independent* binary interaction parameters were used, produce the best results for the binary and ternary mixtures evaluated. However, the one-fluid mixing rules, where one *temperature-independent* binary interaction parameter was used (as represented by VDW-1 or VDW-G), are inadequate for handling asymmetric mixtures involving ethane.

The adequacy of the pairwise interactions was validated with the ternary asymmetric mixtures tested. By applying the one-fluid mixing rules, the models were capable of predicting bubble point pressures of asymmetric ternary mixtures based solely on molecular pairwise interactions. Similarly, the excess Gibbs/Helmholtz energy based models were, in most cases, capable of predicting ternary asymmetric bubble point pressures based solely on pairwise functional-group interactions.

Relating the CEOS covolume to athermal Helmholtz combinatorial expression is an important achievement in the theoretical development of CEOS. By introducing this

new mixing rule, a moderate improvement in the results was realized relative to the VDW-2 model. In comparison; for the hydrogen/n-paraffin systems, the new mixing rule for the covolume outperformed the CHV and LCVM models.

Recommendations

Modeling

1. The UNIFAC and UNIQUAC are based on the two-fluid theory and local composition of Wilson (1964). Several local composition models (e.g., Lee and Sandler, 1987) outperform the Wilson model and should be implemented to develop modified versions of UNIFAC and UNIQUAC.
2. The LLV region is of interest in many applications including enhanced oil recovery. The new model evaluation needs to be extended to this region and to highly non-ideal mixtures, where the local composition models are effective (e.g., polar fluids).
3. Generation of UNIFAC group interaction parameters using computational chemistry or ab initio methods as suggested by Sum and Sandler (1999) should be undertaken.
4. Promising excess Gibbs/Helmholtz combinatorial expressions (e.g., Ye and Zhong, 2000) should be implemented to eliminate the need for non-universal correction factors, which were added to the modified UNIFAC combinatorial expression (Larsen, et al., 1987) when addressing hydrogen/n-paraffin and carbon monoxide/n-paraffin binary mixtures.

Experimental work

5. Additional asymmetric ternary mixtures should be investigated to enrich the current database.

6. The existing solvent injection pump should be automated to allow incremental injection of solvent to the equilibrium cell. Such automation will help generate more efficiently the pressure-versus-total volume plots required for determining the equilibrium phase properties.

LITERATURE CITED

Abildskov, J.; Gani, R.; Rasmussen, P.; O'Connell, J. P., "Analysis of Infinite Dilution Activity Coefficients of Solutes in Hydrocarbons from UNIFAC," *Fluid Phase Equilibria*, 181, 163, 2001.

Abrams, D.; Prausnitz, J., "Statistical Thermodynamics of Liquid Mixtures: A New Expression for the Excess Gibbs Energy of Partly or Completely Miscible Systems," *AIChE J.*, 21, 116, 1975.

Adachi, Y.; Sugie, H., "A New Mixing Rule - Modified Conventional Mixing Rule," *Fluid Phase Equilibria*, 28, 103, 1986.

API Research Project 44, *Selected Values of Properties of Hydrocarbons and Related Compounds*, Thermodynamic Research Center, Texas A&M University, College Station, Texas, 1972.

Azarnoosh, A.; McKetta, J., "Nitrogen-n-Decane System in the Two-Phase Region," *J. Chem. Eng. Data*, 8, 494, 1963.

Azevedo, E. G.; Prausnitz, J. M., "Effects of Molecular Size and Shape on Thermodynamic Properties of Fluid Mixtures," *Fluid Phase Equilibria*, 41, 109, 1988.

Bader, M. S., *Vapor-Liquid Equilibrium Properties of Aqueous and Supercritical Fluids at Infinite Dilution*, Ph.D. Dissertation, Oklahoma State University, Stillwater, OK, 1993.

BenMekki, E.; Mansoori, A., "The Role of Mixing Rules and Three-Body Forces in the Phase Behavior of Mixtures: Simultaneous VLE and VLLE Calculations," *Fluid Phase Equilibria*, 41, 43, 1988.

Bondi, A., *Physical Properties of Molecular Crystals, Liquids and Glasses*, Wiley, New York, 1968.

Boukouvalas, C.; Spiliotis, N.; Coutos, P.; Tzouvaras, N.; Tassios, D., "Prediction of Vapor-Liquid Equilibrium with the LCVM Model: A Linear Combination of the Vidal and Michelsen Mixing Rules Coupled with the Original UNIFAC and the t-mPR Equation of State," *Fluid Phase Equilibria*, 92, 75, 1994.

Bufkin, B., *High Pressure Solubilities of Carbon Dioxide and Ethane in Selected Paraffinic, Naphthenic and Aromatic Solvents*, M. S. Thesis, Oklahoma State University, Stillwater, Oklahoma, 1986.

Cebola, M. J.; Saville, G.; Wakeham, W. A., "VLE Measurements at High Pressures and High Temperatures on (Methane +n-Hexane)," *J. Chem. Thermodynamics*, 32, 1265, **2000**.

Chen, H.; Wagner, J., "An Efficient and Reliable Gas Chromatographic Method for Measuring Liquid-Liquid Mutual Solubilities in Alkylbenzene + Water Mixtures: Toluene + Water from 303 to 373 K," *J. Chem. Eng. Data*, 39, 3, 475, **1994**.

Cunningham, J.; Wilson, G., "Equation of State Analogy to an Activity Coefficient - Equation Calculation of Parameters from Group Contributions," Proc., Annu. Conv., Gas Process. Assoc., Tech. Pap., 53, 77, **1974**.

Dahl, S.; Fredenslund, Aa.; Rasmussen, P., "The MHV2 Model: A UNIFAC-Based Equation of State Model for Prediction of Gas Solubility and Vapor-Liquid Equilibria at Low and High Pressures," *Ind. Eng. Chem. Res.*, 30, 1936, **1991**.

Dahl, S.; Michelsen, M. L., "High Pressure Vapor-Liquid Equilibria with a UNIFAC-Based Equation of State," *AICHE J.*, 36, 1829, **1990**.

Daridon, J-L; Bessieres, D.; Xans, P.; Faissat, B., "Measurement and Calculation of Solid-Liquid and Liquid-Vapor Equilibria in a Ternary Mixture," *High Temperatures - High Pressures*, 29, 3, 337, **1997**.

Darwish, N. A., *Binary Vapor-Liquid Phase Equilibrium for Methane in Selected Heavy Normal Paraffins, Napthenes, and Aromatics*, Ph.D. Dissertation, Oklahoma State University, Stillwater, OK, **1991**.

Deiters, U.K.; Schneider, G., "High Pressure Phase Equilibria: Experimental Methods," *Fluid Phase Equilibria*, 29, 145, **1986**.

Derr, E.; Deal, C., "Analytical Solutions of Groups: Correlation of Activity Coefficients through Structural Group Parameters," *Instn. Chem. Engrs. Symp. Ser. No. 32*, 3, 40, **1969**.

Dohrn, R.; Brunner, G., "High-Pressure Fluid-Phase Equilibria: Experimental Methods and Systems Investigated (1988-1993)," *Fluid Phase Equilibria*, 106, 213, **1995**.

Donohue, M.; Prausnitz, J., "Combinatorial Entropy of Mixing Molecules that Differ in Size and Shape. A Simple Approximation for Binary and Multicomponent Mixtures," *Can. J. Chem. Eng.*, 53, 1586, **1975**.

Doolittle, A. K., "Specific Volumes of n-Alkanes," *J. Chem. Eng. Data*, 9, 275, **1964**.

Eisenberg, B.; Fiato, R.; Mauldin, C.; Say, R.; Soled, S., "Exxon's Advanced Gas-To-Liquids Technology," *Stud. Surf. Sci. Catal.*, 119, 943, **1998**.

Elbro, H. S.; Fredenslund, Aa., Rasmussen, P., "A New Simple Equation for the Prediction of Solvent Activities in Polymer Solutions," *Macromolecules*, 23, 4707, **1990**.

Fernandez, M.; Zollweg, J.; Streett, W., "Vapor-Liquid Equilibrium in the Binary System Carbon Dioxide + n-Butane," *J. Chem. Eng. Data*, 34, 324, **1989**.

Fischer, K.; Gmehling, J., "Further Development, Status and Results of the PSRK Method for the Prediction of Vapor-Liquid Equilibria and Gas Solubilities," *Fluid Phase Equilibria*, 121, 185, **1996**.

Flory, P. J.; Orwoll, A.; Vrij, A., "Statistical Thermodynamics of Chain Molecule Liquids: I. An Equation of State for Normal Paraffin Hydrocarbons," *J. Am. Chem. Soc.*, 86, 3507, **1964**.

Floter, E.; Hollanders, B.; de Loos, Th. W.; de Swaan Arons, J., "The Effect of the Addition of Water, Propane, or Docosane on the Vapor-Liquid and Solid-Fluid Equilibria in Asymmetric Binary n-Alkane Mixtures," *Fluid Phase Equilibria*, 143, 1-2, 185, **1998**.

Fogh, F.; Rasmussen, P., "Detection of High-Pressure Dew and Bubble Points Using a Microwave Technique," *Ind. Eng. Chem. Res.*, 28, 371, **1989**.

Fornari, R. E.; Alessi, P.; Kikic, I., "High Pressure Fluid Phase Equilibria: Experimental Methods and Systems Investigated (1978-1987)," *Fluid Phase Equilibria*, 57, 1, **1990**.

Fredenslund, Aa.; Jones, R.; Prausnitz, J., "Group-Contribution Estimation of Activity Coefficients in Nonideal Liquid Mixtures," *AIChE J.*, 21, 1086, **1975**.

Friend, D. G.; Ingham, H.; Ely, J., "Thermophysical Properties of Ethane," *J. Phys. Chem. Ref. Data*, 20, 2, **1991**.

Gamse, T.; Marr, R., "Phase Equilibrium Properties of the 1-Phenylethanol-Carbon Dioxide and 2-Octanol-Carbon Dioxide Binary Systems at 303.15 K, 313.15 K, and 323.15 K," *J. Chem. Eng. Data*, 46, 117, **2001**.

Gani, R.; Tzouvaras, N.; Rasmussen, P.; Fredenslund, Aa., "Prediction of Gas Solubility and Vapor-Liquid Equilibria by Group Contribution," *Fluid Phase Equilibria*, 47, 133, **1989**.

Gao, W.; Robinson, R. L., Jr.; Gasem, K. A. M., "Improved Correlations for Heavy n-Paraffin Physical Properties," *Fluid Phase Equilibria*, 179, 1-2, 207, **2001**.

Gao, Wuzi, *High Pressure Solubility Measurements for Selected Asymmetric Mixtures and Equation-of-State Developments*, Ph.D. Dissertation, Oklahoma State University, Stillwater, OK, **1999**.

Gasem, K. A. M., *Binary Vapor-Liquid Phase Equilibrium for Carbon Dioxide + Heavy Normal Paraffins*, Ph.D. Dissertation, Oklahoma State University, 1986.

Gasem, K. A. M., GEOS Software, Oklahoma State University, Stillwater, Oklahoma, 1988-1999.

Gasem, K. A. M.; Bufkin, B. A.; Raff, A. M.; Robinson, R. L., Jr., "Solubilities of Ethane in Heavy Normal Paraffins at Pressures to 7.8 MPa and Temperatures from 348 to 423 K," *J. Chem. Eng. Data*, 34, 187, 1989.

Gasem, K. A. M.; Gao, W.; Pan, Z.; Robinson, R. L., Jr., "A Modified Temperature Dependence for the Peng-Robinson Equation of State," *Fluid Phase Equilibria*, 181, 1-2, 113, 2001.

Gasem, K. A. M.; Robinson, R. L., Jr., "Phase Behavior of Light Gases in Hydrocarbon and Aqueous Solvents," DOE Proposal, 1995.

Gasem, K. A. M.; Robinson, R. L., Jr., "Solubilities of Carbon Dioxide in Heavy Normal Paraffins (C₂₀-C₄₄) at Pressures to 9.6 MPa and Temperatures from 323 to 423 K," *J. Chem. Eng. Data*, 30, 53, 1985.

Gasem, K. A. M.; Ross, C. H.; Robinson, R. L., Jr., "Prediction of Ethane and CO₂ Solubilities in Heavy Normal Paraffins using Generalized-Parameters Soave and Peng-Robinson Equation of State," *Can. J. Chem. Eng.*, 71, 805, 1993.

Gehrig, M.; Lentz, H., "Values of P (V_m, T) for n-Decane up to 300 MPa and 673 K," *J. Chem. Thermodynamic*, 15, 1159, 1983.

Gmehling, J., "Present Status of Group-Contribution Methods for the Synthesis and Design of Chemical Processes," *Fluid Phase Equilibria*, 37, 144, 1998.

Gregorowicz, J.; de Loos, Th. W.; de Swaan Arons, J., "Unusual Retrograde Condensation in Ternary Hydrocarbon Systems," *Fluid Phase Equilibria*, 73, 1-2, 109, 1992.

Gregorowicz, J.; Smits, P. J.; de Loos, Th. W.; de Swaan Arons, J., "Liquid-Liquid-Vapor Phase Equilibria in the System Methane + Ethane + Eicosane: Retrograde Behaviour of the Heavy Liquid Phase," *Fluid Phase Equilibria*, 85, 225, 1993.

Gregorowicz, J.; de Loos, Th. W.; de Swaan Arons, J., "Three-Phase Equilibria in the Binary System Ethylene + Eicosane and the Ternary System Propane + Ethylene + Eicosane," *J. Chem. Eng. Data*, 38, 3, 417, 1993.

Guggenheim, E., *Mixtures*, Clarendon Press, Oxford, 1952.

- Gupta, M. K.; Gardner, G. C.; Hegarty, M. J.; Kidnay, A., "Liquid-Vapor Equilibria for the $N_2 + CH_4 + C_2H_6$ System from 260 To 280 K," *J. Chem. Eng. Data*, 25, 313, 1980.
- Gupte, P.; Rasmussen, P.; Fredenslund, Aa., "A New-Group-Contribution Equation of State for Vapor-Liquid Equilibria," *Ind. Eng. Chem. Fundam.*, 25, 636, 1986.
- Haynes, W.; Goodwin, R., *Thermophysical Properties of Normal Butane from 135 to 700 K at Pressures to 70 MPa*, National Bureau of Standard Monograph 169, 1982.
- Heidemann, R. A.; Kokal, S. L., "Combined Excess Free Energy Models and Equations of State," *Fluid Phase Equilibria*, 56, 17, 1990.
- Hicks, C. P., "n-Fluid Models and Phase Equilibrium," *J. Chem. Soc., Faraday Trans.*, 2, 72, 2, 423, 1976.
- Hijmans, J., "Phenomenological Formulation of the Principle of Corresponding States for Liquids Consisting of Chain Molecules," *Physica*, 27, 423, 1961.
- Hildebrand, J. H.; Scott, R. L., *The Solubility of Nonelectrolytes*, Dover, New York, 1964.
- Holderbaum, T.; Gmehling, J., "PSRK: A Group Contribution Equation of State Based on UNIFAC," *Fluid Phase Equilibrium*, 70, 251, 1991.
- Hong, S.-P.; Green, K. A.; Luks, K. D., "Phase Equilibrium of the Mixtures Methane + n-Hexane + n-Hexatricontane, Methane + Toluene + Naphthalene, and Methane + n-Hexane + Naphthalene," *Fluid Phase Equilibria*, 87, 255, 1993.
- Hong, S.-P.; Luks, K. D., "Solid-Liquid-Vapor Phase Equilibria of the Mixture Carbon Dioxide + n-Hexane + n-Hexatricontane," *J. Supercritical Fluids*, 4, 227, 1991.
- Hsu, J. J.-C.; Nagarajan, N.; Robinson, R. L., Jr., "Equilibrium Phase Composition, Phase Densities, and Interfacial Tensions for $CO_2 +$ Hydrocarbon Systems. 1. $CO_2 +$ n-Butane," *J. Chem. Eng. Data*, 30, 485, 1985.
- Huang, H.; Sandler, S.; Orbey, H., "Vapor-Liquid Equilibria of Some Hydrogen + Hydrocarbon Systems with Wong-Sandler Mixing Rule," *Fluid Phase Equilibria*, 96, 143, 1994.
- Huang, S. H.; Lin, H. M.; Tsai, F. N.; Chao, K. C., "Solubility of Synthesis Gases in Heavy n-Paraffins and Fischer-Tropsch Wax," *Ind. Eng. Chem. Res.*, 27, 162, 1988.
- Huie, N. C.; Luks, K. D.; Kohn, J. P., "Phase-Equilibria Behavior of Systems Carbon Dioxide-n-Eicosane and Carbon dioxide-n-Decane-n-Eicosane," *J. Chem. Eng. Data*, 18, 3, 311, 1973.

Humphrey, J. L.; Sebert, A. F.; Koort, R. A., Separation Technologies Advances and Priorities, DOE/ID/12920-1, 1991.

Huron, M.; Vidal, J., "New Mixing Rules in Simple Equation of State for Representing Vapor-Liquid Equilibria of Strongly Non-Ideal Mixtures," *Fluid Phase Equilibria*, 3, 255, 1979.

International Union of Pure and Applied Chemistry, International Thermodynamic Tables of the Fluid State-6 - Nitrogen, Pergamon Press, New York, 1977.

Jangkomkulchai, A.; Luks, K. D., "Partial Miscibility Behavior of the Methane + Ethane + n-Docosane and the Methane + Ethane + n-Tetradecylbenzene Ternary Mixtures," *J. Chem. Eng. Data*, 34, 92, 1989.

Kikic, I.; Alessi, P.; Rasmussen, P.; Fredenslund, Aa., "On the Combinatorial Part of the UNIFAC and UNIQUAC Models," *Can. J. Chem. Eng.*, 58, 253, 1980.

Kim, Y.; Carfagno, J.; McCaffrey, D., Jr.; Kohn, J., "Partial Miscibility Phenomena in the Ternary System Ethane-n-Nonadecane-n-Eicosane," *J. Chem. Eng. Data*, 12, 3, 289, 1967.

Knapp, H.; Zeck, S.; Langhorst, R., "Vapor-Liquid Equilibria for Mixtures of Low Boiling Substances – Ternary Systems," DECHEMA Chemistry Data Series, VI, 4, 1989.

Kontogeorgis, G. M.; Coutsikos, Ph.; Tassios, D.; Fredenslund, Aa., "Improved Models for the Prediction of Activity Coefficients in Nearly Athermal Mixtures," *Fluid Phase Equilibria*, 92, 35, 1994.

Kuo, J. C. W., "Two-Stage Process for Conversion of Synthesis Gas to High Quality Transportation Fuels," Mobil Res. and Dev. Corp., Paulsboro, NJ, Report, DOE/PC/60019-9, 1985.

Kwak, T. Y.; Mansoori, G. A., "van der Waals Mixing Rules for Cubic Equations of State. Applications for Supercritical Fluid Extraction Modeling," *Chem. Eng. Sci.*, 41, 5, 1303, 1986.

Larsen, B.; Rasmussen, P.; Fredenslund, Aa., "A Modified UNIFAC Group-Contribution Model for Prediction of Phase Equilibria and Heats of Mixing," *Ind. Eng. Chem. Res.*, 26, 2274, 1987.

Laursen, T.; Rasmussen, P.; Andersen, S. I., "VLE And VLLE Measurements of Dimethyl Ether Containing Systems," *J. Chem. Eng. Data*, 47, 198, 2002.

Lee, K.; Dodd, L.; Sandler, S., "The Generalized van der Waals Partition Function. V. Mixture of Square Well Fluids of Different Sizes and Energies," *Fluid Phase Equilibria*, 50, 53-77, 1989.

Lee, R.; Chao, K., "Local Composition of Square-Well Molecules of Diverse Energies and Sizes," *Fluid Phase Equilibria*, 37, 327, **1987**.

Lee, S-M; Eubank, P. T.; Hall, K. R., "Truncation Errors Associated with the Virial Equation," *Fluid Phase Equilibria*, 1, 219, **1977**.

Leland, T. W.; Chappellear, P. S., "Recent Developments in the Theory of Fluid Mixtures," *Ind. Engng. Chem.*, 60, 15, **1968a**.

Leland, T. W.; Rowlinson, J. S.; Sather, G. A., "Statistical Thermodynamics of Mixtures of Molecules of Different Sizes," *Trans. Faraday Soc.*, 64, 1447, **1968b**.

Leland, T. W.; Rowlinson, J. S.; Sather, G. A.; Watson, I. D., "Statistical Thermodynamics of Two-Fluid Models of Mixtures," *Trans. Faraday Soc.*, 65, 2034, **1969**.

Leland, T. W., "Equation of State for Phase Equilibrium Computations: Present Capabilities and Future Trends," 2nd International Conference on Phase Equilibria and Fluid Properties in the Chemical Industry, Berlin (West), 21 March **1980**.

Luedecke, D.; Prausnitz, J. M., "Phase Equilibria for Strongly Nonideal Mixtures with an Equation of State with Density-Dependent Mixing Rules," *Fluid Phase Equilibria*, 22, 1, **1985**.

Majeed, A.; Wagner, J., "Parameters from Group Contribution Equation and Phase Equilibria in Light Hydrocarbon Systems," ACS Symp. Ser., 300 (Equation of State), 452, **1986**.

Makamura, S.; Fujiwara, K.; Nagushi, M., "PVT properties for 1,1,1-Trifluoroethane (R-143a)," *J. Chem. Eng. Data*, 42, 334, **1997**.

Marano, J. J.; Holder, G. D., "Prediction of Bulk Properties of Fischer-Tropsch Derived Liquids," *Ind. Eng. Chem. Res.*, 36, 6, 2409, **1997**.

Mathias, P. M.; Klotz, H. C.; Prausnitz, J. M., "Equation of State Mixing Rules for Multicomponent Mixtures: The Problem of Invariance," *Fluid Phase Equilibria*, 67, 31-44, **1991**.

Maurer, G.; Prausnitz, J., "On the Derivation and Extension of the UNIQUAC Equation," *Fluid Phase Equilibria*, 2, 91, **1978**.

McCarty, R.; Hord, J.; Roder, H., *Selected Properties of Hydrogen*, National Bureau of Standards Monograph no. 168, **1981**.

Melhem, G. A.; Saini, R.; Goodwin, B. M., "A Modified Peng-Robinson Equation of State," *Fluid Phase Equilibria*, 47, 189, **1989**.

Michelsen, M. L.; Kistenmacher, H., "On Composition Dependent Interaction Coefficients," *Fluid Phase Equilibria*, 58, 229, 1990.

Michelsen, M. L., "A Method for Incorporating Excess Gibbs Energy Models in Equations of State," *Fluid Phase Equilibria*, 60, 47, 1990a.

Michelsen, M. L., "A Modified Huron-Vidal Mixing Rule for Cubic Equations of State," *Fluid Phase Equilibria*, 60, 213, 1990b.

Mollerup, J., "A Note on the Derivation of Mixing Rules from Excess Gibbs Energy Models," *Fluid Phase Equilibria*, 25, 323, 1986.

Moshfeghian, M.; Shariat, A.; Erbar, J., "Application of the PFGC-MES Equation of State to Synthetic and Natural Gas Systems," ACS Symp. Ser., 133 (Thermody. Aqueous Syst. Ind. Appl.), 22, 1979.

Mundis, C. J.; Yarborough, L.; Robinson, R. L., Jr., "Vaporization Equilibrium Ratios for Carbon Dioxide and Hydrogen Sulfide in Paraffinic, Naphthenic, and Aromatic Solvents," *Ind. Eng. Chem. Process Des. Dev.*, 16, 2, 254, 1977.

Oishi, T.; Prausnitz, J. M., "Estimation of Solvent Activities in Polymer Solutions using Group-Contribution Method," *Ind. Eng. Chem. Process Des. Dev.*, 17, 333, 1978.

Olds, R. H.; Reamer, H. H.; Sage, B. H.; Lacey, W. N., "Phase Equilibria in Hydrocarbon Systems - The Butane + Carbon Dioxide System," *Ind. Eng. Chem.*, 41, 475, 1949.

Orbey, H.; Sandler, S., "A Comparison of Huron-Vidal Type Mixing Rule of Mixtures of Compounds with Large Size Difference, and a New Mixing Rule," *Fluid Phase Equilibria*, 132, 1, 1997.

Orbey, H.; Sandler, S., "On the Combination of Equation of State and Excess Free Energy Models," *Fluid Phase Equilibria*, 111, 53, 1995a.

Orbey, H.; Sandler, S., "Analysis of Excess Free Energy Based Equations of State Models," *AICHE J.*, 42, 2327, 1996.

Orbey, H.; Sandler, S., "Reformulation of Wong-Sandler Mixing Rule for Cubic Equations of State," *AICHE J.*, 41, 683, 1995b.

Orbey, H.; Sandler, S.; Wong, D., "Accurate Equation of State Predictions at High Temperatures and Pressures Using Existing UNIFAC model," *Fluid Phase Equilibria*, 85, 41, 1993.

Osbjornsen, O. A., "Error in the Propagation of Error Formula," *AICHE J.*, 32, 2, 332, 1986.

Panagiotopoulos, A. Z.; Reid, R. C., "Multiphase High Pressure Equilibria in Ternary Aqueous Systems," *Fluid Phase Equilibria*, 29, 525, **1986b**.

Panagiotopoulos, A. Z.; Reid, R. C., "New Mixing Rule for Cubic Equations of State for Highly Polar Asymmetric Mixtures," *ACS Symp. Ser.*, 300, 571, **1986**.

Park, J. K., *Binary Vapor-Liquid Equilibrium Measurements for Selected Asymmetric Mixtures and Equation of State Development*, Ph. D. Dissertation, Oklahoma State University, Stillwater, Oklahoma, **1994**.

Peng, D.-Y.; Robinson, D. B., "A New Two-Constant Equation of State," *Ind. Eng. Chem. Fundam.*, 15, 59, **1976**.

Peters, C. J., *Phase Behavior of Binary Mixtures of Ethane + n-Eicosane and Statistical Mechanical Treatment of Fluid Mixtures*, Ph.D. Dissertation, Delft University, Netherlands, **1986**.

Peters, C. J.; De Roo, J. L.; Lichtenthaler, R. N., "Measurements and Calculations of Phase Equilibria of Binary Mixtures of Ethane + Eicosane. Part I. Vapor + Liquid Equilibria," *Fluid Phase Equilibria*, 34, 2-3, 287, **1987**.

Poston, R. S.; McKetta, J., "Vapor-Liquid Equilibrium in the n-Hexane-Nitrogen System," *J. Chem. Eng. Data*, 11, 3, 364, **1966**.

Prausnitz, J. M., State-of-the-Art Review of Phase Equilibria. In: Storvick, T.S. and Sandler, S. I. (Eds.), *Phase Equilibria and Fluid Properties in Chemical Industry*, American Chemical Society, Washington, D.C., **1977**.

Prausnitz, J. M.; Lichtenthaler, R. N.; Azevedo, E. G., *Molecular Thermodynamics of Fluid-Phase Equilibria*, Prentice Hall, New Jersey, **1999**.

Reamer, H. H.; Sage, B. H., "Phase Equilibria in Hydrocarbon Systems. Volumetric and Phase Behavior of the n-Decane-CO₂ System," *J. Chem. Eng. Data*, 8, 508, **1963**.

Reid, R.; Prausnitz, J. M.; Poling, B., *The Properties of Gases and Liquids*, McGraw-Hill, New York, **1987**.

Renon, H.; Prausnitz, J. M., "Local Compositions in the Thermodynamic Excess Functions for Liquid Mixtures," *AIChE J.*, 14, 135, **1968**.

Sadus, R. J., "Molecular Simulation of the Phase Behavior of Ternary Fluid Mixtures: The Effect of a Third Component on Vapour-Liquid and Liquid-Liquid Coexistence," *Fluid Phase Equilibria*, 157, 2, 169, **1999**.

Saini, R., Ph.D. Dissertation, Northeastern University, Boston, MA, **1990**.

Sandoval, R.; Wilczek-Vera, G.; Vera, J. H., "Prediction of Ternary Vapor-Liquid with PRSV Equation of State," *Fluid Phase Equilibria*, 52, 119, **1989**.

Schwartzentruber, J.; Renon, H., "Extension of UNIFAC to High Pressures and Temperatures by the Use of a Cubic Equation of State," *Ind. Eng. Chem. Res.*, 28, 1049, **1989**.

Schwartzentruber, J.; Renon, H., "Equation of State: How to Reconcile Flexible Mixing Rules, the Virial Coefficient Constraint and the Michelsen-Kistenmacher Syndrome for Multicomponent Systems," *Fluid Phase Equilibria*, 67, 99, **1991**.

Shah, P. P.; Sturlevant, G. C.; Gregor, J. H.; Humbach, M. J.; Steigleder, K. Z., Fisher-Tropsch Wax Characterization and Upgrading, Report, DOE/PC/80017-T1, **1988**.

Shaver, R. D., "Vapor-Liquid Equilibrium Measurements for Selected Ethane and Carbon Dioxide Mixtures and Modification of the SPHCT Equation of State," Ph.D. Dissertation, Oklahoma State University, Stillwater, OK, **1993**.

Shaver, R. D.; Robinson, R. L., Jr.; Gasem, K. A. M., "An Automated Apparatus for Equilibrium Phase Compositions, Densities, and Interfacial tensions: Data for Carbon Dioxide +Decane," *Fluid Phase Equilibria*, 179, 43, **2001**.

Shen, J.; Schmetz, E.; Winslow, J.; Tischer, R., "U.S. DOE Indirect Coal Liquefaction Program: An Overview," US Department of Energy, Proceedings of the 1997 Diesel Engine Emissions Reduction Workshop, University of California-San Diego, July 28-31, **1997**.

Sheng, Y.; Chen, P.; Chen, Y., "Calculation of Solubilities of Aromatic Compounds in Supercritical Carbon Dioxide," *Ind. Eng. Chem. Res.*, 31, 967, **1992**.

Sheng, Y.; Chen, Y., "A Cubic Equation of State for Predicting Vapor-Liquid Equilibria of Hydrocarbon Mixtures using a Group Contribution Mixing Rule," *Fluid Phase Equilibria*, 46, 197, **1989**.

Shibata, S. K.; Sandler, S. I., "High-Pressure Vapor-Liquid Equilibria involving Mixtures of Nitrogen, Carbon Dioxide, and n-Butane," *J. Chem. Eng. Data*, 34, 291, **1989**.

Shibata, S. K.; Sandler, S. I., "Critical Evaluation of Equation of State Mixing Rules for Prediction of High Pressure Phase Equilibria," *Ind. Eng. Chem. Res.*, 28, 1893, **1989**.

Skjold-Jorgensen, S., "Gas Solubility Calculation. II. Application of a New Group-Contribution Equation of State," *Fluid Phase Equilibria*, 16, 317, **1984**.

Skjold-Jorgensen, S., "Group Contribution Equation of State (GC-EOS): A Predictive Method for Phase Equilibrium Computations Over Wide Ranges of Temperature and Pressure up to 30 MPa," *Ind. Eng. Chem. Res.*, 27, 110, **1988**.

- Soave, G., "Improvement of the van der Waals Equation of State," *Chem. Eng. Sci.*, 39, 357, 1984.
- Soave, G., "Equilibrium Constants from a Modified Redlich-Kwong Equation of State," *Chem. Eng. Sci.*, 27, 1197, 1972.
- Staverman, A., "The Entropy of High Polymer Solutions," *Rec. Trav. Chim. Pays-Bas*, 69, 163, 1950.
- Span, R.; Wagner, W., "A New Equation of State for Carbon Dioxide," *J. Phys. Chem. Ref. Data*, 25, 6, 1509, 1996.
- Stryjek, R.; Vera, J. H., "PRSV: An Improved Peng-Robinson Equation of State with New Mixing Rules for Strongly Nonideal Mixtures," *Can. J. Chem. Eng.*, 64, 334, 1986b.
- Sum, A.; Sandler, S., "A Novel Approach to Phase Equilibria Prediction using *Ab initio* Methods," *Ind. Eng. Chem. Res.*, 38, 7, 2849, 1999.
- Tiegs, D.; Gmehling, J.; Medina, A.; Soares, M.; Bastos, J.; Alessi, P.; Kikic, I., *Activity Coefficients at Infinite Dilution*, DECHEMA Chemistry Data Series, IX, 1-2, 1986.
- Tong, J.; Gao, W.; Robinson, R. L., Jr.; Gasem, K. A. M., "Solubilities of Nitrogen in Heavy Normal Paraffins from 323 to 423 K at Pressures to 18.0 MPa," *J. Chem. Eng. Data*, 44, 784, 1999.
- Trivedi, N., *A New Framework for Vapor-Liquid Equilibrium Calculations*, M.S. Thesis, Oklahoma State University, Stillwater, OK, 1996.
- Vargaftik, N. B., *Tables on the Thermophysical Properties of Liquids and Gases in Normal and Dissociated States*, 2nd Ed., John Wiley & Sons, Inc., New York, N. Y., 1975.
- Voutsas, E. C.; Kalospiros, N. S.; Tassios, D. P., "A Combinatorial Activity Coefficient Model for Symmetric and Asymmetric Mixtures," *Fluid Phase Equilibria*, 109, 1, 1995.
- Vukalovich, M. P.; Altunin, V. V., *Thermodynamic Properties of Carbon Dioxide*, Collets, London & Wellingborough, 1968.
- Walas, S. M., *Phase Equilibria in Chemical Engineering*, Butterworth, Stoneham, MA, 1985.
- Weidlich, V.; Gmehling, J., "A Modified UNIFAC Model. 1. Prediction of VLE, H^E , and γ^∞ ," *Ind. Eng. Chem. Res.*, 26, 1372, 1987.

Wilson, G., "Vapor-Liquid Equilibrium. XI. A New Expression for the Excess Free Energy of Mixing," *J. Am. Chem. Soc.*, 86, 127, 1964.

Wong, D. S. H.; Sandler, S., "A Theoretically Correct Mixing Rule for Cubic Equations of State," *AICHE J.*, 38, 671, 1992.

Wong, D. S. H.; Orbey, H. and Sandler, S., "Equation of State Mixing Rule for Nonideal Mixtures using Available Activity Coefficient Model Parameters that Allows Extrapolation over Large Ranges of Temperature and Pressure," *Ind. Eng. Chem. Res.*, 31, 8, 2033, 1992.

Ye, Qi; Zhong, C., "An Improved UNIFAC Model for Prediction of Activity Coefficients of Asymmetric and Symmetric Systems," *Chem. J. Internet*, 2, 10, 45, 2000.

Younglove, B. A.; Ely, J. F., "Thermophysical Properties of Fluids. II. Methane, Ethane, Propane, Isobutane, and Normal Butane," *J. Phys. Chem. Ref. Data*, 16, 4, 577, 1987.

Zavala, M.; Aroche, E.; Bazue, E., "Comparative Study of Mixing Rules for Cubic Equations of State in the Prediction of Multi-Component Vapor-Liquid Equilibria," *Fluid Phase Equilibria*, 122, 99, 1996.

Zhong, C.; Masuoka, H., "Mixing Rules for Accurate Prediction of Vapor-Liquid Equilibria of Gas/Large Alkane Systems using SRK Equation of State Combined with UNIFAC," *J. Chem. Eng. Japan*, 29, 2, 315, 1996.

Zhong, C.; Takeuchi, M.; Masuoka, H., "Vapor-Liquid Equilibria Calculation in Gas/Large Alkane Systems using Group Contribution Equation of State," *J. Chem. Eng. Japan*, 30, 6, 1133, 1997.

DATABASE LITERATURE CITED

Ethane/n-Paraffin Database

- [1] Bufkin, B., *High Pressure Solubilities of Carbon Dioxide and Ethane in Selected Paraffinic, Naphthenic and Aromatic Solvents*, M. S. Thesis, Oklahoma State University, Stillwater, Oklahoma, **1986**.
- [2] de Goede, R.; Peters, C. J.; Van Der Kooi, H. J.; Lichtenthaler, R. N., "Phase Equilibria in Binary Mixtures of Ethane and Hexadecane," *Fluid Phase Equilibria*, **50**, 305, **1989**.
- [3] Estrera, S. S.; Arbuckle, M. M.; Luks, K. D., "Solubility and Partial Miscibility of Ethane in Certain Hydrocarbon Liquids," *Fluid Phase Equilibria*, **35**, 291, **1987**.
- [4] Huang, S. H.; Lin, H.; Chao, K. C., "Solubility of Carbon Dioxide, Methane and Ethane in n-Octacosane," *J. Chem. Eng. Data*, **33**, 143, **1988**.
- [5] Lee, K. H.; Kohn, J. P., "Heterogeneous Phase Equilibrium in the Ethane-n-Dodecane System," *J. Chem. Eng. Data*, **14**, 292, **1969**.
- [6] Lhotak, V.; Wichterle, I., "Vapor-Liquid Equilibrium in the Ethane-n-Butane System at High Pressures," *Fluid Phase Equilibria*, **6**, 229, **1981**.
- [7] Matschke, D. E.; Thodos, G., "Vapor-Liquid Equilibria for the Ethane-Propane System," *J. Chem. Eng. Data*, **7**, 232, **1962**.
- [8] Mehra, V. S.; Thodos, G., "Vapor-Liquid Equilibrium Constants for the Ethane-n-Butane-n-Heptane System at 150⁰, 200⁰, and 250⁰F in the Ethane-n-Heptane System," *J. Chem. Eng. Data*, **11**, 365, **1966**.
- [9] Peters, C. J.; Spiegelaar, J.; de Swaan Arons, J., "Phase Equilibrium in Binary Mixtures of Ethane + Docosane and Molar Volumes of Liquid Docosane," *Fluid Phase Equilibria*, **41**, 245, **1988**.
- [10] Peters, C. J.; Van Der Kooi, H. J.; de Swaan Arons, J., "Measurements and Calculations of Phase Equilibria for (Ethane + Tetracosane) and (p, Vm, T) of Liquid Tetracosane," *J. Chem. Thermodynamics*, **19**, 395, **1987**.
- [11] Reamer, H. H.; Sage, B. H.; Lacey, W. N., "Phase Equilibria Hydrocarbon Systems. Volumetric and Phase Behavior of Ethane-n-Pentane System," *J. Chem. Eng. Data*, **5**, 44, **1960**.

[12] Robinson, R. L., Jr.; Gasem, K. A. M., Phase Behavior of Coal Fluids: Data for Correlation Development, DE-FG22-83PC60039-12, Final Report, Department of Energy, 1987.

[13] Rodrigues, A. B. J.; McCaffrey, D. S., Jr.; Kohn, J. P., "Heterogeneous Phase and Volumetric Equilibrium in the Ethane-n-Octane System," *J. Chem. Eng. Data*, 13, 164, 1968.

[14] Tsai, F.; Huang, S. H.; Lin, H.; Chao, K. C., "Solubility of Methane, Ethane, and Carbon Dioxide in n-Hexatriacontane," *J. Chem. Eng. Data*, 32, 467, 1987.

Carbon Dioxide/n-Paraffin Database

[15] Cheng, H.; Pozo de Fernandez; M. E.; Zollweg, J. A.; Streett, W. B., "Vapor-Liquid Equilibria in the System Carbon Dioxide + n-Pentane from 252 to 458 K at Pressures to 10 MPa," *J. Chem. Eng. Data*, 34, 319, 1989.

[16] Fall, D. J.; Luks, K. D., "Phase Equilibria Behavior of the Systems Carbon Dioxide + n-Dotriacontane and Carbon Dioxide + n-Docosane," *J. Chem. Eng. Data*, 29, 413, 1984.

[17] Fall, D. J.; Fall, J. L.; Luks, K. D., "Liquid-Liquid-Vapor Immiscibility Limits in Carbon Dioxide + n-Paraffin Mixtures," *J. Chem. Eng. Data*, 30, 82, 1985.

[18] Gasem, K. A. M., *Binary Vapor-Liquid Phase Equilibrium for Carbon Dioxide + Heavy Normal Paraffins*, Ph.D. Dissertation, Oklahoma State University, Stillwater, Oklahoma, 1986.

[19] Hsu, J. J.-C.; Nagarajan, N.; Robinson, R. L., Jr., "Equilibrium Phase Compositions, Phase Densities, and Interfacial Tensions for CO₂ + Hydrocarbon Systems. 1. CO₂ + n-Butane," *J. Chem. Eng. Data*, 30, 485, 1985.

[20] Huang, S. H.; Lin, H.; Chao, K. C., "Solubility of Carbon Dioxide, Methane, and Ethane in n-Eicosane," *J. Chem. Eng. Data*, 33, 145, 1988.

[21] Huang, S. H.; Lin, H.; Chao, K. C., "Solubility of Carbon Dioxide, Methane, and Ethane in n-Octacosane," *J. Chem. Eng. Data*, 33, 143, 1988.

[22] Kalra, H.; Kubota, H.; Robinson, D. B.; Ng, H., "Equilibrium Phase Properties of the Carbon Dioxide-n-Heptane System," *J. Chem. Eng. Data*, 3, 317, 1978.

[23] Kim, H.; Lin, H.; Chao, K. C., "Vapor-Liquid Equilibrium in Binary Mixtures of Carbon Dioxide + n-PropylCyclohexane and Carbon Dioxide + n-Octadecane," *AIChE Symp. Ser.*, 81, 244, 96, 1985.

[24] Li, Y.; Dillard, K. H.; Robinson, R. L., Jr., "Vapor-Liquid Phase Equilibrium for Carbon Dioxide-n-Hexane at 40, 80 and 120 °C," *J. Chem. Eng. Data*, 26, 53, 1981.

[25] Ohgaki, K. and Katayama, T., "Isothermal Vapor-Liquid Equilibrium Data for Binary Systems Containing Carbon Dioxide at High Pressures: Methanol-Carbon Dioxide, n-Hexane-Carbon Dioxide, and Benzene-Carbon Dioxide Systems," *J. Chem. Eng. Data*, 21, 53, 1976.

[26] Reamer, H. H.; Sage, B. H., "Phase Equilibria in Hydrocarbon Systems. Volumetric and Phase Behavior of the n-Decane-CO₂ System," *J. Chem. Eng. Data*, 8, 4, 508, 1963.

[27] Sebastian, H. M.; Simnick, J. J.; Lin, H.; Chao, K. C., "Vapor-Liquid Equilibrium in Binary Mixtures of Carbon Dioxide + n-Decane and Carbon Dioxide + n-Hexadecane," *J. Chem. Eng. Data*, 25, 138, 1980.

[28] Tsai, F.; Huang, S. H.; Lin, H.; Chao, K. C., "Solubility of Methane, Ethane, and Carbon Dioxide in n-Hexatriacontane," *J. Chem. Eng. Data*, 32, 467, 1987.

[29] Tsai, F.; Yau, J., "Solubility of Carbon Dioxide in n-Tetracosane and in n-Dotriacontane," *J. Chem. Eng. Data*, 35, 43, 1990.

[30] Wagner, Z.; Wichterle, I., "High-Pressure Vapor-Liquid Equilibrium in Systems containing Carbon Dioxide, 1-Hexene, and n-Hexane," *Fluid Phase Equilibria*, 33, 109, 1987.

Methane/n-Paraffin Database

[31] Darwish, N. A., *Binary Vapor-Liquid Phase Equilibrium for Methane in Selected Heavy Normal Paraffins, Naphthenes and Aromatics*, Ph. D. Dissertation, Oklahoma State University, Stillwater, Oklahoma, 1991.

[32] Huang, S. H.; Lin, H. M.; Chao, K. C., "Solubility of Carbon Dioxide, Methane and Ethane in n-Eicosane," *J. Chem. Eng. Data*, 33, 145, 1988.

[33] Huang, S. H.; Lin, H. M.; Chao, K. C., "Solubility of Carbon Dioxide, Methane and Ethane in n-Octacosane," *J. Chem. Eng. Data*, 33, 143, 1988.

[34] Kohn, J. P.; Bradish, W. F., "Multiphase and Volumetric Equilibria of the Methane-n-Octane System at Temperatures between -110 and 150 °C," *J. Chem. Eng. Data*, 9, 5, 1964.

[35] Lin, H. M.; Sebastian, H. M.; Chao, K. C., "Gas-Liquid Equilibrium in Hydrogen + n-Hexadecane and Methane + n-Hexadecane at Elevated Temperatures and Pressures," *J. Chem. Eng. Data*, 25, 252, 1980.

[36] Poston, R. S.; McKetta, J. J., "Vapor-Liquid Equilibrium in the Methane – n-Hexane System," *J. Chem. Eng. Data*, 1, 29, 1966.

[37] Reamer, H. H.; Olds, R. H.; Sage, B. H.; Lacey, W. N., "Phase Equilibria in Hydrocarbon Systems. Methane-Decane System," *Ind. Eng. Chem.*, 34, 1526, 1942.

[38] Reamer, H. H.; Sage, B. H.; Lacey, W. N., "Volumetric and Phase Behavior of the Methane-n-Heptane System," *Chem. Eng. Data Ser.*, 1, 29, 1956.

[39] Roberts, L. R.; Wang, R. H.; Azarnoosh, A.; McKetta, J. J., "Methane-n-Butane System in the Two-Phase Region," *J. Chem. Eng. Data*, 7, 484, 1962.

[40] Shim, J.; Kohn, J. P., "Multiphase and Volumetric Equilibria of Methane-n-Hexane Binary System at Temperatures between -110 and 150 °C," *J. Chem. Eng. Data*, 7, 3, 1962.

[41] Shipman, L. M.; Kohn, J. P., "Heterogeneous Phase and Volumetric Equilibrium in the Methane-n-Nonane System," *J. Chem. Eng. Data*, 11, 176, 1966.

[42] Srivatsan, S., *Binary Vapor-Liquid Phase Equilibrium for Methane and Carbon Monoxide in Selected Hydrocarbons*, M. S. Thesis, Oklahoma State University, Stillwater, Oklahoma, 1991.

[43] Tsai, F. N.; Huang, S. H.; Lin, H. M.; Chao, K. C., "Solubility of Methane, Ethane and Carbon Dioxide in n-Hexatriacontane," *J. Chem. Eng. Data*, 32, 467, 1987.

[44] Wiese, H. C.; Jacobs, J.; Sage, B. H., "Phase Equilibria in Hydrocarbon Systems: Phase Behavior in the Methane-Propane-n-Butane System," *J. Chem. Eng. Data*, 15, 82, 1970.

Hydrogen/n-Paraffin Database

[45] Connolly, J. F., "Vapor-Liquid Equilibrium Ratios for Four Binary Systems," Proceedings of the American Petrochemical Institute, Section III, 45, 62-67, 1965.

[46] Freitag, N. P.; Robinson, D. B., "Equilibrium Phase Properties of the Hydrogen-Methane-Carbon Dioxide, Hydrogen-Carbon Dioxide-n-Pentane and Hydrogen-n-Pentane Systems," *Fluid Phase Equilibria*, 31, 183, 1986.

[47] Huang, S. H.; Lin, H. M.; Tsai, F. N.; Chao, K. C., "Solubility of Synthesis Gases in Heavy n-Paraffins and Fischer-Tropsch Wax," *Ind. Eng. Chem. Res.*, 27, 162, 1988.

[48] Klink, A. E.; Cheh, H. Y.; Amick, E. H., Jr., "Vapor-Liquid Equilibrium of the Hydrogen-Butane System at Elevated Pressures," *AIChE J.*, 21, 6, 1142, 1975.

[49] Lin, H. M.; Sebastian, H. M.; Chao, K. C., "Gas-Liquid Equilibrium in Hydrogen + n-Hexadecane at Elevated Temperatures and Pressures," *J. Chem. Eng. Data*, 25, 252, 1980.

[50] Park, J. K., *Binary Vapor-Liquid Equilibrium Measurements for Selected Asymmetric Mixtures and Equation of State Development*, Ph. D. Dissertation, Oklahoma State University, Stillwater, Oklahoma, 1993.

[51] Peter, S.; Reinhartz, K., "The Phase Equilibria of the System Hydrogen-n-Heptane, Hydrogen-Methylcyclohexane and Hydrogen- 2, 2, 4-Trimethylpentane at Higher Pressure and Temperature," *Zeit. fur. Phys. Chem.*, 24, 103, 1960.

[52] Gao, Wuzi, *High Pressure Solubility Measurements for Selected Asymmetric Mixtures and Equation-of-State Developments*, Ph.D. Dissertation, Oklahoma State University, Stillwater, OK, 1999.

Carbon Monoxide/n-Paraffin Database

[53] Connolly, J. F.; Kandalic, G. A., "Thermodynamic Properties of Dilute Solutions of Carbon Monoxide in a Hydrocarbon," *J. Chem. Thermodynamics*, 16, 1129, 1984.

[54] Huang, S. H.; Lin, H. M.; Tsai, F. N.; Chao, K. C., "Solubility of Synthesis Gases in Heavy n-Paraffins and Fischer-Tropsch Wax," *Ind. Eng. Chem. Res.*, 27, 162, 1988.

[55] Srivatsan, S., *Binary Vapor-Liquid Phase Equilibrium for Methane and Carbon Monoxide in Selected Hydrocarbons*, M. S. Thesis, Oklahoma State University, Stillwater, Oklahoma, 1991.

[56] Gao, Wuzi, *High Pressure Solubility Measurements for Selected Asymmetric Mixtures and Equation-of-State Developments*, Ph.D. Dissertation, Oklahoma State University, Stillwater, OK, 1999.

[57] Yi, X., *Binary Vapor-Liquid Phase Equilibrium for Carbon Dioxide + Hydrocarbons*, M. S. Thesis, Oklahoma State University, Stillwater, Oklahoma, 1992.

Ternary Mixtures Database

[58] Mehra, V. S.; Thodos, G., "Vapor-Liquid Equilibria Constants for the Ethane-n-Butane-n-Heptane System at 150, 200, and 250 °F," *J. Chem. Eng. Data*, 11, 365, 1966.

[59] Nagarajan, N.; Gasem, K. A. M.; Robinson, R. L., Jr., "Equilibrium Phase Compositions, Phase Densities, and Interfacial Tensions for CO₂ + Hydrocarbon Systems. 6. CO₂ + n-Butane + n-Decane," *J. Chem. Eng. Data*, 35, 228, 1990.

[60] Tanaka, H.; Yamaki, Y.; Kato, M., "Solubility of Carbon Dioxide in Pentadecane, Hexadecane, and Pentadecane + Hexadecane," *J. Chem. Eng. Data*, 38, 386, 1993.

[61] Wiese, H. C.; Reamer, H. H. and Sage, G. H., "Phase Equilibria in Hydrocarbon Systems: Phase Behavior in the Methane-Propane-n-Decane System," *J. Chem. Eng. Data*, 15, 75, **1970**.

Additional Binary Systems

[62] Ohgaki, K.; Katayama, T., "Isothermal Vapor-Liquid Equilibrium Data for the Ethane-Carbon Dioxide System at High Pressure," *Fluid Phase Equilibria*, 1, 27, **1977**.

[63] Tsang, C. Y.; Streett, W. B., "Phase Equilibria in the H₂/ CO₂ System at Temperatures from 220 to 290 K and Pressures to 172 MPa," *Chem. Eng. Sci.*, 36, 993, **1981**.

[64] Gasem, K. A. M.; Bufkin, B. A.; Raff, A. M.; Robinson, R. L., Jr., "Solubilities of Ethane in Heavy Normal Paraffins at Pressures to 7.8 MPa and Temperatures from 348 to 423 K," *J. Chem. Eng. Data*, 34, 2, 187, **1988**.

APPENDIX A

Flow Diagram for Experiment Planning Program

The experiment planning method is based on determining the following variables in sequence:

1. Determine the molar volume and bubble point pressure at the specified temperature and composition (bubble point measurements). Determine the amount of solute and solvent required based on a constant volume equilibrium cell and knowledge of pure component densities.

The first objective is accomplished by determining the bubble point pressure and molar volume of the mixture at constant temperature and composition. If the calculated mixture volume is not equal to equilibrium cell volume, the volume of solvent, V_3 , in cm^3 is adjusted, which accordingly slightly change the mixture composition. Therefore, a new bubble point pressure and composition are determined. The volume of solvent is adjusted until the volume constraint is satisfied.

2. Determine the two-phase equilibrium pressure and liquid/vapor ratio. A flash calculation is performed at constant temperature and overall solute composition subject to constant volume constraint as small increments of solvent is admitted to the equilibrium cell. The number of mole of solvent required to reach bubble point pressure is N_3 . To cover a wide range of mixture's compositions in the two-phase, the initial mole of solvent used is $N_3/10$. After a small increment of solvent is added, the pressure is adjusted in the two-phase region until the volume constraint is satisfied.
3. As the mixture composition reaches beyond the bubble point composition as determined by the vapor over feed ratio (V/F). The pressure is determined in the

liquid region from EOS based on knowledge of molar volume, temperature, and composition. The calculation terminates in the first isotherm when the number of moles of solvent injected exceeds the amount required to reach bubble point by 5 % ($N_{3 \text{ final}} = 1.05 N_3$).

4. Determine the molar volume, the bubble point pressure and the amount of solvent required to reach the bubble point pressure at a lower temperature. After a temperature reduction, the pressure and the molar volume at the bubble point are determined by iteration subject to a variable solvent mole fraction (x_3) until the constant equilibrium cell volume constraint and the bubble point equilibrium condition are satisfied.
5. Determine the two-phase equilibrium pressure and liquid/vapor ratio. A flash calculation is performed at constant temperature and overall solute composition subject to constant volume constraint as small increments of solvent is admitted to the equilibrium cell.

The same procedure continues as the equilibrium cell temperature is reduced further.

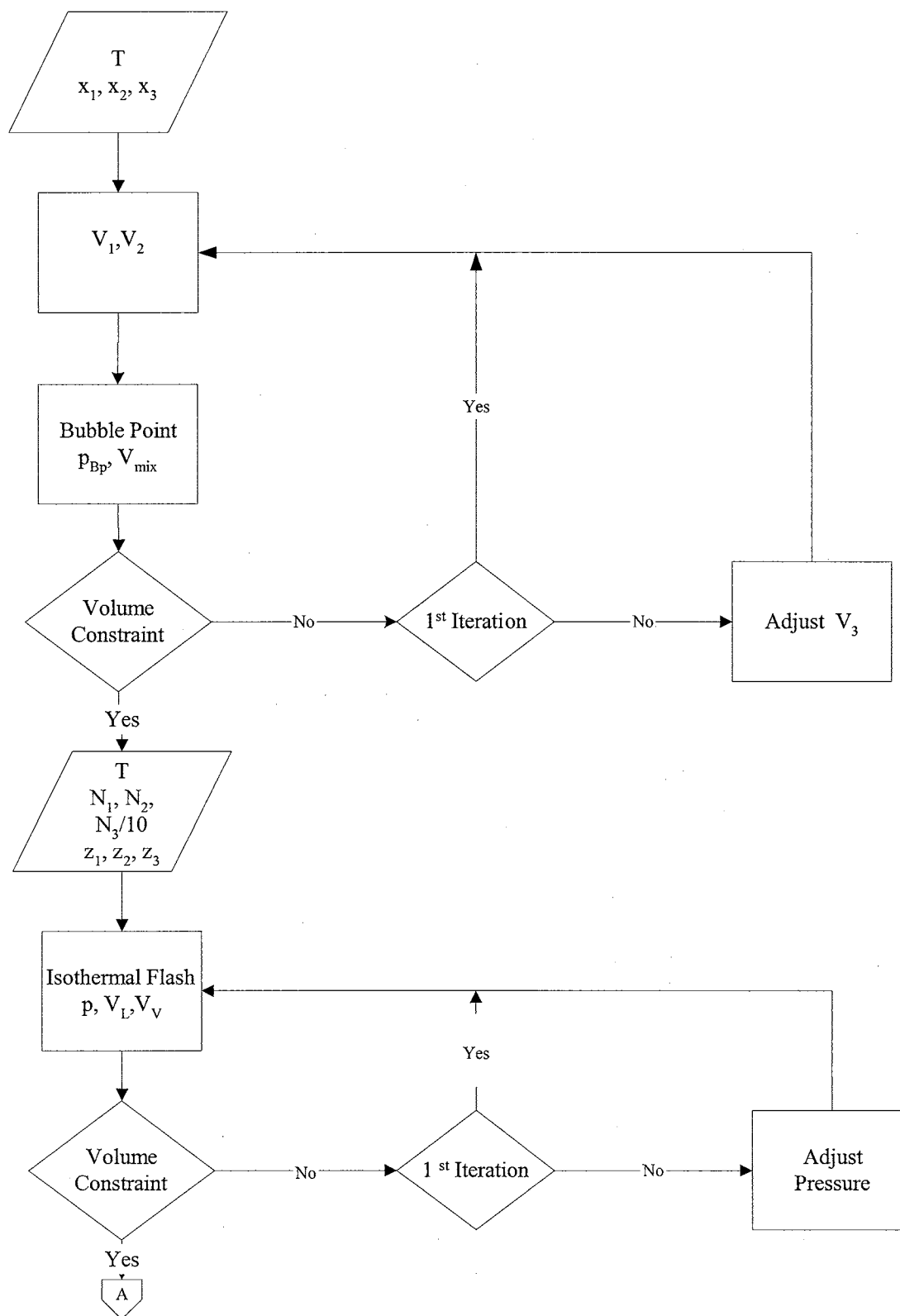


Figure A-1. Flow Diagram for Experiment Planning Program

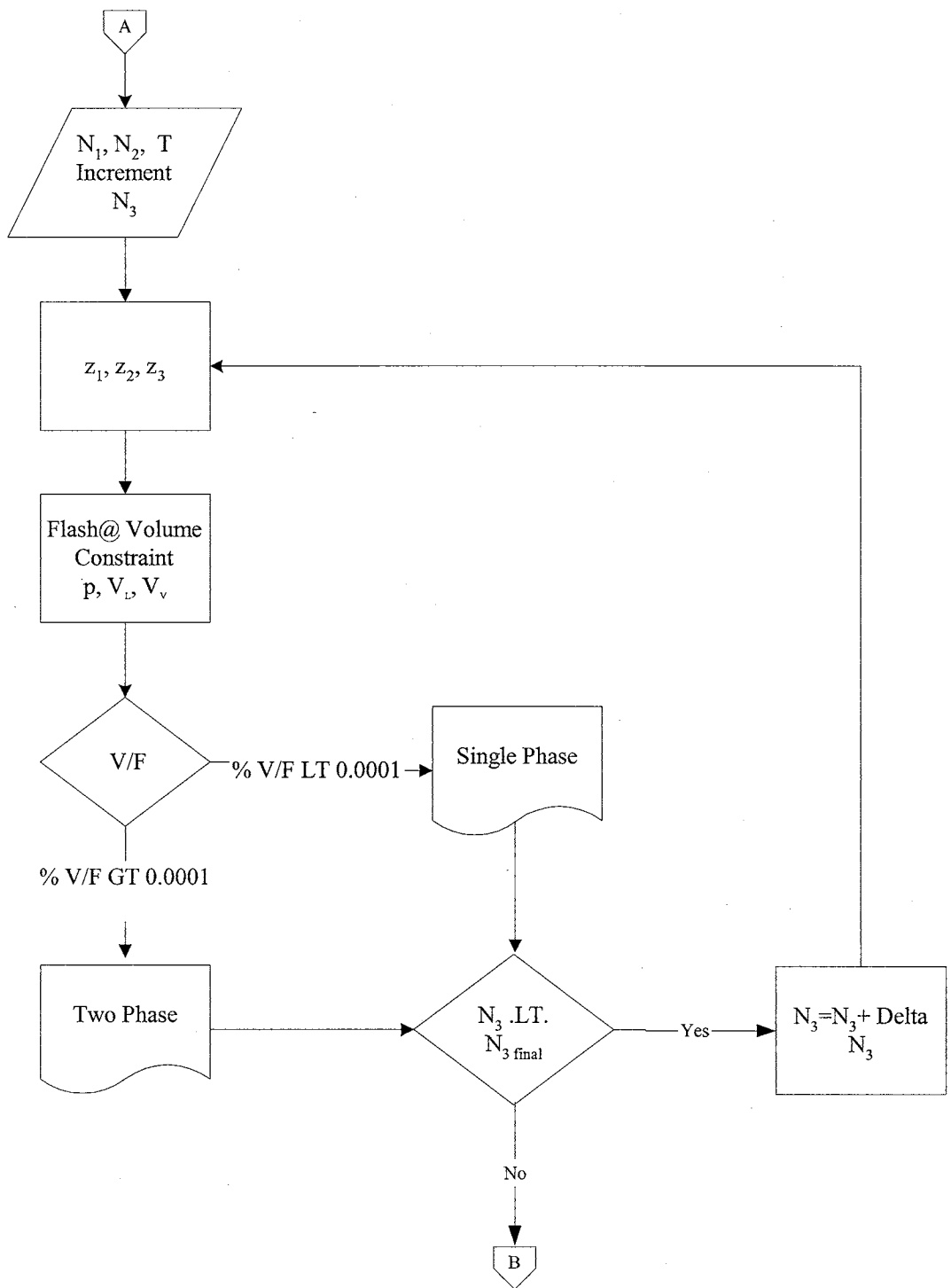


Figure A-1. Flow Diagram for Experiment Planning Program - Continued

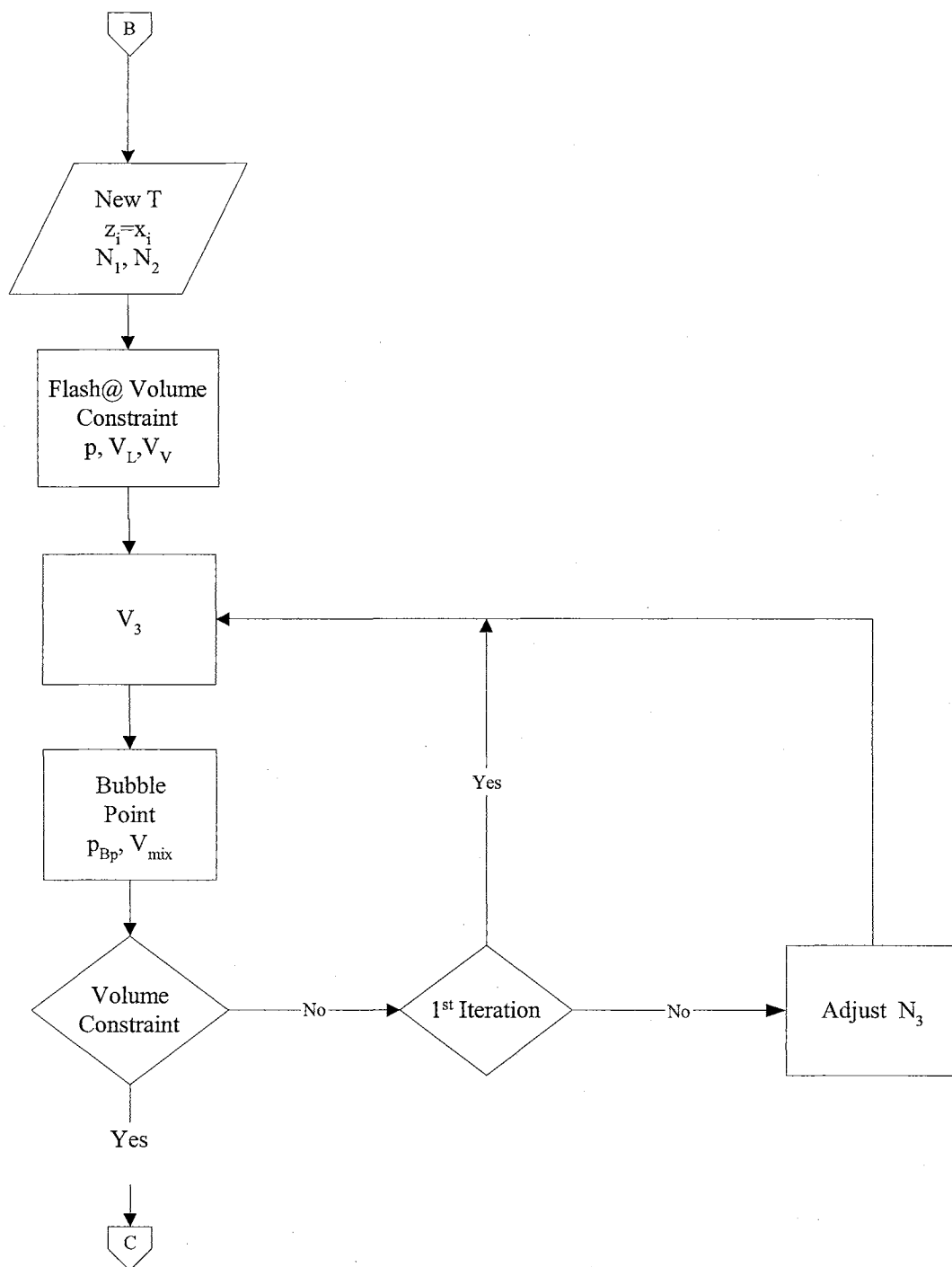


Figure A-1. Flow Diagram for Experiment Planning Program - Continued

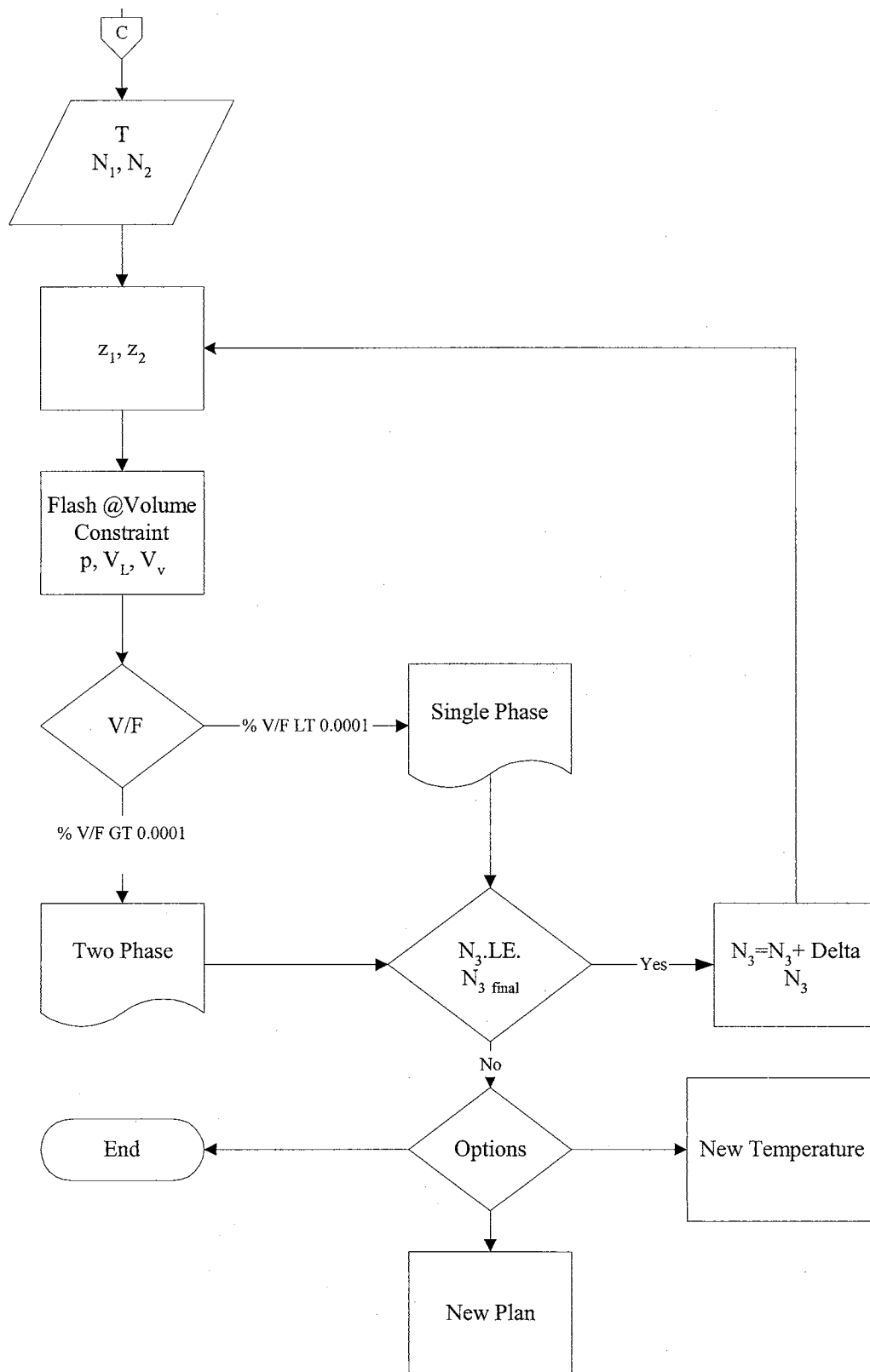


Figure A-1. Flow Diagram for Experiment Planning Program - Continued

APPENDIX B

Error Analysis of Solubility Measurements for Binary and Ternary Mixtures

ERROR ANALYSIS OF
SOLUBILITY MEASUREMENTS FOR BINARY AND TERNARY MIXTURES

Error analysis is a procedure for determining the amount of random variations in experimental measurements and locating the causes of these random variations. The specific objectives of performing error analysis are to: (1) determine the uncertainties in experimental mole fractions and bubble point pressures for binary and ternary mixtures, (2) identify the contributing factors to these uncertainties, and (3) find ways to reduce these uncertainties.

The error analysis used in this work is based on the theory of multivariate error propagation. The experiment model is expressed as a function y of several independent variables x_1, x_2, \dots, x_n , or $y = f(x)$. The usual procedure is to linearize $f(x)$ by a Taylor series and thereafter compute the variance by

$$\sigma_y^2 \cong \sum_i^n \left[\frac{\partial f(x)}{\partial x_i} \right]^2 \sigma_{x_i}^2 \quad (\text{B-1})$$

It is well known that first-order Taylor series expansion is not a valid approximation if the standard deviation in the input variable is large, the second- and higher-order derivative with respect to x are significant (Asbjornsen, 1975) and the independent variable errors are correlated.

For multi-component mixtures, the mole fraction of solute (1) is defined as follows:

$$x_1 = \frac{n_1}{\sum_i n_i} \quad (\text{B-2})$$

Applying Equation (B-1) to the mole fraction definition given in Equation (B-2), we obtain the uncertainty in solute mole fraction for binary mixture:

$$\sigma_{x_1} = \left[\left(-\frac{n_1}{(n_1 + n_2)^2} + \frac{1}{n_1 + n_2} \right)^2 \sigma_{n_1}^2 + \left(\frac{n_1^2}{(n_1 + n_2)^4} \sigma_{n_2}^2 \right) \right]^{1/2} \quad (\text{B-3})$$

The above term can be simplified by dividing σ_{x_1} by $x_1 (1-x_1)$

$$\frac{\sigma_{x_1}}{\{x_1(1-x_1)\}} = \left(\frac{\{n_1 + n_2\}^2}{n_1 n_2} \left(\frac{n_2^2 \sigma_{n_1}^2 + n_1^2 \sigma_{n_2}^2}{\{n_1 + n_2\}^4} \right) \right)^{1/2} \quad (\text{B-4})$$

Thus,

$$\frac{\sigma_{x_1}}{\{x_1(1-x_1)\}} = \left(\frac{\sigma_{n_1}^2}{n_1^2} + \frac{\sigma_{n_2}^2}{n_2^2} \right)^{1/2} \quad (\text{B-5})$$

The moles of solute and solvent injected are defined as follow:

$$n_1 = \left(\frac{I_{n_1} (V_{if} \rho_{1f} - V_{ii} \rho_{1i})}{Mw_1} \right) \quad (\text{B-6})$$

$$n_2 = \left(\frac{I_{n_2} (V_{2f} \rho_{2f} - V_{2i} \rho_{2i})}{Mw_2} \right) \quad (\text{B-7})$$

where

n_1, n_2 : Moles of solute and solvent

V_i and V_f : Initial and final volume

ρ : Density (mass/volume)

x_1 : Solute mole fraction

I_n : Number of injections

Applying Equation (B-1), the uncertainty in number of moles injected is determined as follows:

$$\sigma_{n_1} = \left(\left(\frac{\partial n_1}{\partial V_{1f}} \right)^2 \sigma_{V_{1f}}^2 + \left(\frac{\partial n_1}{\partial \rho_{1f}} \right)^2 \sigma_{\rho_{1f}}^2 + \left(\frac{\partial n_1}{\partial V_{1i}} \right)^2 \sigma_{V_{1i}}^2 + \left(\frac{\partial n_1}{\partial \rho_{1i}} \right)^2 \sigma_{\rho_{1i}}^2 \right)^{1/2} \quad (\text{B-8})$$

$$\sigma_{n_1} = \left(\left(\frac{I_{n_1} \rho_{1f} \sigma_{V_{1f}}}{Mw_1} \right)^2 + \left(\frac{I_{n_1} V_{1f} \sigma_{\rho_{1f}}}{Mw_1} \right)^2 + \left(-\frac{I_{n_1} \rho_{1i} \sigma_{V_{1i}}}{Mw_1} \right)^2 + \left(-\frac{I_{n_1} V_{1i} \sigma_{\rho_{1i}}}{Mw_1} \right)^2 \right)^{1/2} \quad (\text{B-9})$$

$$\sigma_{n_2} = \left(\left(\frac{I_{n_2} \rho_{2f} \sigma_{V_{2f}}}{Mw_2} \right)^2 + \left(\frac{I_{n_2} V_{2f} \sigma_{\rho_{2f}}}{Mw_2} \right)^2 + \left(-\frac{I_{n_2} \rho_{2i} \sigma_{V_{2i}}}{Mw_2} \right)^2 + \left(-\frac{I_{n_2} V_{2i} \sigma_{\rho_{2i}}}{Mw_2} \right)^2 \right)^{1/2} \quad (\text{B-10})$$

Since fluid injections are performed at constant temperature and pressure and the uncertainties of initial and final volumes are the same, then:

$$\rho_{2f} = \rho_{2i} = \rho_2 \quad \sigma_{\rho_{2f}} = \sigma_{\rho_{2i}} = \sigma_{\rho_2} \quad \sigma_{V_{2f}} = \sigma_{V_{2i}} \quad (\text{B-11})$$

$$\rho_{1f} = \rho_{1i} = \rho_1 \quad \sigma_{\rho_{1f}} = \sigma_{\rho_{1i}} = \sigma_{\rho_1} \quad \sigma_{V_{1f}} = \sigma_{V_{1i}} \quad (\text{B-12})$$

This leads to:

$$n_1 = \frac{I_{n_1} (V_{1f} - V_{1i}) \rho_1}{Mw_1} \quad (\text{B-13})$$

Only one solute injection required and the volume of solvent injected is always referenced to the initial volume. Therefore, I_{n_1} and I_{n_2} were set equal to 1.

Dividing Equation (B-8) by Equation (B-13) leads to:

$$\frac{\sigma_{n_1}}{n_1} = \left(\frac{\sigma_{V_{1f}}^2}{(V_{1f} - V_{1i})^2} + \frac{V_{1f}^2 \sigma_{\rho_1}^2}{(V_{1f} - V_{1i})^2 \rho_1^2} + \frac{\sigma_{V_{1i}}^2}{(V_{1f} - V_{1i})^2} + \frac{V_{1i}^2 \sigma_{\rho_1}^2}{(V_{1f} - V_{1i})^2 \rho_1^2} \right)^{1/2} \quad (\text{B-14})$$

Substitute in Equation (B-4) to get:

$$\frac{\sigma_{x_1}}{(x_1(1-x_1))} = \left(\frac{2\sigma_{V_{1f}}^2}{(V_{1f} - V_{1i})^2} + \frac{(V_{1f}^2 + V_{1i}^2)\sigma_{\rho_1}^2}{(V_{1f} - V_{1i})^2 \rho_1^2} + \frac{2\sigma_{V_{2f}}^2}{(V_{2f} - V_{2i})^2} + \frac{(V_{2f}^2 + V_{2i}^2)\sigma_{\rho_2}^2}{(V_{2f} - V_{2i})^2 \rho_2^2} \right)^{1/2} \quad (\text{B-15})$$

Since

$$V_1 = V_{1f} - V_{1i} \quad (\text{B-16})$$

$$\sigma_{V_1} = \sqrt{2} \sigma_{V_{1f}} = \sqrt{2} \sigma_{V_{1i}} \quad (\text{B-17})$$

$$\sigma_{V_{2T}} = \sqrt{2} \sigma_{V_{2f}} = \sqrt{2} \sigma_{V_{2i}} \quad (\text{B-18})$$

Then,

$$\frac{\sigma_{x_1}}{(x_1(1-x_1))} = \left(\frac{\sigma_{V_1}^2}{(V_{1f} - V_{1i})^2} + \frac{(V_{1f}^2 + V_{1i}^2)\sigma_{\rho_1}^2}{(V_{1f} - V_{1i})^2 \rho_1^2} + \frac{\sigma_{V_{2T}}^2}{(V_{2f} - V_{2i})^2} + \frac{(V_{2f}^2 + V_{2i}^2)\sigma_{\rho_2}^2}{(V_{2f} - V_{2i})^2 \rho_2^2} \right)^{1/2} \quad (\text{B-19})$$

Similarity for ternary mixture, the uncertainty in mole fraction is determined as:

$$\frac{\sigma_{x_3}}{(x_3(1-x_3))} = \left(\frac{\sigma_{V_3}^2}{(V_{3f} - V_{3i})^2} + \frac{(V_{3f}^2 + V_{3i}^2)\sigma_{\rho_3}^2}{(V_{3f} - V_{3i})^2 \rho_3^2} + \frac{n_1^2}{(n_1 + n_2)^2} \left(\frac{\sigma_{V_1}^2}{(V_{1f} - V_{1i})^2} + \frac{(V_{1f}^2 + V_{1i}^2)\sigma_{\rho_1}^2}{(V_{1f} - V_{1i})^2 \rho_1^2} \right) + \frac{n_2^2}{(n_1 + n_2)^2} \left(\frac{\sigma_{V_{2T}}^2}{(V_{2f} - V_{2i})^2} + \frac{(V_{2f}^2 + V_{2i}^2)\sigma_{\rho_2}^2}{(V_{2f} - V_{2i})^2 \rho_2^2} \right) \right)^{1/2} \quad (\text{B-20})$$

Equations (B-19) and (B-20) show the effect of the initial and final volumes on the uncertainty in mole fraction.

Uncertainty in the Bubble Point Determination

The uncertainty in bubble point for binary mixture is defined as:

$$\sigma_{Bp}^2 = \left(\frac{\partial P}{\partial x_1} \right)_{T,x_1}^2 \sigma_{x_1}^2 + \left(\frac{\partial P}{\partial T} \right)_{x_1}^2 \sigma_T^2 + \epsilon_{Bp}^2 \quad (\text{B-21})$$

and similarly for ternary mixture,

$$\sigma_{Bp}^2 = \left(\frac{\partial P}{\partial x_1} \right)_{T,x_3}^2 \sigma_{x_1}^2 + \left(\frac{\partial P}{\partial T} \right)_{x_1,x_3}^2 \sigma_T^2 + \left(\frac{\partial P}{\partial x_3} \right)_{T,x_1}^2 \sigma_{x_3}^2 + \epsilon_{Bp}^2 \quad (\text{B-22})$$

where

σ_{Bp} : Uncertainty in bubble point

σ_T : Uncertainty in temperature

ε_{Bp} : Uncertainty in pressure due to experimental procedure and pressure reading

A numerical example is given to demonstrate the method used for determining the uncertainties in measured and calculated variables. Carbon dioxide/decane binary was one of the systems initially investigated, so it is used to demonstrate this evaluation.

Uncertainty in Pressure

The uncertainties in the measured pressure are dependent on the following:

- 1- Uncertainty in the calibrating device. In our case, the Ruska dead-weight gauge has an uncertainty, ε_{pdw} , of 0.015 % of measured pressure.
- 2- The manufacturer reported that the accuracy of pressure transducer is ± 0.05 % of the full scale. For a 2000 psia transducer, the accuracy in pressure is ± 1 psi. The pressure transducer is frequently calibrated against a dead-weight gauge to minimize this inaccuracy. This uncertainty, ε_{pc} , due to inaccuracy in the pressure transducer measurements (and also due to the change with time) is determined by comparing the calibration trend lines over a short time interval. The standard deviation of this reading represents ε_{pc} (for demonstration purpose, $\varepsilon_{pc} = (0.0007 p + 0.5425)/2$).
- 3- The uncertainty in pressure instrument reading, ε_{pi} , after correcting for pressure, is 0.1 psi from dead weight gauge reading.

$$\sigma_p = \left(\varepsilon_{pi}^2 + \varepsilon_{pdw}^2 + \varepsilon_{pc}^2 \right)^{1/2} \quad (B-23)$$

Representing the above factors in Equation (B-23) in mathematical form, the uncertainty in pressure is calculated as follow:

$$\sigma_p = \left(0.1^2 + (.00015 p)^2 + ((0.0007 p + 0.5425)/2)^2 \right)^{1/2} \text{ psia}$$

A separate equation is required for each pressure transducer.

Uncertainty in Temperature

All temperature instruments calibrated frequently against Minco platinum resistance thermometer. The uncertainty in temperature reading, ϵ_{Tr} , is typically 0.05 °F. The temperatures calibration trends over short interval of time revealed a standard deviation or uncertainty, ϵ_{Tc} , of 0.05 °F.

From above, the maximum uncertainty in temperature reading is

$$\sigma_T = \left(\epsilon_{Tc}^2 + \epsilon_{Tr}^2 \right)^{1/2} \tag{B-24}$$

$$\sigma_T = \left((0.05)^2 + (0.05)^2 \right)^{1/2} = 0.07 \text{ °F}$$

For the purpose of this study, $\sigma_T = 0.1 \text{ °F}$

Uncertainty in Solvent Density

Liquid density is a function of temperature and pressure. The uncertainty in the liquid density, σ_{ρ_2} is defined as follows:

$$\sigma_{\rho_2} = \left(\epsilon_{\rho_2}^2 + \left(\frac{\partial \rho_2}{\partial T} \right)_p^2 \sigma_T^2 + \left(\frac{\partial \rho_2}{\partial P} \right)_T^2 \sigma_P^2 \right)^{1/2} \tag{B-25}$$

Grehrig and Lentz (1983) reported a maximum uncertainty of 0.14% for the liquid density of decane. The properties of decane were determined at constant

temperature and pressure, where the liquid density is $\rho_2 = 0.7106 \text{ g/cm}^3$ at 122°F and 565 psia.

where the uncertainty in the experimental liquid density, ε_{ρ_2} , reported is

$$\varepsilon_{\rho_2} = 0.14\% \text{ of solvent density} = 0.0014 \rho_2$$

The derivative of density with respect to temperature and pressure were determined from tabulated results over a narrow temperature and pressure ranges, respectively.

$$\left(\frac{\partial \rho_2}{\partial T}\right)_p = -3.89 \times 10^{-4} \text{ g/cm}^3 \text{ } ^\circ\text{F}$$

$$\left(\frac{\partial \rho_2}{\partial P}\right)_T = 5.95 \times 10^{-6} \text{ g/cm}^3 \text{ psi}$$

Substitute into Equation (B-25), we get:

$$\sigma_{\rho_2} = \left((0.0014 \times 0.71)^2 + (-3.89 \times 10^{-4})^2 \times 0.1^2 + (5.95 \times 10^{-6})^2 \times 0.486 \right)^{1/2}$$

$$\sigma_{\rho_2} = 9.956 \times 10^{-4} \text{ g/cm}^3 \text{ (0.14\%)}$$

Uncertainty in Solute Density

The uncertainty in liquid density, σ_{ρ_2} is defined as follows:

$$\sigma_{\rho_1} = \left(\varepsilon_{\rho_1}^2 + \left(\frac{\partial \rho_1}{\partial T}\right)_p^2 \sigma_T^2 + \left(\frac{\partial \rho_1}{\partial P}\right)_T^2 \sigma_P^2 \right)^{1/2} \quad (\text{B-26})$$

The properties of CO_2 were determined from Vukalovich (1968). The author used a virial equation with fourth order virial coefficients. The maximum reported uncertainty in molar volume is 0.1 to 0.15 %. Gas densities of CO_2 were determined at

constant temperature and pressure, where the density is $\rho_1 = 0.09104 \text{ g/cm}^3$ at 122°F and 650 psia

Where the derivative of density with respect to temperature and pressure were determined from EOS listed in Table 5, to get

$$\left(\frac{\partial \rho_1}{\partial T}\right)_P = -2.47 \times 10^{-4} \text{ g/cm}^3 \text{ } ^\circ\text{F}$$

$$\left(\frac{\partial \rho_1}{\partial P}\right)_T = 1.9246 \times 10^{-4} \text{ g/cm}^3 \text{ psi}$$

$$\varepsilon_{\rho_1} = 0.15 \% \text{ of gas density} = 0.0015 \rho_1$$

Substitute into Equation (B-26), we get:

$$\sigma_{\rho_1} = \left((0.0015 \times 0.09)^2 + (1.92 \times 10^{-4})^2 \times 0.52^2 + (-2.47 \times 10^{-4})^2 \times 0.1^2 \right)^{1/2}$$

$$\sigma_{\rho_1} = 1.7 \times 10^{-4} \text{ g/cm}^3 = 0.19 \%$$

Uncertainty in Volume Injected

Solvent:

The accuracy of amount of solvent injections relies mainly on the accurate determination of the volume of the capillary tube between the injection valve (V-4) and the equilibrium cell. Based on repeated measurements (discontinuity in pressure vs. total-volume-of-solvent-injected plot), an uncertainty of 0.026 cm^3 is determined from repeated measurements. The pump overall scale is from 0 to 25 cm^3 . The scale can be read to 0.005 cm^3 , but below this limit, personal judgment takes place. To be conservative in this estimate, 0.0025 cm^3 will be used, or the uncertainty in volume reading is

$$\varepsilon_{V_{2f}} = 0.0025 \text{ cm}^3$$

The volume of the injected solvent is determined by isolating the equilibrium cell from the liquid-injection line and then the injected volume is determined at constant pressure and temperature. Due to variation of temperature of ± 0.1 °F, a pressure fluctuation of ± 7 psi (at constant volume) is observed with decane. This fluctuation contributes to uncertainties in the volume and density of injected liquid and consequently to the number of moles injected specifically.

The uncertainty in pressure due to temperature fluctuation is approximately defined as

$$\sigma_{P_2} = \left(\sigma_p^2 + \left(\frac{\partial P}{\partial T} \right)_V^2 \sigma_T^2 \right)^{1/2} \quad (\text{B-27})$$

The coefficient of thermal expansion and isothermal coefficient of compressibility for decane estimated from Grehrig and Lentz (1983):

$$\kappa = \frac{1}{V} \left[\frac{\partial V}{\partial T} \right]_{P=60\text{atm}} = 5.64 \times 10^{-4} \text{ } ^\circ\text{F}^{-1}$$

$$\beta = \frac{1}{V} \left[\frac{\partial V}{\partial P} \right]_{T=50\text{C}} = -7.96 \times 10^{-6} \text{ psi}^{-1}$$

where

$$\left(\frac{\partial P}{\partial T} \right)_p = \left(\frac{\frac{1}{V} \left(\frac{\partial V_2}{\partial T} \right)_p}{-\frac{1}{V} \left(\frac{\partial V_2}{\partial P} \right)_T} \right) = 71 \text{ psi}/^\circ\text{F} \quad (\text{B-28})$$

which translates to:

$$\sigma_{P_2} \cong 7.1 \text{ psi}$$

Even though the density is measured at the same pressure and temperature, the effect of this high uncertainty on the pressure is examined:

$$\sigma_{\rho_2} = \left(\varepsilon_{\rho_2}^2 + \left(\frac{\partial \rho_2}{\partial P} \right)_T^2 \sigma_P^2 + \left(\frac{\partial \rho_2}{\partial T} \right)_P^2 \sigma_T^2 \right)^{1/2} \quad (\text{B-29})$$

$$\sigma_{\rho_2} = \left((0.0014 \times .71)^2 + (5.95 \times 10^{-6})^2 \times 7.1^2 + (-3.89 \times 10^{-4})^2 \times .1^2 \right)^{1/2}$$

$$\sigma_{\rho_2} = 9.965 \times 10^{-4} \text{ g/cm}^3 \text{ (0.14 \%)}$$

Accordingly, a negligible change in the uncertainty of the solvent density, σ_{ρ_2} , is noticed due to the pressure and temperature fluctuations.

The uncertainty of volume injected due σ_{p_2} is given as:

$$\sigma_{V_{2f}} = \left(\varepsilon_{V_{2f}}^2 + \left(\frac{\partial V_2}{\partial P} \right)_T^2 \sigma_{p_2}^2 + \left(\frac{\partial V_2}{\partial T} \right)_P^2 \sigma_T^2 \right)^{1/2} \quad (\text{B-30})$$

The derivative of volume with respect to temperature and pressure were determined from κ and β . Assuming 26.26 cm^3 of initial liquid volume, where this volume includes the volume of liquid in pump and connecting tubing to EC injection valve. The initial volume corresponds to the maximum volume to be considered, and consequently from Equation (B-3) to a larger contribution to the volume uncertainty.

The uncertainty in the initial volume injected is defined as:

$$\sigma_{V_{2i}} = \left(\varepsilon_{V_{2i}}^2 + \left(\frac{\partial V_2}{\partial P} \right)_T^2 \sigma_{p_2}^2 + \left(\frac{\partial V_2}{\partial T} \right)_P^2 \sigma_T^2 \right)^{1/2} \quad (\text{B-31})$$

Substitute, in Equation (B-31)

$$\sigma_{V_{2i}} = \left((0.0025)^2 + (5.64 \times 10^{-4} \times 26.26)^2 0.1^2 + (-7.96 \times 10^{-6} \times 26.26)^2 \times 7.094^2 \right)^{1/2}$$

$$\sigma_{V_{2i}} = 0.0038 \text{ cm}^3$$

$$V_2 = V_{2f} - V_{2i} \quad (\text{B-32})$$

$$\sigma_{V_2} = \sqrt{2} \sigma_{V_{2f}} = \sqrt{2} \sigma_{V_{2i}} = 0.0053 \text{ cm}^3 \quad (\text{B-33})$$

The uncertainty in the capillary-tube volume, ε_{cT} , contributes to total uncertainty in the injected liquid volume, since the capillary-tube volume (containing solvent) needs to be subtracted from the total volume of solvent injected.

$$\varepsilon_{cT} = 0.026 \text{ cm}^3$$

$$\sigma_{V_{2T}} = (\varepsilon_{cT}^2 + \sigma_{V_2}^2)^{1/2} \quad (\text{B-34})$$

$$\sigma_{V_{2T}} = (0.026^2 + 0.005^2)^{1/2} = 0.026 \text{ cm}^3$$

Therefore, the change due to uncertainty in temperature and pressure is negligible compared to uncertainty in dead volume.

Solute

Precise determination of the volume of the solute injected requires that the initial compression and the solute bleed to the equilibrium cell to be done at a slow rate. This will eliminate any temperature instability in this process and the consequent error. The solute and solvent injection pumps have the same scale, therefore

$$\varepsilon_{V_{ir}} = 0.0025 \text{ cm}^3$$

In order to determine the uncertainty in the injected volume, the uncertainties in pressure and temperature need to be evaluated. The parameters used in the evaluation, as determined from Vukalovich (1968), are

$Z = 0.806$; $\rho_1 = 0.09104 \text{ g/cm}^3$; $V_1 = 21.83 \text{ cm}^3$; $P = 650 \text{ psia}$; $T = 122 \text{ }^\circ\text{F}$

$$n_1 = \frac{\rho_1 V_1}{Mw_1} = \frac{0.09104 \times 21.83}{44.01} = 4.51 \times 10^{-2} \text{ gmol}$$

$$\left(\frac{\partial P}{\partial V} \right)_T = \frac{-nZRT}{V^2} + \frac{nRT}{V} \left(\frac{\partial Z}{\partial V} \right)_T \quad (\text{B-35})$$

$$\left(\frac{\partial P}{\partial V} \right)_T = 1.6072 \text{ bars/cc} = -23.35 \text{ psi/cm}^3$$

$$\left(\frac{\partial P}{\partial T} \right)_V = \frac{ZnR}{V} + \frac{nRT}{V} \left(\frac{\partial Z}{\partial T} \right)_V \quad (\text{B-36})$$

$$\left(\frac{\partial P}{\partial T} \right)_V = 0.18231 \text{ bars/}^\circ\text{C} = 1.47 \text{ psi/}^\circ\text{F}$$

$$\left(\frac{\partial V}{\partial T} \right)_P = \frac{nZR}{P} + \frac{nRT}{P} \left(\frac{\partial Z}{\partial T} \right)_P \quad (\text{B-37})$$

$$\left(\frac{\partial V}{\partial T} \right)_P = 0.10316 \text{ cc/}^\circ\text{C} = 0.057 \text{ cc/}^\circ\text{F}$$

The thermodynamic derivatives can be determined directly or indirectly, as indicated by Equations (B-35, 36 and 37) from the EOS listed in Table 5.

The uncertainty in solute pressure due to temperature fluctuation is determined as follows:

$$\sigma_{p_1} = (\sigma_p^2 + \left(\frac{\partial P}{\partial T} \right)_V^2 \sigma_T^2)^{1/2} \quad (\text{B-38})$$

$$\sigma_{p_1} = (0.517^2 + (1.47)^2 \times 0.1^2)^{1/2}$$

$$\sigma_{p_1} = 0.538 \text{ psi}$$

The effect of σ_T on σ_{p_1} is very small, so the use of Equation B-38 is valid.

The uncertainty in the injected volume correlates to the uncertainty in temperature and pressure as:

$$\sigma_{V_{ii}} = \left(\varepsilon_{V_{ii}}^2 + \left(\frac{\partial V_1}{\partial P} \right)_T^2 \sigma_P^2 + \left(\frac{\partial V_1}{\partial T} \right)_P^2 \sigma_T^2 \right)^{1/2} \quad (\text{B-39})$$

$$\sigma_{V_{ii}} = (.0025^2 + \left(\frac{-1}{23.35} \right)^2 0.538^2 + (0.0574)^2 .1^2)^{1/2} = 0.02389 \text{ cm}^3$$

For initial and final injections combined:

$$V_1 = V_{if} - V_{ii} \quad (\text{B-40})$$

$$\sigma_{V_1} = \sqrt{2} \sigma_{V_{if}} = \sqrt{2} \sigma_{V_{ii}} \quad (\text{B-41})$$

$$\sigma_{V_1} = \sqrt{2} 0.02389 = 0.0336 \text{ cm}^3$$

Evaluation of the Uncertainty in Mole Fraction and Bubble Point Pressure

For carbon dioxide/decane binary at 280 °F, the relation between bubble point pressure and solute mole fraction were determined from Reamer and Sage (1963) data.

$$P = 2877.6 x_1 - 36.89$$

$$\left(\frac{\partial P}{\partial x_1} \right)_{T=280^\circ\text{F}} = 2877.6 \text{ psia}$$

Also at constant mole fraction, the relation between bubble point pressure and temperature were correlated from Reamer and Sage (1963) data as:

$$P = 1.47 T + 189.71$$

$$\left(\frac{\partial P}{\partial T}\right)_{x_1=0.224} = 1.47 \text{ psia / } ^\circ\text{F}$$

To account for the reproducibility of the bubble point, the bubble point plot for CO₂/decane at 280 °F was examined. By variation of intersection slopes of the lines an uncertainty in bubble point measurement due to experimental procedure is

$$\varepsilon_{pp} = 0.000571 p + 0.8128$$

The total uncertainty in bubble point measurement due to pressure is

$$\varepsilon_{Bp} = \left(\varepsilon_{pp}^2 + \varepsilon_p^2\right)^{1/2} \quad (\text{B-42})$$

or

$$\varepsilon_{Bp} = \left(\left(0.000571 p + 0.8128\right)^2 + (0.1)^2 + (0.00015 p)^2 + \left(\left(0.0007 p + 0.5425\right)/2\right)^2\right)^{1/2} \text{ psia}$$

The initial and final volumes in cm³ in both solute and solvent pumps and associated tubing are as follows:

$$V_{1f} = 21.83 \text{ cm}^3, V_{1i} = 13.83 \text{ cm}^3, V_{2i} = 1 \text{ cm}^3 \text{ and } V_{2f} = 5 \text{ cm}^3$$

Substituting in Equation (B-19), the uncertainty in mole fraction is obtained as:

$$\sigma_{x_1} = 0.0013$$

and similarly substituting in Equation (B-21), the uncertainty in bubble point pressure is estimated as:

$$\sigma_{Bp} = 4.08 \text{ psia}$$

Table E.1 illustrates our error analysis calculation for carbon dioxide/decane binary mixture for four isotherms. Note that only one solute injection was made for all four-bubble point pressures. In addition, the net volume of the solvent injected needs to

be calculated independently at each isotherm because a small volume of solvent is subject to the variation in the equilibrium cell temperature.

Table B.1. Error Analysis for Carbon Dioxide/Decane Binary System

Case		1	2	3	4
Net solute injection		7.96	7.96	7.96	7.96
Solute initial volume	V_{1i}	30	30	30	30
Solute final volume	V_{1f}	22.04	22.04	22.04	22.04
Solute Mwt	Mw1(g/gmol)	44.01	44.01	44.01	44.01
Net solvent injection		15.454	16.247	17.012	17.809
Solvent initial volume	V_{2i}	21.52	21.52	21.52	21.52
Solvent final volume	V_{2f}	6.0656	5.273	4.508	3.7108
Solvent Mwt	Mw2 (g/gmol)	142.285	142.285	142.285	142.285
Solute density	g/cm^3	0.13054	0.13054	0.13054	0.13045
Solvent injection press.	bar	60.85	60.85	60.85	60.85
Solvent density	g/cm^3	0.7125	0.7125	0.7125	0.7125
Mixture gmol/cm3	real				
Total gmol	20.2 cell				
No. of injection-Solute	In_1	1	1	1	1
No. of injection-Solvent	In_2	1	1	1	1
Moles solute	n_1	0.02361	0.02361	0.02361	0.02359
Moles solvent	n_2	0.07739	0.08136	0.08519	0.08918
Mole fraction	X_1	0.23264	0.22383	0.21594	0.20829
Uncertainty in solute volume	σ_{v1}	0.04766	0.04766	0.04766	0.04770
Uncertainty in solute density	$\sigma_{\rho1}$	0.00025	0.00025	0.00025	0.00025
Uncertainty in solvent volume	σ_{v2}	0.02664	0.02664	0.02664	0.02664
Uncertainty in solvent density	$\sigma_{\rho2}$	0.00100	0.00100	0.00100	0.00100
Uncertainty in V_1 term		3.58E-05	3.58E-05	3.58E-05	3.59E-05
Uncertainty in solute density term		8.05E-05	8.05E-05	8.05E-05	8.05E-05
Uncertainty in V_2 term		2.97E-06	2.69E-06	2.45E-06	2.24E-06
Uncertainty in solvent density term		4.11E-06	3.65E-06	3.28E-06	2.95E-06
Multiplying factor $(X_1(1-X_1))^2$		3.19E-02	3.02E-02	2.87E-02	2.72E-02
(Solute volume term) ²		1.14E-06	1.08E-06	1.03E-06	9.76E-07
(Solute density term) ²		2.56E-06	2.43E-06	2.31E-06	2.19E-06
(Solvent volume term) ²		9.47E-08	8.11E-08	7.03E-08	6.08E-08
(Solvent density term) ²		1.31E-07	1.10E-07	9.40E-08	8.03E-08
σ_{X1}		3.93E-06	3.70E-06	3.50E-06	3.31E-06
Uncertainty in V_1 term		0.00107	0.00104	0.00101	0.00099
Uncertainty in solute density term		0.00160	0.00156	0.00152	0.00148
Uncertainty in V_2 term		0.00031	0.00028	0.00027	0.00025
Uncertainty in solvent density term		0.00036	0.00033	0.00031	0.00028
Uncertainty X	σ_{X1}	0.00198	0.00192	0.00187	0.00182

Table B.1. Error Analysis for Carbon Dioxide/Decane Binary System-Continued

Uncertainty in Bubble Point Pressure

Equilibrium cell T	^o F	280	220	160	100
(dP/dx)T		2877.6	2639.5	2131.5	1405.1
(dP/dT)x		1.47	1.47	1.47	1.47
Uncertainty in solute mole fraction		0.00198	0.00192	0.00187	0.00182
Uncertainty in temperature		0.1	0.1	0.1	0.1
Pressure		882.5	882.5	882.5	882.5
(Pressure term) ²		2.098	2.098	2.098	2.098
(Mole fract. Term) ²		32.568	25.795	15.897	6.530
(Temp. term) ²		0.022	0.022	0.022	0.022
Sum		34.687	27.914	18.017	8.649
Pressure term		1.448	1.448	1.448	1.448
Mole fraction		5.707	5.079	3.987	2.555
Temp term		0.147	0.147	0.147	0.147
σ_{Bp}		5.9	5.3	4.2	2.9

Uncertainty in Solvent Density

$\left(\frac{\partial p}{\partial T}\right)_V$	Psia/ ^o F	64.26	64.26	64.26	64.26
ρ_2	g/cm ³	0.7125	0.7125	0.7125	0.7125
$\left(\frac{\partial \rho_2}{\partial T}\right)_P$	g/cm ³ ^o F	-3.82E-04	-3.82E-04	-3.82E-04	-3.82E-04
$\left(\frac{\partial \rho_2}{\partial p}\right)_T$	g/cm ³ psia	5.95E-06	5.95E-06	5.95E-06	5.95E-06
σ_p	psia	0.60	0.60	0.60	0.60
σ_T	^o F	0.1	0.1	0.1	0.1
ϵ_{p2}		0.0010	0.0010	0.0010	0.0010
σ_{p2}	g/cm ³	0.00100	0.00100	0.00100	0.00100
%		0.14	0.14	0.14	0.14

Table B.1. Error Analysis for Carbon Dioxide/Decane Binary System-Continued

Uncertainty in Solute Density

Solute density required @ Cell T		0.05144	0.05144	0.05144	0.05141
Minimum injection pressure	psia	850.38	850.38	850.38	850.38
ρ_1	$\text{g/cm}^3 @ 50$	0.13054	0.13054	0.13054	0.13045
	$^{\circ}\text{C}$	0.13054	0.13054	0.13054	0.13045
$\left(\frac{\partial \rho_1}{\partial T}\right)_P$	$\text{g/cm}^3 \text{ } ^{\circ}\text{F}$	-5.58E-04	-5.58E-04	-5.58E-04	-5.58E-04
$\left(\frac{\partial \rho_1}{\partial P}\right)_T$	$\text{g/cm}^3 \text{ psi}$	2.46E-04	2.46E-04	2.46E-04	2.46E-04
σ_P	psi	0.59	0.59	0.59	0.59
σ_T	$^{\circ}\text{F}$	0.1	0.1	0.1	0.1
$\epsilon_{\rho 1}$	g/cm^3	0.00019	0.00019	0.00019	0.00019
$\sigma_{\rho 1}$	g/cm^3	0.00025	0.00025	0.00025	0.00025
%		0.19	0.19	0.19	0.19

Uncertainty in Solvent Volume

$\left(\frac{\partial P}{\partial T}\right)_V$	psi/ $^{\circ}\text{F}$	77.83	77.83	77.83	77.83
σ_{P2}	psi	7.81	7.81	7.81	7.81
$\kappa = \frac{1}{V} \left[\frac{\partial V}{\partial T} \right]$	$^{\circ}\text{F}^{-1}$	5.46E-04	5.46E-04	5.46E-04	5.46E-04
$\beta = -\frac{1}{V} \left[\frac{\partial V}{\partial P} \right]$	psi $^{-1}$	7.02E-06	7.02E-06	7.02E-06	7.02E-06
σ_T	$^{\circ}\text{F}$	0.1	0.1	0.1	0.1
σ_P	psi	0.60	0.60	0.60	0.60
V	cm^3	21.52	21.52	21.52	21.52
ϵ_{V2f}	cm^3	0.00250	0.00250	0.00250	0.00250
σ_{V2f}	cm^3	0.00300	0.00300	0.00300	0.00300
σ_{V2}	cm^3	0.00423	0.00423	0.00423	0.00423
ϵ_{VcT}	cm^3	0.02630	0.02630	0.02630	0.02630
σ_{V2T}	cm^3	0.02664	0.02664	0.02664	0.02664

Table B.1. Error Analysis for Carbon Dioxide/Decane Binary System-Continued

Uncertainty in Solute Volume

Pressure	psia	850.38	850.38	850.38	850.38
Pressure	bar	58.63	58.63	58.63	58.63
Density g/cm ³	g/cm ³	0.13054	0.13054	0.13054	0.13045
T degree C		50	50	50	50
Z		0.7341	0.7341	0.7341	0.7341
R		83.14	83.14	83.14	83.14
N	gmol	0.0890	0.0890	0.0890	0.0889
V	cm ³	30	30	30	30
Mwt		44.01	44.01	44.01	44.01
$\left(\frac{\partial Z}{\partial V}\right)_T$		0.0076	0.0076	0.0076	0.0076
$\left(\frac{\partial Z}{\partial T}\right)_V$		0.0011	0.0011	0.0011	0.0011
$\left(\frac{\partial Z}{\partial T}\right)_P$		0.0021	0.0021	0.0021	0.0021
$\left(\frac{\partial p}{\partial V}\right)_T$	psi/cm ³	-19.5409	-19.5409	-19.5409	-19.5214
$\left(\frac{\partial p}{\partial T}\right)_V$	psi/°F	2.1620	2.1620	2.1620	2.1605
$\left(\frac{\partial V}{\partial T}\right)_P$	cm ³ /°F	0.0988	0.0988	0.0988	0.0987
σ_T	°F	0.1	0.1	0.1	0.1
σ_p	psi	0.59	0.59	0.59	0.59
σ_{p1}	psi	0.63	0.63	0.63	0.63
ε_{V1f}	cm ³	0.0025	0.0025	0.0025	0.0025
V term		6.25E-06	6.25E-06	6.25E-06	6.25E-06
P term		0.03223	0.03223	0.03223	0.03226
T term		0.00988	0.00988	0.00988	0.00987
σ_{V1f}	cm ³	0.03371	0.03371	0.03371	0.03374
σ_{V1f} (Other method)	cm ³	0.03380	0.03380	0.03380	0.03383
σ_{V1}	cm ³	0.04766	0.04766	0.04766	0.04770
Mole fraction	X	0.2326	0.2238	0.2159	0.2083

APPENDIX C

The PR EOS Representation of Asymmetric Binary Mixtures

This Appendix gives tabulated results for the PR EOS representation of binary mixtures using the van der Waals one-fluid mixing rules. BIPs were determined by fitting the experimental data to minimize the objective function, SS, which represents the sum of squared-relative deviations in bubble point pressure, i.e.:

$$SS = \sum_i^n \left(\frac{P_{cal} - P_{exp}}{P_{exp}} \right)_i^2 \quad (C-1)$$

The critical constants presented in Table 6-6 and the new α function (Gasem et al., 2001) were used in this evaluation.

The BIPs for the CO₂/C₂H₆ and CO₂/H₂ systems at the operating temperatures were obtained by linearly extrapolating from the regressed parameters generated from available VLE data.

For some systems, more than one data source was available, and where binary interaction parameters vary, the evaluation of BIPs from different sources was considered in some cases.

Table C1. PR EOS Interaction Parameters for Carbon Dioxide (1) + n-Paraffins (2) Systems

CN	T, K	C_{ij}	% AAD	$C_{ij}(T)$	% AAD	C_{ij}	D_{ij}	% AAD	$C_{ij}(T)$	$D_{ij}(T)$	% AAD	NPTS	Ref
20	323.15	0.090	3.79	0.097	1.08	0.090	0.000	3.79	0.1074	-0.0034	0.47	14	18
	373.15			0.075	1.82				0.0981	-0.0080	0.34	9	
	323.25	0.084	5.13	0.101	2.21	0.1352	-0.0162	3.93	0.1191	-0.0064	0.42	5	
	373.45			0.078	1.40				0.1016	-0.0071	0.34	5	20
	473.15			0.043	1.12				0.0840	-0.0112	0.29	5	
	573.35			0.060	1.57				0.1848	-0.0349	0.56	5	
28	348.15	0.060	7.24	0.076	6.44	0.1163	-0.0145	2.95	0.1125	-0.0110	0.27	8	18
	373.15			0.058	5.66				0.1112	-0.0129	0.35	9	
	423.15			0.027	6.24				0.1086	-0.0178	1.92	7	
	373.35	0.032	5.34	0.050	3.74	0.1155	-0.0175	4.13	0.1087	-0.0128	1.23	5	
	473.45			0.001	1.41				0.0009	-0.0001	1.38	5	21
	573.45			0.002	1.20				-0.0013	-0.0001	1.20	5	
36	373.15	0.027	5.68	0.032	4.96	0.1065	-0.0133	2.43	0.1014	-0.0113	0.69	10	1
	423.15			0.019	6.16				0.1240	-0.0186	0.71	8	
	373.15	0.0332	3.24	0.044	3.14	0.0960	-0.0103	2.33	0.0886	-0.0076	1.24	5	
	473.35			-0.007	2.36				0.0693	-0.0096	1.10	4	14
	573.25			0.019	1.46				0.0831	-0.0094	1.19	5	
Avg.			5.07		3.06			3.28		0.80			

Table C2. PR EOS Interaction Parameters for Hydrogen + n-Paraffins Systems

CN	T, K	C_{ij}	% ADD	$C_{ij}(T)$	% AAD	$C_{ij}(T)$	$D_{ij}(T)$	% AAD	C_{ij}	D_{ij}	% AAD	NPTS	Ref
20	323.15	0.206	2.29	0.254	0.540	-0.4305	0.0284	1.59	0.1255	0.0055	0.32	4	50
	373.15			0.199	0.56				0.1036	0.0043	0.56	8	
	423.15			0.145	0.26				0.0675	0.0036	0.24	6	
	373.35	0.229	5.14	0.313	1.96	-1.7522	0.0877	2.69	0.1475	0.0071	1.79	5	
	473.55			0.061	0.71				0.0000	0.0029	0.62	5	
	573.25			0.184	1.01				-1.4939	0.0822	0.62	3	
28	348.15	0.312	3.57	0.355	0.55	0.1127	0.0059	3.53	0.1420	0.0066	0.19	6	50
	373.15			0.307	0.36				0.1661	0.0044	0.08	4	
	423.15			0.192	0.43				0.1104	0.0057	0.40	6	
	373.25	0.277	2.22	0.307	1.56	-0.5554	0.0252	1.13	0.1320	0.0051	1.48	5	
	473.25			0.245	1.69				-1.0249	0.0395	0.27	5	
	573.15			0.192	1.31				-0.8558	0.0357	0.88	5	
36	373.15	0.433	2.70	0.473	0.80	0.1780	0.0060	2.5	0.4700	0.000	0.80	6	50
	423.15			0.372	0.46				0.2346	0.0034	0.30	6	
	373.15	0.537	4.78	0.623	3.85	-0.0771	0.0138	3.98	-2.000	0.0563	1.36	5	
	473.05			0.350	3.61				0.3503	0.0000	3.61	5	
	573.15			0.560	3.00				-1.8277	0.0593	1.18	5	
Avg.			3.45		1.33			2.57		0.87			

Table C3. PR EOS Interaction Parameters for Ethane + n-Paraffins Systems

CN	T, K	C_{ij}	% AAD	$C_{ij}(T)$	% AAD	C_{ij}	D_{ij}	% AAD	$C_{ij}(T)$	$D_{ij}(T)$	% AAD	NPTS	Ref
20	323.15	-0.030	7.16	-0.025	7.35	0.0165	-0.0227	2.79	0.0177	-0.0206	0.67	6	64
	373.15			-0.023	8.26				0.0150	-0.0213	0.68	4	
	423.15			-0.049	4.75				0.0131	-0.0280	0.22	5	
	373.75	-0.024	3.7	-0.013	3.48	0.044	-0.031	1.6	-0.0114	-0.0012	3.28	3	
	473.65			-0.043	3.31				0.0452	-0.0329	0.83	4	
	572.85			-0.021	1.83				-0.0012	-0.0074	1.52	4	
28	348.15	-0.060	7.08	-0.052	6.09	-0.0007	-0.0187	2.85	-0.0022	-0.0166	1.07	10	64
	373.15			-0.058	6.80				-0.0062	-0.0159	1.13	7	
	423.15			-0.085	4.80				-0.0113	-0.0213	0.63	6	
	373.25	-0.060	5.88	-0.043	5.91	0.0296	-0.0279	2.98	0.0146	-0.0197	2.33	4	
	473.25			-0.088	4.36				0.0253	-0.0307	0.56	4	
	573.15			-0.081	2.02				-0.0009	-0.0218	0.82	4	
36	373.15	-0.085	7.78	-0.083	7.59	-0.0056	-0.0180	2.06	-0.0062	-0.0168	0.66	7	64
	423.15			-0.087	7.92				-0.0010	-0.0215	1.27	6	
	373.15	-0.077	6.67	-0.059	9.21	0.0276	-0.0258	2.24	0.2424	-0.0232	2.68	4	
	473.05			-0.103	3.91				-0.0194	-0.0180	1.23	4	
	573.05			-0.102	3.13				0.0164	-0.0232	0.70	4	
	Avg.			6.38		5.34						1.19	86

Table C4. PR EOS Interaction Parameters for Carbon Dioxide + Hydrogen

T, K	C_{ij}	% AAD	$C_{ij}(T)$	% AAD	C_{ij}	D_{ij}	% AAD	$C_{ij}(T)$	$D_{ij}(T)$	% AAD	NPTS	Ref
250	0.000	6.39	0.013	8.72	0.000	0.000	6.22	0.013	0.000	8.72	7	
260			0.002	5.98				0.002	0.000	5.98	10	63
290			-0.023	1.17				-0.023	0.000	1.17	5	
		6.39		5.29			6.22			5.29		

Extrapolate: $C_{12} = -0.0009 T (K) + 0.2375$

Table C5. PR EOS Interaction Parameters for Carbon Dioxide + Ethane

T, K	C_{ij}	% AAD	$C_{ij}(T)$	% AAD	C_{ij}	D_{ij}	% AAD	$C_{ij}(T)$	$D_{ij}(T)$	% AAD	NPTS	Ref
283.15	0.1495	1.15	0.129	0.83	0.148	-0.004	0.91	0.197	-0.038	0.60	17	
288.15			0.136	0.83				0.172	-0.020	0.26	15	
291.15			0.150	0.61				0.139	0.001	0.35	17	62
293.15			0.147	0.70				0.147	-0.005	0.55	11	
298.15			0.143	1.37				0.152	-0.013	1.36	6	
		1.15		0.72			0.91			0.52		

Extrapolate: $C_{12} = 0.0016 T (K) - 0.3191$

Regress from high Temperature Ternary data: $C_{12} = -0.003 T (K) + 0.634$

APPENDIX D

Experimental and Calculated Activity Coefficients at Infinite-Dilution using Several Models

Table D.1. Experimental and Calculated Activity Coefficient at Infinite-Dilution using Several Models

CN -1	Solute CN-2*	T °C	Gamma Exp.	γ_2^∞					
				UNIFAC 75	Kikic 80	Larsen 87	Sheng 89	Voulsas 95	Zhong 2000
7	5	20	1.00	0.96	0.98	0.98	1.00	1.00	0.98
7	6	20	1.00	0.99	1.00	1.00	1.00	1.00	1.00
8	5	20	1.01	0.93	0.97	0.96	1.00	1.00	0.97
8	5	20	0.97	0.93	0.97	0.96	1.00	1.00	0.97
8	5	55	1.07	0.93	0.97	0.96	1.00	1.00	0.97
8	5	75	1.06	0.93	0.97	0.96	1.00	1.00	0.97
8	5	115	1.04	0.93	0.97	0.96	1.00	1.00	0.97
8	6	55	1.07	0.97	0.99	0.99	1.00	1.00	0.99
8	6	75	1.04	0.97	0.99	0.99	1.00	1.00	0.99
8	6	115	1.02	0.97	0.99	0.99	1.00	1.00	0.99
8	7	55	1.06	0.99	1.00	1.00	1.00	1.00	1.00
8	7	75	1.03	0.99	1.00	1.00	1.00	1.00	1.00
8	7	115	1.00	0.99	1.00	1.00	1.00	1.00	1.00
12	5	20	0.89	0.79	0.90	0.89	1.01	0.95	0.88
12	5	20	0.97	0.79	0.90	0.89	1.01	0.95	0.88
12	5	30	0.95	0.79	0.90	0.89	1.01	0.95	0.88
16	3	25	0.96	0.50	0.72	0.69	1.04	0.70	0.63
16	3	40	0.82	0.50	0.72	0.69	1.04	0.70	0.63
16	4	30	0.89	0.59	0.78	0.76	1.02	0.79	0.72
16	4	40	0.85	0.59	0.78	0.76	1.02	0.79	0.72
16	4	70	0.84	0.59	0.78	0.76	1.02	0.79	0.72
16	4	90	0.83	0.59	0.78	0.76	1.02	0.79	0.72
16	5	25	0.83	0.67	0.83	0.81	1.01	0.86	0.79
16	5	25	0.93	0.67	0.83	0.81	1.01	0.86	0.79
16	5	30	0.92	0.67	0.83	0.81	1.01	0.86	0.79
16	5	40	0.87	0.67	0.83	0.81	1.01	0.86	0.79
16	5	50	0.90	0.67	0.83	0.81	1.01	0.86	0.79
16	5	70	0.86	0.67	0.83	0.81	1.01	0.86	0.79
16	5	90	0.85	0.67	0.83	0.81	1.01	0.86	0.79
16	6	20	0.89	0.74	0.87	0.86	1.00	0.91	0.84
16	6	20	0.90	0.74	0.87	0.86	1.00	0.91	0.84
16	6	20	0.91	0.74	0.87	0.86	1.00	0.91	0.84
16	6	20	0.90	0.74	0.87	0.86	1.00	0.91	0.84
16	6	25	0.89	0.74	0.87	0.86	1.00	0.91	0.84
16	6	25	0.87	0.74	0.87	0.86	1.00	0.91	0.84
16	6	25	0.90	0.74	0.87	0.86	1.00	0.91	0.84
16	6	30	0.90	0.74	0.87	0.86	1.00	0.91	0.84
16	6	30	0.90	0.74	0.87	0.86	1.00	0.91	0.84
16	6	30	0.90	0.74	0.87	0.86	1.00	0.91	0.84
16	6	31.7	0.91	0.74	0.87	0.86	1.00	0.91	0.84
16	6	35	0.90	0.74	0.87	0.86	1.00	0.91	0.84
16	6	40	0.88	0.74	0.87	0.86	1.00	0.91	0.84
16	6	40	0.89	0.74	0.87	0.86	1.00	0.91	0.84
16	6	40	0.91	0.74	0.87	0.86	1.00	0.91	0.84
16	6	40	0.91	0.74	0.87	0.86	1.00	0.91	0.84
16	6	42.2	0.92	0.74	0.87	0.86	1.00	0.91	0.84

Table D1. Experimental and Calculated Activity Coefficient at Infinite-Dilution using Several Models- *Continued*

CN-1	Solute CN-2	T °C	Gamma Exp.	UNIFAC	Kikic 80	Larsen 87	Sheng 89	Voulsas 95	Zhong 2000
						γ_2^∞			
16	6	50	0.90	0.74	0.87	0.86	1.00	0.91	0.84
16	6	50	0.90	0.74	0.87	0.86	1.00	0.91	0.84
16	6	51.3	0.87	0.74	0.87	0.86	1.00	0.91	0.84
16	6	60	0.90	0.74	0.87	0.86	1.00	0.91	0.84
16	6	60	0.89	0.74	0.87	0.86	1.00	0.91	0.84
16	6	60	0.91	0.74	0.87	0.86	1.00	0.91	0.84
16	6	60	0.89	0.74	0.87	0.86	1.00	0.91	0.84
16	6	60	0.89	0.74	0.87	0.86	1.00	0.91	0.84
16	6	60	0.89	0.74	0.87	0.86	1.00	0.91	0.84
16	6	70	0.88	0.74	0.87	0.86	1.00	0.91	0.84
16	6	90	0.89	0.74	0.87	0.86	1.00	0.91	0.84
16	6	90	0.88	0.74	0.87	0.86	1.00	0.91	0.84
16	6	120	0.89	0.74	0.87	0.86	1.00	0.91	0.84
16	6	120	0.88	0.74	0.87	0.86	1.00	0.91	0.84
16	6	150	0.88	0.74	0.87	0.86	1.00	0.91	0.84
16	6	180	0.86	0.74	0.87	0.86	1.00	0.91	0.84
16	7	20	0.91	0.80	0.90	0.89	1.00	0.95	0.88
16	7	25	0.93	0.80	0.90	0.89	1.00	0.95	0.88
16	7	25	0.91	0.80	0.90	0.89	1.00	0.95	0.88
16	7	30	0.92	0.80	0.90	0.89	1.00	0.95	0.88
16	7	30	0.93	0.80	0.90	0.89	1.00	0.95	0.88
16	7	31.7	0.93	0.80	0.90	0.89	1.00	0.95	0.88
16	7	40	0.91	0.80	0.90	0.89	1.00	0.95	0.88
16	7	40	0.90	0.80	0.90	0.89	1.00	0.95	0.88
16	7	42.2	0.93	0.80	0.90	0.89	1.00	0.95	0.88
16	7	50	0.90	0.80	0.90	0.89	1.00	0.95	0.88
16	7	51.3	0.93	0.80	0.90	0.89	1.00	0.95	0.88
16	7	60	0.90	0.80	0.90	0.89	1.00	0.95	0.88
16	7	70	0.90	0.80	0.90	0.89	1.00	0.95	0.88
16	7	90	0.90	0.80	0.90	0.89	1.00	0.95	0.88
16	7	90	0.90	0.80	0.90	0.89	1.00	0.95	0.88
16	7	120	0.90	0.80	0.90	0.89	1.00	0.95	0.88
16	7	120	0.88	0.80	0.90	0.89	1.00	0.95	0.88
16	7	150	0.90	0.80	0.90	0.89	1.00	0.95	0.88
16	7	180	0.87	0.80	0.90	0.89	1.00	0.95	0.88
16	8	25	0.99	0.85	0.93	0.92	1.00	0.97	0.91
16	8	40	0.93	0.85	0.93	0.92	1.00	0.97	0.91
16	8	50	0.91	0.85	0.93	0.92	1.00	0.97	0.91
16	8	70	0.92	0.85	0.93	0.92	1.00	0.97	0.91
16	8	90	0.91	0.85	0.93	0.92	1.00	0.97	0.91
16	8	90	0.92	0.85	0.93	0.92	1.00	0.97	0.91
16	8	120	0.90	0.85	0.93	0.92	1.00	0.97	0.91
16	8	150	0.90	0.85	0.93	0.92	1.00	0.97	0.91
16	8	180	0.89	0.85	0.93	0.92	1.00	0.97	0.91
16	9	40	0.95	0.89	0.95	0.94	1.00	0.99	0.94
16	9	70	0.94	0.89	0.95	0.94	1.00	0.99	0.94

Table D1. Experimental and Calculated Activity Coefficient at Infinite-Dilution using Several Models- *Continued*

Sol CN-1	Sol CN-2	T °C	Gamma Exp.	UNIFAC 75	Kikic 80	Larsen 87	Sheng 89	Voulsas 95	Zhong 2000
γ_2^∞									
16	9	90	0.94	0.89	0.95	0.94	1.00	0.99	0.94
16	9	90	0.93	0.89	0.95	0.94	1.00	0.99	0.94
16	9	120	0.92	0.89	0.95	0.94	1.00	0.99	0.94
16	9	150	0.92	0.89	0.95	0.94	1.00	0.99	0.94
16	10	70	0.96	0.92	0.96	0.96	1.00	0.99	0.96
16	10	90	0.95	0.92	0.96	0.96	1.00	0.99	0.96
17	5	22.5	0.88	0.65	0.82	0.80	1.01	0.84	0.77
17	5	30	0.86	0.65	0.82	0.80	1.01	0.84	0.77
17	5	40	0.86	0.65	0.82	0.80	1.01	0.84	0.77
17	5	50	0.85	0.65	0.82	0.80	1.01	0.84	0.77
17	5	60	0.84	0.65	0.82	0.80	1.01	0.84	0.77
17	5	70	0.83	0.65	0.82	0.80	1.01	0.84	0.77
17	5	80	0.82	0.65	0.82	0.80	1.01	0.84	0.77
17	6	22.5	0.91	0.72	0.86	0.84	1.00	0.90	0.82
17	6	30	0.90	0.72	0.86	0.84	1.00	0.90	0.82
17	6	40	0.88	0.72	0.86	0.84	1.00	0.90	0.82
17	6	50	0.89	0.72	0.86	0.84	1.00	0.90	0.82
17	6	50	0.89	0.72	0.86	0.84	1.00	0.90	0.82
17	6	60	0.88	0.72	0.86	0.84	1.00	0.90	0.82
17	6	70	0.88	0.72	0.86	0.84	1.00	0.90	0.82
17	6	80	0.87	0.72	0.86	0.84	1.00	0.90	0.82
17	7	22.5	0.95	0.77	0.89	0.88	1.00	0.93	0.86
17	7	30	0.93	0.77	0.89	0.88	1.00	0.93	0.86
17	7	40	0.20	0.77	0.89	0.88	1.00	0.93	0.86
17	7	50	0.93	0.77	0.89	0.88	1.00	0.93	0.86
17	7	60	0.92	0.77	0.89	0.88	1.00	0.93	0.86
17	7	70	0.91	0.77	0.89	0.88	1.00	0.93	0.86
17	7	80	0.92	0.77	0.89	0.88	1.00	0.93	0.86
18	4	35	0.88	0.55	0.75	0.73	1.02	0.75	0.68
18	5	30	0.85	0.62	0.80	0.78	1.01	0.82	0.74
18	5	30	0.80	0.62	0.80	0.78	1.01	0.82	0.74
18	5	35	0.87	0.62	0.80	0.78	1.01	0.82	0.74
18	5	35	0.87	0.62	0.80	0.78	1.01	0.82	0.74
18	6	30	0.87	0.69	0.84	0.83	1.00	0.88	0.80
18	6	30	0.84	0.69	0.84	0.83	1.00	0.88	0.80
18	6	30	0.87	0.69	0.84	0.83	1.00	0.88	0.80
18	6	35	0.88	0.69	0.84	0.83	1.00	0.88	0.80
18	6	35	0.88	0.69	0.84	0.83	1.00	0.88	0.80
18	6	40	0.86	0.69	0.84	0.83	1.00	0.88	0.80
18	6	50	0.88	0.69	0.84	0.83	1.00	0.88	0.80
18	6	50	0.86	0.69	0.84	0.83	1.00	0.88	0.80
18	6	51.4	0.85	0.69	0.84	0.83	1.00	0.88	0.80
18	6	61.4	0.86	0.69	0.84	0.83	1.00	0.88	0.80
18	6	70.5	0.88	0.69	0.84	0.83	1.00	0.88	0.80
18	6	80	0.84	0.69	0.84	0.83	1.00	0.88	0.80

Table D1. Experimental and Calculated Activity Coefficient at Infinite-Dilution using Several Models- *Continued*

Sol CN-1	Sol CN-2	T °C	Gamma Exp.	UNIFAC	Kikic 80	Larsen 87	Sheng 89	Voulsas 95	Zhong 2000
γ_2^∞									
18	6	80.5	0.86	0.69	0.84	0.83	1.00	0.88	0.80
18	7	30	0.89	0.75	0.88	0.86	1.00	0.92	0.85
18	7	30	0.88	0.75	0.88	0.86	1.00	0.92	0.85
18	7	30	0.88	0.75	0.88	0.86	1.00	0.92	0.85
18	7	30	0.91	0.75	0.88	0.86	1.00	0.92	0.85
18	7	35	0.89	0.75	0.88	0.86	1.00	0.92	0.85
18	7	40	0.88	0.75	0.88	0.86	1.00	0.92	0.85
18	7	40	0.90	0.75	0.88	0.86	1.00	0.92	0.85
18	7	50	0.88	0.75	0.88	0.86	1.00	0.92	0.85
18	7	50	0.88	0.75	0.88	0.86	1.00	0.92	0.85
18	7	51.4	0.86	0.75	0.88	0.86	1.00	0.92	0.85
18	7	60	0.89	0.75	0.88	0.86	1.00	0.92	0.85
18	7	61.4	0.89	0.75	0.88	0.86	1.00	0.92	0.85
18	7	70.5	0.89	0.75	0.88	0.86	1.00	0.92	0.85
18	7	80.5	0.88	0.75	0.88	0.86	1.00	0.92	0.85
18	8	30	0.91	0.80	0.90	0.89	0.99	0.95	0.88
18	8	35	0.91	0.80	0.90	0.89	0.99	0.95	0.88
18	8	40	0.89	0.80	0.90	0.89	0.99	0.95	0.88
20	4	80	0.83	0.51	0.72	0.70	1.02	0.70	0.64
20	5	40	0.83	0.58	0.77	0.75	1.01	0.78	0.71
20	5	53.2	0.85	0.58	0.77	0.75	1.01	0.78	0.71
20	5	74.1	0.83	0.58	0.77	0.75	1.01	0.78	0.71
20	5	80	0.84	0.58	0.77	0.75	1.01	0.78	0.71
20	5	93.9	0.82	0.58	0.77	0.75	1.01	0.78	0.71
20	6	40	0.85	0.65	0.81	0.80	1.00	0.84	0.76
20	6	53.2	0.89	0.65	0.81	0.80	1.00	0.84	0.76
20	6	74.1	0.88	0.65	0.81	0.80	1.00	0.84	0.76
20	6	80	0.87	0.65	0.81	0.80	1.00	0.84	0.76
20	6	93.9	0.87	0.65	0.81	0.80	1.00	0.84	0.76
20	7	40	0.88	0.71	0.85	0.84	1.00	0.89	0.81
20	7	53.2	0.92	0.71	0.85	0.84	1.00	0.89	0.81
20	7	74.1	0.91	0.71	0.85	0.84	1.00	0.89	0.81
20	7	80	0.90	0.71	0.85	0.84	1.00	0.89	0.81
20	7	93.9	0.92	0.71	0.85	0.84	1.00	0.89	0.81
20	8	80	0.92	0.76	0.88	0.87	0.99	0.93	0.85
20	10	80	0.97	0.84	0.93	0.92	0.99	0.97	0.91
22	4	50	0.79	0.47	0.69	0.67	1.02	0.66	0.60
22	5	50	0.80	0.54	0.75	0.73	1.01	0.74	0.67
22	5	60	0.79	0.54	0.75	0.73	1.01	0.74	0.67
22	6	50	0.81	0.61	0.79	0.77	1.00	0.81	0.73
22	6	60	0.80	0.61	0.79	0.77	1.00	0.81	0.73
22	7	50	0.82	0.67	0.83	0.81	0.99	0.86	0.78
22	8	50	0.83	0.72	0.86	0.85	0.99	0.90	0.82
24	4	60	0.77	0.44	0.67	0.64	1.02	0.62	0.57
24	5	51.3	0.73	0.51	0.72	0.70	1.01	0.70	0.64
24	5	55	0.76	0.51	0.72	0.70	1.01	0.70	0.64

Table D1. Experimental and Calculated Activity Coefficient at Infinite-Dilution using Several Models- *Continued*

Sol CN-1	Sol CN-2	T °C	Gamma Exp.	UNIFAC	Kikic 80	Larsen 87	Sheng 89	Voulsas 95	Zhong 2000
γ_2^∞									
24	5	60	0.76	0.51	0.72	0.70	1.01	0.70	0.64
24	5	60.6	0.73	0.51	0.72	0.70	1.01	0.70	0.64
24	5	65	0.76	0.51	0.72	0.70	1.01	0.70	0.64
24	5	70.4	0.74	0.51	0.72	0.70	1.01	0.70	0.64
24	5	80.3	0.73	0.51	0.72	0.70	1.01	0.70	0.64
24	6	51.3	0.78	0.57	0.77	0.75	1.00	0.77	0.70
24	6	55	0.78	0.57	0.77	0.75	1.00	0.77	0.70
24	6	60	0.78	0.57	0.77	0.75	1.00	0.77	0.70
24	6	60.6	0.78	0.57	0.77	0.75	1.00	0.77	0.70
24	6	65	0.78	0.57	0.77	0.75	1.00	0.77	0.70
24	6	70.4	0.77	0.57	0.77	0.75	1.00	0.77	0.70
24	6	76	0.79	0.57	0.77	0.75	1.00	0.77	0.70
24	6	80	0.79	0.57	0.77	0.75	1.00	0.77	0.70
24	6	80.3	0.76	0.57	0.77	0.75	1.00	0.77	0.70
24	6	84	0.79	0.57	0.77	0.75	1.00	0.77	0.70
24	6	88	0.79	0.57	0.77	0.75	1.00	0.77	0.70
24	7	20	0.81	0.63	0.80	0.79	0.99	0.83	0.75
24	7	51.3	0.80	0.63	0.80	0.79	0.99	0.83	0.75
24	7	60.6	0.80	0.63	0.80	0.79	0.99	0.83	0.75
24	7	70.4	0.79	0.63	0.80	0.79	0.99	0.83	0.75
24	7	76	0.82	0.63	0.80	0.79	0.99	0.83	0.75
24	7	80	0.82	0.63	0.80	0.79	0.99	0.83	0.75
24	7	80.3	0.78	0.63	0.80	0.79	0.99	0.83	0.75
24	7	84	0.81	0.63	0.80	0.79	0.99	0.83	0.75
24	7	88	0.82	0.63	0.80	0.79	0.99	0.83	0.75
24	8	60	0.83	0.68	0.83	0.82	0.99	0.87	0.79
24	8	76	0.85	0.68	0.83	0.82	0.99	0.87	0.79
24	8	80	0.85	0.68	0.83	0.82	0.99	0.87	0.79
24	8	84	0.85	0.68	0.83	0.82	0.99	0.87	0.79
24	8	88	0.85	0.68	0.83	0.82	0.99	0.87	0.79
24	9	76	0.88	0.73	0.86	0.85	0.98	0.90	0.83
24	9	80	0.88	0.73	0.86	0.85	0.98	0.90	0.83
24	9	84	0.88	0.73	0.86	0.85	0.98	0.90	0.83
24	9	88	0.87	0.73	0.86	0.85	0.98	0.90	0.83
28	5	70	0.72	0.46	0.68	0.66	1.01	0.64	0.58
28	5	80.2	0.69	0.46	0.68	0.66	1.01	0.64	0.58
28	5	100	0.69	0.46	0.68	0.66	1.01	0.64	0.58
28	5	120	0.69	0.46	0.68	0.66	1.01	0.64	0.58
28	7	80.2	0.74	0.57	0.76	0.75	0.99	0.77	0.69
28	7	100	0.75	0.57	0.76	0.75	0.99	0.77	0.69
28	7	120	0.76	0.57	0.76	0.75	0.99	0.77	0.69
28	8	80.2	0.77	0.62	0.79	0.78	0.98	0.81	0.74
28	8	100	0.80	0.62	0.79	0.78	0.98	0.81	0.74
28	8	120	0.79	0.62	0.79	0.78	0.98	0.81	0.74
28	10	80.2	0.83	0.71	0.85	0.84	0.98	0.89	0.81

Table D1. Experimental and Calculated Activity Coefficient at Infinite-Dilution using Several Models- *Continued*

Sol CN-1	Solute CN-2	T °C	Gamma Exp.	UNIFAC	Kikic 80	Larsen 87	Sheng 89	Voulsas 95	Zhong 2000
γ_2^∞									
28	10	100	0.86	0.71	0.85	0.84	0.98	0.89	0.81
28	10	120	0.86	0.71	0.85	0.84	0.98	0.89	0.81
30	6	76	0.69	0.49	0.70	0.68	0.99	0.68	0.62
30	6	80	0.70	0.49	0.70	0.68	0.99	0.68	0.62
30	6	84	0.70	0.49	0.70	0.68	0.99	0.68	0.62
30	6	88	0.69	0.49	0.70	0.68	0.99	0.68	0.62
30	7	76	0.72	0.54	0.74	0.73	0.98	0.74	0.67
30	7	80	0.72	0.54	0.74	0.73	0.98	0.74	0.67
30	7	84	0.70	0.54	0.74	0.73	0.98	0.74	0.67
30	7	88	0.72	0.54	0.74	0.73	0.98	0.74	0.67
30	8	76	0.74	0.59	0.78	0.76	0.98	0.79	0.71
30	8	80	0.74	0.59	0.78	0.76	0.98	0.79	0.71
30	8	84	0.73	0.59	0.78	0.76	0.98	0.79	0.71
30	8	88	0.75	0.59	0.78	0.76	0.98	0.79	0.71
30	9	76	0.77	0.63	0.80	0.79	0.97	0.83	0.75
30	9	80	0.77	0.63	0.80	0.79	0.97	0.83	0.75
30	9	84	0.76	0.63	0.80	0.79	0.97	0.83	0.75
30	9	88	0.77	0.63	0.80	0.79	0.97	0.83	0.75
32	7	75	0.70	0.52	0.72	0.71	0.98	0.71	0.64
32	8	75	0.72	0.56	0.76	0.74	0.98	0.76	0.69
36	6	76	0.64	0.43	0.65	0.63	0.99	0.60	0.55
36	6	80	0.63	0.43	0.65	0.63	0.99	0.60	0.55
36	6	84	0.63	0.43	0.65	0.63	0.99	0.60	0.55
36	6	88	0.63	0.43	0.65	0.63	0.99	0.60	0.55
36	7	76	0.65	0.47	0.69	0.67	0.98	0.66	0.60
36	7	80	0.65	0.47	0.69	0.67	0.98	0.66	0.60
36	7	84	0.65	0.47	0.69	0.67	0.98	0.66	0.60
36	7	88	0.65	0.47	0.69	0.67	0.98	0.66	0.60
36	8	76	0.68	0.52	0.72	0.71	0.97	0.71	0.64
36	8	80	0.68	0.52	0.72	0.71	0.97	0.71	0.64
36	8	84	0.68	0.52	0.72	0.71	0.97	0.71	0.64
36	8	88	0.67	0.52	0.72	0.71	0.97	0.71	0.64
36	9	76	0.73	0.56	0.75	0.74	0.96	0.75	0.68
36	9	80	0.72	0.56	0.75	0.74	0.96	0.75	0.68
36	9	84	0.72	0.56	0.75	0.74	0.96	0.75	0.68
36	9	88	0.72	0.56	0.75	0.74	0.96	0.75	0.68
AAD				0.17	0.03	0.04	0.15	0.04	0.06
AAD%				20.78	4.75	5.61	20.17	5.28	8.72
BIAS				-0.16	-0.01	-0.03	0.15	0.01	-0.06
RMSE				0.18	0.06	0.06	0.18	0.06	0.09

*CN-1 and CN-2 correspond to n-paraffin carbon number of components 1 and 2, respectively.

- All experimental data listed are reported by Tiegs, et al. (1986)

APPENDIX E

Mixing Rules and Component Fugacity Coefficients
for the Thermodynamic Models
used in this Work

In addition to the new thermodynamics models introduced, two other models were used in this work for the purpose of evaluation and comparison. Accordingly, the necessary mixing rules and component fugacity coefficients for all five models are listed here for completeness. The PR equation-of-state is the starting point for the derivation of a general form for component fugacity coefficient.

$$\ln \hat{\phi}_i = -\ln(Z - B) + \frac{\bar{b}_i}{b} (Z - 1) - \frac{a}{2\sqrt{2}bRT} \left[\frac{\bar{a}_i}{na} - \frac{\bar{b}_i}{b} \right] \ln \left[\frac{Z + 2.414B}{Z - 0.414B} \right] \quad (\text{E-1})$$

Equation (E-1) was derived and verified against fugacity coefficient expression reported by Bader (1993), where

$$\bar{a}_i = \frac{\partial (n^2 a)}{\partial n_i} \quad (\text{E-2})$$

and

$$\bar{b}_i = \frac{\partial (nb)}{\partial n_i} \quad (\text{E-3})$$

The mixing rules for all models is defined in terms of α , where α is defined as follows

$$\alpha = \frac{a}{bRT} \quad (\text{E-4})$$

Differentiating with respect to n_i ,

$$\frac{\partial n\alpha}{\partial n_i} = \frac{1}{nbRT} \bar{a}_i - \frac{n^2 a}{RT(nb)^2} \bar{b}_i \quad (\text{E-5})$$

thus

$$\frac{\partial n\alpha}{\partial n_i} = \frac{a}{bRT} \left(\frac{\bar{a}_i}{na} - \frac{\bar{b}_i}{b} \right) \quad (\text{E-6})$$

Combining Equations (E-1) and (E-6), the general expression for fugacity coefficient of a component in a mixture is then defined as:

$$\ln \hat{\phi}_i = -\ln(Z - B) + \frac{\bar{b}_i}{b} (Z - 1) - \frac{1}{2\sqrt{2}} \frac{\partial n\alpha}{\partial n_i} \ln \left[\frac{Z + 2.414B}{Z - 0.414B} \right] \quad (\text{E-7})$$

A complete set of equations for a thermodynamic model require mixing rules for energy constant, a , and covolume, b . Also, \bar{b}_i and $\frac{\partial n\alpha}{\partial n_i}$ are required for the component fugacity coefficient. Following are the main equations used for each model.

Model-1

$$\alpha = \frac{a}{bRT} = \frac{1}{C_N} \left[\frac{A^{\text{exe}}}{RT} + (1 - \delta_1) \sum_1^{\text{NC}} z_i \ln \frac{b}{b_i} \right] + \sum_1^{\text{NC}} \frac{a_i}{b_i RT} \quad (\text{E-8})$$

Two cases were considered in the model evaluations, where they differ in the expression used for covolume parameter.

Case 1: New Mixing Rule for the covolume

$$b = \exp \left(\sum_1^{\text{NC}} z_i \ln b_i - (1 - \delta_2) \frac{A^{\text{exe}}_{\text{comb}}}{RT} \right) \quad (\text{E-9})$$

$$\frac{\partial n\alpha}{\partial n_i} = \frac{1}{C_N} \left[\ln \tilde{\gamma}_i + (1 - \delta_1) \left[\ln \frac{b}{b_i} + \sum_{j=1}^{\text{NC}} n_j \frac{1}{b} \frac{\partial b}{\partial n_j} \right] \right] + \frac{a_i}{b_i RT} \quad (\text{E-10})$$

where

$$\ln \tilde{\gamma}_i = \frac{\partial \left(\frac{nA^{\text{exe}}}{RT} \right)_{T,P,n_j}}{\partial n_i} \quad (\text{E-11})$$

and

$$\ln \tilde{\gamma}_{i,\text{comb}} = \frac{\partial \left(\frac{nA^{\text{exe}}_{\text{comb}}}{RT} \right)_{T,P,n_j}}{\partial n_i} \quad (\text{E-12})$$

Differentiating the covolume parameter with respect to n_i

$$n \frac{1}{b} \frac{\partial b}{\partial n_i} + \ln b = -(1 - \delta_2) \ln \tilde{\gamma}_{i,\text{comb}} + \ln b_i \quad (\text{E-13})$$

then

$$\frac{\partial b}{\partial n_i} = \frac{b}{n} \left(\ln \frac{b_i}{b} - (1 - \delta_2) \ln \tilde{\gamma}_{i,\text{comb}} \right) \quad (\text{E-14})$$

Substitute in Equation (E-10), to get:

$$\frac{\partial n\alpha}{\partial n_i} = \frac{1}{C_N} \left[\ln \gamma_i + (1 - \delta_1) \left(- \{1 - \delta_2\} \ln \tilde{\gamma}_{i,\text{comb}} \right) \right] + \frac{a_i}{b_i RT} \quad (\text{E-15})$$

Taking the derivative of b with respect to n_i leads to

$$\frac{\partial nb}{\partial n_i} = b + n \frac{\partial b}{\partial n_i} \quad (\text{E-16})$$

then

$$\frac{\partial nb}{\partial n_i} = b \left(1 + \ln \frac{b_i}{b} - (1 - \delta_2) \ln \tilde{\gamma}_{i,\text{comb}} \right) \quad (\text{E-17})$$

Case 2: Quadratic Mixing Rule

$$b = \sum_i \sum_j z_i z_j b_{ij} \quad (\text{E-18})$$

where

$$b_{ij} = (1 + D_{ij}) \frac{b_i + b_j}{2} \quad (\text{E-19})$$

and

$$\frac{\partial nb}{\partial n_i} \equiv \bar{b}_i = 2 \sum_j z_j b_{ij} - b \quad (\text{E-20})$$

then

$$\frac{\partial n\alpha}{\partial n_i} = \frac{1}{C_N} \left[\ln \tilde{\gamma}_i + (1 - \delta_i) \left[\ln \frac{b}{b_i} + \frac{\bar{b}_i - b}{b} \right] \right] + \frac{a_i}{b_i RT} \quad (\text{E-21})$$

LCVM Model

$$\alpha = \left(\frac{\lambda}{C_V} + \frac{1 - \lambda}{C_M} \right) \frac{G^{\text{exe}}}{RT} + \frac{1 - \lambda}{C_M} \sum_1^{\text{NC}} z_i \ln \frac{b}{b_i} + \sum_1^{\text{NC}} z_i \frac{a_i}{b_i RT} \quad (\text{E-22})$$

A linear mixing rule is used for covolume, where b is defined as:

$$b = \sum_1^{\text{NC}} z_i b_i \quad (\text{E-23})$$

where

$$\frac{\partial nb}{\partial n_i} = b_i \quad (\text{E-24})$$

and

$$\frac{\partial b}{\partial n_i} = \frac{1}{n} (b_i - b) \quad (\text{E-25})$$

then

$$\frac{\partial n\alpha}{\partial n_i} = \left(\frac{\lambda}{C_V} + \frac{1 - \lambda}{C_M} \right) \ln \gamma_i + \frac{1 - \lambda}{C_M} \left[\ln \frac{b}{b_i} + \frac{b_i}{b} - 1 \right] + \frac{a_i}{b_i RT} \quad (\text{E-26})$$

where

$$\ln \gamma_i = \frac{\partial \left(\frac{nG^{\text{exe}}}{RT} \right)_{T,P,n_j}}{\partial n_i} \quad (\text{E-27})$$

CHV Model

$$\alpha = \frac{1}{C_{OS}} \left(\frac{A^{exe}}{RT} \right) + \frac{1-\lambda}{C_{OS}} \sum_1^{NC} z_i \ln \frac{b}{b_i} + \sum_1^{NC} z_i \frac{a_i}{b_i RT} \quad (E-28)$$

and

$$\frac{\partial n \alpha}{\partial n_i} = \frac{1}{C_{OS}} \ln \tilde{\gamma}_i + \frac{1-\lambda}{C_{OS}} \left[\ln \frac{b}{b_i} + \frac{b_i}{b} - 1 \right] + \frac{a_i}{b_i RT} \quad (E-29)$$

Similar to the LCVM model, a linear mixing rule was used for the covolume as defined by Equations (E-23) and (E-24).

Model-2 & -3

$$\alpha = \frac{1}{C_N} \left(\frac{A_{residual}^{exe}}{RT} \right) + \sum_1^{NC} z_i \frac{a_i}{b_i RT} \quad (E-30)$$

$$\frac{\partial n \alpha}{\partial n_i} = \frac{1}{C_N} \ln \tilde{\gamma}_{i,residual} + \frac{a_i}{b_i RT} \quad (E-31)$$

where

$$\ln \tilde{\gamma}_{i,residual} = \frac{\partial \left(\frac{n A_{residual}^{exe}}{RT} \right)_{T,P,n_j}}{\partial n_i} \quad (E-32)$$

Case 1: Linear mixing rule for the covolume was used as defined by Equations (E-23) and (E-24) leading to Model-3.

Case 2: New mixing rule for the covolume was used as defined by Equations (E-9) and (E-17) leading to Model-2.

Appendix F

Auxiliary VLE Properties Measurements

In this appendix, an external consistency test for liquid molar volumes measured in this study was performed. In addition, experimental measurements of dew point pressures and the corresponding molar volumes are presented for selected systems. In most of the experiments performed, the solvents were high-molecular weight hydrocarbons with very low vapor pressures. Accordingly, the vapor phase consists mainly of solute gas. For the two gas/light hydrocarbon systems, CO₂/butane and N₂/hexane, examined, dew point pressures were determined from the discontinuity in the pressure-total volume of solvent injected plot. The molar volumes at the corresponding dew point and bubble point pressures were determined from knowledge of the total amount of material injected to reach the bubble or dew point pressure and the volume of the equilibrium cell.

Determination of the Equilibrium Cell Volume

Volumetric method was used in determining the equilibrium cell volume. The equilibrium cell was evacuated and isolated from gas injection pump by valve V-4. The pump was pressurized with hydrogen gas (or any other gas with known properties) and the equilibrium pressure and temperature were recorded. V-4 valve was opened to admit gas to the equilibrium cell. The gas injection pump piston was forwarded until the original pressure is reached. The system was allowed to stabilize and then the net volume injected and the gas temperatures in both the pump and the equilibrium cell were recorded. From the data collected, the cell was determined. The temperature effect on the equilibrium cell volume expansion was determined in this evaluation and accordingly, the following correlation produced:

$$V_{EC} = 18.895 + 0.00038 * T (^{\circ}F)$$

Based on repeated measurements, the uncertainty in equilibrium cell molar volume, $\sigma_{V_{EC}}$, is 0.04 cm^3 .

The uncertainty in reported molar volume is determined as follows:

$$\rho = \frac{n_1 + n_2 + n_3}{V_{EC}} \quad (F-1)$$

where

$$n_1 = \frac{(V_{if}\rho_{if} - V_{li}\rho_{li})}{Mw_1} \quad (F-2)$$

Applying Equation (B-1) to the mole fraction definition given in Equation (F-1) and taking into consideration the effect of pressure and temperature on vapor or liquid density (at bubble or dew point pressure), we obtain the uncertainty in density for ternary mixtures:

$$\begin{aligned} \sigma_p^2 = & \left(\frac{1}{V_{EC}}\right)^2 \sigma_{n_1}^2 + \left(\frac{1}{V_{EC}}\right)^2 \sigma_{n_2}^2 + \left(\frac{1}{V_{EC}}\right)^2 \sigma_{n_3}^2 + \left(-\frac{n}{V_{EC}^2}\right)^2 \sigma_{V_{EC}}^2 + \\ & \left(\frac{\partial \rho}{\partial T}\right)^2 \sigma_T^2 + \left(\frac{\partial \rho}{\partial P}\right)^2 \sigma_P^2 \end{aligned} \quad (F-3)$$

The uncertainties in number of moles determined from equations similar to Equation B-14 for binary mixtures. As indicated in the numerical example applied to Equation (B-25), the effect of the uncertainties in pressures and temperatures on liquid densities is negligible, therefore they were not considered in the reported uncertainties in liquid densities presented.

The uncertainty in molar volume is related to the uncertainty in density as follows:

$$\sigma_v^2 = \left(-\frac{1}{\rho^2} \right)^2 \sigma_p^2 \quad (\text{F-4})$$

Consistency Test of Liquid Molar Volume

Table F.1 presents a comparison between experimental results for liquid densities for carbon dioxide/decane mixtures measured in this work in comparison to published results by Reamer and Sage (1963). In most cases, good agreement observed between both sets of data, where the deviations in liquid molar volumes are within or slightly over the uncertainty in our experimental results estimated at 0.5 % of liquid molar volume. The volume of the equilibrium cell is critical in determining the molar volume, therefore, further tests are required to confirm the equilibrium cell volume.

Table F.1. Liquid Molar Volume for Carbon Dioxide (1)/Decane (2) Mixtures.

Mole Fraction, x_1	T/K	This Work	Reamer & Sage (1963)	AAD	%AAD
cm^3/gmol					
	344.3				
0.2030		175.2	174.4	0.77	0.44
0.2040		176.5	174.2	2.37	1.34
0.2159		173.3	172.4	0.90	0.52
	377.6				
0.2208		181.8	179.1	2.65	1.46
0.2104		181.8	180.7	1.09	0.60
0.2123		183.4	180.4	2.95	1.60
0.2238		179.9	178.6	1.24	0.69
	410.9				
0.2294		189.1	186.5	2.57	1.34
0.2187		189.4	188.2	1.22	0.64
0.2199		190.2	188.0	2.19	1.15
0.2274		188.1	186.8	1.28	0.68
0.2259		187.8	187.1	0.76	0.41
0.2326		187.2	186.0	1.25	0.66

Determination of Dew Point Pressures

As indicated in Table F.2, high deviations are observed in the measured dew point pressures obtained in this work in comparison to the published results by Olds, et al. (1949). The pressure vs. volume injected trends for nitrogen/hexane system is shown in Figure F.1 for the first composition ($y_1 = 0.826$) listed in Table F.3. A major contribution to vapor-phase mole fraction uncertainty (0.005 in the first case) is due to limited data points taken in the two-phase region close to the dew point pressure intersection. As shown in Figure F.2, the uncertainty of vapor-phase mole fraction due to limited data in the two-phase region is 0.001, where three data point taken in the two-phase region nearly fall in a straight line. The second major contribution to the high uncertainties in vapor-phase molar volume is due to the uncertainty in the capillary tube volume. Both contributions can be minimized to achieve better results for dew point pressures measurements. Measurements in the dew point region are preliminary and further work is required.

Table F.2. Dew Point Pressures for Carbon Dioxide (1)/Butane (2) System

T/K	Mole Fraction, y_2	This Work	Olds, et al. (1949)	AAD	%AAD
		MPa			
377.6	0.445	5.33	5.67	0.34	6.4
377.6	0.450	5.24	5.49	0.25	4.8

Table F.3. Dew Point Pressures and Molar Volumes for Nitrogen (1)/Hexane (2) System

T/K	Mole Fraction, y_1	Dew Point		
		Molar Volume, cm^3/gmol	p, MPa	σ_{y_1}
410.9	0.826	747	4.399	0.007
410.9	0.589	1569	1.896	0.005

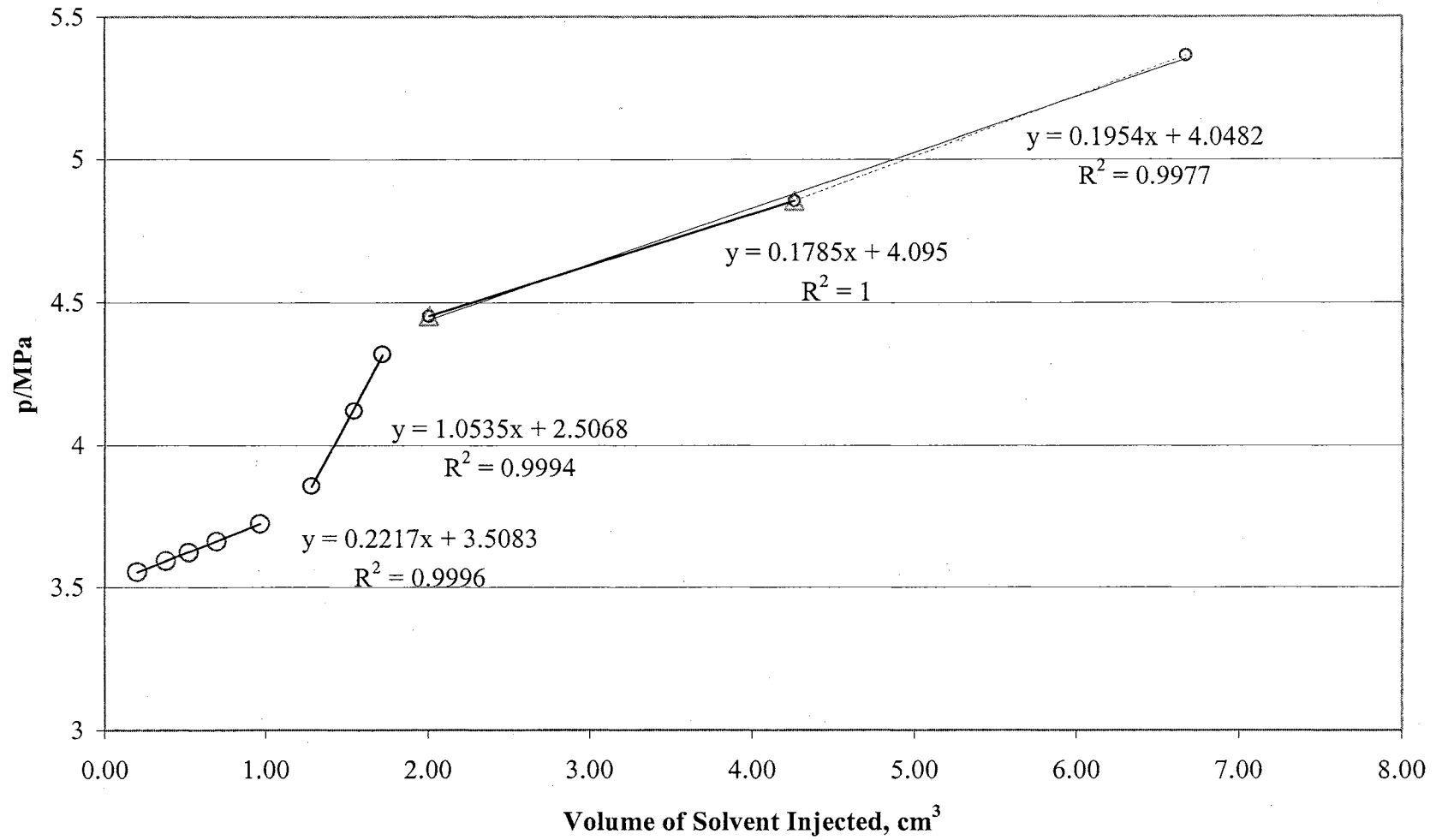


Figure F.1 Dew Point Pressure for Nitrogen/Hexane System at 410.9 K – Case 1.

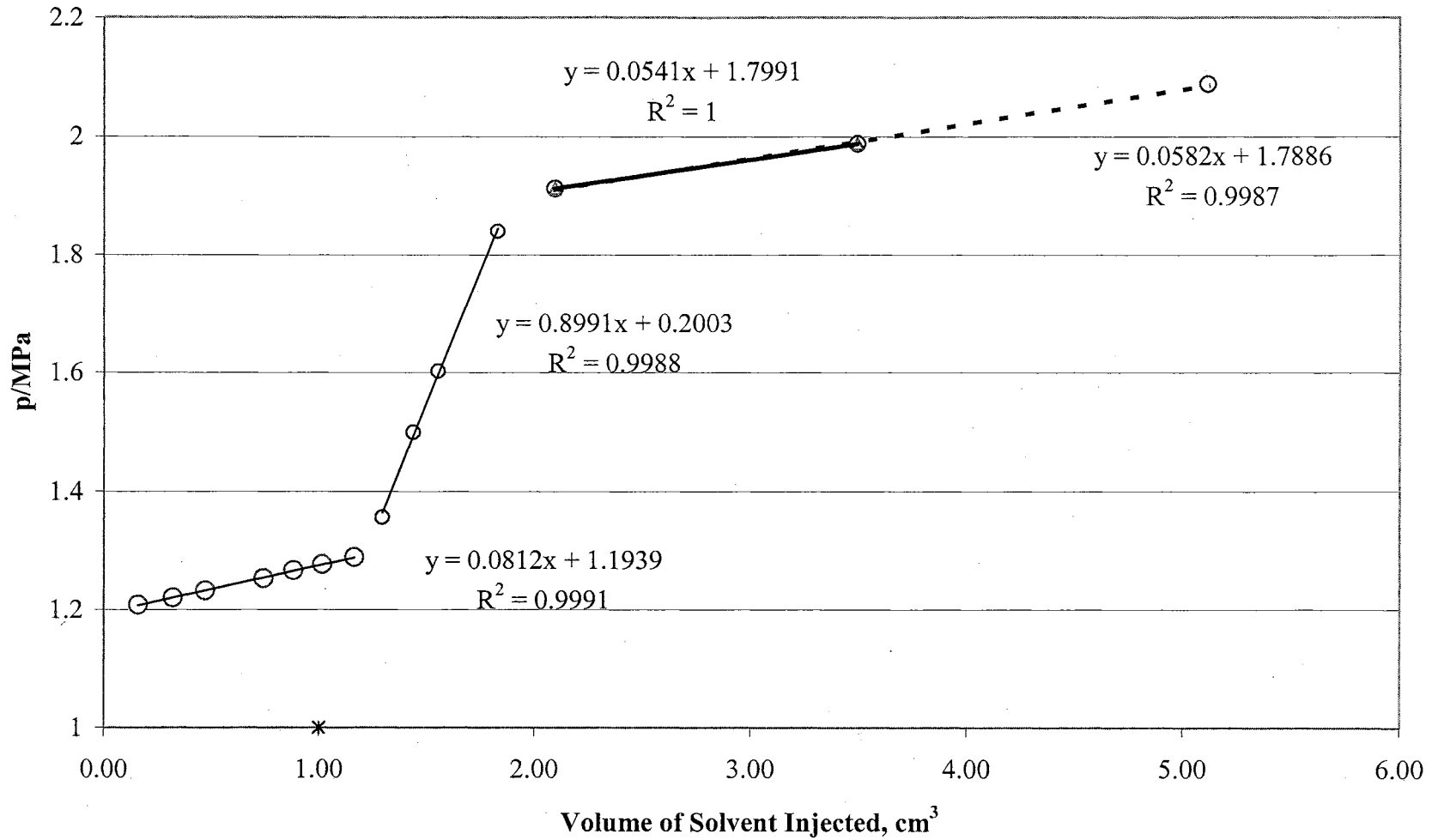


Figure F.2 Dew Point Pressure for Nitrogen/Hexane System at 410.9 K – Case 2.

VITA

Khalid Farouk Omar Z

Candidate for the Degree of

Doctor of Philosophy

Thesis: PHASE EQUILIBRIUM MEASUREMENTS AND MODELING OF SELECTED
ASYMMETRIC TERNARY MIXTURES

Major Field: Chemical Engineering

Biographical:

Personal Data: Born in Baton Rouge, Louisiana, the son of Dr. Farouk Omar and Mrs. Nifisa Muhammad. Married to Azza Ahmad and has two sons and a daughter.

Education: Received Bachelor of Science degree in Chemical Engineering from Texas A&M University – College Station in August 1989 and Master of Chemical Engineering degree from University of Houston – University Park in May 1993. Completed the requirements for the Doctor of Philosophy degree in Chemical Engineering at Oklahoma State University in December 2002.

Experience: Research Assistant, School of Chemical Engineering, Oklahoma State University, January 1999 to July, 2002; Project Engineer, Emissions Technology Inc./Thermal Recovery Inc., June 1991 to December 1998. Research Associate (temporary), Kraft General Food Co., October 1990 to May 1991.

Professional Memberships: American Institute of Chemical Engineers, American Society of Heating, Refrigeration, and Air-Conditioning Engineers, Inc.. Registered Professional Engineer in the State of Texas in February 1999.